UNIVERSITÉ DE STRASBOURG

ÉCOLE DOCTORALE des Science de la Vie et de la Santé **IGBMC - CNRS UMR 7104 - INSERM U1258**

THÈSE présentée par :

Rana EL BIZRI

soutenue le : **31 Juillet 2018**

pour obtenir le grade de : **Docteur de l'université de Strasbourg**

Discipline : Sciences de la Vie et de la Santé

Spécialité : Aspects Moléculaires et Cellulaires de la Biologie

Characterization of Pten and Trp53-deficient prostatic tumors in mice

THÈSE dirigée par :
Dr. METZGER Daniel Directeur de recherches - IGBMC - Université de Strasbourg

Codirecteur de THÈSE :
Pr. DAHER Ahmad Professeur - Faculté de Sciences - Université Libanaise

RAPPORTEURS :
Dr. GOFFIN Vincent Directeur de recherches - INEM - Université Paris Descartes
Dr. ORIAN-ROUSSEAU Véronique Directeur de recherches - KIT - ITG - Université de Karlsruhe

---

AUTRES MEMBRES DU JURY :
Dr. CERALINE Jocelyn MCU - PH - IGBMC - Université de Strasbourg

اهداء:

أهدي انجازي العلم ي اليوم الى صاحبة الفضل الكبير علي، الى من قضت من حياتها عمرا كاملا كي تراني على ملأ عليين لآ ه، الى مصدر قوتي وسبب سعادتي وملجئي عند التعب، الى من أستمد من خطوط وجهها الأملأ، ومن ارتعاشة يديها الثبات، ومن دعائها التوفيو ،قمن دموعهقوقلا ا، ومن رماد عينها نور الحال ،قاي ى أمي زيند ب مكي، ومن مثلكي ا أمي.

فالشكر الأول وا لأخير لك يا أمي بعد . الله لجو ز.

Acknowledgments

After 3 years of continuous hard work, long days, and sleepless nights, I finally made my dream come true and was able to successfully achieve what I came here for. My perseverance has finally paid off.

But all this period, I was never alone. God was always here for me. He has armed me with the strength to tolerate being away from home and enlightened my way and steadied my steps to the intended goal. The awaited day has finally come, and it couldn't have happened without God, whom I'm deeply grateful for and whose mercy and satisfaction I seek all my days.

I thank Dr. Daniel Metzger, my advisor throughout these years who taught me how to be rigid in the hardest times, how to think differently and have new perspectives that could yield very positive results, and how to utilize both knowledge and experience to support my thesis work. He was not only my advisor, he was my support, my guide, and my family.

I thank Pr. Pierre Chambon who was always my inspiration. Seeing him working in the weekends has always given me the motivation and determination to continue what I have started, even when I was at my worst.

I thank Maxime, the former Post doctor who has commenced the research work I have been working on and whose paper I was the second co-author for.

I thank Elise who participated with me in my first paper as a second co-author and that was published in "JEM" journal. We both have put the time and effort into this paper and wholeheartedly worked together as a team to obtain unique findings and achieve a quite satisfactory impact factor.

I Thank Gilles and Delphine, the researchers who were ready to give pieces of advice during my presence in the lab and give constructive feedback in lab meetings. Also, I thank Delphine for all her efforts to translate for me scientific documents to French.

I thank Annabelle and Daniela, my dearest friends who stood on my side in good and bad times. We have formed together a unique trio that I've truly enjoyed. We have strengthened each other, rejoiced in our sense of humor, and had lots of fun times together. I will not forget asking everyday Annabelle to see what is the problem in my computer, and asking Daniela to reread each paragraph I wrote in my papers. Thank you a lot my best friends and lab partners….

I thank Justine for being there when I was at the hospital. She was like a sister taking care of me…

I thank Jean Marc who has a beautiful soul, was always fun to be around in the animal house, and has triggered my laughs many times. His humor has made it easier for me to deal with mice. He was never reluctant to help me especially during my first period here at IGBMC. I thank Camille for teaching me how to castrate mice and she was very sympathetic.

I thank Alaa who is a great listener and a true friend who was always there for me and has helped me assemble my thesis work. His presence has always given me positive vibes. I will not forget his words: "Don't worry be happy".

I Thank Naima who was the first person I met in Strasbourg. We both have supported each other away from home. Her experience here have taught me to be stronger than I've ever been and prepared to deal with the unexpected.

I thank my friends Hussien, Najwa, Hassan, Jackey, leaticia, Nada, Ali and Hanin for their full support and their kind souls.

I thank IGBMC for making all the required facilities and equipment available and accessible for researchers, helping me excel in my experimental work.

I thank Al Bizri Association for funding me during my PhD period.

I thank mom, dad, my elder sister Mona, and my brother Youssef for being my support system till the end.

I thank my sister Dana from whom I've obtained much strength and inspiration, and whose hard personal experience with cancer has been my biggest incentive to put much effort into my research and be able to transform the lives of suffering patients and their families and dearest ones.

I thank the jury members who will allocate the time to be present on my thesis day.

I thank everyone whom I missed to mention and who have impacted me positively in my long journey, even in the simplest ways.

Résumé de thèse

Le cancer de la prostate (CaP) est la forme de cancer la plus fréquente et la troisième cause de décès par cancer chez l'homme dans les sociétés occidentales, ce qui lui confère un impact socio-économique important (Siegel et al., 2017). La progression du CaP chez l'homme se fait sur des décennies via un processus en plusieurs étapes, commençant par le développement de néoplasies prostatiques intraépithéliales (PINs), suivis d'adénocarcinomes et de métastases (Abate-Shen and Shen, 2000). Quand il est détecté alors qu'il est encore confiné localement, le CaP est éradiqué dans 70-80% des cas par prostatectomie ou radiothérapie. Cependant, ces traitements induisent souvent des complications (impuissance, incontinence) (Resnick et al., 2013). De ce fait, une surveillance active des CaP à faible risque pathologique est favorisée la plupart du temps afin d'éviter des traitements trop agressifs (Wadman et al., 2015). Malheureusement, la sévérité du CaP est souvent sous-estimée au moment du diagnostic et 20-30% des patients pour lesquels un CaP localisé a été diagnostiqué développent des métastases (Loeb et al., 2014). A l'heure actuelle, les tumeurs locales avancées ou métastatiques sont traitées par des anti-androgènes. Les tumeurs prostatiques peuvent néanmoins développer une résistance au traitement conduisant à une résurgence tumorale au bout de 1 à 3 ans conduisant à des formes agressives de CaP, alors qualifiées de cancer de la prostate résistant à la castration (CRPC) (Yuan et al., 2009). Le CRPC est actuellement traité par le Docetaxel, qui n'améliore malheureusement la survie des patients que de quelques mois (Berthold et al., 2008). Ainsi, il est important d'identifier les facteurs contribuant à la progression, mais aussi à la régression des tumeurs prostatiques, afin de développer de nouveaux composés pour traiter le CRPC.

Le gène suppresseur de tumeur PTEN étant fréquemment muté dans le CaP chez l'homme, le laboratoire a établi un modèle murin dans lequel PTEN est sélectivement invalidé post-puberté dans les cellules luminales épithéliales prostatiques (souris $Pten^{(i)pe-/-}$) (Ratnacaram et al., 2008). Les souris $Pten^{(i)pe-/-}$ développent une hyperplasie de la prostate dans le mois suivant l'ablation de Pten et des PINs dans les 3 mois. Au bout de 10 mois, certains de ces PINs évoluent en adénocarcinomes. Nous n'avons cependant observé aucune métastase au cours des 20 mois d'analyse, indiquant qu'une ou plusieurs mutations additionnelles sont requises pour le développement de métastases (Ratnacaram et al., 2008).

Plusieurs études ont montré que la progression des PINs induite par la perte de Pten est antagonisée par la sénescence cellulaire (Alimonti et al., 2010; Chen et al., 2005; Di Mitri et al., 2014). La sénescence est induite par de nombreux stimuli, notamment par les oncogènes [oncogene-induced senescence (OIS) (Bartkova et al., 2006; Bartek et al., 2007; Courtois-Cox et al., 2008). L'expression de certains oncogènes stimule la prolifération cellulaire, induisant un stress de réplication et une activation de la voie de réponse aux dommages de l'ADN (DDR) (Bartkova et al., 2006; Bartek et al., 2007). La sénescence induite par la perte de Pten est dépendante du facteur de transcription Trp53 (Chen et al., 2005) et est considérée comme un type de sénescence particulier (Astle et al., 2012; Chen et al., 2005; Courtois-Cox et al., 2008) du fait qu'elle n'est pas associée à de l'hyperprolifération (Alimonti et al., 2010; Astle et al., 2012). De plus, Di Mitri et al. ont montré que les cellules suppressives dérivées de myéloïdes infiltrées (MDSCs) dans les tumeurs (e.g. GR-1) antagonisent la sénescence induite par la perte de Pten et favorisent la croissance tumorale (Di Mitri et al., 2014).

Afin de caractériser en détails la sénescence induite par la perte de Pten *in vivo*, les souris $Pten^{(i)pe-/-}$ ont été analysées sur une période de 12 mois après invalidation de Pten. La perte de Pten stimule la prolifération des cellules épithéliales de la prostate formant des PINs au cours des 3 premiers mois. La

croissance de ces PINs est ensuite ralentie et à 5 mois, nous avons mis en évidence que ces PINs entre en sénescence. Ils sont en effet positifs pour la coloration à la SA-β-galactosidase, un marqueur de la sénescence cellulaire (Collado and Serrano, 2006), et les niveaux d'expression des marqueurs sénescence (e.g. p16, $p19^{ARF}$, p21 et p27) et des gènes impliqués dans le phénotype sécrétoire associé à la sénescence (SASP) (e.g. IL-1α, IL-1β, M-CSF et TNFα) sont augmentés.

Il est important de noter que nous avons également prouvé que les cellules épithéliales de la prostate en prolifération et déficientes pour Pten montrent des signes de stress de réplication et de DDR (expression de γH2AX, ATR et 53BP1), conduisant à la stabilisation de Trp53. Ceci est cependant retardé par la diminution des niveaux d'expression de Trp53. Afin de démontrer que Mdm2 est impliqué dans la dégradation de Trp53 à des temps précoces, les souris $Pten^{(i)pe-/-}$ ont été traitées à la Nutlin-3, un inhibiteur de l'interaction Mdm2-Trp53 (Vassilev et al., 2004) 1 mois après la perte de Pten. Nos résultats ont montré qu'un traitement à la Nutlin-3 stimule les niveaux protéiques de Trp53 dans les cellules épithéliales de la prostate, et active les niveaux transcriptionnels de p21, une cible de Trp53. Ainsi, les faibles niveaux de Trp53 observés à des temps précoces résultent très probablement de sa dégradation par Mdm2. Nous avons également montré que les MDSCs ne rentrent pas en compte dans le retard de la sénescence des cellules épithéliales de la prostate et la stabilisation de Trp53, aucune cellule myéloïde positive pour GR-1 n'ayant été observée après l'ablation de Pten. Ainsi, même si la perte de Pten induit la sénescence cellulaire pour restreindre la progression de la tumeur en induisant un stress de réplication, les stratégies pour promouvoir la sénescence induite par la perte de Pten constituent néanmoins un risque pour la prévention et le traitement du cancer **[manuscript 1]**.

Des mutations dans Trp53 ayant été trouvées dans les CaP chez l'homme, nous avons établi des souris $Pten/Trp53^{(i)pe-/-}$, chez lesquelles les allèles de Pten et Trp53 sont sélectivement invalidés dans les cellules épithéliales de la prostate, et avons analysés ces animaux sur une période de 9 mois. De 1 à 5 mois, le poids de la prostate des souris $Pten/Trp53^{(i)pe-/-}$ est similaire à celui des souris $Pten^{(i)pe-/-}$, mais le taux de prolifération déterminé par un immunomarquage au Ki67 est supérieur chez les souris $Pten/Trp53^{(i)pe-/-}$ 2 mois après ablation. Cela peut ainsi expliquer le délai observé en l'absence de Trp53 dans la mise en place de la sénescence des cellules épithéliales prostatiques invalidées pour Pten. Entre 5 et 9 mois, 27% des souris $Pten/Trp53^{(i)pe-/-}$ développent adénocarcinomes hyperprolifératifs (ADK) et des tumeurs sarcomatoïdes (SARC), et 1/3 de ces dernières métastasent au niveau péritonéal et des ganglions lymphatiques. Néanmoins, 73% des souris $Pten/Trp53^{(i)pe-/-}$ développent des PINs similaires à ceux des souris $Pten^{(i)pe-/-}$. Ainsi, la perte de Trp53 affecte la stimulation précoce de la prolifération des cellules épithéliales prostatiques invalidées en l'absence de Pten conduisant par la suite au développement de tumeurs de la prostate à des temps tardifs, mais cela n'est certainement pas suffisant pour contrer la sénescence.

L'analyse transcriptomique des PINs des souris $Pten/Trp53^{(i)pe-/-}$ et contrôles a montré un enrichissement des voies de signalisation jouant un rôle dans l'inflammation, la réponse immunitaire et la sénescence. Parmi les gènes dont l'expression est la plus augmentée chez les mutants, nous avons identifié des régulateurs du cycle cellulaire (e.g. Cdkn2a et p16), des gènes impliqués dans la SASP qui permettent le recrutement de cellules immunitaires (e.g. Cxcl1, Cxcl2, Cxcl5, Tnf, Il1β et Csf1), ainsi que des marqueurs de cellules souches (e.g. Cd44). L'analyse par RT-qPCR a montré que les niveaux d'expression des marqueurs de sénescence (p16, $p19^{ARF}$ and p21) de même que les SASP (M-CSF et CXCL-1) sont d'avantage exprimés dans les PINs des souris $Pten/Trp53^{(i)pe-/-}$ par rapport aux souris $Pten^{(i)pe-/-}$, dans les 5 mois suivant l'ablation des gènes. De plus, nous avons observé un marquage

nucléaire de pHP1γ (Adams, 2007) dans la majorité des PINs des souris Pten/Trp53$^{(i)pe-/-}$ confirmant le fait que ces cellules positives pour la coloration SA-βGal soient en sénescence même en l'absence de Trp53. Ainsi, la sénescence des cellules épithéliales prostatiques observée en l'absence de Pten n'est pas dépendante de Trp53.

Les chimiokines (faisant partie la SASP) et les MDSCs peuvent contribuer au recrutement de cellules immunosuppressive, et ainsi promouvoir la tumorigenèse (Katoh et al., 2013). A 5 mois, les niveaux de transcrits des MDSCs Cd11b et Ly6g sont plus élevés dans les PINs des souris Pten/Trp53$^{(i)pe-/-}$ par rapport aux souris Pten$^{(i)pe-/-}$, suggérant que la perte de Trp53 dans les cellules dans lesquelles Pten est sélectivement invalidé active le recrutement de MDSCs via la SASP pour favoriser la tumorigenèse.

Il a également était montré que les cellules en sénescence relarguent des facteurs pouvant promouvoir la reprogrammation des cellules voisines (Mosterio et al., 2016; Ritschka et al., 2017). Nous montrons par RT-qPCR et immunohistochimie que Sox2 et Nanog, 2 facteurs essentiels de la reprogrammation pour générer des cellules souches pluripotentes (iPSCs) (Bracken et al., 2003), sont d'avantage induits dans les PINs des souris Pten/Trp53$^{(i)pe-/-}$ que dans ceux des souris Pten$^{(i)pe-/-}$ à 5 mois. Ainsi, la perte de Trp53 dans les cellules dans lesquelles Pten est sélectivement invalidé induit des facteurs de reprogrammation, pouvant créer un environnement de type cellule souche, permissif pour la plasticité de la lignée cellulaire (Mu et al., 2017). Nous montrons par RT-qPCR et immunohistochimie que les niveaux d'expression du marqueur neuroendocrine Syp dans les PINs des souris sont plus élevés chez les souris Pten/Trp53$^{(i)pe-/-}$ que chez les souris Pten$^{(i)pe-/-}$ à 5 mois. Ainsi, en l'absence de Trp53, les caractères de sénescence, de pluripotence et de celulles neuroendocrines sont induits, indiquant que Trp53 joue un rôle dans l'interaction entre la sénescence cellulaire et la reprogrammation *in vivo* **[manuscript 2]**.

Afin de caractériser le rôle des androgènes dans la progression tumorale, les souris Pten$^{(i)pe-/-}$ and Pten/Trp53$^{(i)pe-/-}$ ont été chirurgicalement castrées dans les 2 mois suivant l'invalidation de ces gènes à un stade auquel nous observons la formation de PINs, et sacrifiées 3 mois plus tard (au stade de sénescence). Nos résultats montrent que la castration des souris Pten$^{(i)pe-/-}$ et Pten/Trp53$^{(i)pe-/-}$ réduit la masse de la tumeur ainsi que la surface des glandes. Cependant, l'architecture des PINs des souris mutantes castrées ressemble à celle des souris mutantes dont l'opération a été simulée (sham), avec un taux de prolifération similaire (% Ki67), montrant que certaines cellules épithéliales prostatiques sont résistantes à la castration. Ces tumeurs résistantes expriment des niveaux similaires des marqueurs de sénescence et de SASP par rapport aux mutants sham. Ainsi, l'absence d'androgènes n'affecte pas la sénescence des cellules épithéliales prostatiques en l'absence de Pten seul ou de Pten/Trp53. Les analyses de RT-qPCR et d'immunohistochimie montrent que les niveaux d'expression de Sox2 et de Syp sont cependant augmentés chez les souris Pten$^{(i)pe-/-}$ et Pten/Trp53$^{(i)pe-/-}$ après castration. Ainsi, la déprivation d'androgènes facilite la dédifférenciation des cellules épithéliales prostatiques des souris mutantes Pten et Pten/Trp53 en cellules focales neuroendocrines **[manuscript 3]**.

Nos données démontrent que la sénescence induite par la perte de Pten dans les cellules épithéliales de la prostate advient après une phase au cours de laquelle la prolifération est activée et est relayée par le stress de réplication et la réponse aux dommages de l'ADN *in vivo*, ressemblant ainsi à la sénescence induite par l'activation oncogènes contrairement à ce qui avait été préalablement proposé (Alimonti et al., 2010). Nous avons également montré que la sénescence induite par la perte de Pten dans les cellules épithéliales de la prostate est retardée par la diminution des niveaux protéiques de

Trp53 par Mdm2. En accord avec ces observations, nous montrons que l'hyperprolifération cellulaire est activée en l'absence de Trp53 dans les cellules épithéliales de la prostate mutées pour Pten à des temps précoces. Cependant, seules 27% des souris Pten/Trp53$^{(i)pe-/-}$ développent des adénocarcinomes et des tumeurs sarcomatoïdes, tandis que les cellules épithéliales de la prostate de 73% de ces animaux sénescentes même en l'absence de Trp53. Ainsi, la sénescence induite par la perte de Pten dans les cellules épithéliales de la prostate n'est pas pleinement dépendante de Trp53 *in vivo*, contrairement à ce qui avait été préalablement observé (Chen et al., 2005).

Concomitamment avec la sénescence observée en l'absence de Trp53, nous avons identifié des facteur de la SASP, de MDSCs et de marqueurs de pluripotence dans les cellules épithéliales de la prostate ne possédant plus Pten promouvant leur différenciation en cellules focales neuroendocrines. Ainsi, Trp53 pourrait jouer un rôle dans le cross-talk entre la sénescence et la reprogrammation cellulaire *in vivo*.

Par ailleurs, l'absence d'androgènes n'empêche pas la prolifération des cellules épithéliales de la prostate dépourvues de Pten ou de Pten/Trp53, stimule leur pluripotence et induit leur différenciation en cellules neuroendocrines. De ce fait, la différenciation neuroendocrine fait partie du mécanisme de résistance à la castration.

L'identification des voies de signalisation supprimant la reprogrammation des cellules épithéliales de la prostate en l'absence de Pten et de Trp53, ainsi qu'après castration, devrait ouvrir de nouvelles perspectives de développement de thérapies efficaces pour le traitement des formes avancées de cancer de la prostate.

Contents

List of figures

List of tables

List of Abbreviations

Abbreviation	Description
	A
ADT	androgen deprivation therapy
AF1	activation function 1
AKT/PKB	protein kinase B
AP	anterior prostate
AR	androgen receptor
ARA70	androgen receptor-associated protein 70
ARE	androgen-responsive element
ATM	ataxia telangiectasia mutated
ATR	ATM and Rad3-related
	B
53BP1	tumor suppressor p53 binding protein 1
BPH	benign prostatic hyperplasia
BRAC1	breast cancer gene 1
BrdU	5-bromodeoxyuridine
	C
CCL	C-C motif chemokine ligand
CDK	cyclin dependent kinase
CHGA	chromogranin A
CHK	checkpoint kinase
CRPC	castration-resistant prostate cancer
CSCs	cancer stem-like cells
CXCL	C-X-C motif chemokine ligand
CYP17A	cytochrome P450 17alpha-hydoxylase
	D
DBD	DNA-binding domain
DDR	DNA damage response
DHEA	dehydroepiandrosterone
DNA-PK	DNA-dependent protein kinase
DP	dorsal prostate
DSBs	DNA double-strand breaks
	E
ECM	extracellular matrix
EGF	epidermal growth factor
EMT	epithelial-mesenchymal transition
ERbB2	Erb-B2 receptor tyrosine kinase 2
Ezh2	enhancer of zeste 2 polycomb repressive complex 2
	G
G-CSF	granulocyte-colony stimulatory factor
GEMMs	genetically engineered mouse models
GM-CSF	granulocyte-macrophage colony stimulatory factor
G-MDSC	granulocytic MDSC
GnRH	gonadotropin-releasing hormone

GR	glucocorticoid receptor
	H
H2AX	H2A histone family member X
HGPINs	high grade PINs
HP1γ	heterochromatin protein 1-γ
	I
IGF1	insulin-like growth factor
IL	interleukin
IL1β	interleukin-1 β
IL-1R	interleukin-1 receptor
IL-1RA	interleukin-1 receptor antagonist
	L
LBD	ligand binding domain
LGPINs	low grade PINs
LP	lateral prostate
	M
MAPK	mitogen-activated protein kinase
MCPs	monocyte chemoattractant proteins
MDSCs	myeloid derived suppressor cells
Mdm2	Mouse double-minute 2 homolog
MEK	mitogen-activated protein kinase kinase
MET	mesenchymal-epithelial transition
MIPs	macrophage inflammatory proteins
M-MDSCs	monocytic-MDSCs
MMTV	mouse mammary tumor virus
	N
NANOG	Nanog homeobox
NCoR	nuclear receptor corepressor
NEPC	neuroendocrine prostate cancer
NF-κB	nuclear factor-κB
NK	natural killer
Nkx3.1	Nk3 homeobox 1
NSE	neuron specific enolase
	O
OIS	oncogene-induced senescence
	P
PCa	prostate cancer
PGE2	prostaglandin E2
PICS	PTEN loss-induced senescence
PI3K	phosphatidylinositol-3-kinase
PIP2	phosphatidylinositol-2-phosphate
PIP3	phosphatidylinositol-3-phosphate
POU5F1	POU class 5 homeobox 1
PSA	prostate specific antigen
PTEN	phosphatase and tensin homolog deleted on chromosome 10
PZ	peripheral zone

	R
RAF	proto-oncogene, Serine/Threonine kinase
RAS	proto-oncogen, GTPase
RB	retinoblastoma
ROS	reactive oxygen species
RPA	replication protein A
	S
SA-βGal	senescence-associated β-galactosidase
SAHF	senescence-associated heterochromatin foci
Slug	snail family transcriptional repressor 2
Snail	snail family transcriptional repressor 1
Sox2	sex determining region Y-box2
Sox11	sex determining region Y-box11
ssDNA	single-stranded genomic DNA
Stat3	signal transducer and activator of transcription 3
SV	simian virus
Syp	Synaptophysin
	T
TGF-β	transforming growth factor-β
TMPRSS2	transmembrane protease, serine 2
TNFα	tumor necrosis factor α
TP53	tumor protein p53
TRAMP	transgenic adenocarcinoma mouse prostate
TSP-1	thrombospondin-1
Twist	twist family BHLH transcription factor
TZ	transitional zone
	U
UGM	urogenital sinus mesenchyme
UGS	urogenital sinus
	V
VEGF	vascular endothelial growth factor
	Z
Zeb1/2	Zinc finger E-box binding homeobox 1/2

INTRODUCTION

Chapter I:

1. Hallmarks of cancer:

Six hallmarks of cancer constitute an organizing principle for rationalizing the complexities of neoplastic diseases. As normal cells evolve progressively to a neoplastic state, they acquire a succession of these hallmark capabilities (Hanahan and Weinberg, 2000). The hallmarks comprise sustaining proliferative signaling, evading growth suppressors, resisting cell death, enabling replicative immortality, inducing angiogenesis, and activating invasion and metastasis **(Figure 1)** (Fouad and Aanei, 2017; Hanahan and Weinberg, 2000).

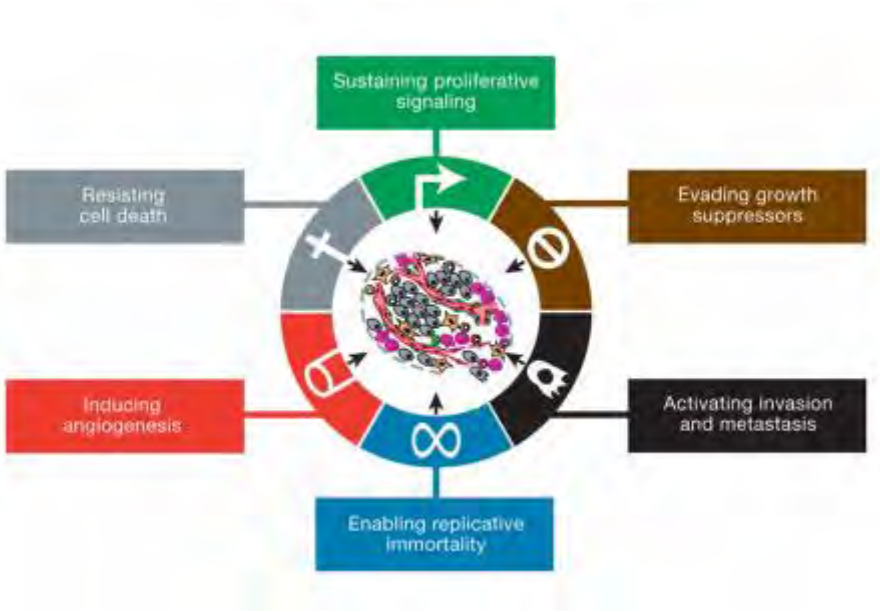

Figure 1: The Hallmarks of Cancer. Schematic illustration showing the six hallmarks of cancer (Hanahan and Weinberg, 2000).

1.1 Sustaining proliferative signaling:

Cancer cells acquire the capability to sustain proliferative signaling in different ways: they may produce growth factor ligands themselves, to which they can respond by the expression of relative receptors, resulting in autocrine proliferative stimulation. Alternatively, cancer cells may send signals to stimulate normal cells within the supporting tumor-associated stromal fibroblasts, which reciprocate by supplying the cancer cells with various growth factors (Bhowmick et al., 2004; Cheng et al., 2008).

1.1.1. Excessive proliferative signaling can trigger cell senescence:

Increased expression of oncogenes and the signals manifested in their protein products would correspondingly result in increased cancer cell proliferation and thus tumor growth. Recently, it was shown that excessively elevated signaling by oncoproteins such as RAS, MYC, and RAF can provoke counteracting responses from cells, specifically induction of cell senescence and/or apoptosis (Collado and Serrano, 2010; Evan and d'Adda di Fagagna, 2009; Lowe et al., 2004).

1.1.1.1. Cellular Senescence:

Loenard Hayflick and Paul Moorhead discovered that normal human fibroblasts have a limited proliferative capacity in culture, a phenomenon that they named “cellular senescence” (Hayflick and Moorhead, 1961). Cellular senescence is an irrevesible growth arrest that constrains cell cycle progression in case proliferation becomes aberrant, thus limiting tumorigenesis (Collado and Serrano, 2010; Di Mitri et al., 2015b). Moreover, senescent cells recruit phagocytic immune cells and promote tissue renewal, followed by clearance and then regeneration. However, these events may not be efficiently completed in cancer or in aged tissues, thereby resulting in the accumulation of senescent cells **(Figure 2)**. Both pro-senescent and anti-senescent therapies can be beneficial in chronic disorders, cancer and ageing. In cancer and during active tissue repair, pro-senescent therapies engage to reduce the damage by limiting both proliferation and fibrosis, whereas anti-senescent therapies may help to eliminate accumulated senescent cells and to recover tissue function (Munoz-Espin and Serrano, 2014).

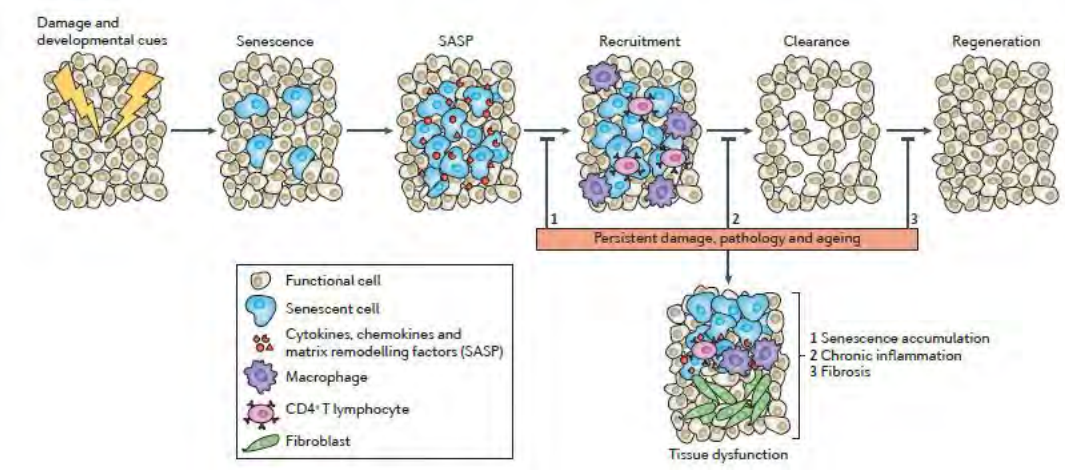

Figure 2: Schematic model of senescence. Senescence primes for a tissue remodeling process via recruiting immune cells by the senescence-associated secretory phenotype (SASP). Macrophages clear senescent cells, and progenitor cells regenerate the damaged tissue. This order of senescence-clearance-regeneration may be impaired upon persistent damage, pathology and ageing. Therefore, senescent cells are not cleared and the tissue is not fully regenerated, resulting in senescence accumulation, chronic inflammation and fibrotic tissue (Munoz-Espin and Serrano, 2014).

1.1.1.2. Morphology of senescent cells and biomarkers:

Cellular senescence in *in vitro* culture is accompanied by morphological changes in which cells become large, flat and multinucleated. However, *in vivo* senescent cells retain the normal morphology dictated by tissue architecture. Senescent cells display specific characteristics such as the absence of proliferative markers [e.g. Ki67 protein or 5-bromodeoxyuridine (BrdU)] and the presence of senescence-associated β-galactosidase (SA-βGal) activity. This activity is based on the increased lysosomal content of senescent cells, which enables the detection of lysosomal βGal at a suboptimal pH (pH=6), and this probably reflects the increased autophagy occurring in senescent cells together with an enlargement of the lysosomal compartment (Young et al., 2009). Moreover, senescent cells express tumor suppressor proteins (e.g. p53 and hypo-phosphorylated Rb) and cyclin-dependent kinase (CDK) inhibitors such as p16 (also known as INK4A; encoded by CDKN2A), p15 (also known as INK4B; encoded by CDKN2B), p21 (also known as WAF1; encoded by CDKN1A) and p27 (encoded by CDKN1B) (Munoz-Espin and Serrano, 2014). The inhibition of CDK-cyclin complexes results in proliferative arrest, and the critical component responsible for the implementation of senescence is the hypo-phosphorylated form of Rb (Chicas et al., 2010).

There are multiple senescence triggers and senescence-activating pathways. However, it is conceivable that the mechanisms that ultimately lead to senescence may also vary depending on the cell type and conditions. The main mechanisms involved in "damage-induced senescence" which comprises various subtypes, such as replicative senescence, DNA-damage-induced senescence, stress-induced senescence and oncogene induced senescence.

1.1.1.3. Molecular Mechanisms of cellular senescence:

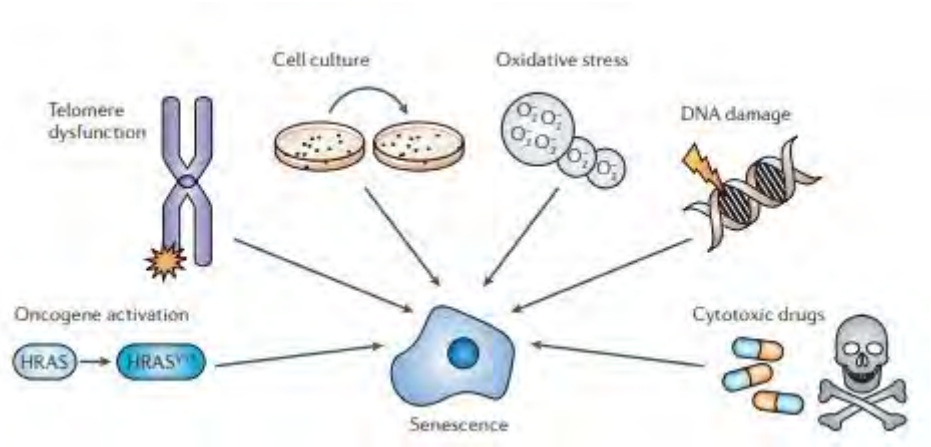

Figure 3: Several factors inducing senescence. Distinct factors can participate in the establishment of a stable growth arrest known as senescence. All of these stimuli represent stressful conditions for the cell, many of which exist in the tumor environment (Collado and Serrano, 2006).

1.1.1.3.1. Telomere shortening and DNA-damage response:

Telomeres function as molecular clocks that keep a record of the replicative history of primary cells (Harley et al., 1990). The loss of telomeres **(Figure 3)** is detected by cells as a type of DNA damage, and therefore triggers a DNA damage response (DDR) which is a complex molecular mechanism developed to detect and repair DNA damage. The principle mediators of the DDR are the DNA damage kinases ATM, ATR, CHK1 and CHK2, which in turn phosphorylate and activate several cell cycle proteins including p53. Hence, phosphorylated p53 protein activates the expression of p21, which binds to and inhibits some CDK-cyclin complexes, especially those involving CDK2 **(Figure 6)** (Munoz-Espin and Serrano, 2014).

1.1.1.3.2. CDKN2A derepression:

CDKN2A derepression senescence is related to the CDKN2A locus (also known as INK4A and ARF), which encodes two main tumor suppressors, p16 and ARF (also known as $p19^{ARF}$and $p14^{ARF}$). p16 is an inhibitor of CDK4 and CDK6, whereas ARF regulates p53 stability through the inactivation of the p53-degrading E3 ubiquitin protein ligase "Mdm2" **(Figure 4)** (Kim and Sharpless., 2006). The CDKN2A locus is normally expressed at very low levels in young tissues but becomes derepressed with aging (Krishnamurthy et al., 2004). Loss of Polycomb repressive proteins (e.g. BMI-1) can lead to CDKN2A derepression (Bracken et al., 2007).

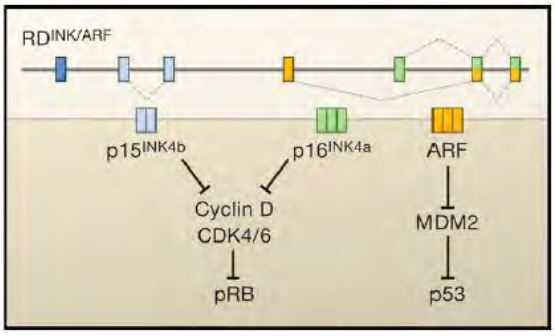

Figure 4: The INK4a/ARF/INK4b locus. Also known as CDKN2A and CDKN2B that encodes three genes within 35 kilobases: $p15^{INK4b}$, $p16^{INK4a}$ and ARF. Members of the INK4 family of cyclin dependent kinase inhibitors bind to and inactivate CDK4/6. ARF inhibits Mdm2, resulting in p53 stabilization (Kim and Sharpless., 2006).

1.1.1.3.2.1. p53 activation is regulated via Mdm2:

p53, the tumor suppressor gene, is a potent transcription factor that effectively blocks cell cycle progression or induces apoptosis in response to diverse forms of stress, thus protecting normal cells from malignant transformation (Levine, 1997; Vogelstein et al., 2000). Mouse double-minute 2

homolog (Mdm2) oncoprotein is a major negative regulator of p53, which promotes p53 ubiquitination and subsequent destruction in unstressed cells (Haupt et al., 1997). The N-terminus of the mdm2 protein interacts with the p53 and its C-terminal ring-finger, which possesses the ubiquitin E3 ligase activity, ubiquitinates p53 (Kussie et al., 1996). Endogenous levels of Mdm2 are sufficient to regulate p53 stability, and overexpression of Mdm2 can reduce the amount of endogenous p53. Since Mdm2 is transcriptionally activated by p53, this degradative pathway may contribute to the maintenance of low p53 concentrations in normal cells (Perry et al., 1993). Inhibition of Mdm2-p53 interaction can stabilize p53 and may offer a novel strategy for cancer therapy (Vassilev et al., 2004).

The binding of Mdm2 to p53 is a subject of many types of regulation. Among them, the DNA damage-induced ATM/ATR/CHK kinase cascade plays a critical role. In response to stress such as DNA damage, activation of the ATM/ATR/CHK kinase pathway results in p53 phosphoryrlation, which in turn disrupts the interaction between Mdm2 and p53, permitting p53 to escape Mdm2-mediated proteolysis and become stabilized (Chehab et al., 2000; Hirao et al., 2000). Then, Mdm2 protein is quickly degraded by auto-ubiquitination, allowing p53 to accumulate and become fully activated (Stommel and Wahl, 2004). However, the molecular mechanism still remain unclear. It is reported using transgenic mice that E3 ligase activity of Mdm2 is not required for its proper destruction (Itahana et al., 2007), and thus the molecular mechanisms governing Mdm2 ubiquitination and destruction have not yet been discovered.

1.1.1.3.2.1.1. Inhibition of Mdm2-p53 interaction:

Vassilev et al. identified potent and selective small-molecule antagonists of Mdm2 (e.g. Nutlin-1, Nutlin-2 and Nutlin-3) and confirm their mode of action through the crystal structures of complexes. These compounds bind Mdm2 in the p53-binding pocket, inhibiting Mdm2-p53 interaction, and in turn activate the p53 pathway in cancer cells, leading to cell cycle arrest, apoptosis, and growth inhibition of human tumor xenografts in nude mice (Vassilev et al., 2004).

1.1.1.3.3. Stress-induced senescence and reactive oxygen species (ROS):

Levels of ROS increase after many distinct types of stresses including chemotherapeutic drugs, loss of telomeric protective functions, DNA damage and oncogene activation **(Figure 3)**. Mechanistically, high intracellular levels of ROS induced by the RAS-RAF-MEK-ERK cascade activate the p38 MAPK, which leads to increased transcriptional activity of p53 and upregulation of p21 **(Figure 6)** (Sun et al., 2007).

1.1.1.3.4. Oncogene-induced senescence:

Cells undergo cellular senescence via the activation of various oncogenes **(Figure 3)**. Oncogene-induced senescence (OIS) was originally observed when an oncogenic form of RAS was expressed in

human fibroblasts (Serrano et al., 1997). OIS may also prompt a robust DDR due to the DNA damage that is caused by aberrant DNA replication [e.g. DNA double-strand breaks (DSBs)] (Bartkova et al., 2006; Di Micco et al., 2006).

In addition, it is reported that in mice the ARF-p53 pathway is a crucial activator of oncogene-induced senescence, whereas in humans the DDR-p53 pathway seems to have a more important role than the ARF-p53 pathway (**Figure 6**) (Halazonetis et al., 2008).

1.1.1.3.4.1. Mechanisms underlying oncogene-induced senescence*:*

1.1.1.3.4.1.1. DNA damage and replication stress:

DNA double-strand breaks are the most deleterious DNA lesions. They are a type of DNA damage in which two complementary strands of the double helix of DNA are damaged simultaneously in locations close to each other. DSBs are the most dangerous type of DNA damage, which if left unrepaired may cause severe consequences for cell survival, as they lead to chromosome aberrations, genomic instability, or cell death (Podhorecka et al., 2010). Several physical, chemical, and biological factors are involved in DSBs induction. Cells respond to DNA damage by activating the so-called DDR, a complex molecular mechanism developed to detect and repair DNA damage. The formation of DSBs triggers activation of many factors, including phosphorylation of the histone variant H2AX on Serine 139, producing γH2AX (Rogakou et al., 1998). Phosphorylation of H2AX plays a key role in DDR and is required for the assembly of DNA repair proteins at the sites containing damaged chromatin as well as for activation of checkpoints proteins which arrest the cell cycle progression (Podhorecka et al., 2010).

1.1.1.3.4.1.1.1. H2AX phosphorylation*:*

Histone H2AX is a substrate of various phosphoinositide 3-kinase-related protein kinases (PIKKs), such as ATM (ataxia telangiectasia mutated), ATR (ATM and Rad3-related), or DNA-dependent protein kinase (DNA-PK) (Podhorecka et al., 2010). ATM kinase is a major physiological mediator of H2AX phosphorylation in response to DSBs formation (Bakkenist and Kastan, 2003; Kastan and Lim, 2000). ATM is activated by its autophosphorylation at Serine 1981 position, which allows the dissociation of the inactive ATM dimers into single protein molecules with increased kinase activity **(Figure 5)** (Bakkenist and Kastan, 2003; Helt et al., 2005; Kastan and Lim, 2000; Rogakou et al., 1998)**.** Other than H2AX, the target substrates phosphorylated by ATM are BRCA1, NBS1, 53BP1 and p53 as well as checkpoint proteins, CHK1 and CHK2. These processes are aimed to stop the progression of the cell cycle and to activate proteins responsible for DNA repair (Podhorecka et al., 2010).

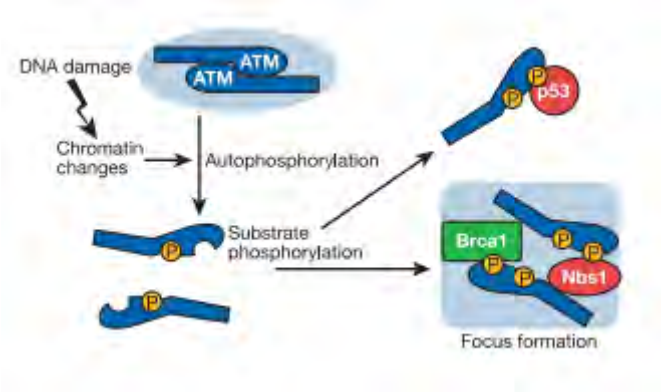

Figure 5: Schematic representation of ATM activation after DNA damage. DNA strand breaks lead to an alteration of chromatin structures that promote intermolecular autophosphorylations of an ATM dimer on serine 1981, and dissociation of the previously inert dimer. Active ATM monomers are then free to migrate and phosphorylate substrates e.g. [Brac1, Nbs1, p53 and H2AX (not shown)] (Bakkenist and Kastan, 2003).

Notably, ATR phosphorylates H2AX in response to single-stranded DNA breaks coated with replication protein A (RPA) during replication stress, such as replication fork arrest (Ward and Chen, 2001; Ward et al., 2004). RPA acts during DNA replication stress conditions to recruit and activate checkpoint kinase ATR (Namiki and Zou, 2006; Zou and Elledge, 2003). RPA32 is a subunit of the single-stranded genomic DNA (ssDNA) complex RPA (Branzei and Foiani, 2005; Byun et al., 2005). RPA phosphorylation at distinct sites occurs at stalled replication forks, and DSBs produced from stalled DNA replication induce phosphorylation of RPA32 at Serine 4 and 8 (Liaw et al., 2011; Sirbu et al., 2011).

Moreover, DNA-PK mediates phosphorylation of H2AX in mammalian cells under hypertonic conditions and during apoptotic DNA fragmentation (Mukherjee et al., 2006; Reitsema et al., 2005). However, DNA damage caused by ionizing radiation leads to phosphorylation of H2AX that is mediated by all PIKK kinases, ATM, ATR and DNA-PK (Wang et al., 2005a).

1.1.1.4. Senescence-associated heterochromatin foci:

The irreversibility of senescence may be mediated through chromatin changes by the formation of senescence-associated heterochromatin foci (SAHF) (Narita et al., 2003). SAHFs bear the hallmarks of heterochromatin, such as the trimethylation of lysine 9 in histone 3 (H3K9me3) (Narita et al., 2003), or the recruitment of heterochromatin protein 1-γ (HP1γ) (Narita et al., 2003) and macroH2A histone (Zhang et al., 2005). SAHFs accumulate during oncogene-induced senescence via a multi-step process and suppress the expression of E2F target genes through the recruitment of Rb and heterochromatin proteins (Adams, 2007; Narita et al., 2003). It has also been shown that DNA damage may precede and trigger SAHF formation, thus linking these two processes (Hemann and Narita, 2007). Whether SAHFs always occur in response to OIS and what is/are the mechanism/s underlying their formation are still not addressed.

1.1.1.3.5. Senescence-associated secretory phenotype (SASP):

Senescent phenotype is not limited to an arrest of cell proliferation. Indeed, a senescent cell is a persisting cell that is metabolically active and has undergone extensive changes in protein expression and secretion, basically developing the SASP (Coppe et al., 2010). SASP is mediated by the transcription factor, nuclear factor-κB (NF-κB), and includes the secretion of pro-inflammatory cytokines (interleukins e.g. IL-6, IL-8 and IL-10), chemokines [monocyte chemoattractant proteins (MCPs) and macrophage inflammatory proteins (MIPs)], growth factors [transforming growth factor-β (TGFβ) **(Figure 6)** and granulocyte-macrophage colony-stimulatory factor (GM-CSF)] and proteases (Munoz-Espin and Serrano, 2014). SASP components, most notably TGFβ, can provoke senescence in neighboring cells in a paracrine manner, through a mechanism that generates ROS and DNA damage (Hubackova et al., 2012). Thus, SASP has potent autocrine and paracrine activities, which suggests that senescence creates an inflammatory microenvironment that may lead to the elimination of senescent cells (Munoz-Espin and Serrano, 2014). However, Coppé et al reported the ability of SASP to facilitate cancer progression through paracrine effects on nearby cells (Coppe et al., 2010).

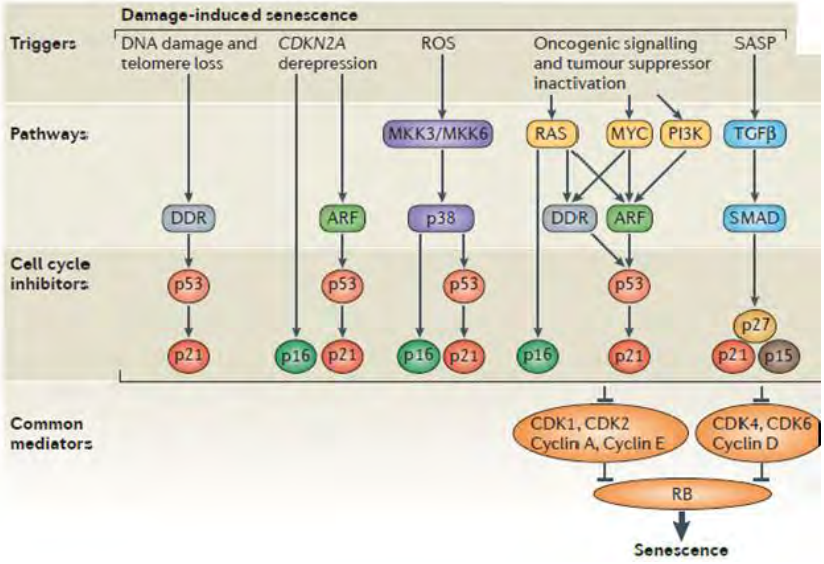

Figure 6: Molecular pathways involved in damage-induced senescence. DNA damage agents and telomere loss activate the DNA-damage response (DDR), which in turn activates p53 and its downstream transcriptional target p21. Multiple types of senescence are associated with the epigenetic derepression of the cyclin-dependent kinase inhibitor 2A (CDKN2A) locus (encoding p16 and the p53 activator ARF). Reactive oxygen species (ROS) can activate p16 and p53 via the kinases (MKK3/MKK6) and their downstream kinase effector p38. Oncogenic signaling or loss of tumor suppressors activate of p16 and p53 with the involvement of the DDR and ARF. Finally, transforming growth factor-β (TGF-β) is a prominent component of the senescence-associated secretory phenotype (SASP) pathway, which induces p27, p21 and p15 through the SMAD complex (adapted from Munoz-Espin and Serrano, 2014).

1.1.1.4. Myeloid-derived suppressor cells antagonize senescence in cancer:

1.1.1.4.1. Myeloid-derived suppressor cells and its role:

Tumor-infiltrating myeloid derived suppressor cells (MDSCs) are the major mediator of immunosuppression in tumors. MDSCs are an immune cell population coexpressing GR-1 and CD11b myeloid lineage differentiation markers in mouse and either or both of the common myeloid markers CD33 or CD11b in cancer patients (Gabrilovich et al., 2012; Talmadge and Gabrilovich, 2013). MDSCs represent a heterogenous population that includes both cells of granulocytic (G-MDSC) and monocytic (M-MDSC) origin. Human monocytic MDSCs are characterized by a HLA-DR$^-$ CD11b$^+$ CD33$^+$ CD14$^+$ phenotype (CD11b$^+$ Ly6G$^-$ /Ly6C$^+$ in mice), whereas human granulocytic MDSCs are defined by a HLA-DR$^-$ CD11b$^+$ CD33$^+$ CD15$^+$ phenotype (CD11b$^+$ Ly6G$^+$ /Ly6C^{low} in mice). Distinct studies have shown that tumor formation induces the migration of MDSCs from the bone marrow to the tumors. Mechanistically, this is associated with tumor secretion of cytokines and chemokines that promote myeloid cell trafficking, proliferation and infiltration to the tumor (Di Mitri et al., 2015a). In the bone marrow, MDSCs can be produced in response to cancer-derived factors such as granulocyte colony-stimulating factor (G-CSF), interleukin-6 (IL-6), granulocyte monocyte colony-stimulating factor (GM-CSF), IL1β, prostaglandin E2 (PGE2), tumor necrosis factor α (TNFα) and vascular endothelial growth factor (VEGF), and are then recruited to the tumor site by mean of chemokines belonging to the CCL and CXCL family (Di Mitri et al., 2015a; Wesolowski et al., 2013). Upon recruitment to tumors, MDSCs mediate immunosuppression of antitumor effector cells such as T and natural killer (NK) cells (Ostrand-Rosenberg and Sinha, 2009). MDSCs may also affect key events in tumorigenesis such as angiogenesis and metastasis formation **(Figure 7)** (Di Mitri et al., 2015a).

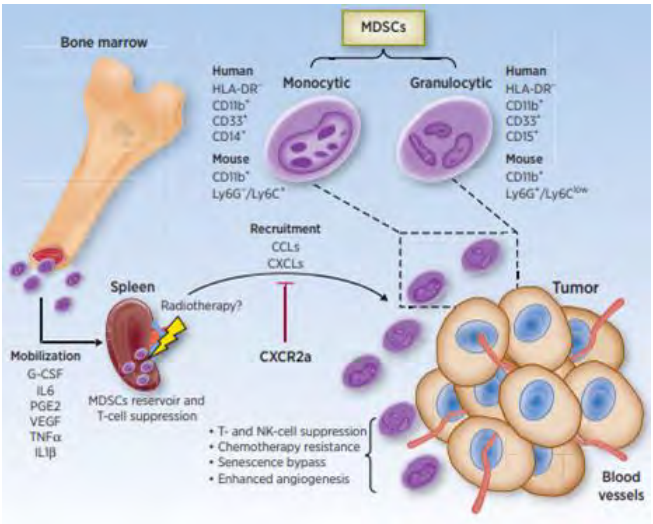

Figure 7: Schematic representation depiciting recruitment and function of MDSCs in tumor (Di Mitri et al., 2015a).

1.2. Evading growth suppressors:

In addition to the hallmark capability of inducing and sustaining positively growth-stimulatory signals, cancer cells also circumvent powerful programs that negatively regulate cell proliferation; many of these programs (e.g. senescence) depend on the actions of the tumor suppressor genes (Hanahan and Weinberg, 2000). For example, PTEN (Phosphatase and tensin homolog deleted on chromosome 10), a tumor suppressor gene located on chromosome 10q23.31, is one of the most frequent genetic alterations in human cancers. It encodes a lipid phosphatase that has an essential function in blocking the PI3K pathway by dephosphorylating phosphatidylinositol-3-phosphate (PIP_3) to generate (PIP_2) leading to the downregulation of the survival Akt pathway **(Figure 8)** (Molinari and Frattini, 2014).

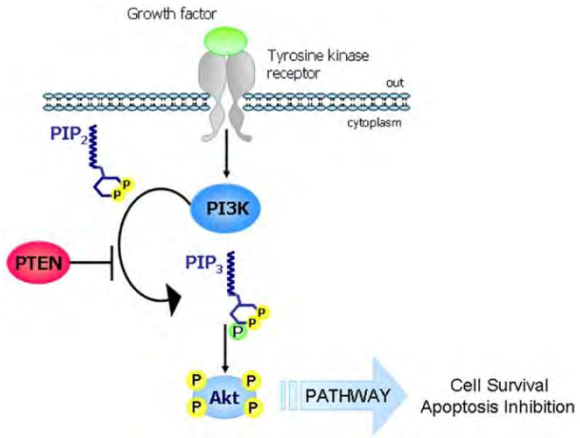

Figure 8: The PI3K-PTEN-Akt pathway. The major function of PTEN depends on the regulation of the PI3K/Akt/mTOR. In response to extracellular stimuli (e.g. presence of insulin, growth factors and chemokines), PI3K is activated by tyrosine kinase receptors or G-protein-coupled receptors and it phosphorylates PIP2 to generate PIP3 which in turn phosphorylates and activates Akt. PTEN is a lipid phosphatase that antagonizes the action of PI3K by dephosphorylating PIP3 to generate PIP2, and thus blocking the PI3K signaling cascade (Molinari and Frattini, 2014).

Moreover, Retinoblastoma (RB) and Tumor protein P53 (p53) are tumor suppressors that operate as central control in activating senescence and apoptotic programs in cells. These two tumor suppressors are also altered in most of human cancers (Hanahan and Weinberg, 2000).

1.3. Resisting cell death:

Over the last two decades, it has been established that programmed cell death by apoptosis serves as a natural barrier to cancer development (Adams and Cory, 2007; Evan and Littlewood, 1998; Lowe et al., 2004). Elucidation of the signaling pathways governing the apoptotic program has shown how apoptosis is triggered in response to various physiologic stresses that cancer cells experience during the course of tumorigenesis or as a result of anticancer therapy. Notably, among the apotosis-inducing stresses are signaling imbalances resulting from increased levels of oncogene signaling and DNA damage associated with the hyperproliferation (Adams and Cory, 2007; Lowe et al., 2004). The main cellular abnormality that triggers apoptosis is the activation of DNA damage that functions via p53 (Junttila and Evan, 2009). Tumor cells evolve a variety of strategies to limit or circumvent apoptosis. The most common one, is the loss of p53 function, which eliminates the critical DNA damage sensor from the apoptosis-inducing pathway (Hanahan and Weinberg, 2000).

1.4. Enabling replicative immortality:

Cancer cells require unlimited replicative potential in order to generate macroscopic tumors. This capability is in contrast to the behavior of normal cells, which are able to pass through only a limited number of successive cell growth. This limitation is associated with two distinct barriers: senescence and apoptosis (Hanahan and Weinberg, 2000). Multiple lines of evidence indicate that telomeres protecting the ends of chromosomes are centrally involved in the capability for unlimited proliferation (Shay and Wright, 2000). The telomeres, comprised of multiple tandem hexanucleotide repeats, shorten progressively in nonimmortalized cells, and thus reducing cell viability (Hanahan and Weinberg, 2000).

Telomerase, the DNA polymerase that adds telomere repeat segments to the ends of telomeric DNA, is almost absent in nonimmortalized cells but expressed at functionally significant levels in immortalized cells, including human cancer cells. The presence of telomerase activity in immortalized cells is correlated with cells resistance to both proliferative barriers: senescence and apoptosis. Conversely, suppression of telomerase activity leads to telomere shortening and to activation of one or the other of these proliferative barriers. Hence, telomere shortening has been viewed as a clocking device that determines the limited replicative potential of normal cells and thus one that must be overcome by cancer cells (Hanahan and Weinberg, 2000).

1.5. Inducing Angiogenesis:

Like normal tissues, tumors require sustenance in the form of nutrients and oxygen as well as the ability to evacuate metabolic wastes and carbon dioxide. The tumor-associated neovasculature, generated by the process of angiogenesis, addresses these needs (Hanahan and Weinberg, 2000). During embryogenesis, the development of the vasculature involves the birth of new endothelial cells and their assembly into tubes (vasculogenesis) in addition to the growth (angiogenesis) of new vessels from existing ones. Following this morphogenesis, the normal vasculature becomes largely quiescent. In adults, as part of physiologic processes such as wound healing and female reproductive cycling, angiogenesis is turned on, but only transiently. In contrast, during tumor progression, an "angiogenic switch" is almost always activated and remains on, causing normally quiescent vasculature to continualy sprout new vessels that help sustain expanding neoplastic growths (Hanahan and Folkman, 1996). Several factors induce or oppose angiogenesis such as signaling proteins that bind to stimulatory or inhibitory cell surface receptors displayed by vascular endothelial cells. The well-known angiogenesis inducers and inhibitors are vascular endothelial growth factor-A (VEGF-A) and thrombospondin-1 (TSP-1), respectively (Baeriswyl and Christofori, 2009; Bergers and Benjamin, 2003).

1.6. Activating invasion and metastasis:

It is known that as carcinomas arising from epithelial tissues progressed to higher pathological grades of malignancy, reflected in local invasion and distant metastasis, the associated cancer cells typically developed alterations in their shape as well as in their attachment to other cells and to the extracellular matrix (ECM) (Hanahan and Weinberg, 2000). The main characterized alteration involved the loss by carcinoma cells of E-cadherin, a key cell to cell adhesion molecule. By forming adherens junctions with adjacent epithelial cells, E-cadherin helps to assemble epithelial cell sheets and maintain the quiescence of the cells within these sheets. The frequently observed downregulation of E-cadherin in human carcinomas provides strong evidence for its role as a key suppressor of this hallmark capability (Berx and van Roy, 2009; Cavallaro and Christofori, 2004). In contrast, N-cadherin, which is normally expressed in migrating neurons and mesenchymal cells during organogenesis, is upregulated in many invasive carcinoma cells (Cavallaro and Christofori, 2004).

1.6.1. Epithelial-mesenchymal transition regulates invasion and metastasis:

EMT was described as a developmental process that is crucial for the cell type interconversions that underlie organogenesis and wound healing (Acloque et al., 2009; Hay, 2005; Shook and Keller, 2003). Throughout EMT process, epithelial cells lose the characteristics of differentiated cells, including cell-cell adhesion and apical basal polarity, and gain features of mesenchymal cells, including invasive,

migration capacity and increased resistance to apoptosis **(Figure 9)** (Acloque et al., 2009; Hay, 2005; Nieto, 2011; Nieto, 2013; Shook and Keller, 2003; Thiery et al., 2009).

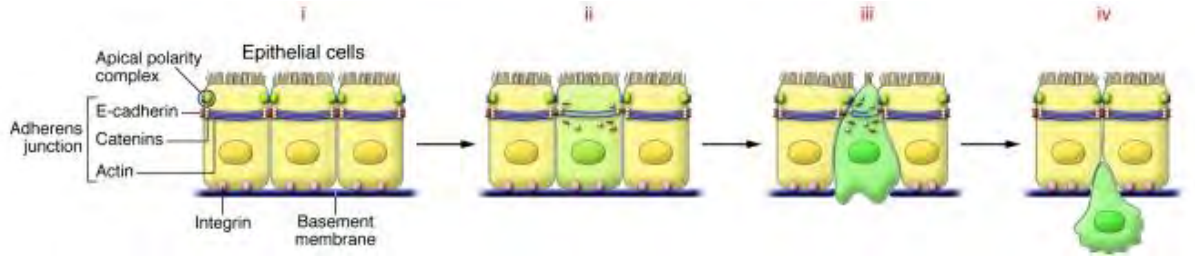

Figure 9: Cellular aspect of EMT. (i) Normal epithelial cells consist of adherens junctions composed of E-cadherin together with catenins and actin rings. Tight junctions are associated with apical polarity complexes, whereas integrins interact with components of the basal membrane. (ii) Loss of cell-cell adhesion. EMT inducers repress the transcription of the genes encoding the components of both adherens and tight junctions, inducing the loss of cell polarity. E-cadherin is internalized and targeted for degradation. (iii) Breakdown of the basal membrane and apical contraction. Profound cytoskeletal remodeling will favor cell delamination by inducing apical contraction and disorganization of the basal membrane. (iv) Cell delamination and invasion. Expression of integrin receptors and continued activation of metalloproteases favors migration through the extracellular matrix and invasion of adjacent tissues (Acloque et al., 2009).

Transcription factors, including Snail, Slug, Twist, and Zeb1/2 coordinate in the EMT program. These transcriptional regulators are expressed in various malignant tumor types and have been shown in experimental models of carcinoma formation to be important for programming invasion; some have been found to elicit metastasis when they are overexpressed (Micalizzi et al., 2010; Schmalhofer et al., 2009; Taube et al., 2010; Yang and Weinberg, 2008).

1.6.2. Epithelial-mesenchymal transition and the acquisition of a stem cell-like phenotype:

Studies have shown that terminally differentiated adult cells can be reprogrammed into pluripotent stem cells (Takahashi and Yamanaka, 2006; Yu et al., 2007), suggesting that by expressing the right combination of transcription factors, dedifferentiation or transdifferentiation of most cell types is possible. Transdifferentiation programes include EMT and mesenchymal-epithelial transition (MET)

Partial EMT is a state in which carcinoma cells progress through multiple transitional states between epithelial and mesenchymal phenotype (active EMT and MET program) (Davies et al., 2018). Importantly, cells that have undergone partial EMT have a stem-like cell properties, such as the ability of self-renewal, growth, and therapeutic resistance (Bae et al., 2010). The origin and characterization of these stem cells [referred as cancer stem-like cells (CSCs)] in cancer is controversial.

Chapter II:

1. Prostate gland:

1.1. Development of prostate gland:

The prostate is a tubuloalveolar exocrine gland of the male reproductive tract. It originates from the solid epithelial outgrowths (prostatic buds) that emerge from the urogenital sinus (UGS) under the influence of the underlying mesenchyme (Cunha et al., 1992; Meeks and Schaeffer, 2011). The mesenchymal-epithelial interactions are crucial in the development of the male urogenital tract. The urogenital sinus mesenchyme (UGM) induces ductal morphogenesis, promotes the expression of epithelial androgen receptors (AR), regulates epithelial proliferation, and specifies the expression of prostatic lobe-specific secretory proteins **(Figure 10)** (Cunha et al., 1992).

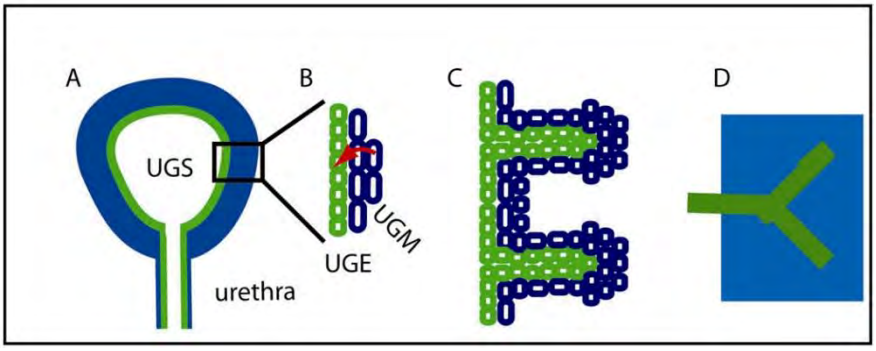

Figure 10: Schematic illustration of phases of prostatic development. (A) The prostate develops from the Urogenital sinus (UGS) in response to androgens. The UGS comprises of both epithelium (green) and mesenchyme (blue). **(B)** Androgens bind to androgen receptor in the mesenchyme and induce epithelial budding. **(C)** Epithelial buds elongate into solid cords of tissue that canalize into ducts. **(D)** Latter phases of prostate development include epithelial branching (Meeks and Schaeffer, 2011).

In human, prostatic development is initiated at 10 to 12 weeks of gestation (Kellokumpu-Lehtinen et al., 1980), followed after birth by limited prostatic regression and growth-quiescence until puberty, when rising androgen levels trigger renewed prostatic growth. When adulthood is reached, prostatic growth is stopped, however, it is reinitiated in old aged men during the pathogenesis of benign prostatic hyperplasia (BPH) (Cunha et al., 1992). In rats and mice, prostatic growth and ductal branching morphogenesis are mandatory continuous processes that extend from late fetal life until early adulthood, when these processes stop (Cunha et al., 1992).

2. Anatomy of human and mouse prostate:

2.1. Human prostate:

The human prostate is a glandular organ composed of central, peripheral and transitional zones. The three zones contain acini located within a fibromuscular stroma **(Figure 11A)**. Acini are formed by columnar epithelial cells which secrete prostatic proteins and fluids from their apical surfaces into a lumen, and are surrounded by basal cells attached to the basement membrane and scattered neuroendocrine cells (Bostwick and Qian, 2004; McNeal and Bostwick, 1986; McNeal et al., 1986; Timms, 2008). The peripheral zone (PZ) is the predominant location for the origin of prostatic adenocarcinoma, whereas the benign prostatic outgrowth occurs exclusively in the transitional zones (TZ) (Noel et al., 2008).

2.2. Mouse prostate:

The mouse prostate is composed of four distinct lobes [e.g. anterior (AP), ventral (VP), dorsal (DP) and lateral (LP)] **(Figure 11B)**. Although the overall anatomy of mouse prostate differs from that of human prostate, the prostate of both species are composed of glands and ducts of similar organization (Cunha et al., 1987). However, mouse prostatic glands comprise fewer basal and neuroendocrine cells, less fibromuscular stroma and only few smooth muscle cells **(Figure 11C)** (Marker et al., 2003).

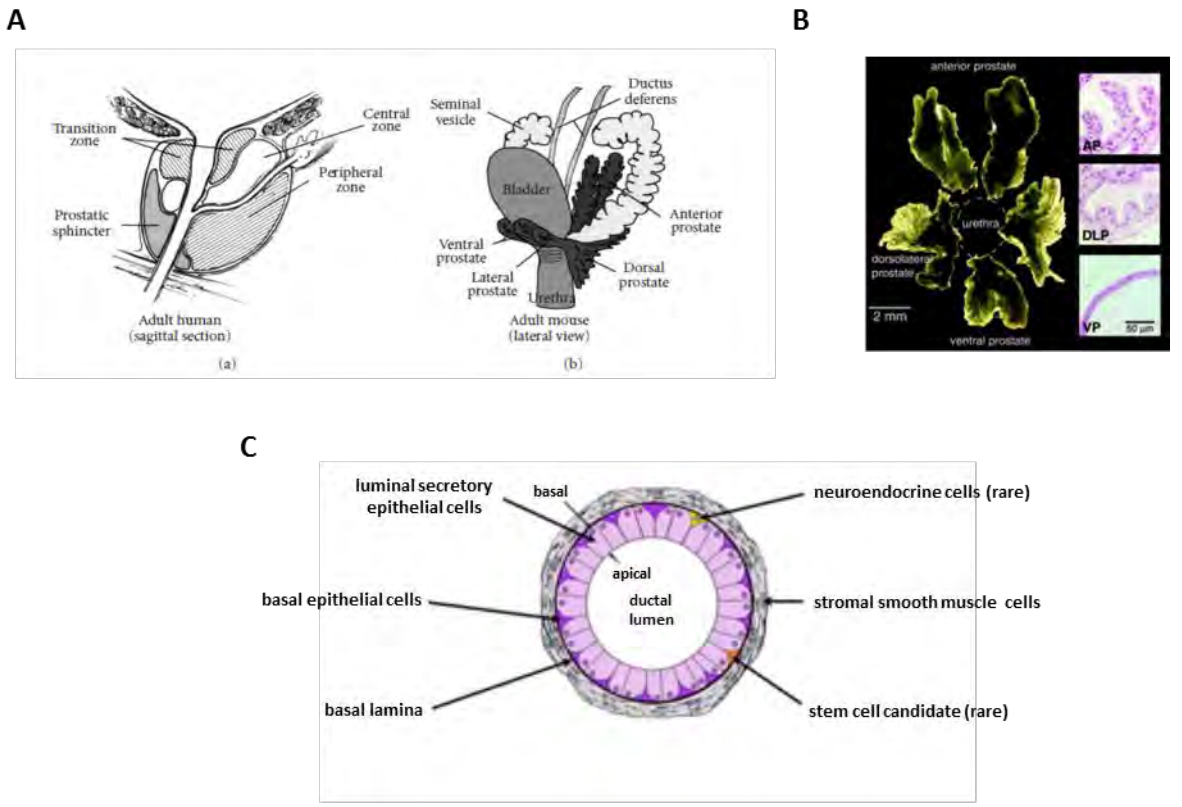

Figure 11: Anatomy of human and mouse prostate. (A) Schematic illustration of the anatomy of the human prostate (a) and mouse prostate (b) (adapted from Valkenburg., 2011). **(B)** The lobes of the adult mouse prostate together with hematoxalin and eosin-stained sections of prostatic ducts from each lobe (adapted from Marker et al., 2003). **(C)** A diagram of a mouse ductal cross-section with labels indicating cell types that are present in prostatic ducts including luminal secretory epithelial cells, basal epithelial cells, neuroendocrine cells, stromal smooth muscle cells, and stem cell candidates. Beneath the label for each cell type is a list of differentiation markers commonly used to distinguish these cell types (adapted from Marker et al., 2003).

3. Prostate cancer:

Prostate cancer (PCa) is the most common malignant visceral neoplasm and the third leading cause of cancer-related death in males of western societies (Siegel et al., 2017), and thus has a high socio-economic impact. The PTEN and p53 tumor suppressors are among the most commonly inactivated or mutated genes in human cancer including prostate cancer (Di Cristofano and Pandolfi, 2000; Vogelstein et al., 2000). Although they are functionally distinct, reciprocal cooperation has been proposed, as PTEN is thought to regulate p53 stability, and p53 to enhance PTEN transcription (Freeman et al., 2003; Stambolic et al., 2001). Human PCa progression takes decades and proceeds through multistage process: prostatic intraepithelial neoplasia (PIN), locally adenocarcinoma, invasive adenocarcinoma and metastasis **(Figure 12)** (Abate-Shen and Shen, 2000). PINs usually appear after the fifth decade, and its etiology remain largely unknown and its clinical course unpredictable. Serum prostate specific antigen (PSA) is widely used as a biomarker for prostate cancer detection, but it does not predict whether tumors will remain indolent or become clinically aggressive. Thus, systematic use of this marker leads to many unnecessary transrectal prostatic needle biopsies, over diagnosis and over treatment with severe side effects on patients and increased costs for healthcare systems (Schroder et al., 2012; Whitson and Carroll, 2010).

If detected when locally confined, PCa is eradicated in 70-80% of the patients by radical prostatectomy, cryotherapy or radiation therapy. However, these treatments often induce complications, such as impotence and incontinence (Resnick et al., 2013). Therefore, active surveillance of low-risk PCa is often preferred to avoid aggressive treatments (Wadman et al., 2015). However, the severity of PCa is often underestimated at diagnosis, and 20-30% of patients diagnosed with localized PCa develop metastasis (Loeb et al., 2014). Locally advanced and/or metastatic PCa are treated with anti-androgens to induce tumor regression. Nonetheless, due to treatment resistance, prostate tumors relapse after 1-3 years and develop aggressive forms of PCa, termed castration-resistant prostate cancer (CRPC) **(Figure 12)** (Yuan et al., 2009). In addition, Docetaxel the major cytotoxic agent for CRPC treatment has only a median survival benefit of 3 months (Berthold et al., 2008). Thus, it is important to identify factors that promote, as well as means to prevent tumor progression.

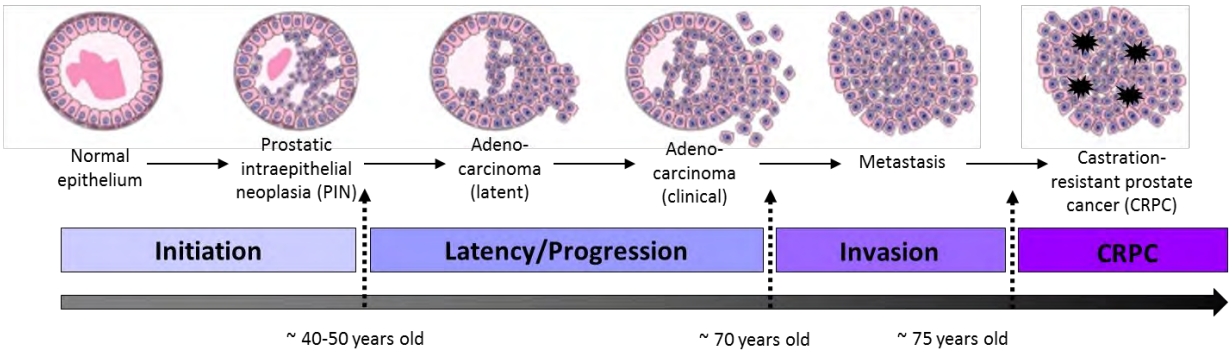

Figure 12: Prostate cancer progression. Prostate cancer evolution from precancerous lesions (PIN) to adenocarcinoma, metastasis and CRPC (adated from Abate-Shen and Shen, 2000).

3.1. Low and High grade PINs:

PIN lesions are formed by cells that proliferate within the prostatic epithelium and disrupt its well-defined architecture (Bostwick and Qian, 2004; McNeal and Bostwick, 1986; McNeal et al., 1986; Timms, 2008). In addition, PINs are associated with progressive abnormalities of phenotype and genotype, which are intermediate between normal prostatic epithelium and cancer, indicating impairment of cell differentiation and regulatory control with advancing stages of prostatic carcinogenesis (Bostwick and Qian, 2004). Low grade PINs (LGPINs) define areas of proliferative glandular epithelial cells that display enlarged nuclei, variable in size, non-prominent nucleoli and intact basal cells layer (Bostwick, 1989). High grade PINs (HGPINs) differ from LGPINs by the presence of prominent nucleoli, nuclear hyperchromasia and fragmented or lack of basal cells layer (Montironi et al., 2011). HGPINs are known to be precursors of prostate adenocarcinoma (Chrisofos et al., 2007; Montironi et al., 2011). Almost all human prostate cancers correspond to acinar adenocarcinoma, and less than 2% of the cases correspond to neuroendocrine cancers (Grignon, 2004). However, focal regions of neuroendocrine differentiation are more commonly observed following recurrence after prostatectomy and androgen deprivation therapy (Yuan et al., 2007; Komiya et al., 2009).

4. Limitations of *in vitro* and *ex vivo* studies:

A wide number of studies have been done with immortalized human prostate cancer cell lines, such as LnCap, VCap, PC-3 or MDA-PCa, to understand the biology of tumor progression, androgen-independent diseases and metastatic prostate cancer, and to test putative chemo-preventive compounds (Wang et al., 2005b). However, these lines are derived from advanced/metastatic tumors that cannot recapitulate the various stages of the human disease. In addition, *in vitro* studies do not show the interaction of tumors cells with the various cellular compartments of prostate such as basal

and neuroendocrine epithelial cells, stromal cells, or of the metastatic site (e.g. osteoblasts), as well as vascular and lymphatic circulation and immune cells.

Moreover, xenograft transplantation models based on transformed human cell lines do not mimic the heterogeneity of human tumors and their microenvironment, and require immunodeficient host animals that lack crucial modulators of tumorigenesis (Parisotto and Metzger, 2013).

These major limitations require the development of genetically engineered mice (GEM) to investigate tumor genetics of its initiation and progression, and to evaluate new therapies.

5. Development of animal models of prostate cancer:

5.1. Examples of Diverse GEM lines of prostate cancer with their strengths and weaknesses:

5.1.1. Prostate cancer mouse models established by targeted protein overexpression:

Maroulakou et al. generated the first GEM line for prostate cancer [C3(1)-Tag] by expressing, under the control of C3(1) promoter, the simian virus (SV) 40 large T antigen (Tag), a viral oncogene encoded by the SV 40 early sequence which is known to inactivate vital cellular tumor-supppressor proteins (e.g. p53 and Rb). C3(1)-Tag mice develop prostatic hyperplasia in the dorsal and ventral prostate at 2-3 months of age, PINs by 6 months and adenocarcinoma by 7-11 months (Maroulakou et al., 1994). However, their use is limited now, since T antigen is expressed in other tissues including the thyroid, salivary gland and cartilage, and induces lethal lesions in these tissues by 1 year (Shibata et al., 1998).

TRAMP (transgenic adenocarcinoma mouse prostate) model was developed by linking rat probasin promotor region (-426 bp to +28 bp) to the SV 40 early sequence (Greenberg et al., 1995). TRAMP mice develop PINs between 2 to 3 months of age and they are poorly differentiated to neuroendocrine carcinoma by 4-7 months (Gingrich et al., 1996; Kaplanlefko et al., 2003). TRAMP mice develop distant metastases primarily in lymph nodes, lung, and sometimes in the liver, kidney and adrenal glands by 4 to 9 months. In contrast to C3(1)-Tag transgenic mice, TRAMP mice do not develop other primary pathologies.

Moreover, C3(1)-c-Myc, ARR_2PB-Myc and probasin-Myc transgenic mouse lines that express c-Myc under the control of the rat C3(1), rat probasin ARR_2PB and the (-426 bp to +28 bp) rat probasin promoter/enhancer elements, respectively, were generated to determine the consequences of c-Myc overexpression in the prostate (Zhang et al., 2000; Ellwood-Yen et al., 2003). c-Myc is a transcription factor known to regulate cell proliferation and apoptosis in which it is frequently overexpressed or amplified in prostate cancer (Qian et al., 1997). Overexpression of c-Myc in the epithelial cells of ventral prostate in C3(1)-c-Myc transgenic mice prompts LGPINs that do not progress to adenocarcinoma during the lifetime of these mice. C3(1)-c-Myc mice lose their capacity to reproduce

within five generations, which most probably results from the transgene expression in male and female reproductive tissues (Zhang et al., 2000), thereby limiting the use of these transgenic mice. However, ARR_2PB-Myc and Pb-Myc transgenic mice express c-Myc in the prostate as early as at 2 weeks of age, and at higher levels than in C3(1)-c-Myc mice (Ellwood-Yen et al., 2003). ARR_2PB-Myc mice develop PIN lesions from 2 weeks of age in which they progress to invasive adenocarcinoma by 3-6 months of age with a reliable kinetics. Full penetrance of lesions occurs in the ventral and dorsolateral prostate with a lower extent in the anterior prostate. Pb-Myc mice develop similar pathological changes, but with a slower kinetics. Both ARR_2PB-Myc and Pb-Myc mice have advantages over those expressing SV40 T antigen since they express a non-viral oncogene and develop invasive adenocarcinoma. However, they do not develop metastasis.

5.1.2. Prostate cancer mouse models generated by loss of function mutations:

Bi-allelic ablation of the tumor suppressor PTEN in mice results in embryonic lethality, however, heterozygous mutant ($PTEN^{+/-}$) mice develop neoplasia in multiple tissues, including intestines, lymphoid cells, mammary gland, thyroid, endometrial and adrenal glands (Di Cristofano et al., 1998), and most of them die within 8 months. Moreover, $PTEN^{+/-}$ exhibit PINs by 8-10 months of age, but with no invasive adenocarcinoma. Moreover, as the gene encoding the homeobox transcription factor NKX3.1 maps to a region of chromosome 8p21 that undergoes allelic deletion in about 80% of human prostatic neoplasia, mice with Nkx3.1 null alleles were generated. Both $Nkx3.1^{+/-}$ and $Nkx3.1^{-/-}$ mice develop PINs by one year of age (Bhatia-Gaur et al., 1999; Kim et al., 2002a). In addition, $PTEN^{+/-}$ /$Nkx3.1^{-/-}$ develop high grade PINs (HGPINs), invasive adenocarcinoma and lymph node metastasis (Abate-Shen et al., 2003; Kim et al 2002b).

5.1.3. Prostate cancer mouse models generated by targeted somatic mutations:

The technique to introduce targeted somatic mutations in the mouse depend on site specific recombinases that catalyze recombination of DNA segments flanked by adjacent recognition sites. The most vastly used conditional system is based on the bacteriophage P1 Cre recombinase that recognizes DNA elements called LoxP sites, and stimulates recombination between two of them, leading to the deletion or inversion of the intermediate sequence (Sternberg et al., 1981). Conditional inactivation of a gene is carried out by flanking, through homologous recombination in embryonic stem (ES) cells, one or various exons of interest with LoxP sites (floxed allele; L2). Using convenient promoters, Cre recombinase is expressed in a cell/tissue specific manner, and thus the targeted exon(s) are selectively excised in a controlled pattern (Gu et al., 1994).

The Pb-Cre mouse line, expressing Cre in the prostatic epithelium under the control of rat probasin promotor/enhancer region, were first established (Maddison et al., 2000). The Cre coding sequence is inserted downstream of the rat probasin promotor/enhancer region (-426 bp to +28 bp). Although Cre expression is higher in the VP of Pb-Cre line, Cre-mediated excision occurs in all lobes. Moreover, recombination might also occur in the bladder and seminal vesicles, since Cre is also expressed at low levels in these tissues (Maddison et al., 2000) **(Table 1)**. In addition, PB-Cre4 and ARR_2PBi-Cre expressing Cre under the control of the ARR_2PB promoter/enhancer regions were established (Wu et al., 2001; Jin et al., 2003). Recombination efficiency of young PB-Cre4 mice is higher in the luminal epithelial cells of LP than in the VP, DP and AP (Wu et al., 2001). Moreover, Cre is also expressed in basal and stromal cells of the prostate, in seminal vesicles, as well as in seminiferous tubules **(Table 1)** (Wang et al., 2006; Wu et al., 2001). ARR_2PBi-Cre line displays efficient recombination in epithelial cells of all prostatic lobes, as well as in seminal vesicles and ductus deferens **(Table 1)** (Jin et al., 2003)**.**

Two additional transgenic mouse line, expressing Cre under the control of the 6 kb promoter/enhancer region of the human PSA gene were independently established (PSA-Cre)(Abdulkadir et al., 2002; Ma et al., 2005). Recombination in these lines is restricted to luminal epithelial cells of mature prostate, in contrast to Probasin-based transgenic Cre lines **(Table 1)**.

Mouse line	Transcriptional regulatory elements	Cre recombinase activity	Ectopic Cre expression	References
Pb-Cre	Rat probasin (−426 bp to +28 bp)	VP > DP, AP, LP	Bladder, seminal vesicles	(Maddison et al., 2000)
PB-Cre4	ARR_2PB	LP > VP, DP, AP, starting before puberty	Prostatic basal and stromal cells; seminal vesicles, seminiferous tubules	(Wang et al., 2006; Wu et al., 2001)
ARR_2PBi-Cre	ARR_2PB	LP, VP, DP, AP	Seminal vesicles, ductus deferens	(Jin et al., 2003)
PSA-Cre	PSA (6 kb)	All lobes of mature prostate	None reported	(Abdulkadir et al., 2002)
PSA-Cre	PSA (6 kb)	All lobes of mature prostate	None reported	(Ma et al., 2005)

Table 1: Mouse lines expressing Cre recombinase in prostatic epithelial cells (Parisotto and Metzger, 2013).

These transgenic Cre lines were extensively used to define the consequences of loss of function of several genes in the prostate (e.g. PTEN). Diverse laboratories generated mice in which PTEN is ablated in the prostate via intercrossing mice bearing floxed (L2) PTEN alleles with Pb-Cre, PB-Cre4, PSA-Cre and mouse mammary tumor virus (MMTV)-Cre mice (Trotman et al., 2003; Backman et al., 2004; Ma et al., 2005; Wang et al., 2003, 2006). Differences in genetic background, variable efficiencies of PTEN ablation in luminal epithelial cells and/or PTEN ablation in prostatic basal and stromal cells in some lines might cause alterations in tumor progression and aggressiveness among the lines. Accordingly, all lines develop HGPINs and invasive carcinoma, but tumorigenesis and its penetrance were markedly

increased in PB-Cre4/PTEN$^{L2/L2}$ (PTEN$^{pe-/-}$) and MMTV-Cre/PTEN$^{L2/L2}$ mice in which PTEN is ablated before full development of prostate gland (before puberty). In addition, PTEN$^{pe-/-}$ and PSA-Cre/PTEN$^{L2/L2}$ mice develop lymph node metastasis, but only the former develop lung metastasis (Ma et al., 2005; Wang et al., 2003).

5.1.3.1. Diverse studies using transgenic Cre lines of prostate cancer:

Chen et al. demonstrate, using PTEN$^{loxP/loxP}$/PB-Cre4 and p53$^{loxP/loxP}$/PB-Cre4 transgenic mice, that complete PTEN inactivation in mouse prostatic epithelium (PTEN$^{pe-/-}$ mice) elicits non-lethal invasive prostate cancer after long latency, whereas complete p53 inactivation in the prostate (p53$^{pe-/-}$ mice) fails to produce a tumor phenotype. Strikingly, they show that combined inactivation of PTEN and p53 triggers invasive prostate cancer as early as 2 weeks after puberty and is invariably lethal by 7 months of age. Importantly, PTEN inactivation induces growth arrest through the p53-dependent cellular senescence pathway both *in vitro* and *in vivo*, which can be fully rescued by combined loss of p53. Their results demonstrate the relevance of cellular senescence in restricting tumorgenesis *in vivo* and support a model for cooperative tumor suppression in which p53 is an essential failsafe protein of PTEN-deficient tumors **(Figure 13A and 13B)** (Chen et al., 2005).

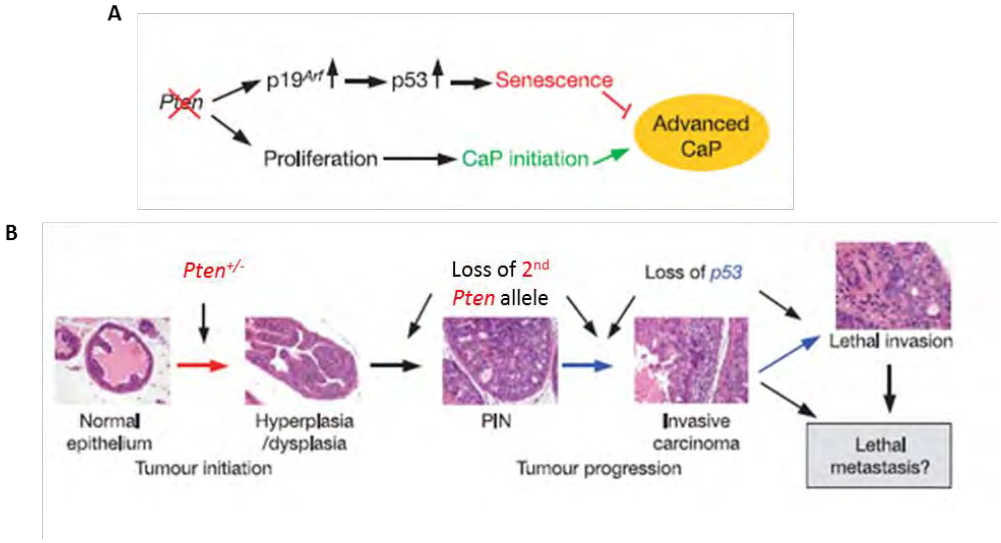

Figure 13: The p53-dependent cellular senescence restricts PTEN-deficient prostate tumorgenesis. (A) A model for PTEN-deficient tumorgenesis and p53 cooperativity. **(B)** A model for prostate tumor initiation, development and progression synergistically participated by PTEN and p53. Loss of p53 accelerates cancer progression by a senescence escape mechanism in PTEN-deficient prostate tumors (adapted from Chen et al., 2005).

In addition, Pandolfi and coworkers suggested *PTEN* loss-induced cellular senescence as a prosenescence therapy feasible for blocking tumor progression, in particular prostate cancers driven by *PTEN* loss (Alimonti et al., 2010). The researchers compared PICs to OIS *in vitro*. The cell-cycle arrest

of OIS is preceded by a period of hyperproliferation. At least for some activated oncogenes, this is accompanied by hyperreplication stress and a DNA damage response (DDR). Upon *Pten* loss, mouse embryo fibroblasts (MEFs) activate p53 and its downstream effectors p21. The authors reported that, in contrast to OIS, PICs directly appears after *Pten* loss, resulting in increased SA-βGal activity and restrained proliferation. In contrast to OIS, MEFs undergoing PICs showed no signs of a DDR. Correspondingly, PIN lesions in $Pten^{pe-/-}$ mice (Probasin-Cre/$Pten^{lox/lox}$ mice) exhibited increased SA-βGal activity and lacked γ-H2AX foci which is a marker for DNA breaks (Alimonti et al., 2010; Di Mitri et al., 2014). The uncoupling of PICs from DDR activation prompted the authors to consider the possibility of activating PICs in early prostate tumors, in an effort to restrain these tumors from evolving to full malignancy.

Interestingly, Di Mitri et al. showed that GR1-positive myeloid cells infiltrate the prostate of $PTEN^{pe-/-}$ mice and secrete to tumor microenvironment the cytokine IL-1RA, an antagonist of IL-1R, which opposes PICs in a paracrine manner **(Figure 14)** (Di Mitri et al., 2014). Moreover, *PTEN* loss-induced senescence was enhanced *in vivo* when Il1ra knockout myeloid cells were transferred to PTEN null mice (Di Mitri et al., 2014). Therapeutically, docetaxel-induced senescence and efficacy were higher in PTEN null tumors when the percentage of $CD11b^{+}$ $GR\text{-}1^{+}$ myeloid cells was decreased by CXCR2, an antagonist of CXC chemokine receptor 2 (Di Mitri et al., 2014; Gabrilovich et al., 2012). These findings identify a novel factors, established by innate immunity, that controls senescence evasion and chemoresistance. Thus targeting MDSCs provides novel opportunities for cancer therapy.

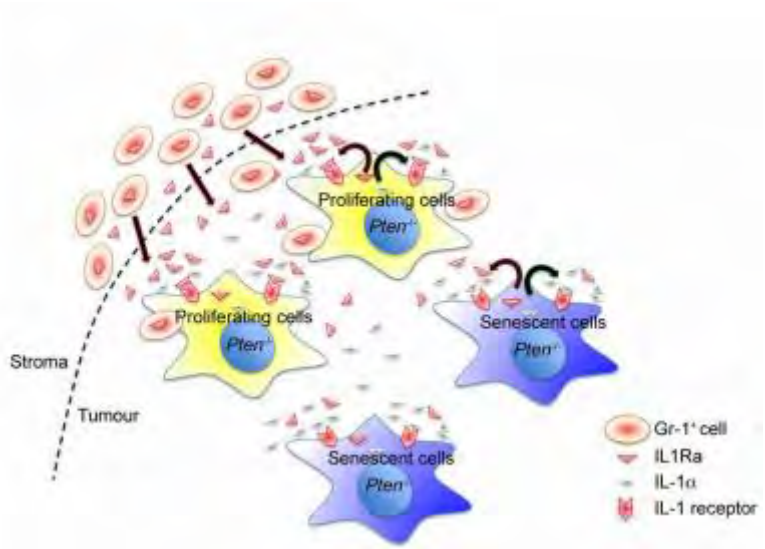

Figure 14: Model describing GR-1+ myeloid cells recruited to the tumor site and antagonize Pten loss-induced cellular senescence via secreting IL-1RA in the tumor microenvironment (Di Mitri et al., 2014).

5.1.3.2. Limitations of transgenic Cre lines of prostate cancer:

Despite the fact that the above transgenic Cre mouse lines of prostate cancer show that specific gene alterations (e.g. PTEN) can lead to prostate cancer in mice, pathological lesions develop in young animals and disease progression is frequently very fast. However, prostate cancer in men occurs in late adulthood and can prolong to a period of many years. The initiation of genetic mutations in a vast number of cells in mouse prostate before its full development, and even sometimes in several cell types could justify these differences. Thus, in order to strictly model periodic prostate cancer, mutations should arise in a confined number of cells of the prostate after puberty (Parisotto and Metzger, 2013).

5.1.4. Development of transgenic lines expressing ligand-dependent Cre recombinases:

Development of ligand-controlled site-specific recombinases over the recent years allows to circumvent most of the above limitations. The host laboratory established Cre-ER^{T2} recombinase to introduce spatio-temporally controlled targeted somatic mutations in the mouse. Cre-ER^{T2} recombinase is based on a fusion protein between Cre and a mutated human estrogen receptor, in which the activity of Cre is selectively induced by the synthetic ligand Tamoxifen (Tam) (Metzger and Chambon, 2001). Consequently, the host laboratory generated PSA-Cre-ER^{T2} mice expressing Tamoxifen-dependent Cre-ER^{T2} recombinase selectively in prostatic luminal epithelium under the control of the 6 kb human PSA promoter, and thus allowing us to target floxed genes selectively in luminal epithelial cells of fully differentiated prostate of adult mice and to modulate the number of genetically altered cells (Ratnacaram et al., 2008). PSA-Cre-ER^{T2} mice exhibit a high recombination efficiency in the DLP and VP (>up to 80%) and a lower efficiency in the AP (10-60%) (Ratnacaram et al., 2008).

To assess the consequences of PTEN loss in luminal epithelial cells of adult mice, PTEN ablation was induced by Tamoxifen administration [(from D1 to D5 (1 mg/day)] to adult PSA-Cre-ER^{T2} mice bearing floxed (L2) PTEN alleles (PTEN$^{pe-/-}$ mice) (Ratnacaram et al., 2008). Indeed, mutant mice develop prostate epithelium hyperplasia within 4 weeks after PTEN ablation and PINs in all lobes within 2-3 months, with the highest incidence in the dorsolateral lobe, which is considered to be the most similar to the peripheral zone of the human prostate, in which adenocarcinoma is preferentially localized. Some PINs of the dorsolateral lobe progress to invasive adenocarcinoma 8-10 months after PTEN ablation. However, no distant metastases are found up to 20 months after PTEN ablation. In contrast, monoallelic Cre-ER^{T2} –mediated PTEN ablation in luminal epithelial cells of adult prostate (PTEN$^{pe+/-}$ mice) induced only few PIN lesions in DLP, and no progression to adenocarcinoma is observed (Ratnacaram et al., 2008). The lack of PTEN protein expression in PINs of these mice demonstrates that

loss of PTEN function is a permissive event for uncontrolled cell proliferation. Thus, Cre-ER^{T2}-mediated PTEN ablation in luminal cells of adult prostate mimics well early stages of prostate cancer formation in humans. This mouse model (PTEN$^{(i)pe-/-}$ mice) is valuable both for exploring the molecular mechanisms underlying prostate cancer and its progression and for the development and validation of preventive and therapeutic approaches in preclinical settings.

Chapter III:

1. Androgen receptor:

1.1. Overview of androgen receptor structure, regulation and function:

The human androgen receptor (AR) is a member of the nuclear receptor superfamily, and plays a central role in normal prostate development and in prostate cancer initation and progression. AR regulates multiple cellular events such as proliferation, apoptosis, migration, invasion and differentiation. It is located on the X chromosome (q11-12) and consists of 8 exons. It codes for a protein of 919 amino acids with a mass of 110 kDa. AR functions as ligand-induced transcription factor that contains conserved C-terminal functional domains (hinge, DNA-binding domain [DBD] and ligand binding domain [LBD]), but harbors a unique N-terminal region. Unlike many of other nuclear receptors, the N-terminal region (activation function 1 [AF1]) maintains the transcriptional transactivation function **(Figure 15)** (Agoulnik and Weigel, 2008; Centenera et al., 2008; Claessens et al., 2008; Culig and Bartsch, 2006; Dehm and Tindall, 2007; Lonergan and Tindall, 2011).

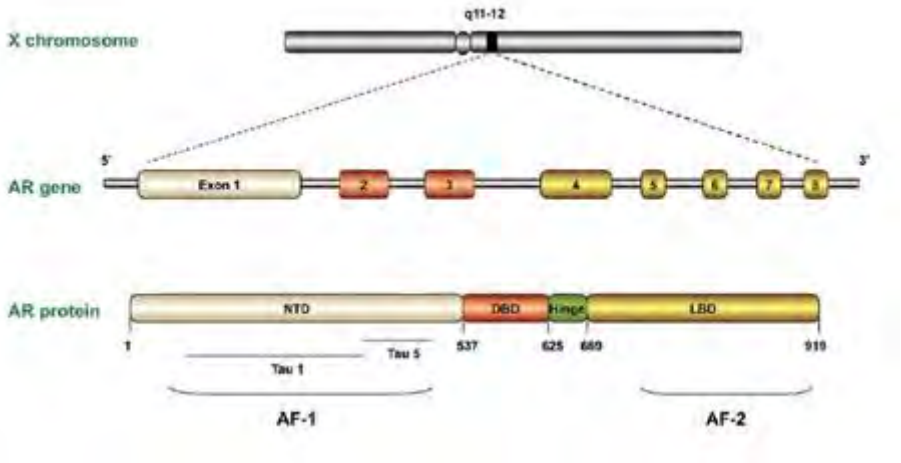

Figure 15: Schematic representation of the human androgen receptor gene and protein with its specific motifs and domains (Lonergan and Tindall, 2011).

In the absence of androgens, AR is present in the cytoplasm and is held inactive through its association with inhibitory molecules such as heat-shock proteins (e.g. Hsp90 chaperone complex) (Knudsen and Kelly, 2011; Yuan and Balk, 2009). Testosterone, the most prevalent androgen in the serum, bind and activate AR, whereas in the context of the prostate, this androgen is converted to dihydrotestosterone (DHT) via the action of the enzyme 5α-reductase in order to activate AR (Askew et al., 2007). Androgen binding, to the C-terminal LBD of the receptor, results in the dissociation of inhibitory proteins, homodimerization of the receptor, and conformational changes that trigger transcriptional

transactivation potential, post translational modifications and rapid translocation of ligand-bound AR into the nucleus (Knudsen and Kelly, 2011). These activated AR bind to androgen-responsive elements (AREs) of androgen regulated genes and increased the transcription of the latter genes **(Figure 16)** (Knudsen and Kelly, 2011; Yuan and Balk, 2009). Importantly, one of the main AR target genes encodes prostate-specific antigen (PSA) **(Figure 16)** (Cleutjens et al., 1996), a secreted protein marker used clinically for detecting prostate cancer development and progression (Greene et al., 2009; Lilja et al., 2008). However, limited evidence suggest that the PSA protein participates in the ability of AR to promote tumor development or progression (Knudsen and Kelly, 2011). Genome-wide analyses of AR function have not yet identified a single AR target that promote disease progression, and thus the means by which AR promotes prostate cancer survival and proliferation is complex (Knudsen and Kelly, 2011).

Prostate tumors which could not be cured by surgery or radiotherapy are treated with therapies based on downregulation of androgen levels in the circulation or blockade of the androgen receptor (AR) (Culig and Santer, 2014).

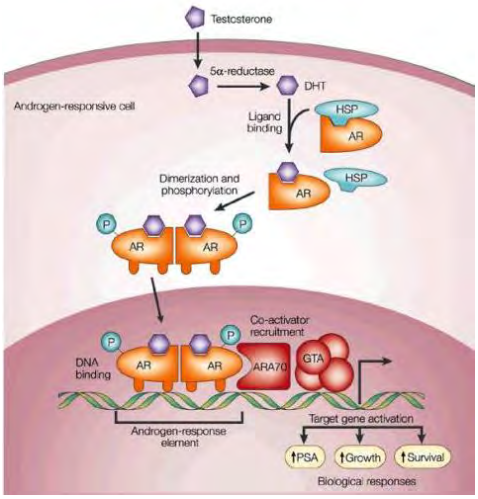

Figure 16: Action of androgens. Free testosterone enters prostate cells and is converted to DHT via the enzyme 5α-reductase. Binding of DHT to AR induces AR dissociation from HSPs and phosphorylation. AR dimerizes and bind to androgen-response elements (AREs) in the promoter regions of target genes. Coactivators (such as ARA70) and corepressors (not shown) also bind to the AR complex, facilitating or preventing, respectively, its interaction with the GTA. Activation (or repression) of target genes leads to biological responses including growth, survival and the production of PSA (Harris et al., 2009).

2. Targeting AR in prostate cancer:

Huggins and Hodges demonstrated that androgen deprivation therapy (ADT) results in prostate cancer regression (Huggins, 1942; Huggins, 1944; Huggins and Hodges, 1972), and this therapy remains the underlying basis for clinical management to avoid the spread of the disease. Currently, suppression of testicular androgen synthesis, which accounts for up to 95 % of serum testosterone) is efficiently achieved through the utilization of gonadotropin-releasing hormone (GnRH) agonist (Knudsen and Scher, 2009). Such strategies, which suppress AR activity by limiting access to the ligand, can be supplemented with direct AR antagonists such as bicalutamide, flutamide, or nilutamide. These AR antagonists, in combination with surgical or medical castration, result in further suppression of AR (Klotz, 2008). AR antagonists competes with testosterone or DHT for the AR ligand-binding domain and inhibits receptor activity by passive means. AR binds to anatagonist as a ligand that promotes nuclear entry and DNA binding; however, once bound to DNA, bicalutamide-bound receptors can induce recruitment of corepressor molecules such as nuclear receptor corepressor (NCoR) and SMRT (or NCoR 2) to actively suppress transcriptional transactivation (Shang et al., 2002). Whereas the majority of patients respond effectively to AR-directed therapeutics strategies (Knudsen and Scher, 2009), the responses are still transient. Thus, within a median time period of only 2-3 years, recurrent "castration-resistant prostate cancer (CRPC) progress (Knudsen and Kelly, 2011).

3. Castration-resistant prostate cancer (CRPC):

3.1. Overview of CRPC:

Patients with advanced and metastatic prostate cancer often receive hormonal therapy which decreases the production of testotesterone by the testes and block AR capacity. However, after an initial response which varies markedly among patients, prostate cancer progresses despite low levels of testosterone in the systemic circulation (<20 ng/dl) (Harris et al., 2009). This state of the disease is metastatic and is termed as castration-resistant prostate cancer (CRPC) (Yuan et al., 2009), and the average overall survival is 1.5 years with significant variability between patients with lymph node metastasis, bone metastasis and both lymph node and bone metastasis (Wu et al., 2014). In addition, chemotherapy agents such as Docetaxel and Cabazitaxel are approved therapies for CRPC with median survival benefit of only few months (Berthold et al., 2008; de Bono et al., 2010; Tannock et al., 2004). Thus, a better understanding of the mechanisms that give rise to CRPC as well as development of means that can delay or prevent this process are needed.

3.2. Mechanisms involved in CRPC:

3.2.1. AR hypersensitivity:

AR become sensitive to low levels of residual androgens via increased protein production (Katsogiannou et al., 2015), and up to 30 % of CRPC tumors show marked upregulation of the receptor (Ford et al., 2003; Linja and Visakorpi, 2004; Mohler, 2008a). Increased AR production could result from AR locus amplification, increased mRNA transcription rates and/or stabilization of the mRNA or protein (Bubendorf et al., 1999; Edwards et al., 2003). Enzalutamide is a novel antiandrogen selected for novel clinical development with promising results (Scher et al., 2010), displaying great affinity to AR, lacks agonists effects and inhibits not only ligand binding to the receptor in a competitive manner, but also AR nuclear translocation and DNA fixation **(Figure 17)**. It slow down cancer cell growth and induces cancer cell apoptosis resulting in tumor regression (Schalken and Fitzpatrick, 2016).

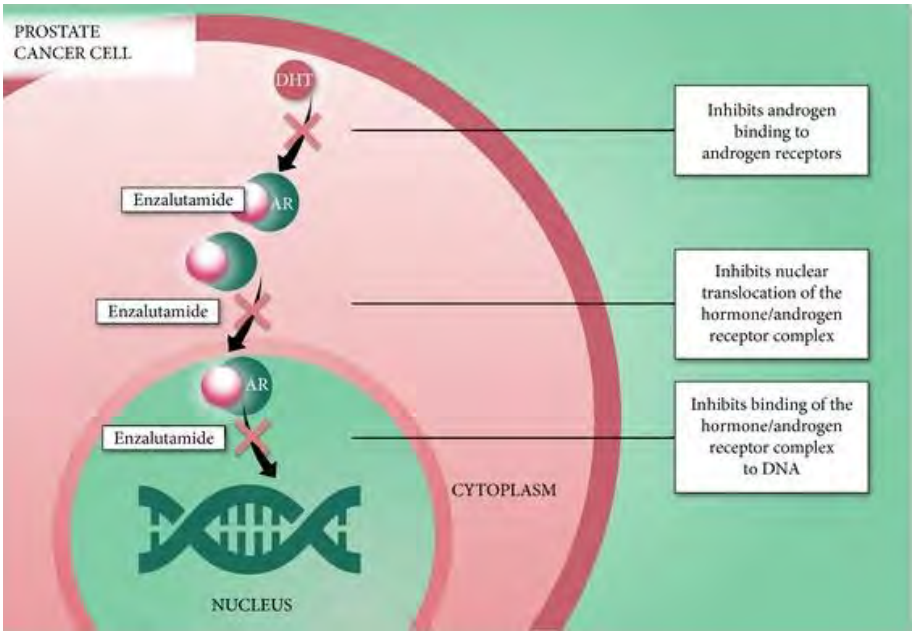

Figure 17: Mechanisms of Enzalutamide action (Schalken and Fitzpatrick, 2016).

Recent studies showed a link between AR expression and the retinoblastoma (RB) tumor suppressor, in which RB acts as a transcriptional repressor at the AR locus. In contrast, RB suppression results in deregulation of AR expression that is sufficient to induce CRPC *in vivo* **(Figure 18)**. Clincally, RB loss is markedly overrepresented in CRPC and inversely correlated with AR expression. These findings indicate that in prostate cancer, RB inhibits AR expression and signaling (Macleod, 2010; Sharma et al., 2010).

Figure 18: Loss of RB is associated with CRPC. Detectable loss of RB at late stages upon disease progression to CRPC (Macleod, 2010).

3.2.2. Intracrine androgen synthesis:

Prostate cancer cells can survive and compensate ADT via regulating intracrine androgen synthesis within the prostate. This local androgen synthesis is due to the overproduction of 5α-reductase enzyme that lead to the increased testosterone conversion to DHT (Holzbeierlein et al., 2004; Montgomery et al., 2008). Intratumoral androgens can also be synthesized from cholesterol or other precursors such as DHEA (dehydroepiandrosterone). DHEA could be converted to androstenedione, a substrate for conversion to testosterone **(Figure 19)**. The expression of all the genes necessary for androgen synthesis are significantly increased in CRPC compared to early stage of prostate cancer (Locke et al., 2008; Mohler, 2008a; Mohler, 2008b; Montgomery et al., 2008). Abiraterone acetate is a novel drug that inhibits CYP17A enzyme involved in the intratumoral androgen biosynthesis. Abiraterone, an effective and very potent drug, represents the first hormonal therapy to be approved in the post-chemotherapy setting for CRPC (Galsky et al., 2012; Suzman and Antonarakis, 2014).

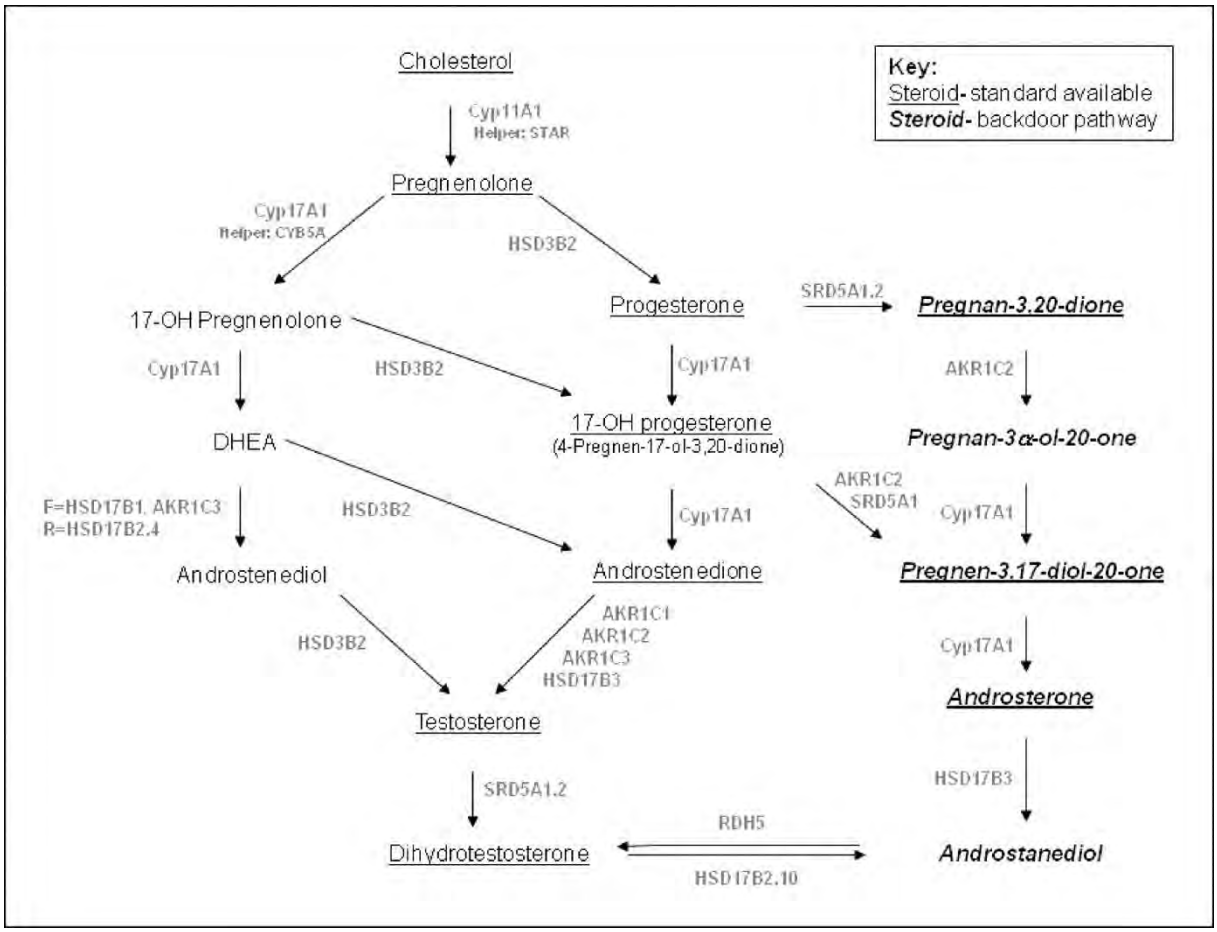

Figure 19: Schematic outline of the steroidogenic metabolism from cholesterol to dihydrotestosterone, including the backdoor pathway (shown in bold italics) (Locke et al., 2008).

3.2.3. AR mutations and alternative splicing:

3.2.3.1. AR mutations:

AR mutations enhance AR ligand binding specificity (Marcelli et al., 2000; Taplin et al., 1995; Tilley et al., 1996) and its activation by weak adrenal androgens and other steroid hormones such as DHEA, progesterone, estrogens and cortisol (Brooke and Bevan, 2009; Culig et al., 1994; Taplin, 2007; Veldscholte et al., 1992; Zhao et al., 2000). These mutations have several consequences depending on their localization (Bergerat and Ceraline, 2009; Brooke and Bevan, 2009; Culig et al., 2001). For example, cells from LNCaP cell line exhibit an AR missense mutation in the ligand-binding domain. At codon 877, the threonine is substituted to alanine, which opens the AR sensitivity to a wide number of steroid ligands (Suzuki et al., 1993; Taplin et al., 1999). Stikingly, this mutation may also convert AR antagonists (flutamide and bicalutamide) to AR agonist (Steinkamp et al., 2009). Moreover, mutations occur in the AR DNA-binding domain or in the N-terminal domain modulate the binding specificity of its co-regulators and the transcriptional activation of its target genes (Black et al., 2004; Chmelar et al.,

2007). Accordingly, T877A and Q640Stop/T877A are two mutations that activate AR. Q640Stop/T877A harbor the nonsense mutation Q640Stop just downstream the DNA binding domain together with the T877A point mutation leading to c-terminal truncated AR (Ceraline et al., 2004).

3.2.3.2. AR splice variants:

AR splice variants (AR3, 4 and 5) which lack their C-terminal protein domain (ligand-binding domain) including the canonical nuclear localization signal (NLS), can activate AR target genes (Chan et al., 2012; Guo et al., 2009; Hu et al., 2009; Sun et al., 2010). However, truncated AR at their N-terminal domain (DNA-binding domain) can translocate to the nucleus and have ligand-independent transcriptional activity. AR variants such as AR-V7 is associated with a short time to disease recurrence following radical prostatectomy (Guo et al., 2009; Hornberg et al., 2011; Hu et al., 2009). A small molecule (EPI-001), targeting the AR N-terminal domain, is still under study for its efficiency against tumors expressing AR splice variants (Andersen et al., 2010).

3.2.4. AR activation by growth factors, cytokines and receptor tyrosine kinases:

Growth factor pathways such as insulin-like growth factor (IGF1) and epidermal growth factor (EGF) bind and activate AR in CRPC, when they are overexpressed (Manin et al., 2000). IGF1 triggers cell growth, survival and differentiation of prostate cells and is increased in advanced metastatic prostate cancer (Wu et al., 2006). Cytokines such as interleukin-6 (IL-6) and interleukin-4 (IL-4) are also activators of AR pathway in CRPC (Lee et al., 2003a; Lee et al., 2003b). Importantly, IL-6 activate AR via the activation of MAPK (mitogen-activated protein kinase) and Stat3 pathways (Ueda et al., 2002). In addition, tyrosine kinase receptors (e.g. ERbB2) are overexpressed in CRPC, resulting in the increase of AR expression and activity through the activation of MAPK and phosphoinositide-3 kinase (PI3K)/AKT signaling pathways (Lemmon and Schlessinger, 2010; Manin et al., 2002; Wen et al., 2000; Yeh et al., 1999), and AKT mutant or PI3K disruption reduce AR protein levels (Manin et al., 2002).

3.2.5. Post translational modifications and cofactor alteration:

Post-translational modifications have been suggested to contribute to enhance AR function in CRPC. These modifications include serine/threonine phosphorylation (Ward and Weigel, 2009), tyrosine phosphorylation **(Figure 20)** (Guo et al., 2006), acetylation (Popov et al., 2007), ubiquitination (Dirac and Bernards, 2010; Xu et al., 2009) and sumolyation (Kaikkonen et al., 2009) of the receptor, and could act synergistically with other AR alteration events (Knudsen and Kelly, 2011).

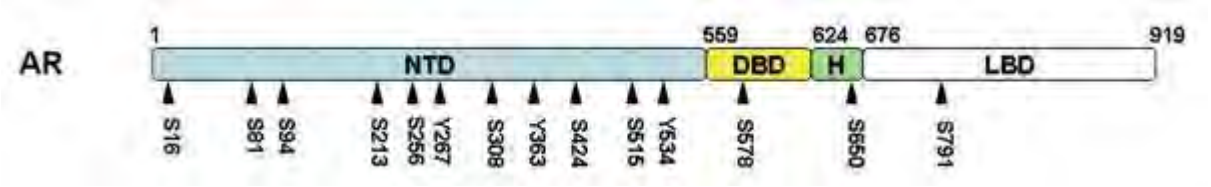

Figure 20: Phosphorylation site locations of human AR (Ward and Weigel, 2009).

In addition, AR cofactors are altered in prostate cancer, involving the upregulation of coactivators (Agoulnik and Weigel, 2008). Coactivator levels are increased in CRPC, enhancing the sensitivity of AR to several ligands rather than androgens. For examples, ARA70, ARA55, SRC-1, P/CAF and GRIP1/TIF2 are overexpressed in prostate cancer (Dehm and Tindall, 2005; Feldman and Feldman, 2001; Gregory et al., 2001; Heemers and Tindall, 2007; Mestayer et al., 2003). Moreover, loss of AR corepressor function may trigger AR transcription activity in CRPC, for example, exclusion of NCoR from the AR complex (Katsogiannou et al., 2015).

3.2.6. TMPRSS2-ERG fusion:

The ERG oncogene, a member of the large family of ETS transcription factors, is overexpressed in early stage PCa and CRPC (Kumar-Sinha et al., 2008; Smit et al., 2013). This family is involved in various biological processes such as cell proliferation, differentiation, apoptosis, metastasis and angiogenesis (Hollenhorst et al., 2011; Tomlins et al., 2005). ERG gene fuse with the first exon(s) of the transmembrane protease serine 2 (TMPRSS2), a prostate-specific and androgen-regulated gene located close to ERG on the same 21q22 chromosome region **(Figure 21)** (Perner et al., 2006; Tomlins et al., 2005). Fusion of these genes can occur either by interstitial deletion leading to the loss of genomic region between the two genes (60 % of fusion-positive tumors), or by complex genomic rearrangements involving several chromosomes (Hermans et al., 2009). Importantly, ETS genes are frequently involved in gene fusions, resulting in the formation of altered expression of ETS proteins.

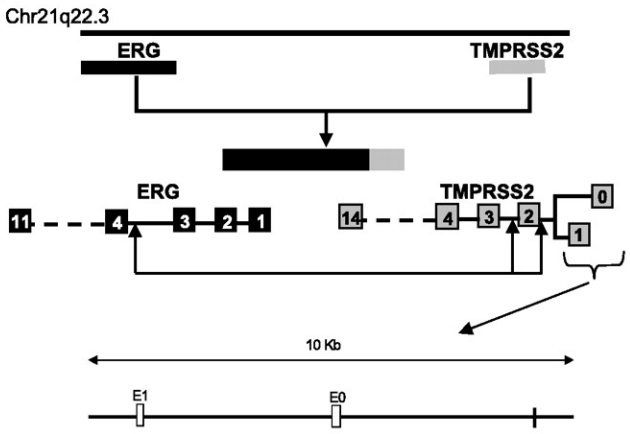

Figure 21: Schematic representation of the TMPRSS2-ERG locus on chromosome band 21q22.3. The most frequent gene fusion events are shown. The enlarged genomic region containing TMPRSS2 shows exon 0 and 1 and repeat sequences (Hermans et al., 2009).

3.2.7. Glucocorticoid receptor bypass AR blockade:

Induction of glucocorticoid receptor (GR) levels and/or activity bypass enzalutamide-mediated AR blockade without the need for restored AR function (Arora et al., 2013; Isikbay et al., 2014), and this is due to the fact that GR associates with the canonical AR binding sites to activate a transcriptional machinery similar to that activated by AR itself (Arora et al., 2013). Arora et al., showed that GR expression was upregulated in ~ 30 % of patient tumors at 8 weeks after enzalutamide treatment, whereas in only ~ 10 % of tumors obtained before therapy (Arora et al., 2013). These findings establish a mechanism of escape from AR blockade through expansion of cells primed to drive AR target genes through an alternative nuclear receptor (GR) upon therapy.

3.3. Histological dedifferentiation and alterations in the lineage of prostate cancer cells:

3.3.1. EMT in prostate cancer:

Prostate cancer cells acquire EMT program to gain malignancy associated traits, such as motility, invasiveness and drug resistance (Nieto, 2011; Thiery, 2002). Clinically, the induction of EMT and the gain of mesenchymal characteristics has been linked to a high Gleason score, a shortented time to biological recurrence, and the presence of bone and lymph node metastasis (Davies et al., 2018).

ADT increases the expression of AR splice variants such as AR-V7 (also termed as AR3), which can induce EMT **(Figure 22)** and the expression of stem-cell-assocaited marker genes (Cottard et al., 2013; Kong et al., 2015).

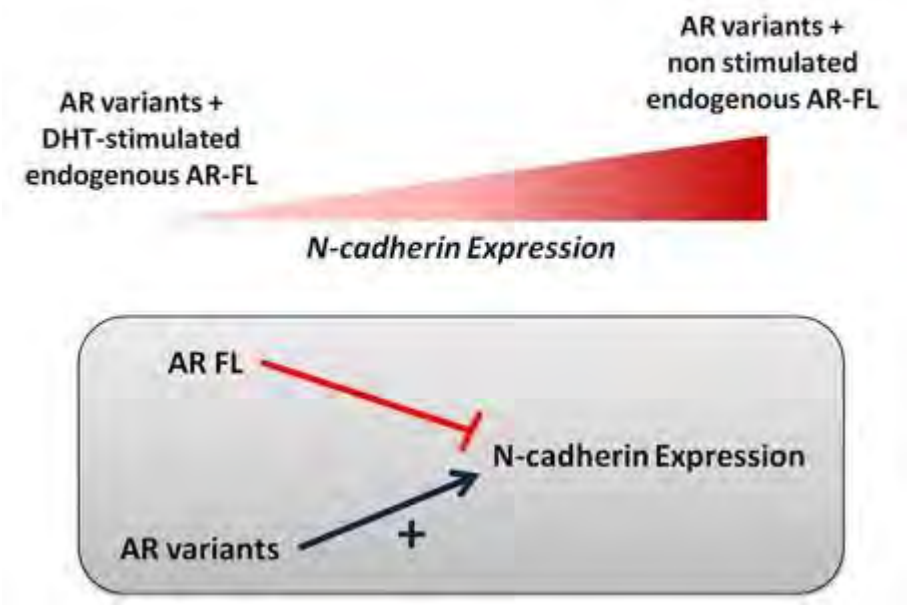

Figure 22: Androgens abrogate N-cadherin upregulation induced by active androgen receptor variants (e.g. AR-V7) in LNCaP cells. N-cadherin expression induced by constitutively active AR variants (AR variants) was negatively regulated when LNCaP cells were grown in the presence of DHT. Thus, endogenous AR-FL present in LNCaP cells and AR variants could act differently. In this model, DHT-stimulated endogenous AR-FL represses N-cadherin expression, whereas AR variants upregulate its expression (Cottard et al., 2013).

Stikingly, AR3Tg transgenic mice, which express AR-V7 in the prostatic epithelium, exhibit a population of murine prostate progenitor cells (known as those cells positive for Lin-Sca-1 and CD49f^{high}), indicating that AR-V7 antagonizes the differentiation program mediated by full-length AR by an unknown mechanism (Sun et al., 2014).

3.3.2. EMT acquire a stem cell-like phenotype:

Several studies linked activation of the EMT program with the acquisition of a CSC phenotype. For example, gene expression profiling of LuCaP35 human prostate cancer xenografts following ADT showed that the EMT program was activated in parallel with the upregulation of stem-cell-associated genes WNT5A and WNT5B (Sun et al., 2012). In addition, specific epithelial stem/progenitor cells (Lin^{-}Epcam^{low}CD24^{low}cells; defined as expressing low levels of epithelial cell adhesion molecule (Epcam^{low}) and signal transducer CD24 (CD24^{low}) isolated from a Pten-null, activated Kras^{G12D}-driven GEMM of prostate cancer had a greater capacity to reconstitute an EMT and drive distant metastasis than populations of epithelial cells (Mulholland et al., 2012).

In contrast, some studies on prostate cancer indicate that EMT and mesenchymal features can also be associated with non-CSC populations. For example, an epithelial derivative of PC-3 cells had induced self-renewal capacity, pluripotency, and metastatic capacity relative to its mesenchymal coordinate (Celia-Terrassa et al., 2012). In addition, the epithelial (E-cadhrin-positive) fraction of PC-3 and DU145 cells expressed pluripotency associated transcription factors (SOX2, POU5F1, and NANOG) and was strongly tumorigenic *in vivo* (Bae et al., 2010).

These findings support the concept that CSC phenotype, plasticity, and tumorigenicity are associated with partial EMT rather than with the isolated epithelial or mesenchymal state. Therefore, understanding the molecular underpinnings of the partial EMT phenotype is needed to better explain the context-dependent requirements for plasticity during tumor evolution.

3.3.3. Lineage plasticity and neuroendocrine phenotype:

The success of inhibitors for AR pathway, such as abiraterone and enzalutamide, in treating PCa has been hampered by the emergence of therapeutic resistance. This acquired drug resistance is driven via the ability of prostate cancer cells to reprogram to a phenotypic state that is no longer dependent on AR pathway which is being initially targeted by therapeutic drugs (Ku et al., 2017; Mu et al., 2017). Around one-quarter of resistant prostate tumors consist cells that have undergone cellular reprogramming and acquire neuroendocrine characteristics (Davies et al., 2018). These highly aggressive tumors, termed neuroendocrine prostate cancer (NEPC), display reactivation of developmental programmes that are associated with epithelial-mesenchymal plasticity and gain of stem-like cell properties (Davies et al., 2018; Qin et al., 2012). Understanding the cross-talk between lineage plasticity and the emergence of NEPC phenotype has been increased in the last few years.

3.3.3.1. Neuroendocrine phenotype in prostate cancer:

Neuroendocrine prostate cancers (NEPCs) represent <2 % of newly diagnosed prostate cancers (Helpap et al., 1999). However, NEPC are widely known as a subset of resistant tumors that evade AR pathway and acquire histological features of neuroendocrine differentiation (Aparicio et al., 2011; Beltran et al., 2012; Nadal et al., 2014). NEPC is associated with altered histology, reduced AR levels, and expression of neuroendocrine markers such as Synaptophysin (Syp), Chromogranin A (CHGA) and Neuron Specific Enolase (NSE) (Beltran et al., 2016; Wang and Epstein, 2008). Tumors exhibiting NEPC are typically negative for luminal prostate differentiation markers, such as PSA and prostatic acid phosphatase (Wang and Epstein, 2008). Currently, there are no targeted therapies available for NEPC, and the survival of patients with NEPC ranges from 7 months to 2 years (Davies et al., 2018).

Data from *in vitro* and *in vivo* human prostate cancer models (Beltran et al., 2011; Beltran et al., 2012; Mu et al., 2017), as well as genetically engineered mouse models (GEMMs) **(Table 2)** (Dardenne et al., 2016; Ku et al., 2017; Zou et al., 2017), indicate that a lineage switch from epithelial cells to neuroendocrine cells makes tumors independent on AR signaling, enabling them to resist inhibition of the AR pathway.

Name or characteristic	Origin of cells	Histology	Evidence of plasticity
Cell line			
NCI-H660	Lymph node metastasis from a patient with small-cell prostate cancer	NA	Dependency on EZH2
GEMMs			
Rb1 deletion and *Pten* loss	Mouse prostate epithelium	Mixed adenocarcinoma and NEPC (SYP^+) cells	EZH2 inhibition reverses antiandrogen (enzalutamide) resistance
Tp53 deletion and *Pten* loss	Mouse prostate epithelium (luminal cells)	Divergent differentiation, including squamous, sarcomatoid, and small-cell NE-like (SYP^+CHGA^+) cells	Lineage tracing demonstrates that luminal adenocarcinoma cells give rise to NE tumours in response to antiandrogen (abiraterone) treatment
Mycn induction and *Pten* loss	Mouse prostate epithelium	Foci of poorly differentiated carcinoma with divergent differentiation, including sarcomatoid and small-cell NE ($CHGA^+$) cells	Upregulation of AR-regulated genes following EZH2 inhibition
Xenografts			
MYCN induction and *AKT* activation	Human prostate epithelium	Divergent differentiation, including small-cell NE and mixed NE–acinar adenocarcinoma ($SYP^+CHGA^+NCAM1^+$) cells	Upregulation of epigenetic regulators (EZH2 and DNMT1); CSC features
PDX			
LTL331R	PDX adenocarcinoma (LTL331)	NEPC ($SYP^+CHGA^+CD56^+$) cells	Rapid emergence of NE tumour following castration

Table 2: Description of plasticity in NEPC models. AR, androgen receptor; CHGA, chromogranin A; CSC, cancer stem-like cell; DNMT1, DNA (cytosine-5)-methyltransferase 1; EZH2, enhancer of zeste homologue 2; GEMM, genetically engineered mouse model; NA, not applicable; NCAM1, neural cell adhesion molecule 1; NE, neuroendocrine; NEPC, neuroendocrine prostate cancer; PDX, patient-derived xenograft; SYP, Synaptophysin (Davies et al., 2018).

3.3.3.2. Mechanisms of neuroendocrine differentiation after ADT:

3.3.3.2.1. Hierarchical model:

Prostate tumor are heterogeneous, in which they consist of a mixture of cells whose stemness and/or proliferative capacity differs. AR pathway inhibitors (ARPIs) can decrease tumor by eliminating the higly proliferative AR-dependent cells (referred as the luminal epithelial cells), but not the AR-independent cells (cancer stem-like cells (CSCs) and/or neuroendocrine cells). The tumorigenic CSC population spreads after ARPI treatment. The plasticity of these cells enables them to differentiate into neuroendocrine-like malignant cells, which comprise NEPC. Also, the acquisition of new mutations in pre-existing neuroendocrine cells, could lead to the emergence of NEPC **(Figure 23)** (Davies et al., 2018).

3.3.3.2.2. Transdifferentiation model:

After ARPIs, luminal epithelial cells can be reprogrammed into neuroendocrine cells (Zou et al., 2017). Activation of the partial EMT endows cells with a plastic phenotype and underlies the transdifferentiation program, which can progress by a transient pluripotent and stem-like state to generate CSCs. The capacity for migration and invasion, therapy resistance, and stem-like properties differ over the spectrum of adenocarcinoma to neuroendocrine transdifferentiation **(Figure 23)** (Davies et al., 2018).

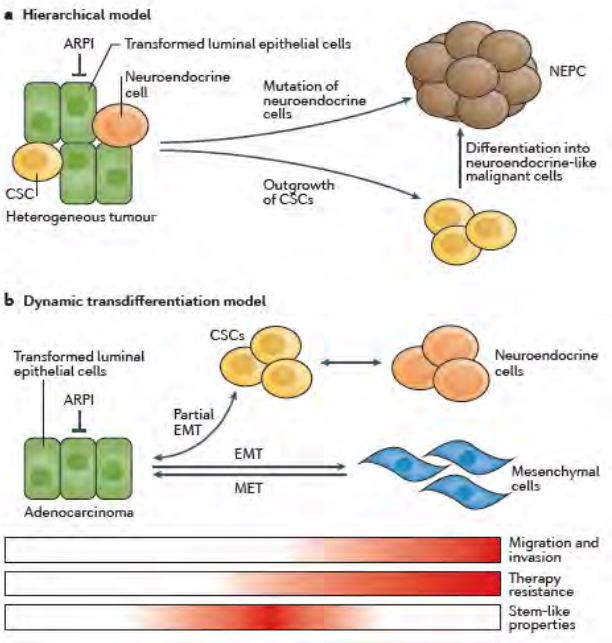

Figure 23: Mechanisms of neuroendocrine differentiation in response to AR pathway inhibitors. (**a**) Hierarchical model and (**b**) Transdifferentiation model as described above. Red indicates a high level.

Notably, Zou et al. showed that abiraterone-treated NPp53 prostate tumors, in which Pten and p53 genes are co-inactivated in the prostate, contain regions of focal and/or overt neuroendocrine differentiation, distinguished by their proliferative potential. Strikingly, lineage tracing *in vivo* indicates that focal and overt neuroendocrine regions arise via the transdifferentiation of the luminal adenocarcinoma cells **(Table 2 ; Figure 24)** (Zou et al., 2017).

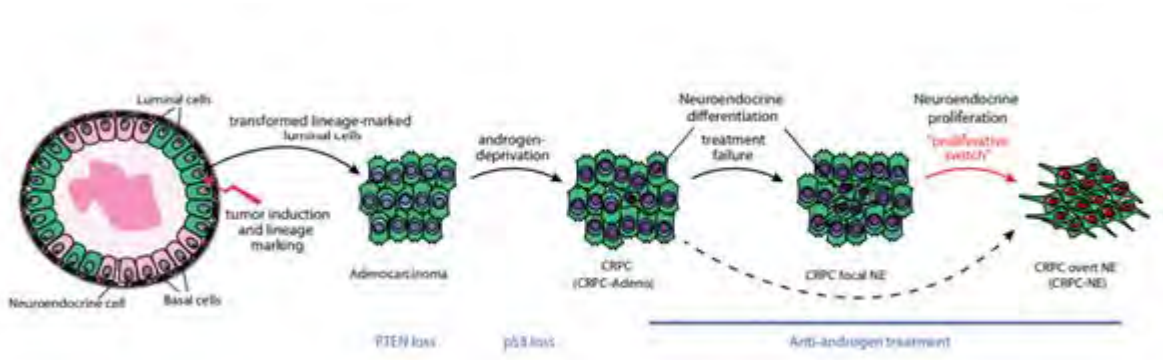

Figure 24: NP and NPp53 prostate cancer mouse models. The phenotypic events associated with the progression to CRPC including the anti-androgen treatment failure and the transdifferentation of luminal adenocarcinoma cells into neuroendocrine cells (Zou et al., 2017).

3.3.3.3. Relationship between cellular plasticity and neuroendocrine differentiation:

Several evidences support the relationship between epithelial plasticity and the emergence of a neuroendocrine differentiation. First, AR pathway inhibition in prostate cancer cell lines and clinical samples drives to the induction of EMT (Sun et al., 2012), enrichment of CSC populations (Germann et al., 2012; Lee et al., 2013; Qin et al., 2012; Seiler et al., 2013), and neuroendocrine differentiation (Beltran et al., 2011; Hirano et al., 2004; Lipianskaya et al., 2014; Yuan et al., 2006). NEPC tumors can use the EMT program, but whether this is a consequence of cellular reprogramming or an independent process remains unclear (Beltran et al., 2016; Dardenne et al., 2016). Strikingly, the transcription factor Sox11 (sex determining region Y-box11), which has been implicated in EMT and MET (Hargrave et al., 1997), was identified as a driver of neuroendocrine differentiation in NPp53 mouse model following abiraterone treatment (Zou et al., 2017). Thus, these data provide evidence that EMT program and neuroendocrine differentiation are linked.

3.3.3.4. Cell surface markers in lineage plasticity and neuroendocrine differentiation:

CD44, a well-established cell surface marker for prostate CSCs, is selectively expressed in NEPC supporting the evidence of the relationship between lineage plasticity and neuroendocrine differentiation (Davies et al., 2018). CD44 expression is correlated with cell invasion, cell migration, and cell-self renewal capacity after ADT, thus bridging the EMT and CSC phenotypes **(Figure 25)** (Shang et al., 2015).

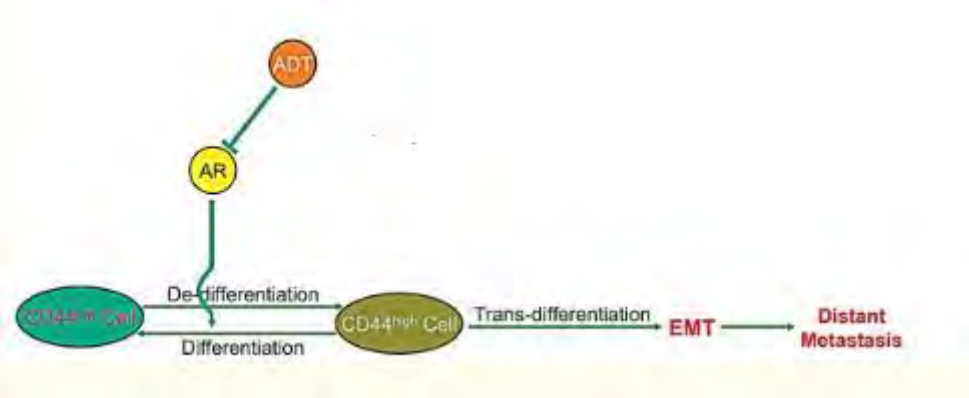

Figure 25: CD44 marker. Schematic representation of the mechanism of ADT enhanced prostate cancer metastasis via CD44 (Shang et al., 2015).

Furthermore, it was shown that CD44 expression in LnCaP, DU145, and PC-3 cell lines is selectively induced in cells positive for the neuroendocrine marker (NSE) (Palapattu et al., 2009). The association between CSCs, EMT, and neuroendocrine differentiation was also shown by transplanting CSCs into mice; inoculating mice with $CD44^{+}CD24^{-}$CSCs isolated from the DU145 cell line resulted in invasive mesenchymal-like tumors which exhibit low levels of E-cadherin and β-catenin and high levels of vimentin with a high density of $CHGA^{+}$ neuroendocrine cells (Salvatori et al., 2012). Clinically, immohistological analysis of prostate tumors showed that > 90 % of neuroendocrine cells (referred as $CHGA^{+}$ cells) are $CD44^{+}$ cells (Palapattu et al., 2009). Therefore, all these data provide evidences in the correlation between CSCs, EMT and neuroendocrine phenotype.

3.3.3.5. Genetic and epigenetic mediators of cellular plasticity:

Genomic analysis showed that RB1 loss and the mutation or deletion of p53 occur together more commonly in NEPC (~ 50 %) than in prostatic adenocarcinoma (~ 14 %) (Beltran et al., 2016). Indeed, loss of Rb1 and p53 in a conditional mouse model for metastaic prostate cancer promotes lineage plasticity and neuroendocrine differentiation (Zhou et al., 2006). Moreover, one study reported that silencing RB1 and p53 in the antiandrogen sensitive LNCaP-AR human prostate cancer cell line allow

resistance to enzalutamide by causing a phenotypic shift from AR-dependent luminal epithelial cells to AR independent basal and neuroendocrine cells (Mu et al., 2017). Sox2, sex determining region Y-box2, which has a role in both inducing and maintaining pluripotency as well as in balancing neuronal progenitor cell proliferation and differentiation (Sarkar and Hochedlinger, 2013), was shown to promote lineage plasticity and enzalutamide resistance in the latter study **(Figure 26)** (Mu et al., 2017). In a related study, loss of Rb1 in Pten-null prostate cancer mouse model promotes the formation of neuroendocrine cells, which arise from pre-existing luminal cells **(Table 2)** (Ku et al., 2017). The additional loss of Trp53 in this model facilitates neuroendocrine differentiation and antiandrogen resistance with the upregulation of the reprogramming factors such as Sox2 and the enhancer of zeste 2 polycomb repressive complex 2 subunit (Ezh2) (Ku et al., 2017). This observation is consistent with the role of p53 activity in reducing efficiency of somatic cell reprogramming (Kawamura et al., 2009). Clinically, Ezh2 inhibitors restore androgen receptor expression and sensitivity to antiandrogen (enzalutmide) therapy. These findings uncover genetic alterations that enable prostate cancer evolution, and suggest an epigenetic approach for enhancing clinical responses to antiandrogen therapy.

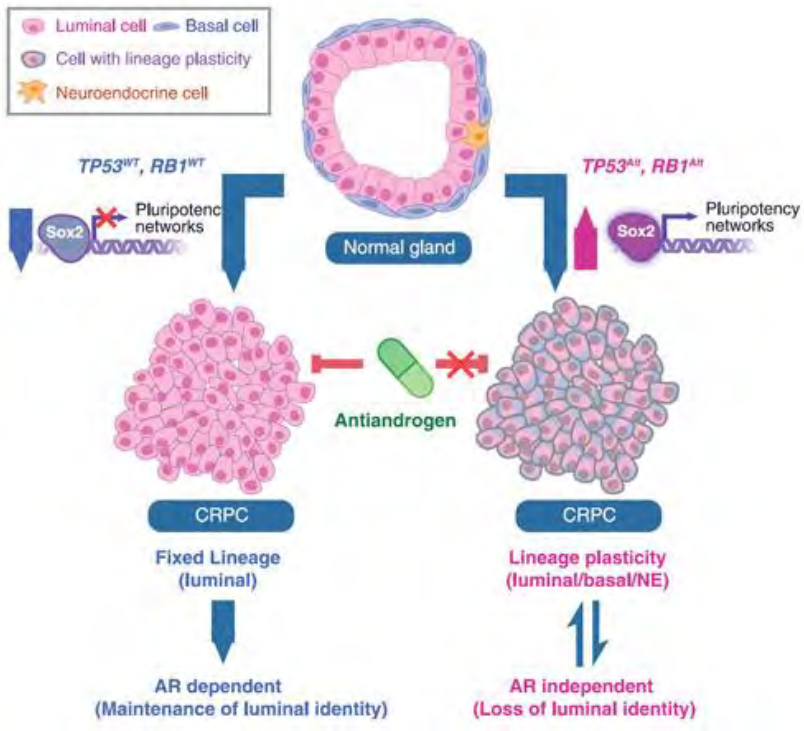

Figure 26: Model. Model describing the lineage plasticity variation and antiandrogen resistance in CRPC-Adeno due to *TP53* and *RB1* alterations (*TP53*^{Alt}, *RB1*^{Alt}) compared to CRPC-Adeno with WT *TP53* and *RB1* (*TP53*^{WT}, *RB1*^{WT}) (Mu et al., 2017).

Objectives of the Thesis:

1. ***Characterizing the key events underpinning the formation of prostatic intraepithelial neoplasia (PIN) after Pten loss in mature prostatic epithelial cells (PECs) in vivo.***

2. ***Determine the role of Trp53 in Pten-deficient prostatic epithelial cells (PECs) of adult mice.***

3. ***Study the role of androgens in Pten and Pten/Trp53-deficient prostatic epithelial cells (PECs) of adult mice.***

RESULTS

PART I

Manuscript I

Summary Part I: Characterization of Pten deletion in mature luminal PECs

Previously, the host laboratory showed that temporally controlled somatic biallelic ablation of the tumor suppressor gene *PTEN* via the CreER^{T2} system in adult mice (PTEN$^{(i)pe-/-}$ mice), closely mimics the course of human prostate cancer formation (Ratnacaram et al., 2008). Several studies have shown that the progression of *PTEN* loss induced prostatic intraepithelial neoplasia (PINs) is antagonized by cell senescence *in vivo* (Alimonti et al., 2010; Chen et al., 2005; Di Mitri et al., 2014). However, unlike oncogene-induced senescence, *PTEN* loss-induced senescence (PICs) was reported to be a novel type of cellular senescence, as no hyperproliferation phase and no sign of DNA damage response (DDR) were observed in PTEN-deficient prostatic epithelial cells (PECs); however, this mouse model is hampered by the lack of the temporal control of *PTEN* loss (Alimonti et al., 2010; Chen et al., 2005; Di Mitri et al., 2014). Therefore, we aimed to further characterize PICs in PTEN$^{(i)pe-/-}$ mice in which *PTEN* is selectively ablated in prostatic luminal cells after puberty.

Following *PTEN* ablation, PECs actively proliferate forming PINs within a few months. This hyper-proliferation induces replication stress and mount a DNA damage response (DDR), which in turn lead to a progressive growth arrest with characteristics of cell senescence. Notably, as these senescent PECs secrete a large number of cytokines and chemokines that can accumulate other mutations, they contribute to tumor progression into adenocarcinoma.

Together, the most promising strategy for prostate cancer treatment remains the elimination of senescent cells from preneoplastic lesions.

Keywords: prostate cancer, prostatic epithelial cells, prostatic intraepithelial neoplasia, replication stress, DNA damage response, and cell senescence.

Graphical abstract I:

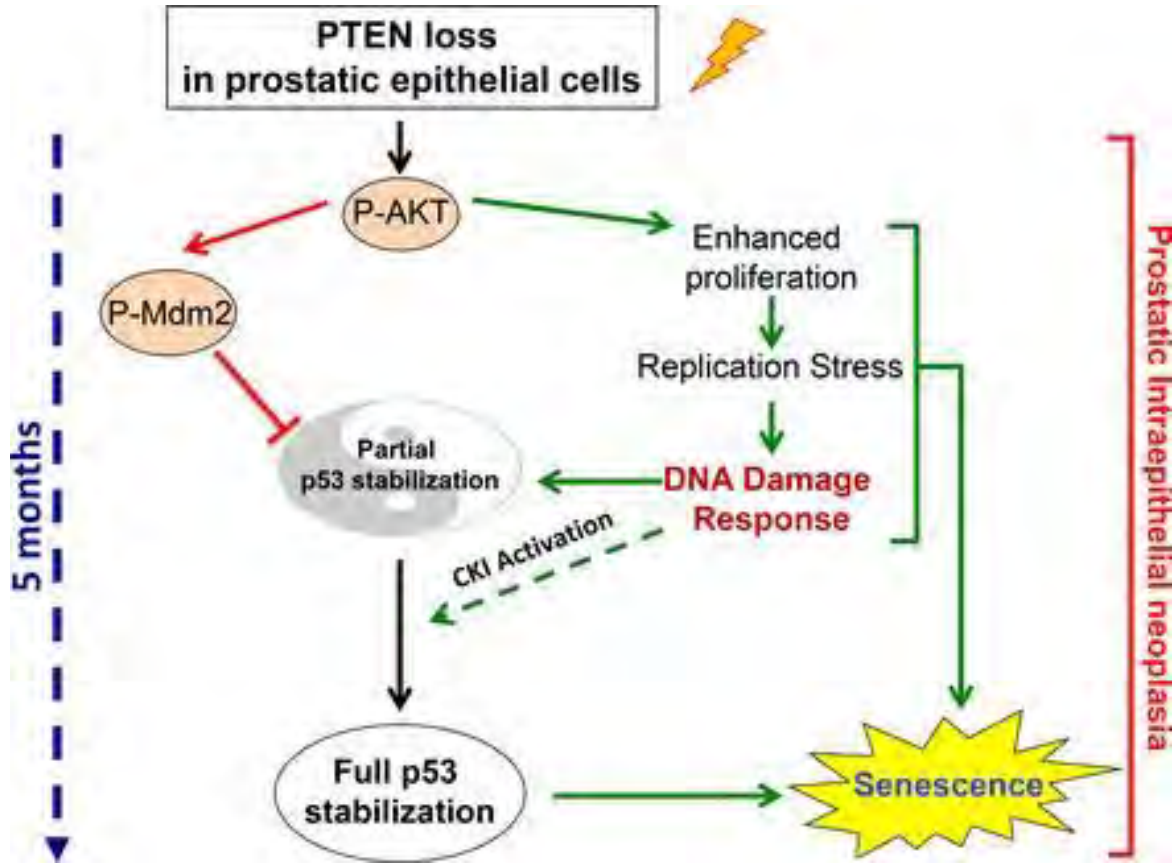

Figure 27: Schematic representation describing factors inducing cellular senescence after PTEN loss in prostatic epithelial cells in vivo (Parisotto et al., 2018).

JEM Journal of Experimental Medicine

ARTICLE

PTEN deletion in luminal cells of mature prostate induces replication stress and senescence in vivo

Maxime Parisotto, Elise Grelet*, Rana El Bizri*, Yongyuan Dai, Julie Terzic, Doriane Eckert, Laetitia Gargowitsch, Jean-Marc Bornert, and Daniel Metzger

Genetic ablation of the tumor suppressor *PTEN* in prostatic epithelial cells (PECs) induces cell senescence. However, unlike oncogene-induced senescence, no hyperproliferation phase and no signs of DNA damage response (DDR) were observed in *PTEN*-deficient PECs; *PTEN* loss-induced senescence (PICS) was reported to be a novel type of cellular senescence. Our study reveals that *PTEN* ablation in prostatic luminal epithelial cells of adult mice stimulates PEC proliferation, followed by a progressive growth arrest with characteristics of cell senescence. Importantly, we also show that proliferating *PTEN*-deficient PECs undergo replication stress and mount a DDR leading to p53 stabilization, which is however delayed by Mdm2-mediated p53 down-regulation. Thus, even though *PTEN*-deficiency induces cellular senescence that restrains tumor progression, as it involves replication stress, strategies promoting *PTEN* loss–induced senescence are at risk for cancer prevention and therapy.

Introduction

Mutations or deletion of the *PTEN* locus are common and associated with metastasis and resistance to therapeutic castration in prostate cancer (Cairns et al., 1997; Choucair et al., 2012; Krohn et al., 2012; Costa et al., 2015). Genetic ablation of *PTEN* or expression of a dominant-negative mutant of PTEN in mouse prostate epithelial cells (PECs) induces prostatic intraepithelial neoplasia (PIN) with full penetrance (Chen et al., 2005; Luchman et al., 2008; Ratnacaram et al., 2008; Papa et al., 2014).

Several studies have shown that the progression of *PTEN* loss–induced PINs is antagonized by cell senescence in mice (Chen et al., 2005; Alimonti et al., 2010; Di Mitri et al., 2014). Senescence is triggered in response to various stimuli (Yaswen and Campisi, 2007; Courtois-Cox et al., 2008), including the expression of oncogenes in untransformed cells (e.g., Ras^{G12V}, E2F1, Raf, Mos, Cdc6, cyclin E, Stat5, and PML; Serrano et al., 1997; Ferbeyre et al., 2000; Michaloglou et al., 2005; Mallette et al., 2007; Courtois-Cox et al., 2008). Oncogene-induced senescence (OIS), by permanently halting cell proliferation and promoting immune surveillance of premalignant lesions, is a barrier against cell transformation (Braig et al., 2005; Chen et al., 2005; Kang et al., 2011). Accordingly, markers of senescence have been observed in premalignant lesions in various human tissues, including the prostate, but not in the corresponding tumors (Chen et al., 2005; Michaloglou et al., 2005; Collado and Serrano, 2010; Vernier et al., 2011). Thus, escaping or avoiding OIS likely represents a critical step toward transformation.

The DNA damage response (DDR) pathway is a central regulator of OIS (Bartkova et al., 2006; Bartek et al., 2007; Mallette et al., 2007; Courtois-Cox et al., 2008). Indeed, the expression of oncogenes has been shown to stimulate cell proliferation, causing replication stress and a robust activation of the DDR pathway (Bartkova et al., 2006; Bartek et al., 2007), whereas inactivation of components of the DDR pathway bypasses OIS (Di Micco et al., 2006; Mallette et al., 2007). Induction of the DDR stabilizes p53 through its phosphorylation by DDR kinases (ATR, ATM, DNA-PK, CHK1, and CHK2; Zhou and Elledge, 2000; Lavin and Gueven, 2006). p53 promotes OIS through transcriptional regulation of an array of genes, including p21, an inhibitor of cell cycle progression (Mirzayans et al., 2012).

PTEN loss–induced senescence (PICS) was also shown to be p53-dependent (Chen et al., 2005), but as no hyperproliferation and DDR activation was observed (Alimonti et al., 2010; Astle et al., 2012), it was concluded that PICS is a new type of senescence (Chen et al., 2005; Courtois-Cox et al., 2008; Astle et al., 2012). Moreover, Di Mitri et al. reported that tumor-infiltrated GR-1–positive myeloid cells antagonize PICS and sustain tumor growth (Di Mitri et al., 2014).

Department of Functional Genomics and Cancer, Institut de Génétique et de Biologie Moléculaire et Cellulaire (IGBMC), Centre National de la Recherche Scientifique UMR7104/Institut National de la Santé et de la Recherche Médicale U1258, Université de Strasbourg, Illkirch Cedex, France.

*E. Grelet and R. El Bizri contributed equally to this paper; Correspondence to Daniel Metzger: metzger@igbmc.fr; M. Parisotto's current address is Université de Montréal, Montréal, Québec, Canada.

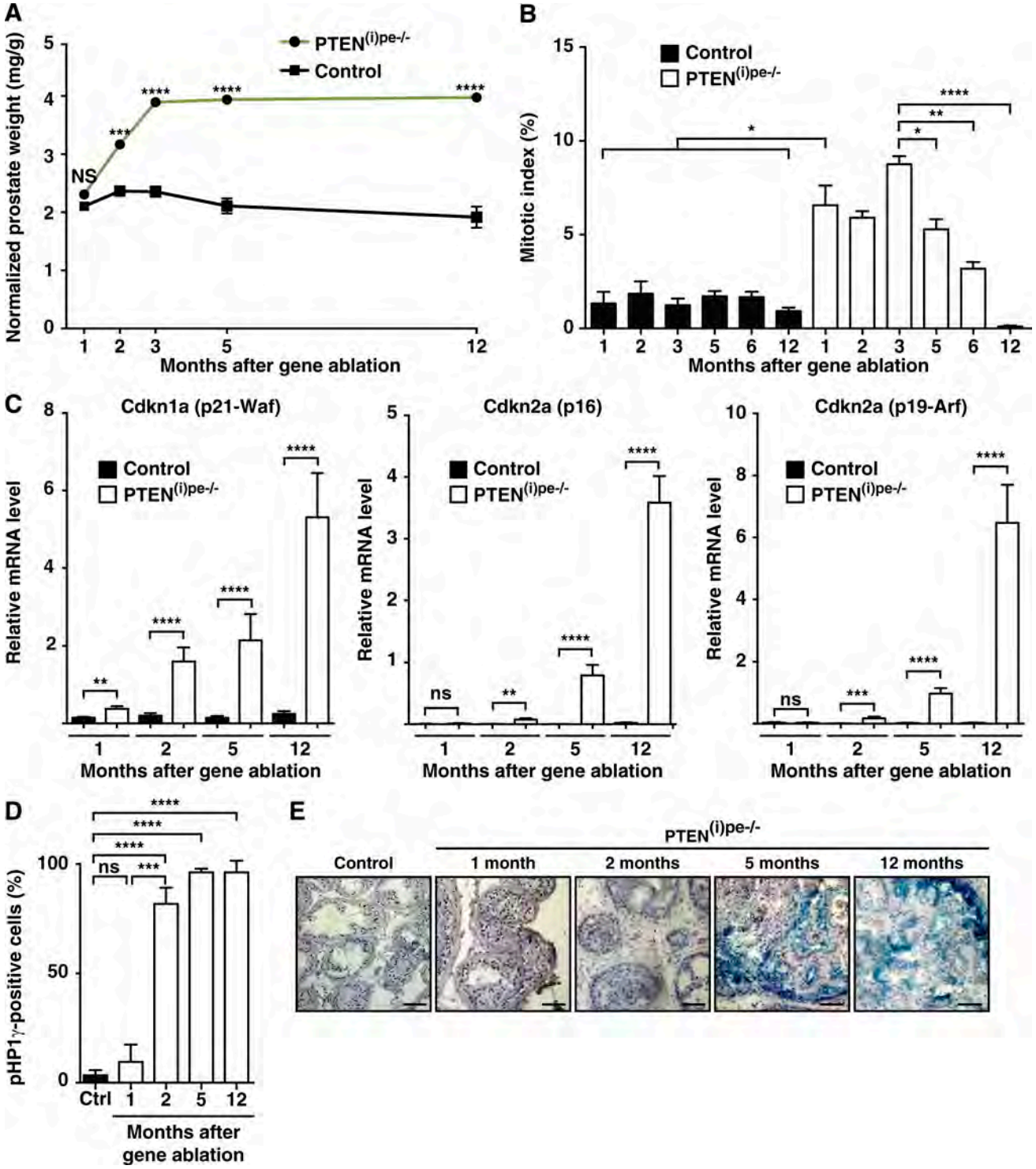

Figure 1. **Characterization of prostate tumors in PTEN$^{(i)pe-/-}$ mice. (A)** Prostate weight (normalized over body weight) in PTEN$^{(i)pe-/-}$ and control mice over 12 mo after *PTEN* ablation. Values are mean of four to six mice ± SEM. **(B)** Proliferation index (percentage of Ki67-positive epithelial cells) of DLP in PTEN$^{(i)pe-/-}$ and control mice over 12 mo after gene ablation. Values are mean of four to eight mice ± SEM. Data are representative of two experiments. **(C)** Relative transcript levels of *Cdkn1a* (*p21*) and *Cdkn2a* (*p16* and *p19ARF*) in the prostate of PTEN$^{(i)pe-/-}$ and control mice over 12 mo after gene ablation. Values are mean from four to eight mice ± SEM. **(D)** Quantification of pHP1γ-positive cells in DLP epithelium of PTEN$^{(i)pe-/-}$ and control mice over 12 mo after gene ablation. Values are mean from four to six mice ± SEM. **(E)** Representative SA-βGal staining (blue) of DLP sections of PTEN$^{(i)pe-/-}$ and control mice sacrificed at indicated time points after gene ablation. Pink, hematoxylin staining. Bars, 250 µm. Four to six mice were analyzed for each time point. ns, not significant, P value ≥ 0.05; *, P value < 0.05; **, P value < 0.01; ***, P value < 0.001; ****, P value < 0.0001.

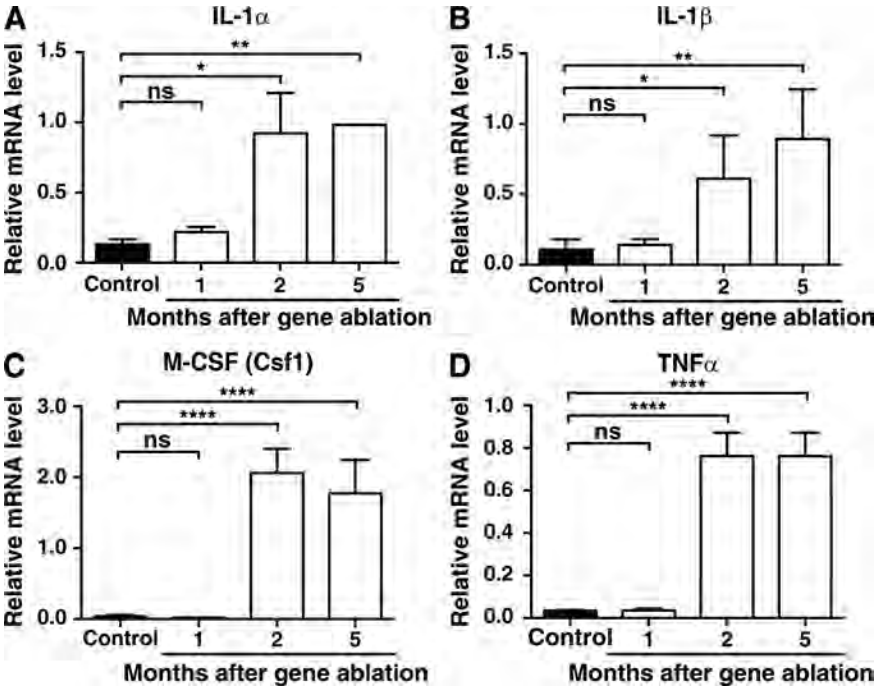

Figure 2. **Characterization of the senescence-associated secretory phenotype in the prostate of PTEN$^{(i)pe-/-}$ mice. (A–D)** Relative transcript levels of *Il-1α* (A), *Il-1β* (B), *M-CSF* (C), and *TNFα* (D) in the prostate of PTEN$^{(i)pe-/-}$ and control mice over 5 mo after gene ablation. Values are mean of four to six mice ± SEM. Data are representative of three experiments. ns, not significant. *, P value < 0.05; **, P value < 0.01; ****, P value < 0.0001.

To further characterize PICS in vivo, we analyzed PTEN$^{(i)pe-/-}$ mice in which *PTEN* is selectively ablated in prostatic luminal cells at adulthood, via the tamoxifen (Tam)-dependent Cre-ER^{T2} system (Ratnacaram et al., 2008). These mice develop slowly progressing PIN lesions with a highly reproducible kinetics. We took advantage of the strict temporal control of *PTEN* ablation in this model to characterize the fate of *PTEN*-deficient PECs. Our study reveals that *PTEN* ablation stimulates proliferation of PECs during several months, followed by a progressive growth arrest with characteristics of cell senescence. Importantly, we also show that proliferating *PTEN*-deficient PECs undergo replication stress and mount a DDR that stabilizes p53. However, as p53 is actively down-regulated at early time by Mdm2, cell senescence is delayed by several months.

Results

PTEN-deficient PECs actively proliferate to generate PINs prior to becoming senescent

To study the consequences of *PTEN* loss in PECs of adult mice, we analyzed PTEN$^{(i)pe-/-}$ and PTEN$^{pe+/+}$ (control) mice over a period of 12 mo after *PTEN* ablation (Fig. S1 A). The prostate weight of PTEN$^{(i)pe-/-}$ mice increased during the first 3 mo after *PTEN* ablation to reach twice that of control mice and remained stable for the following 9 mo (Fig. 1 A). In agreement with previous results (Ratnacaram et al., 2008), the levels of pAKT S473 were enhanced in the prostate of PTEN$^{(i)pe-/-}$ mice, and >75% of the glands in the dorsolateral prostate (DLP) contained PINs between 1 and 12 mo (Fig. S1, B–E). The mitotic index of PECs was approximately four- to fivefold higher in PTEN$^{(i)pe-/-}$ mice than in control mice between 1 and 3 mo, but progressively decreased at a later time (Fig. 1 B). No terminal deoxynucleotidyl transferase dUTP nick end labeling (TUNEL)-positive apoptotic cells were observed in PECs of PTEN$^{(i)pe-/-}$ mice (Fig. S1 F), but transcript levels of the negative regulators of cell cycle progression *Cdkn1a* (*p21*) and *Cdkn2a* (*p16* and *p19ARF*) were markedly increased at 5 mo and 12 mo (Fig. 1 C). In contrast, transcript levels of *p16* and *p19ARF* were similar in PTEN$^{(i)pe-/-}$ and control mice at 1 mo and slightly increased at 2 mo, whereas those of *p21* were increased by 2-fold at 1 mo and by 10-fold at 2 mo (Fig. 1 C). From 2 to 12 mo, >95% PIN cells in DLP of PTEN$^{(i)pe-/-}$ mice displayed nuclear foci of phosphorylated HP1γ (pHP1γ; Fig. 1 D and Fig. S2), indicative of senescence-associated heterochromatin foci (SAHF; Adams, 2007). At 12 mo, most of PIN cells in PTEN$^{(i)pe-/-}$ mice exhibited staining for senescence-associated β-galactosidase (SA-βGal), a well-accepted marker of cell senescence (Dimri et al., 1995; Collado and Serrano, 2006), and ∼20–50% of PIN cells were SA-βGal positive at 2 and 5 mo, respectively (Fig. 1 E). In contrast, at 1 mo, only ∼7% of PEC were pHP1γ-positive in PTEN$^{(i)pe-/-}$ mice, and almost no SA-βGal staining was observed. Transcript levels of several members of the senescence-associated secretory phenotype (SASP; e.g., *IL-1α*, *IL-1β*, *M-CSF*, and *TNFα*) (Pérez-Mancera et al., 2014) were increased by 4- to 15-fold at 2 and 5 mo in the prostate of PTEN$^{(i)pe-/-}$ mice, whereas their levels were similar in control and PTEN$^{(i)pe-/-}$ mice at 1 mo (Fig. 2). Thus, *PTEN* deficiency stimulates the proliferation of PECs within 1 mo to form PINs, which become progressively senescent within the following months.

PTEN deficiency in PECs induces replication stress

Because DDR is an inducer of OIS (Bartkova et al., 2006; Di Micco et al., 2006; Mallette et al., 2007), we investigated the levels of phosphohistone H2AX S139 (γH2AX), a faithful marker of DDR activation (Rogakou et al., 1998; Mah et al., 2010). Western blot analysis showed increased levels of γH2AX in DLP extracts of PTEN$^{(i)pe-/-}$ mice at 1 mo (Fig. S3 A), and immunohistological analyses revealed that most PECs in DLP of PTEN$^{(i)pe-/-}$ mice present a nuclear staining of γH2AX, whereas no staining was observed in the prostatic epithelium of age-matched control

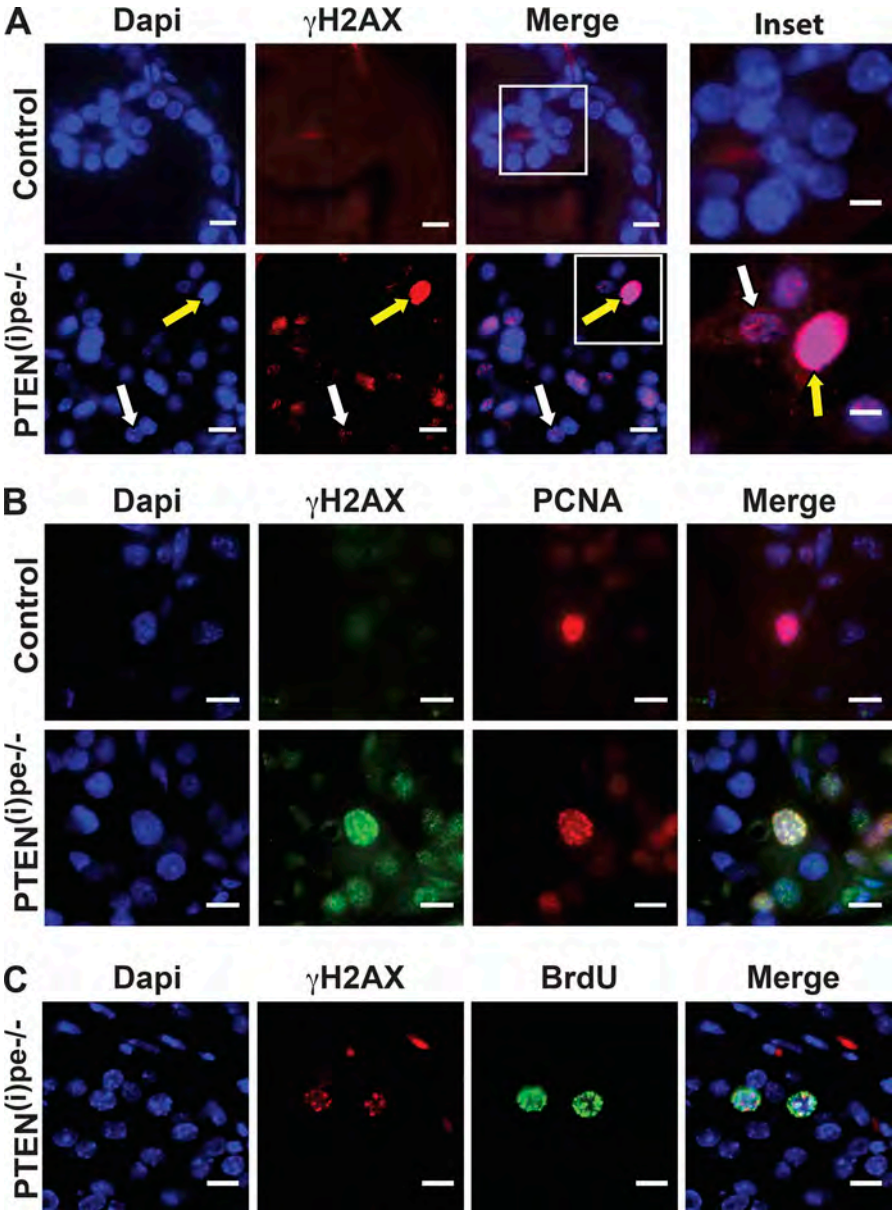

Figure 3. **Characterization of replication stress in *PTEN*-deficient PECs. (A)** Representative γH2AX immunofluorescence staining (red) of DLP sections of PTEN$^{(i)pe-/-}$ and control mice sacrificed 1 mo after gene ablation. Yellow arrow, example of γH2AX-high staining; white arrow, example of γH2AX-low staining. **(B)** Representative immunofluorescence staining of γH2AX (green) and PCNA (red) of a DLP section of a PTEN$^{(i)pe-/-}$ and of a control mouse sacrificed 1 mo after gene ablation. **(C)** Representative immunofluorescence staining of γH2AX (red) and BrdU (green) of a DLP section of a PTEN$^{(i)pe-/-}$ mouse sacrificed 1 mo after gene ablation. Blue, Dapi. Bars: main images, 10 µm; insets, 5 µm. Four PTEN$^{(i)pe-/-}$ mice and four control mice were analyzed.

mice (Fig. 3 A). Although most cells displayed numerous small nuclear foci, ∼5% of the cells exhibited a very intense γH2AX nuclear staining (γH2AX-high), and often, no individual γH2AX foci could be distinguished in these cells (Fig. 3 A). Importantly, γH2AX-high PECs stained positive for the proliferation marker PCNA (Fig. S3 B), and individual γH2AX foci colocalized with foci of PCNA (Fig. 3 B). In contrast, no γH2AX foci were observed in PCNA-positive PECs of age-matched control mice. Therefore, in γH2AX-high PECs, γH2AX foci are localized at the vicinity or at the site of DNA replication, which is characteristic of replication stress (Ward and Chen, 2001). In addition, labeling of DNA-replicating cells with BrdU revealed that all γH2AX-high PECs were BrdU-positive in PTEN$^{(i)pe-/-}$ mice (Fig. 3 C). Moreover, at 1 and 2 mo, PECs of PTEN$^{(i)pe-/-}$ mice displayed numerous nuclear foci of RPA32, a subunit of the single-stranded genomic DNA (ssDNA) complex replication protein A (RPA) that coats stretches of ssDNA in replication stress (Branzei and Foiani, 2005; Byun et al., 2005), although such foci were rarely observed in prostatic epithelial cells of age-matched control mice (Fig. 4 A and not depicted). RPA phosphorylation at various sites occurs at stalled replication forks, and DNA double strand breaks (DSB) produced from stalled DNA replication induce phosphorylation of RPA32 at S4 and S8 (Liaw et al., 2011; Sirbu et al., 2011). Interestingly, at 1 mo, many PEC nuclei of PTEN$^{(i)pe-/-}$ mice contained high levels of S4/S8 phosphorylated RPA32 (Fig. 4 B), indicating that DSB follow replication fork stalling. Numerous nuclear foci of ATR (Ataxia telangiectasia and Rad3-related) and 53BP1 (p53-binding protein 1) were also observed in PECs of PTEN$^{(i)pe-/-}$ mice, whereas none were observed in PECs of age-matched control mice (Fig. 4, C and D), further supporting activation of DDR signaling (Cortez et al., 2001; Lukas et al., 2011). Together these results show that replication stress-mediated DDR signaling is induced in proliferating *PTEN*-deficient PECs. In agreement with the DDR mediating senescence induction, discrete foci of γH2AX were present in most PIN cells of PTEN$^{(i)pe-/-}$ mice at 5 mo (Fig. S3 C), similar to long term γH2AX foci observed in OIS (Rodier et al., 2011).

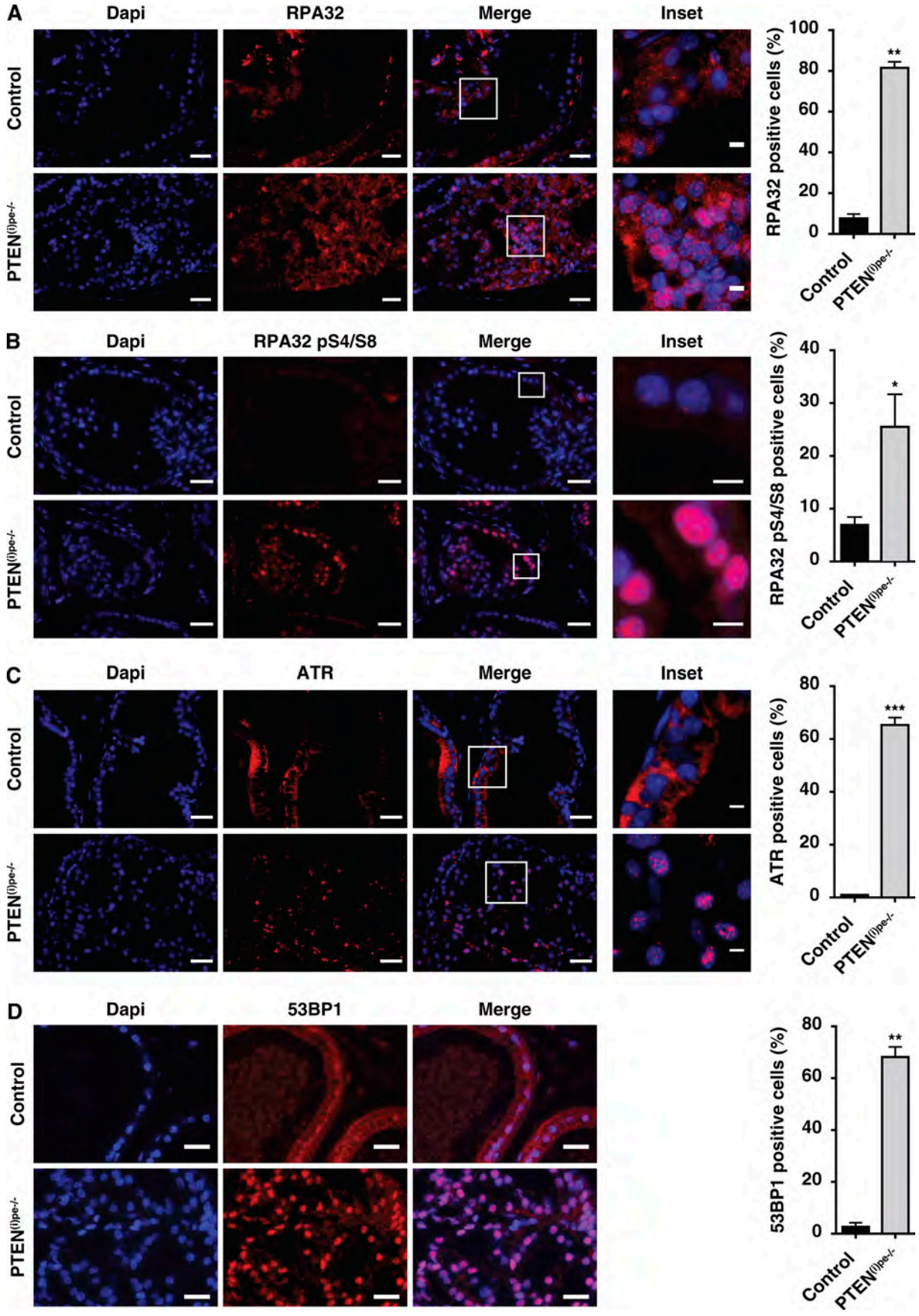
A
Dapi
RPA32
Merge
Inset
Control
PTEN(i)pe-/-
RPA32 positive cells (%)
100
80
60
40
20
0
**
Control
PTEN(i)pe-/-
B
Dapi
RPA32 pS4/S8
Merge
Inset
Control
PTEN(i)pe-/-
RPA32 pS4/S8 positive cells (%)
40
30
20
10
0
*
Control
PTEN(i)pe-/-
C
Dapi
ATR
Merge
Inset
Control
PTEN(i)pe-/-
ATR positive cells (%)
80
60
40
20
0
***
Control
PTEN(i)pe-/-
D
Dapi
53BP1
Merge
Control
PTEN(i)pe-/-
53BP1 positive cells (%)
80
60
40
20
0
**
Control
PTEN(i)pe-/-

DDR stabilizes p53 in proliferating PECs of PTEN$^{(i)pe-/-}$ mice.
Because p53 can be stabilized by the DDR (Meek, 2009), we immunodetected p53. Nuclear accumulation of p53 was observed in >90% PECs of PTEN$^{(i)pe-/-}$ mice at 2 mo, whereas almost all PECs displayed nuclear p53 at 5 and 12 mo (Fig. 5 A and Fig. S4 A). No p53-positive nuclei were detected in prostate epithelium of control mice at any time point. Therefore, *PTEN* ablation induced nuclear accumulation of p53 in PECs within 2 mo and up to 12 mo. In contrast, at 1 mo, only ∼6% of PECs were p53-positive in PTEN$^{(i)pe-/-}$ mice (Fig. 5 A and Fig. S4 A), and most of them were Ki67- and BrdU-positive (Fig. 5 B and Fig. S4 B). This is in agreement with the slightly increased expression of the p53-target gene p21 at 1 mo (Fig. 1 C) and shows that activation of p53 signaling precedes senescence.

Activation of the DDR increases p53 stability and its transcriptional activity through phosphorylation of its serine 15 (Meek, 2009). p53 pS15 nuclear staining was observed in ∼5% PECs of PTEN$^{(i)pe-/-}$ mice at 1 mo, and these cells also stained for the proliferation marker Ki67 (Fig. 5 C). Therefore, p53 is stabilized in proliferating PECs of PTEN$^{(i)pe-/-}$ mice by a DDR-mediated pathway.

p53 stabilization is counteracted by the protein kinase B (AKT)–Mdm2 axis.
To investigate the role of p53 in the control of senescence induced by *PTEN* loss, we administered Tam to 8-wk-old PSA-CreER^{T2} mice bearing LoxP-flanked *PTEN* and *p53* alleles to generate PTEN/p53$^{(i)pe-/-}$ mice in which both *PTEN* and *p53* are ablated in PECs at adulthood.

As expected, no nuclear staining for p53 was observed in PECs of PTEN/p53$^{(i)pe-/-}$ mice (Fig. S4, C and D). At 1 and 2 mo, the prostate weights were similar in PTEN/p53$^{(i)pe-/-}$ and in PTEN$^{(i)pe-/-}$ mice (Fig. 6 A). The mitotic index of PECs was similar in PTEN/p53$^{(i)pe-/-}$ and PTEN$^{(i)pe-/-}$ mice at 1 mo, but was higher in PTEN/p53$^{(i)pe-/-}$ mice than in PTEN$^{(i)pe-/-}$ at 2, 5, and 6 mo (Fig. 6 B). At 5 and 6 mo, the prostate weight was threefold higher in PTEN/p53$^{(i)pe-/-}$ than in PTEN$^{(i)pe-/-}$ mice (Fig. 6 A). Whereas PIN lesions in DLP were similar in PTEN/p53$^{(i)pe-/-}$ and in PTEN$^{(i)pe-/-}$ mice at 1 and 2 mo, they were more severe in PTEN/p53$^{(i)pe-/-}$ mice than in PTEN$^{(i)pe-/-}$ mice at 5 and 6 mo with, in some cases, a loss of prostate epithelium architecture (compare Fig. 6 C and Fig. S1 C). Therefore, *p53* ablation does not affect early stimulation of *PTEN*-null PEC proliferation and PIN formation, but impairs their subsequent growth arrest.

Di Mitri et al. reported that GR1-positive myeloid cells infiltrate the prostate of PTEN$^{pe-/-}$ mice and secrete the cytokine IL-1RA, an antagonist of IL-1R, which opposes PICS in a paracrine fashion (Di Mitri et al., 2014). FACS analysis of dissociated prostates of PTEN$^{(i)pe-/-}$ mice revealed that GR-1–positive myeloid cells represent ∼2.5–3% of all prostatic cells at 2 and 5 mo after *PTEN* ablation, but <0.07% at 1 mo in both in PTEN$^{(i)pe-/-}$ and control mice (Fig. 7 A). Moreover, the transcript levels of the marker of the myeloid lineage *CD11b*, and of *Ly6g* and *Ly6c*, the two GR-1 variants, were increased in PTEN$^{(i)pe-/-}$ mice at 2 and 5 mo, but not at 1 mo (Fig. 7, B–D). In agreement with these results, the transcript levels of *IL-1rn*, coding for IL-1RA protein, were markedly increased at 2 and 5 mo in the prostate PTEN$^{(i)pe-/-}$ mice, whereas they were similar in control and PTEN$^{(i)pe-/-}$ mice at 1 mo (Fig. 7 E). Therefore, IL-1RA–producing GR-1–positive cells cannot account for the delay of PEC senescence entry induced by *PTEN* ablation.

In unstressed cells, p53 is maintained at low level by proteasomal degradation through mouse double-minute 2 (Mdm2)-mediated polyubiquitylation (Rodriguez et al., 2000). Stabilization of p53 involves the dissociation of p53 from Mdm2 through modifications of p53, including phosphorylation by DDR kinases ATR or ATM. Once stabilized, p53 translocates to the nucleus, whereas Mdm2 is submitted to proteasomal degradation. At 1 mo, high levels of Mdm2 were present in the nuclei of pAKT S473–positive PECs of PTEN$^{(i)pe-/-}$ mice (Fig. 8 A). Moreover, Mdm2-positive cells were p53-negative, and p53 was only detected in Mdm2-low cells (Fig. 8 B). To demonstrate that Mdm2 was involved in p53 degradation at early time, PTEN$^{(i)pe-/-}$ mice were treated with Nutlin-3, an inhibitor of Mdm2–p53 interaction (Vassilev et al., 2004) 1 mo after *PTEN* ablation. Our results show that Nutlin-3a treatment increases p53 protein levels in prostatic epithelial cells and enhances the transcript levels of p53 target gene *p21* (Fig. 8, C–E). Thus, low p53 levels at early time result from Mdm2-mediated p53 degradation.

Because AKT can phosphorylate Mdm2 at several serine residues (S166 and S186 in human, equivalent to S163 and S183, in mouse), inducing its nuclear translocation and accumulation (Feng et al., 2004; Wei et al., 2013), and increasing both its association and E3 ligase activity toward p53 (Ashcroft et al., 2002; Mayo et al., 2002; Ogawara et al., 2002), AKT might promote Mdm2-mediated p53 proteasomal degradation in PECs of PTEN$^{(i)pe-/-}$ mice. Importantly, most nuclei of PECs were Mdm2 pS163–positive at 1 mo, whereas Mdm2 pS163 was not immunodetected in normal prostate epithelium of PTEN$^{(i)pe-/-}$ mice and of control mice (Fig. 9 A and not depicted). The level of Mdm2 pS163 decreased, however, between 1 and 2 mo, while p53 increased and was detected in most cells at 5 mo, whereas Mdm2 pS163 was detected no more (Fig. 9 A and Fig. 5 A). Moreover, because Casein Kinase I (CKI) family members have been shown to phosphorylate N-terminal sites of p53 and to decrease p53 affinity to Mdm2, and because phosphorylation of Mdm2 by CKIδ leads to Mdm2 degradation and p53 expression (Knippschild et al., 2014), we determined their transcript levels in *PTEN*-deficient PINs at various time points. Interestingly, the transcript levels of *CKIα*, *-δ*, *-γ*, and *-ε* were induced 3 and 5 mo after gene invalidation, and at 5

Figure 4. **Immunodetection of DDR markers in *PTEN*-deficient PECs. (A)** Representative immunofluorescence staining of RPA32 (red) of DLP sections of PTEN$^{(i)pe-/-}$ or control mice sacrificed 2 mo after gene ablation. **(B)** Representative RPA32 pS4/S8 immunofluorescence staining (red) of DLP sections of PTEN$^{(i)pe-/-}$ and control mice sacrificed 1 mo after gene ablation. **(C)** Representative ATR immunofluorescence staining (red) of DLP sections of PTEN$^{(i)pe-/-}$ and control mice sacrificed 2 mo after gene ablation. **(D)** Representative immunofluorescence staining of 53BP1 (red) of DLP sections of PTEN$^{(i)pe-/-}$ or control mice sacrificed 2 mo after gene ablation. Blue, Dapi. Bars: main images, 20 µm; insets, 5 µm. Four PTEN$^{(i)pe-/-}$ mice and four control mice were analyzed. A quantification of immunolabeled epithelial cells is shown in each panel. *, P value < 0.05; **, P value < 0.01; ***, P value < 0.001.

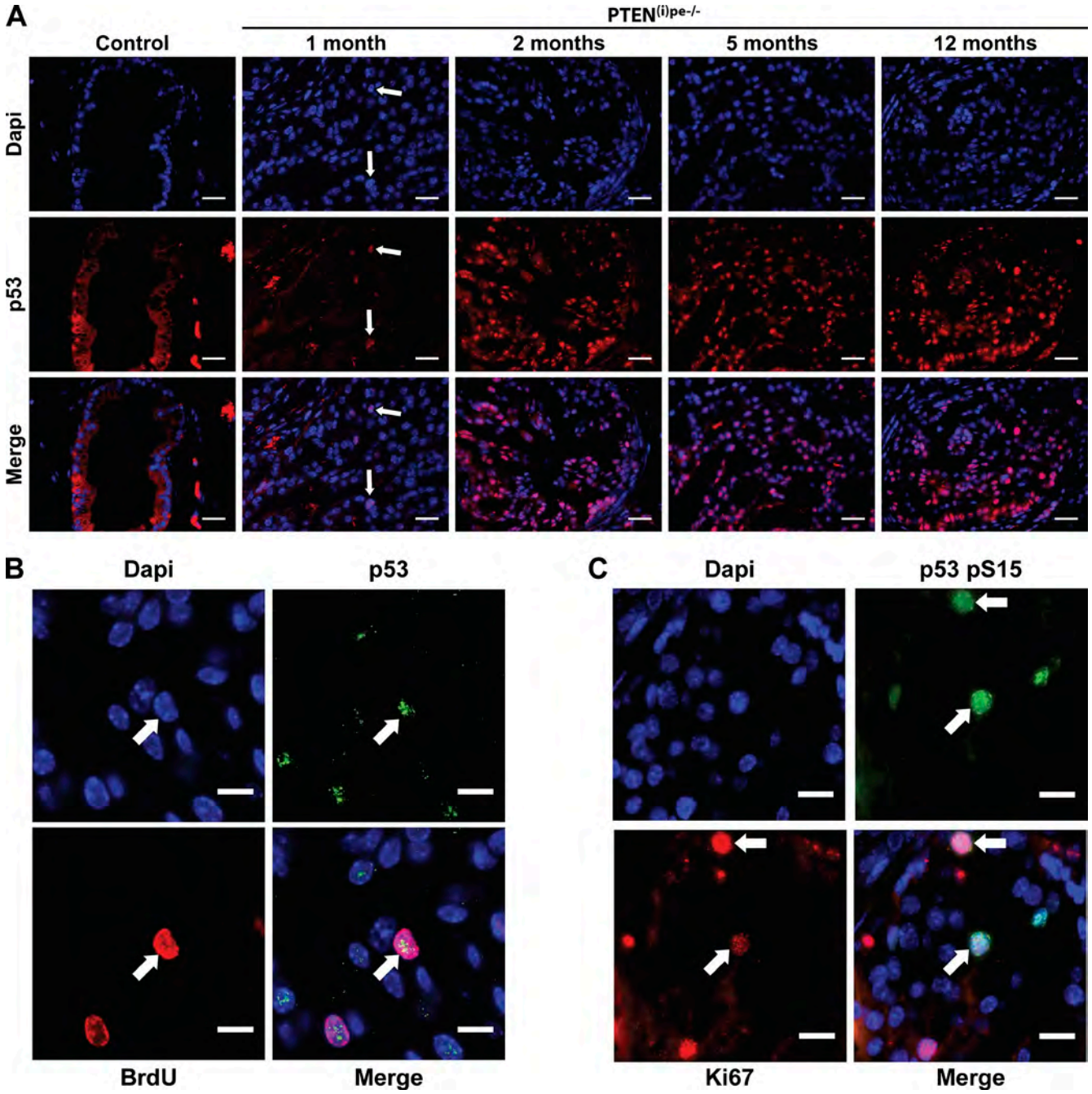

Figure 5. **Characterization of p53-positive *PTEN*-deficient PECs. (A)** Representative p53 immunofluorescence staining (red) of DLP sections of PTEN$^{(i)pe-/-}$ and control mice sacrificed at indicated time points after gene ablation. White arrow, example of a stained nucleus at 1 mo. **(B)** Representative BrdU (red) and p53 (green) immunofluorescence staining of DLP sections of PTEN$^{(i)pe-/-}$ and control mice sacrificed 1 mo after gene ablation. White arrow, example of a double-stained nucleus. **(C)** Representative p53 pS15 (green) and Ki67 (red) immunofluorescence staining of DLP sections of PTEN$^{(i)pe-/-}$ and control mice sacrificed 1 mo after gene ablation. White arrow, example of a double-stained nucleus. Blue, Dapi. Bars: 25 µm (A); 10 µm (B and C). Four PTEN$^{(i)pe-/-}$ mice and four control mice were analyzed.

mo, the transcript levels of *CKIε* correlated with *p21* levels (Fig. 9, B and C; and Fig. S5).

Thus, as DNA damage has been shown to induce the interaction between Mdm2 and CKI (Inuzuka et al., 2010), it is likely that 3 mo after *PTEN* ablation, CKI-mediated Mdm2 degradation, and/or decreased binding of Mdm2 to p53 overcomes early Mdm2 activation and contributes to p53 stabilization.

Discussion

We show here that *PTEN* ablation in PECs of adult mice induces PINs formation, the progression of which is antagonized by a cell senescence barrier, in agreement with previous studies (Chen et al., 2005; Di Mitri et al., 2014). Because PTEN knockdown in cultured cells was shown to induce a rapid senescence state in the absence of proliferation and DDR, in contrast to OIS

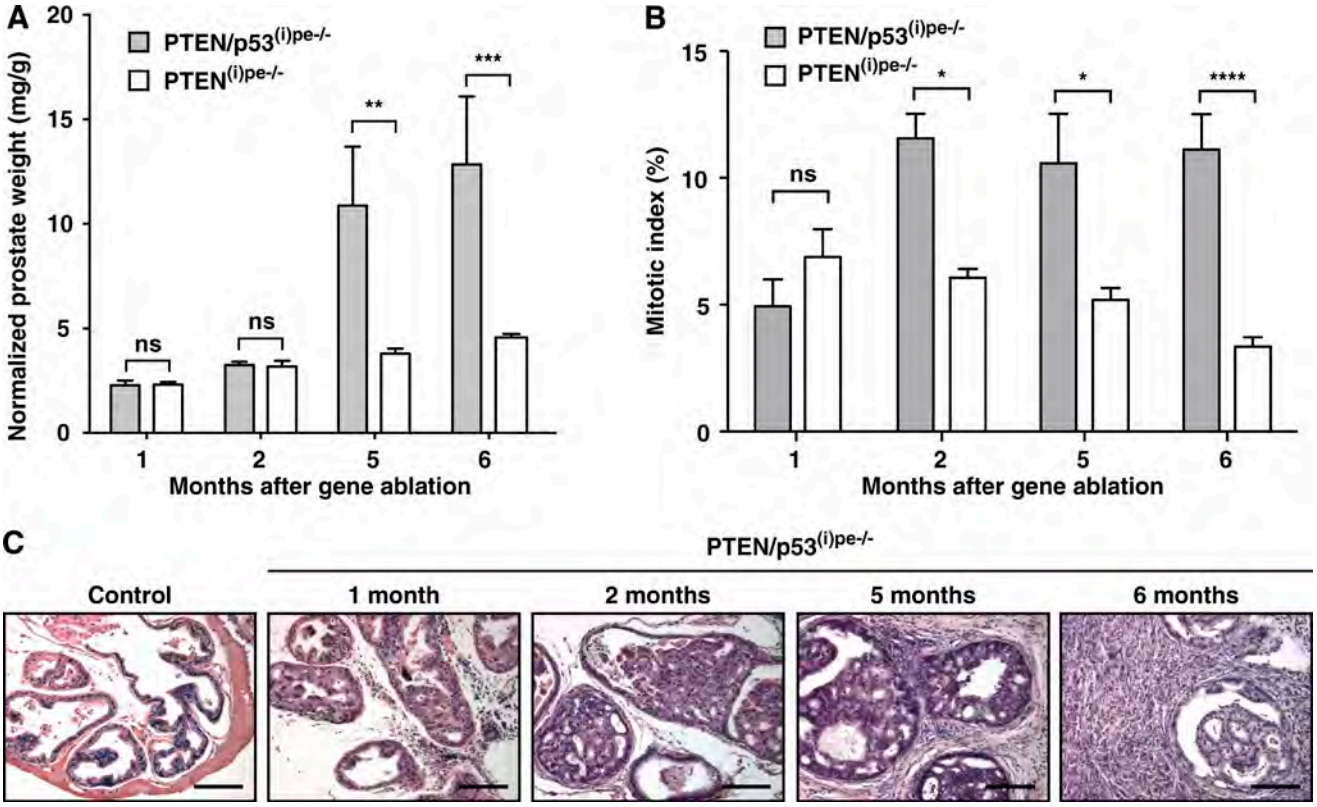

Figure 6. **Prostate tumor evolution in PTEN/p53$^{(i)pe-/-}$ mice. (A)** Evolution of normalized prostate weight (prostate weight over body weight) in PTEN$^{(i)pe-/-}$ and PTEN/p53$^{(i)pe-/-}$ mice over 6 mo after gene ablation. Values are mean from of four to eight mice ± SEM. **(B)** Proliferation index (percentage of Ki67-positive cells) of DLP epithelial cells in PTEN$^{(i)pe-/-}$ and PTEN/p53$^{(i)pe-/-}$ mice over 6 mo after gene ablation. Values are mean from of four to eight mice ± SEM. **(C)** Representative views of DLP sections of PTEN/p53$^{(i)pe-/-}$ and control mice sacrificed at 1, 2, and 5 mo after gene ablation and of DLP sections of PTEN/p53$^{(i)pe-/-}$ mice with large tumors, sacrificed 6 mo after gene ablation. Sections were stained with H&E. Bars, 125 µm. Four to eight PTEN/p53$^{(i)pe-/-}$ mice per time point and eight control mice were analyzed. ns, not significant, P value ≥ 0.05; *, P value < 0.05; **, P value < 0.01; ***, P value < 0.001; ****, P value < 0.0001.

(Alimonti et al., 2010; Astle et al., 2012), it was proposed that PICS is a new type of senescence. Moreover, it was shown that PICS is antagonized by IL-1RA secreted by infiltrated GR1-positive myeloid cells, allowing proliferation of a subset of *PTEN*-deficient PECs and, thereby, PIN formation (Alimonti et al., 2010; Di Mitri et al., 2014).

We demonstrate here that GR1-positive cells and IL-1RN are not present in the prostate 1 mo after *PTEN* ablation in PTEN$^{(i)pe-/-}$ mice and, thus, cannot contribute to the high proliferation rate and the absence of senescence markers at this stage. Therefore, we conclude that the first temporal consequence of *PTEN* ablation in mouse PECs is to increase their rate of proliferation, allowing PIN formation in most prostate ducts within 1 mo. Signs of senescence are observed only later, after several weeks of active proliferation.

Unlike previous studies (Alimonti et al., 2010; Astle et al., 2012), *PTEN* ablation in PECs induced γH2AX nuclear foci, clearly reflecting activation of the DDR. Our results are in agreement with a previous study showing that PTEN knock-down in human-immortalized fibroblasts induces cell senescence with accumulation of γH2AX foci (Kim et al., 2007). Importantly, proliferating PECs in PTEN$^{(i)pe-/-}$ mice displayed a very strong γH2AX staining, with numerous intense foci, and presented characteristics of replication stress, including accumulation of foci of RPA32 and RPA32 pS4/S8, as well as ATR, the DDR kinase activated by replication stress and a major effector of replication stress–mediated DDR (Mazouzi et al., 2014).

ATR can phosphorylate p53 S15 directly or via activation of CHK1 (Mazouzi et al., 2014), and our results show that actively proliferating cells exhibit a nuclear staining for p53 pS15 and that p53 mainly accumulates in Ki67-positive and BrdU-positive PECs. Therefore, p53 is stabilized by replication stress–mediated DDR activation in *PTEN*-deficient PECs, and replication stress–mediated p53 activation contributes to trigger senescence, as in OIS (Bartkova et al., 2006; Bartek et al., 2007).

In addition, we show that Mdm2 accumulates in the nuclei of AKT pS473–positive PECs at 1 mo and that nuclear Mdm2 is phosphorylated at S163. It is well documented that Mdm2 can be phosphorylated at S163 by AKT, resulting in its translocation in the nucleus, while it increases its E3-ligase activity toward p53 and thus down-regulates p53 (Mayo and Donner, 2001; Mayo et al., 2002; Ogawara et al., 2002; Feng et al., 2004; Fenouille et al., 2011). It has been shown that *PTEN* ablation in mouse cells and tissue results in a dramatic decrease of p53 expression (Freeman et al., 2003), and pharmacological inhibition of PI3K prevents p53 activation by DNA damage (Bar et al., 2005). Moreover, activation of AKT by Her2 in breast cancer cells increases Mdm2-mediated p53 degradation via AKT-mediated Mdm2 phosphorylation on S163 (Zhou et al., 2001). Importantly, we show that early p53 degradation in *PTEN*-deficient PECs is mediated by Mdm2 and

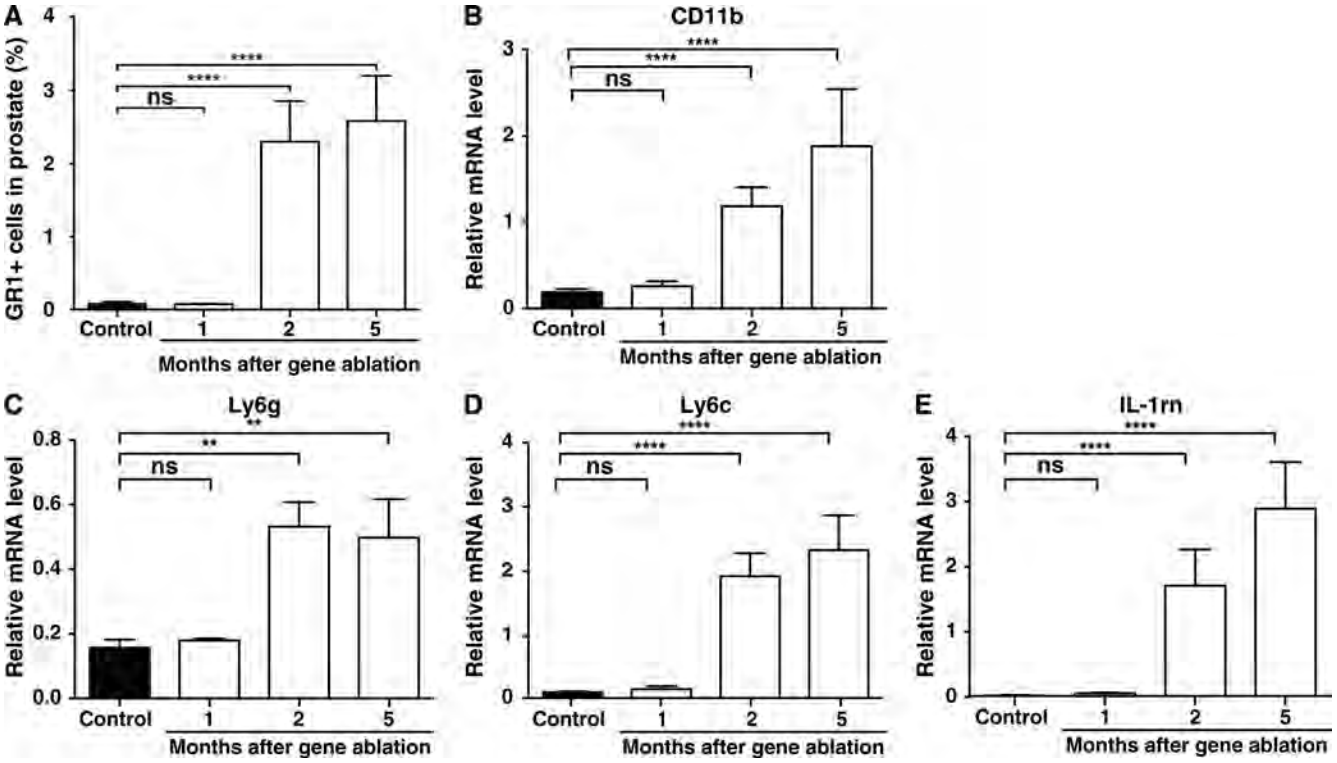

Figure 7. **Characterization of GR1-positive myeloid cells and *IL1rn* expression during PIN evolution in PTEN$^{(i)pe-/-}$ mice. (A)** FACS quantification of GR1-positive myeloid (CD11b-positive) cells in the prostate of PTEN$^{(i)pe-/-}$ and control mice (percentage of the total cells in dissociated prostates) sacrificed at the indicated time points after gene ablation. **(B–E)** Values are mean of three to six mice ± SEM. Relative transcript levels of *CD11b* (B), *Ly6g* (C), *Ly6c* (D) and *IL-1rn* (E) in the prostate of PTEN$^{(i)pe-/-}$ and control mice sacrificed at indicated time points after gene ablation. Values are mean of four to ten mice ± SEM. ns, not significant, P value ≥ 0.05; **, P value < 0.01; ****, P value < 0.0001.

provide evidence that CKI contributes to p53 stabilization at later time. We thus propose that *PTEN* loss has two simultaneous and opposed consequences. Besides initiating a senescence program through replication stress mediated activation of the DDR and p53 stabilization, AKT activation induced by *PTEN* ablation contributes to delay senescence via enhanced Mdm2-mediated p53 degradation.

An important characteristic of our mouse model is the possibility to strictly control the time of floxed genes ablation by induction of the CreER^{T2} recombinase activity. In other models, *PTEN* ablation occurs in the undifferentiated prostate of young mice (Chen et al., 2005; Alimonti et al., 2010), because of the early activity of the Pb-4 promoter (in the prostate bud of the newborn) that drives the expression of a constitutively active Cre recombinase (Wu et al., 2001). As we induced Cre-mediated recombination selectively in luminal prostatic epithelial cells after puberty, *PTEN* was ablated in a fully developed prostate and well-differentiated PECs. It was shown that PIN development is accelerated when *PTEN* is ablated before puberty (Luchman et al., 2008). Thus, the lower proliferation rate of PECs in our model, which reaches a maximum of ∼10%, although it reaches ∼40% in previously studied models (Chen et al., 2005; Alimonti et al., 2010), might contribute to the slow establishment of cell senescence, as replication stress might be less intense.

Our results diverge from several published studies on PICS. The discrepancy between our observations made in vivo in epithelial cells and in vitro results obtained in nonepithelial cells (Alimonti et al., 2010; Astle et al., 2012) might result from the obvious growth conditions differences. Indeed, in vitro cell culture conditions induce cellular stress, because partial O_2 pressure is much higher in culture medium than in tissues, and because high levels of growth factors push the cells to actively proliferate (Serrano and Blasco, 2001). Thus, cells in culture might induce pathways to cope with such stress conditions. In any event, our data highlight that in vitro data on senescence should not be extrapolated to in vivo situations.

As we demonstrate here that *PTEN* loss–induced cell senescence in prostate epithelial cells is mediated at least in part by replication stress after a phase of enhanced proliferation in vivo, this type of senescence resembles other types of senescence, in particular OIS, in contrast to previous conclusions drawn from others (Alimonti et al., 2010). Thus, approaches for cancer prevention and therapy based on PICS induction are at risk, because replication stress induced by *PTEN* loss might result in an accumulation of mutations, including of *p53*, before p53 is stabilized and senescence initiated, and/or in senescent cells, leading to senescence escape and formation of adenocarcinoma. Supporting this idea, *p53* mutations cooccur with *PTEN* mutations in a high proportion of advanced prostate tumors (Chen et al., 2005; Lotan et al., 2011; Markert et al., 2011).

In contrast, selective inhibitors of AKT or of Mdm2-p53 interaction might enforce senescence and prevent or delay prostate cancer progression. However, the safest approach remains probably the elimination of senescent cells.

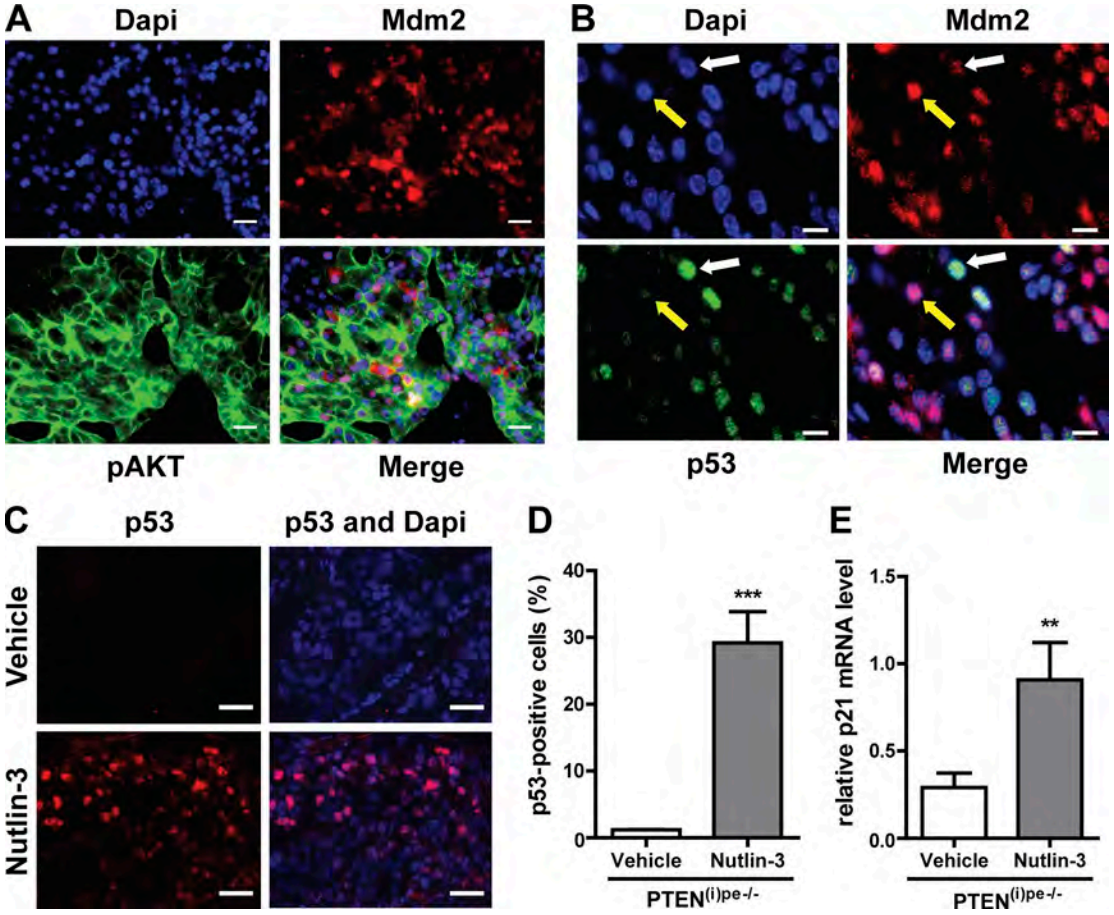

Figure 8. **Characterization of Mdm2 expression in the prostate of PTEN$^{(i)pe-/-}$ mice. (A)** Representative pAKT S473 (green) and Mdm2 (red) immunofluorescence staining of DLP sections of a PTEN$^{(i)pe-/-}$ mouse sacrificed 1 mo after gene ablation. Blue, Dapi. Four mice were analyzed. **(B)** Representative p53 (green) and Mdm2 immunofluorescence staining (red) of DLP sections of a PTEN$^{(i)pe-/-}$ mouse sacrificed 1 mo after gene ablation. Four mice were analyzed. **(C)** Representative p53 immunofluorescence staining (red) of DLP sections of PTEN$^{(i)pe-/-}$ mice treated with vehicle- and Nutlin-3 1 mo after gene ablation (n = 3 for each condition). Blue, Dapi. Bars: 20 µm (A and C); 10 µm (B). Data are representative of two experiments; n = 3 vehicle and n = 3 Nutlin-treated PTEN$^{(i)pe-/-}$ mice. **(D)** Quantification of p53 positive epithelial cells in PINs of PTEN$^{(i)pe-/-}$ mice treated 1 mo after gene ablation with vehicle and Nutlin-3. Data are cumulative of two experiments; n = 3 for each group. Unpaired-t test. ***, P value < 0.001. **(E)** Relative transcript levels of *p21* in the DLP and AP of vehicle- and Nutlin-3 treated PTEN$^{(i)pe-/-}$ mice. n = 7 vehicle and n = 8 Nutlin-3 treated PTEN$^{(i)pe-/-}$ mice. Unpaired-t test. **, P value <0.01.

Materials and methods

Mouse care

Mice were maintained in a temperature- and humidity-controlled animal facility with a 12 h light/dark cycle. Breeding and maintenance of mice were performed in the accredited IGBMC/ICS animal house (C67-2018-37), in compliance with French and EU regulations on the use of laboratory animals for research, under the supervision of D. Metzger who holds animal experimentation authorizations from the French Ministry of Agriculture and Fisheries (Nos. 67-209 and A 67-227). All animal experiments were approved by the Ethical committee Com'Eth (Comité d'Ethique pour l'Expérimentation Animale, Strasbourg, France). Animals were euthanized with carbon dioxide and cervical dislocation, and tissues were immediately collected, weighed and frozen in liquid nitrogen, or processed for biochemical and histological analysis.

Generation of mouse cohorts

PTEN$^{(i)pe-/-}$ mice were generated as described (Ratnacaram et al., 2008). In brief, mice carrying one copy of the PSA-Cre-ER^{T2} transgene, expressing the Tam-inducible Cre-ER^{T2} recombinase in prostate epithelium under the control of the human PSA promoter, were crossed with mice carrying LoxP-flanked (floxed) alleles of *PTEN* (L2 allele; a gift from T. Mak, Campbell Family Institute for Breast Cancer Research, Toronto, Canada, and A Suzuki, Akita University School of Medicine, Akita, Japan) to generate PSA-Cre-ER$^{T2(tg/0)}$/PTEN$^{L2/L2}$ (tg, transgenic) and PSA-Cre-ER$^{T2(0/0)}$/PTEN$^{L2/L2}$ mice. PTEN/p53$^{(i)pe-/-}$ mice were generated by intercrossing PSA-Cre-ER$^{T2(tg/0)}$/PTEN$^{L2/L2}$ mice with p53$^{L2/L2}$ mice carrying floxed alleles of *p53* (a gift of A. Berns, The Netherlands Cancer Institute, Amsterdam, Netherlands; Jonkers et al., 2001) to generate PSA-Cre-ER$^{T2(tg/0)}$/PTEN$^{L2/L2}$/p53$^{L2/L2}$ and PSA-Cre-ER$^{T2(0/0)}$/PTEN$^{L2/L2}$/p53$^{L2/L2}$ mice. Gene ablation was induced by intraperitoneal injection of Tam performed daily for 5 d (1 mg/mouse) to 8- to 10-wk-old mice, as described (Fig. S1 A; Metzger et al., 2005), to generate mutant PTEN$^{(i)pe-/-}$ and PTEN/p53$^{(i)pe-/-}$ mice. Respective control mice (PTEN$^{pe+/+}$ and PTEN/p53$^{pe+/+}$) did not bear the PSA-Cre-ER^{T2} transgene (pe, prostate epithelium; (i), induced).

PSA-Cre-ER^{T2}, PTEN$^{L2/L2}$, and p53$^{L2/L2}$ mice were backcrossed on C57BL/6 mice for more than eight generations before

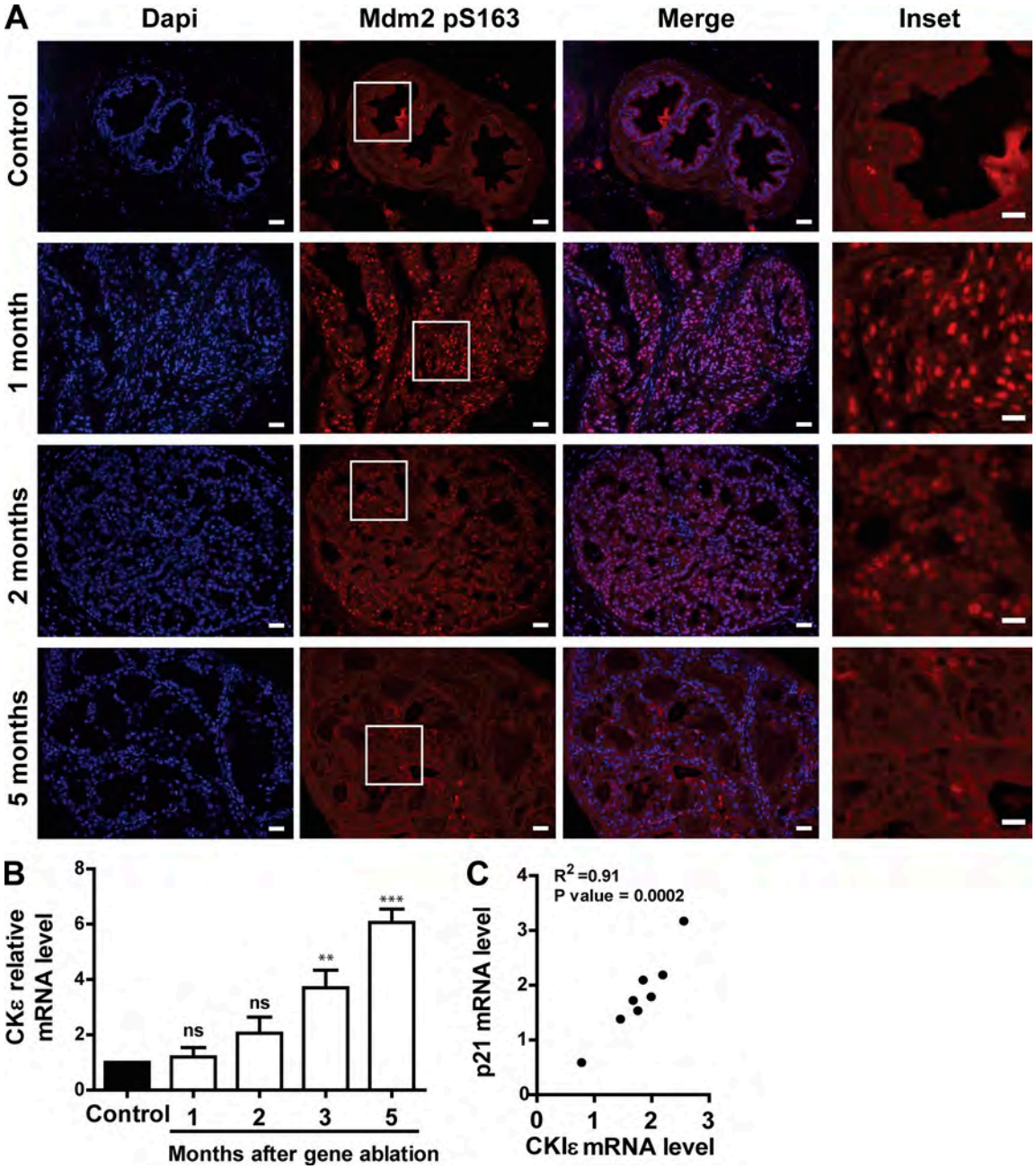

Figure 9. **Immunodetection of Mdm2 pS163 and quantification of *CKIε* and *p21* transcript levels in DLP of PTEN$^{(i)pe-/-}$ mice. (A)** Representative Mdm2 pS163 (red) immunofluorescence staining of DLP sections of control and PTEN$^{(i)pe-/-}$ mice sacrificed at the indicated time after gene ablation. Blue, Dapi. Bars: main images, 40 µm; insets, 10 µm. Data are representative of three experiments with $n = 3$ mice per time point and two prostate sections per mouse. **(B)** Transcript levels of *CKIε* in the DLP and AP of PTEN$^{(i)pe-/-}$ and control mice at the indicated time points. $n = 3$ for control mice at 5 mo and $n = 4$, $n = 4$, $n = 4$, $n = 3$, and $n = 8$ for PTEN$^{(i)pe-/-}$ mice at 1, 2, 3, and 5 mo after gene ablation, respectively. Bars represent the mean ± SEM. One way ANOVA. ns; not significant; **, P < 0.01; ***, P < 0.001. **(C)** Correlation between *p21* and *CKI1ε* transcript levels in the prostate of PTEN$^{(i)pe-/-}$ mice 5 mo after *PTEN* ablation.

intercrossing. Mice were genotyped by PCR performed on genomic DNA isolated from ear biopsies, using the DirectPCR extraction kit (102-T; Viagen) and primers as described (Jonkers et al., 2001; Ratnacaram et al., 2008).

Treatment of mice

Control and PTEN$^{(i)pe-/-}$ mice were administered i.p. with 5-bromo-2'-deoxyuridine (BrdU, Sigma-Aldrich) at 50 mg/kg in 100 µl of sterile saline solution (0.9% NaCl), 3 h before sacrifice. 1 mo after gene ablation, PTEN$^{pe-/-}$ mice were treated (i.p.) with Nutlin-3 (daily 100 mg/kg; AdooQ Biosciences) or vehicle for 2 d and sacrificed 4 h after the last administration.

Histological analysis

Prostate tissue samples were immediately fixed in ice-cold 4% formaldehyde supplemented with 1 tablet/10 ml of PhoSTOP (04 906 837 001; Roche). Prostate samples were embedded in paraffin, and 5-µm serial sections were cut. For histopathological

analyses, paraffin sections were stained with H&E. For immunofluorescence staining, sections were processed as previously described (Ratnacaram et al., 2008), except that sections were incubated over night with primary antibodies diluted 1:200, unless indicated. Primary antibody used for immunofluorescence were directed against AKT pS473 (4060; Cell Signaling Technology), γH2AX (05-636; EMD Millipore; 1:600), p53 (CM5; Vector Labs), p53 pS15 (12571; Cell Signaling Technology), pHP1γ (2600; Cell Signaling Technology), RPA32 (GTX113004; Tebu-Bio), RPA32 pS4/S8 (A300-245A; Bethyl Laboratories), ATR (2790; Cell Signaling Technology), Ki67 (M7248; Dako), BrdU (600-401-C29; Rockland), ATM pS1966 (200-301-400; Rockland), Mdm2 (sc-965; Santa Cruz Biotechnology), Mdm2 pS166 (human)/pS163 (mouse; 3521; Cell Signaling Technology), PCNA (ab2426; AbCam), 53BP1 (NB100-305; Novus Biologicals). Secondary antibodies (CY3 AffiniPure goat anti–rabbit IgG [H+L], CY3 AffiniPure goat anti–mouse IgG [H+L], CY5 AffiniPure goat anti–mouse IgG [H+L], and CY5 AffiniPure donkey anti–rabbit IgG [H+L]) were from Jackson Immunoresearch.

SA-βGal staining

10-µm frozen prostate sections were cut, fixed in 2% formaldehyde and 0.2% glutaraldehyde, stained in 100 mM $K_3Fe(CN)_6$, 100 mM $K_4Fe(CN)_6$, 2 mM $MgCl_2$, 150 mM NaCl, citric acid phosphate buffer (0.2 M Na_2HPO_4 and 0.1 M Citric acid), and 1 mg/ml X-gal (Roche) for 6 h and counterstained in hematoxylin (Dimri et al., 1995).

TUNEL assays

10-µm paraffin-embedded prostate sections were cut and stained with TUNEL kit (11684817910; In Situ Cell Death Detection kit; Roche) following manufacturer's instructions.

Microscope image acquisition

Microscopic analyses were performed at 21°C using a Leica Microsystems DM4000B with the following objectives: 10×, N Plan, dry, numerical aperture (NA): 0.25; 20×, HC Plan Apo dry, NA: 0.7; 40×, N Plan, dry, NA: 0.65; 63×, HCX Plan Apo, oil immersion, NA: 1.32–0.6; and 100, HCX PL Fluotar, oil immersion, NA: 1.30–0.6. Images were acquired with a 12-bit Photometrics Cool Snap FX camera by the Micro-Manager software. Pictures were edited with the Fiji software (Schindelin et al., 2012). The Cell Counter Fiji plugin was used for quantification of pathological features and histological markers.

RNA extraction and analysis

RNA was isolated from DLP and anterior prostate samples, and quantitative PCR of retrotranscribed RNAs were performed as described (Gali Ramamoorthy et al., 2015). Primer sequences were as follows: p16 forward: 5′-GAACTCTTTCGGTCGTACCC-3′, reverse: 5′-CAGTTCGAATCTGCACCGTA-3′; $p19^{ARF}$ forward: 5′-GCTCTGGCTTTCGTGAACAT-3′, reverse: 5′-GTGAACGTTGCC CATCATC-3′; p21 forward: 5′-TCTTCTGCTGTGGGTCAGGAG-3′, reverse: 5′-GAGGGCTAAGGCCGAAGATG-3′; IL-1α forward: 5′-AGACGGCTGAGTTTCAGTGAG-3′, reverse: 5′-TAAGGTGCT GATCTGGGTTG-3′; IL-1β forward: 5′-ACGACAAAATACCTG TGGCC-3′, reverse: 5′-TGGGTATTGCTTGGGATCCA-3′; M-CSF forward: 5′-GACCCAGGATGAGGACAGAC-3′, reverse: 5′-TTCCCA TATGTCTCCTTCCA-3′; TNFα forward: 5′-CACTTGGTGGTTTGC TACGA-3′, reverse: 5′-CCCCAAAGGGATGAGAAGTT-3′; IL-1rn forward: 5′-TGAGCTGGTTGTTTCTCAGG-3′, reverse: 5′-GAA AAGACCCTGCAAGATGC-3′; Ly6c forward: 5′-ATAGCACTCGTA GCACTGCA-3′, reverse: 5′-ACCTTGTCTGAGAGGAACCC-3′; Ly6g forward: 5′-TGTGCTCATCCTTCTTGTGG-3′, reverse: 5′-AGGGGC AGGTAGTTGTGTTG-3′; CD11b forward: 5′-CAAAGAACAACA CACGCAGG-3′, reverse: 5′-GGCTCCCCAACCAGTGTATA-3′; CKIε forward: 5′-TGAAGCATGGAGTTGCGTGT-3′, reverse: 5′-TGTTGG CACCCAGGTAGATG-3′; CKIα1 forward: 5′-TCCGCATCCTTTTCA GGACC-3′, reverse: 5′-AGAAACCTGTGGGGGTTTGG-3′; CKIδ forward: 5′-TACCTCACACACGGCCAACA-3′, reverse: 5′-GCAGCC GCATACTCACTTTC-3′; CKIγ1 forward: 5′-GGGTGGTTGAGAGAA GCAGT-3′, reverse: 5′-CCTGTCCTCCTAAATCAGCGG 3′; CKIγ2 forward: 5′-GCTATCAAGCTGGAGCCCAT-3′; reverse: 5′-TAGTAG ACCTGAGGGACGCC 3′; CKIγ3 forward: 5′-TGGCAAGGCTTAAAG GCTGA-3′; reverse: 5′-TGGGAAGTTCTCACACAACACT-3′; 18S forward: 5′- TCGTCTTCGAAACTCCGACT-3′, reverse: 5′-CGCGGT TCTATTTTGTTGGT-3′.

Preparation and analysis of prostate tissue protein extracts

Prostates were crushed in ice-cold modified radioimmunoprecipitation assay buffer (50 mM Tris, pH 7.5, 1% Nonidet P40, 0.5% sodium deoxycholate, 0.1% SDS, 150 mM NaCl, 5 mM EDTA, 5% glycerol, supplemented with protease inhibitor cocktail [05892970001; Sigma-Aldrich], PhoSTOP [PHOSS-RO; Sigma-Aldrich] and 1,4-dithiothreitol 10 mM) with a potter. Protein extracts (25 µg) were electrophoresed on 8–15% SDS-polyacrylamide gels and electroblotted to Hybond nitrocellulose membranes (Amersham Biosciences). Proteins were detected using primary antibodies directed against γH2AX (05-636; EMD Millipore; 1:1,000), AKT (4691; Cell Signaling Technology; 1:1,000), AKT pS473 (4060; Cell Signaling Technology; 1:1,000), and tubulin (TUB-2A2; IGBMC; 1:10,000). Membranes were probed with secondary HRP-conjugated secondary antibodies (Amersham Biosciences; 1:10,000), which were revealed using an enhanced chemiluminescence detection system (Pierce).

FACS analysis

Fresh prostates were chopped with a scalpel blade immediately after dissection, and dissociated for 4 h in 1 ml/50 mg of prostate tissue of dissociation buffer (RPMI-1640 cell culture medium [Thermo Fisher Scientific] supplemented with 10% heat-inactivated FBS, Hepes, pH 7.2, 10 mM, 200 µg/ml hyaluronidase [H3506; Sigma-Aldrich], 2.5 mg/ml collagenase [C0130; Sigma-Aldrich], and 25 mM $CaCl_2$) at 37°C with gentle shaking. After centrifugation (400 *g*; 5 min), pellets were washed twice with 10 ml of PBS and resuspended in 2 ml of prewarmed 0.05% trypsin (Thermo Fisher Scientific) supplemented with 5 mM EDTA. After a 5 min incubation at 37°C with gentle shaking, trypsin was inactivated by addition of RPMI-1640 supplemented with 10% heat-inactivated FBS, Hepes, pH 7.2, 10 mM, and 300 µg/ml DNase I (DN25; Sigma-Aldrich). Remaining cell clumps were physically dissociated by 10 passages through an 18-G needle and 10 passages through in a 20-G needle. After filtration on a 40-µm cell strainer, cell suspensions were centrifuged at 400 *g* for 5 min, washed twice in ice-cold PBS, and resuspended in

FACS buffer (PBS supplemented with 5 mM EDTA and 1% heat-inactivated FBS).

Cells were incubated with anti-CD16/32 antibodies (BD PharMingen; 1:50) for 15 min on ice to block nonspecific binding sites to Fc receptors, stained with antibodies directed against Epcam (PE-Cy7; Biolegend), CD45 (PerCP-Cy5.5; eBiosciences), CD11b (BV421; BD biosciences), and GR1 RB6-8C5 (FITC; eBiosciences; 1:50 each) for 15 min on ice, and analyzed on a BD LSR II Flow Cytometer (IGBMC; cytometry service) with FlowJo software. The presence of GR1-positive cells was determined by gating $CD11b^{high}GR1^{high}$ cells in $Epcam^{low}CD45^{high}$ cells. The proportion of $CD11b^{high}GR1^{high}$ cells was determined as the number of $CD11b^{high}GR1^{high}$ relative to the total number of single cells of dissociated prostate cells that were analyzed.

Statistical analysis

Statistical analysis was performed with the one-way ANOVA test with Prism (GraphPad).

Online supplemental material

Fig. S1 shows the generation and characterization of $PTEN^{(i)pe-/-}$ mice. Fig. S2 shows pHP1γ immunodetection in PEC of $PTEN^{(i)pe-/-}$ mice. Fig. S3 shows DDR marker immunodetection of in PEC of $PTEN^{(i)pe-/-}$ mice. Fig. S4 shows p53 expression PEC of $PTEN^{(i)pe-/-}$ mice and efficient ablation of p53 in PTEN/$p53^{(i)pe-/-}$ mice. Fig. S5 shows CKIα1, -δ, -γ1, -γ2 and -γ3 transcript levels in the prostate of $PTEN^{(i)pe-/-}$, and control mice at various time points after gene ablation.

Acknowledgments

We thank T. Mak and A. Suzuki for floxed *PTEN* mice and A. Berns for floxed *p53* mice; the staff of the mouse, histopathology, cell sorting, and imaging facilities from Institut de Génétique et de Biologie Moléculaire et Cellulaire and Institut Clinique de la Souris for excellent assistance; P. Kessler and G. Laverny for helpful discussions; and E. Weiss and B. Keyes for critical reading of the manuscript.

This work was supported by funds from the Centre National de la Recherche Scientifique, the Institut National de la Santé et de la Recherche Médicale, the Université de Strasbourg, the Fondation ARC pour la Recherche sur le Cancer, the Ligue Contre le Cancer, Alsace Contre le Cancer, the Association pour la Recherche sur les Tumeurs de la Prostate, the Centre d'Ingénierie Moléculaire Européen, and by French state funds through the Agence Nationale de la Recherche grant ANR-10-LABX-0030-INRT under the frame program Investissements d'Avenir labeled ANR-10-IDEX-0002-02. M. Parisotto was supported by the Association pour la Recherche à l'IGBMC (ARI), E. Grelet by the Ministère de l'enseignement supérieur et de la recherché, R. El Bizri by the Al Bizri Foundation, Y. Dai. by the China Scholarship Council, J. Terzic by the Ecole de l'Institut National de la Santé et de la Recherche Médicale Liliane Bettencourt, and D. Eckert by the Ligue Contre le Cancer.

The authors declare no competing financial interests.

Author contributions: D. Metzger conceived the study together with M. Parisotto; M. Parisotto, E. Grelet, R. El Bizri, Y. Dai, J. Terzic, D. Eckert, L. Gargowitsch, and J.-M. Bonert performed experiments; D. Metzger and M. Parisotto analyzed data and wrote the manuscript.

Submitted: 8 July 2017
Revised: 3 February 2018
Accepted: 10 April 2018

References

Adams, P.D. 2007. Remodeling of chromatin structure in senescent cells and its potential impact on tumor suppression and aging. *Gene.* 397:84–93. https://doi.org/10.1016/j.gene.2007.04.020

Alimonti, A., C. Nardella, Z. Chen, J.G. Clohessy, A. Carracedo, L.C. Trotman, K. Cheng, S. Varmeh, S.C. Kozma, G. Thomas, et al. 2010. A novel type of cellular senescence that can be enhanced in mouse models and human tumor xenografts to suppress prostate tumorigenesis. *J. Clin. Invest.* 120:681–693. https://doi.org/10.1172/JCI40535

Ashcroft, M., R.L. Ludwig, D.B. Woods, T.D. Copeland, H.O. Weber, E.J. MacRae, and K.H. Vousden. 2002. Phosphorylation of HDM2 by Akt. *Oncogene.* 21:1955–1962. https://doi.org/10.1038/sj.onc.1205276

Astle, M.V., K.M. Hannan, P.Y. Ng, R.S. Lee, A.J. George, A.K. Hsu, Y. Haupt, R.D. Hannan, and R.B. Pearson. 2012. AKT induces senescence in human cells via mTORC1 and p53 in the absence of DNA damage: implications for targeting mTOR during malignancy. *Oncogene.* 31:1949–1962. https://doi.org/10.1038/onc.2011.394

Bar, J., N. Lukaschuk, A. Zalcenstein, S. Wilder, R. Seger, and M. Oren. 2005. The PI3K inhibitor LY294002 prevents p53 induction by DNA damage and attenuates chemotherapy-induced apoptosis. *Cell Death Differ.* 12:1578–1587. https://doi.org/10.1038/sj.cdd.4401677

Bartek, J., J. Bartkova, and J. Lukas. 2007. DNA damage signalling guards against activated oncogenes and tumour progression. *Oncogene.* 26:7773–7779. https://doi.org/10.1038/sj.onc.1210881

Bartkova, J., N. Rezaei, M. Liontos, P. Karakaidos, D. Kletsas, N. Issaeva, L.V. Vassiliou, E. Kolettas, K. Niforou, V.C. Zoumpourlis, et al. 2006. Oncogene-induced senescence is part of the tumorigenesis barrier imposed by DNA damage checkpoints. *Nature.* 444:633–637. https://doi.org/10.1038/nature05268

Braig, M., S. Lee, C. Loddenkemper, C. Rudolph, A.H. Peters, B. Schlegelberger, H. Stein, B. Dörken, T. Jenuwein, and C.A. Schmitt. 2005. Oncogene-induced senescence as an initial barrier in lymphoma development. *Nature.* 436:660–665. https://doi.org/10.1038/nature03841

Branzei, D., and M. Foiani. 2005. The DNA damage response during DNA replication. *Curr. Opin. Cell Biol.* 17:568–575. https://doi.org/10.1016/j.ceb.2005.09.003

Byun, T.S., M. Pacek, M.C. Yee, J.C. Walter, and K.A. Cimprich. 2005. Functional uncoupling of MCM helicase and DNA polymerase activities activates the ATR-dependent checkpoint. *Genes Dev.* 19:1040–1052. https://doi.org/10.1101/gad.1301205

Cairns, P., K. Okami, S. Halachmi, N. Halachmi, M. Esteller, J.G. Herman, J. Jen, W.B. Isaacs, G.S. Bova, and D. Sidransky. 1997. Frequent inactivation of PTEN/MMAC1 in primary prostate cancer. *Cancer Res.* 57:4997–5000.

Chen, Z., L.C. Trotman, D. Shaffer, H.K. Lin, Z.A. Dotan, M. Niki, J.A. Koutcher, H.I. Scher, T. Ludwig, W. Gerald, et al. 2005. Crucial role of p53-dependent cellular senescence in suppression of Pten-deficient tumorigenesis. *Nature.* 436:725–730. https://doi.org/10.1038/nature03918

Choucair, K., J. Ejdelman, F. Brimo, A. Aprikian, S. Chevalier, and J. Lapointe. 2012. PTEN genomic deletion predicts prostate cancer recurrence and is associated with low AR expression and transcriptional activity. *BMC Cancer.* 12:543. https://doi.org/10.1186/1471-2407-12-543

Collado, M., and M. Serrano. 2006. The power and the promise of oncogene-induced senescence markers. *Nat. Rev. Cancer.* 6:472–476. https://doi.org/10.1038/nrc1884

Collado, M., and M. Serrano. 2010. Senescence in tumours: evidence from mice and humans. *Nat. Rev. Cancer.* 10:51–57. https://doi.org/10.1038/nrc2772

Cortez, D., S. Guntuku, J. Qin, and S.J. Elledge. 2001. ATR and ATRIP: partners in checkpoint signaling. *Science.* 294:1713–1716. https://doi.org/10.1126/science.1065521

Costa, H.A., M.G. Leitner, M.L. Sos, A. Mavrantoni, A. Rychkova, J.R. Johnson, B.W. Newton, M.C. Yee, F.M. De La Vega, J.M. Ford, et al. 2015. Discovery and functional characterization of a neomorphic PTEN mutation.

Proc. Natl. Acad. Sci. USA. 112:13976–13981. https://doi.org/10.1073/pnas.1422504112

Courtois-Cox, S., S.L. Jones, and K. Cichowski. 2008. Many roads lead to oncogene-induced senescence. *Oncogene.* 27:2801–2809. https://doi.org/10.1038/sj.onc.1210950

Di Micco, R., M. Fumagalli, A. Cicalese, S. Piccinin, P. Gasparini, C. Luise, C. Schurra, M. Garre', P.G. Nuciforo, A. Bensimon, et al. 2006. Oncogene-induced senescence is a DNA damage response triggered by DNA hyper-replication. *Nature.* 444:638–642. https://doi.org/10.1038/nature05327

Di Mitri, D., A. Toso, J.J. Chen, M. Sarti, S. Pinton, T.R. Jost, R. D'Antuono, E. Montani, R. Garcia-Escudero, I. Guccini, et al. 2014. Tumour-infiltrating Gr-1+ myeloid cells antagonize senescence in cancer. *Nature.* 515:134–137. https://doi.org/10.1038/nature13638

Dimri, G.P., X. Lee, G. Basile, M. Acosta, G. Scott, C. Roskelley, E.E. Medrano, M. Linskens, I. Rubelj, O. Pereira-Smith, et al. 1995. A biomarker that identifies senescent human cells in culture and in aging skin in vivo. *Proc. Natl. Acad. Sci. USA.* 92:9363–9367. https://doi.org/10.1073/pnas.92.20.9363

Feng, J., R. Tamaskovic, Z. Yang, D.P. Brazil, A. Merlo, D. Hess, and B.A. Hemmings. 2004. Stabilization of Mdm2 via decreased ubiquitination is mediated by protein kinase B/Akt-dependent phosphorylation. *J. Biol. Chem.* 279:35510–35517. https://doi.org/10.1074/jbc.M404936200

Fenouille, N., A. Puissant, M. Tichet, G. Zimniak, P. Abbe, A. Mallavialle, S. Rocchi, J.P. Ortonne, M. Deckert, R. Ballotti, and S. Tartare-Deckert. 2011. SPARC functions as an anti-stress factor by inactivating p53 through Akt-mediated MDM2 phosphorylation to promote melanoma cell survival. *Oncogene.* 30:4887–4900. https://doi.org/10.1038/onc.2011.198

Ferbeyre, G., E. de Stanchina, E. Querido, N. Baptiste, C. Prives, and S.W. Lowe. 2000. PML is induced by oncogenic ras and promotes premature senescence. *Genes Dev.* 14:2015–2027.

Freeman, D.J., A.G. Li, G. Wei, H.H. Li, N. Kertesz, R. Lesche, A.D. Whale, H. Martinez-Diaz, N. Rozengurt, R.D. Cardiff, et al. 2003. PTEN tumor suppressor regulates p53 protein levels and activity through phosphatase-dependent and -independent mechanisms. *Cancer Cell.* 3:117–130. https://doi.org/10.1016/S1535-6108(03)00021-7

Gali Ramamoorthy, T., G. Laverny, A.I. Schlagowski, J. Zoll, N. Messaddeq, J.M. Bornert, S. Panza, A. Ferry, B. Geny, and D. Metzger. 2015. The transcriptional coregulator PGC-1β controls mitochondrial function and anti-oxidant defence in skeletal muscles. *Nat. Commun.* 6:10210. https://doi.org/10.1038/ncomms10210

Inuzuka, H., A. Tseng, D. Gao, B. Zhai, Q. Zhang, S. Shaik, L. Wan, X.L. Ang, C. Mock, H. Yin, et al. 2010. Phosphorylation by casein kinase I promotes the turnover of the Mdm2 oncoprotein via the SCF(beta-TRCP) ubiquitin ligase. *Cancer Cell.* 18:147–159. https://doi.org/10.1016/j.ccr.2010.06.015

Jonkers, J., R. Meuwissen, H. van der Gulden, H. Peterse, M. van der Valk, and A. Berns. 2001. Synergistic tumor suppressor activity of BRCA2 and p53 in a conditional mouse model for breast cancer. *Nat. Genet.* 29:418–425. https://doi.org/10.1038/ng747

Kang, T.W., T. Yevsa, N. Woller, L. Hoenicke, T. Wuestefeld, D. Dauch, A. Hohmeyer, M. Gereke, R. Rudalska, A. Potapova, et al. 2011. Senescence surveillance of pre-malignant hepatocytes limits liver cancer development. *Nature.* 479:547–551. https://doi.org/10.1038/nature10599

Kim, J.S., C. Lee, C.L. Bonifant, H. Ressom, and T. Waldman. 2007. Activation of p53-dependent growth suppression in human cells by mutations in PTEN or PIK3CA. *Mol. Cell. Biol.* 27:662–677. https://doi.org/10.1128/MCB.00537-06

Knippschild, U., M. Krüger, J. Richter, P. Xu, B. García-Reyes, C. Peifer, J. Halekotte, V. Bakulev, and J. Bischof. 2014. The CK1 Family: Contribution to Cellular Stress Response and Its Role in Carcinogenesis. *Front. Oncol.* 4:96. https://doi.org/10.3389/fonc.2014.00096

Krohn, A., T. Diedler, L. Burkhardt, P.S. Mayer, C. De Silva, M. Meyer-Kornblum, D. Kötschau, P. Tennstedt, J. Huang, C. Gerhäuser, et al. 2012. Genomic deletion of PTEN is associated with tumor progression and early PSA recurrence in ERG fusion-positive and fusion-negative prostate cancer. *Am. J. Pathol.* 181:401–412. https://doi.org/10.1016/j.ajpath.2012.04.026

Lavin, M.F., and N. Gueven. 2006. The complexity of p53 stabilization and activation. *Cell Death Differ.* 13:941–950. https://doi.org/10.1038/sj.cdd.4401925

Liaw, H., D. Lee, and K. Myung. 2011. DNA-PK-dependent RPA2 hyperphosphorylation facilitates DNA repair and suppresses sister chromatid exchange. *PLoS One.* 6:e21424. https://doi.org/10.1371/journal.pone.0021424

Lotan, T.L., B. Gurel, S. Sutcliffe, D. Esopi, W. Liu, J. Xu, J.L. Hicks, B.H. Park, E. Humphreys, A.W. Partin, et al. 2011. PTEN protein loss by immunostaining: analytic validation and prognostic indicator for a high risk surgical cohort of prostate cancer patients. *Clin. Cancer Res.* 17:6563–6573. https://doi.org/10.1158/1078-0432.CCR-11-1244

Luchman, H.A., H. Benediktsson, M.L. Villemaire, A.C. Peterson, and F.R. Jirik. 2008. The pace of prostatic intraepithelial neoplasia development is determined by the timing of Pten tumor suppressor gene excision. *PLoS One.* 3:e3940. https://doi.org/10.1371/journal.pone.0003940

Lukas, C., V. Savic, S. Bekker-Jensen, C. Doil, B. Neumann, R.S. Pedersen, M. Grøfte, K.L. Chan, I.D. Hickson, J. Bartek, and J. Lukas. 2011. 53BP1 nuclear bodies form around DNA lesions generated by mitotic transmission of chromosomes under replication stress. *Nat. Cell Biol.* 13:243–253. https://doi.org/10.1038/ncb2201

Mah, L.J., A. El-Osta, and T.C. Karagiannis. 2010. gammaH2AX: a sensitive molecular marker of DNA damage and repair. *Leukemia.* 24:679–686. https://doi.org/10.1038/leu.2010.6

Mallette, F.A., M.F. Gaumont-Leclerc, and G. Ferbeyre. 2007. The DNA damage signaling pathway is a critical mediator of oncogene-induced senescence. *Genes Dev.* 21:43–48. https://doi.org/10.1101/gad.1487307

Markert, E.K., H. Mizuno, A. Vazquez, and A.J. Levine. 2011. Molecular classification of prostate cancer using curated expression signatures. *Proc. Natl. Acad. Sci. USA.* 108:21276–21281. https://doi.org/10.1073/pnas.1117029108

Mayo, L.D., and D.B. Donner. 2001. A phosphatidylinositol 3-kinase/Akt pathway promotes translocation of Mdm2 from the cytoplasm to the nucleus. *Proc. Natl. Acad. Sci. USA.* 98:11598–11603. https://doi.org/10.1073/pnas.181181198

Mayo, L.D., J.E. Dixon, D.L. Durden, N.K. Tonks, and D.B. Donner. 2002. PTEN protects p53 from Mdm2 and sensitizes cancer cells to chemotherapy. *J. Biol. Chem.* 277:5484–5489. https://doi.org/10.1074/jbc.M108302200

Mazouzi, A., G. Velimezi, and J.I. Loizou. 2014. DNA replication stress: causes, resolution and disease. *Exp. Cell Res.* 329:85–93. https://doi.org/10.1016/j.yexcr.2014.09.030

Meek, D.W. 2009. Tumour suppression by p53: a role for the DNA damage response? *Nat. Rev. Cancer.* 9:714–723. https://doi.org/10.1038/nrc2716

Metzger, D., M. Li, and P. Chambon. 2005. Targeted somatic mutagenesis in the mouse epidermis. *Methods Mol. Biol.* 289:329–340.

Michaloglou, C., L.C. Vredeveld, M.S. Soengas, C. Denoyelle, T. Kuilman, C.M. van der Horst, D.M. Majoor, J.W. Shay, W.J. Mooi, and D.S. Peeper. 2005. BRAFE600-associated senescence-like cell cycle arrest of human naevi. *Nature.* 436:720–724. https://doi.org/10.1038/nature03890

Mirzayans, R., B. Andrais, A. Scott, and D. Murray. 2012. New insights into p53 signaling and cancer cell response to DNA damage: implications for cancer therapy. *J. Biomed. Biotechnol.* 2012:170325. https://doi.org/10.1155/2012/170325

Ogawara, Y., S. Kishishita, T. Obata, Y. Isazawa, T. Suzuki, K. Tanaka, N. Masuyama, and Y. Gotoh. 2002. Akt enhances Mdm2-mediated ubiquitination and degradation of p53. *J. Biol. Chem.* 277:21843–21850. https://doi.org/10.1074/jbc.M109745200

Papa, A., L. Wan, M. Bonora, L. Salmena, M.S. Song, R.M. Hobbs, A. Lunardi, K. Webster, C. Ng, R.H. Newton, et al. 2014. Cancer-associated PTEN mutants act in a dominant-negative manner to suppress PTEN protein function. *Cell.* 157:595–610. https://doi.org/10.1016/j.cell.2014.03.027

Pérez-Mancera, P.A., A.R. Young, and M. Narita. 2014. Inside and out: the activities of senescence in cancer. *Nat. Rev. Cancer.* 14:547–558. https://doi.org/10.1038/nrc3773

Ratnacaram, C.K., M. Teletin, M. Jiang, X. Meng, P. Chambon, and D. Metzger. 2008. Temporally controlled ablation of PTEN in adult mouse prostate epithelium generates a model of invasive prostatic adenocarcinoma. *Proc. Natl. Acad. Sci. USA.* 105:2521–2526. https://doi.org/10.1073/pnas.0712021105

Rodier, F., D.P. Muñoz, R. Teachenor, V. Chu, O. Le, D. Bhaumik, J.P. Coppé, E. Campeau, C.M. Beauséjour, S.H. Kim, et al. 2011. DNA-SCARS: distinct nuclear structures that sustain damage-induced senescence growth arrest and inflammatory cytokine secretion. *J. Cell Sci.* 124:68–81. https://doi.org/10.1242/jcs.071340

Rodriguez, M.S., J.M. Desterro, S. Lain, D.P. Lane, and R.T. Hay. 2000. Multiple C-terminal lysine residues target p53 for ubiquitin-proteasome-mediated degradation. *Mol. Cell. Biol.* 20:8458–8467. https://doi.org/10.1128/MCB.20.22.8458-8467.2000

Rogakou, E.P., D.R. Pilch, A.H. Orr, V.S. Ivanova, and W.M. Bonner. 1998. DNA double-stranded breaks induce histone H2AX phosphorylation on serine 139. *J. Biol. Chem.* 273:5858–5868. https://doi.org/10.1074/jbc.273.10.5858

Schindelin, J., I. Arganda-Carreras, E. Frise, V. Kaynig, M. Longair, T. Pietzsch, S. Preibisch, C. Rueden, S. Saalfeld, B. Schmid, et al. 2012. Fiji: an open-source platform for biological-image analysis. *Nat. Methods.* 9:676–682. https://doi.org/10.1038/nmeth.2019

Serrano, M., and M.A. Blasco. 2001. Putting the stress on senescence. *Curr. Opin. Cell Biol.* 13:748–753. https://doi.org/10.1016/S0955-0674(00)00278-7

Serrano, M., A.W. Lin, M.E. McCurrach, D. Beach, and S.W. Lowe. 1997. Oncogenic ras provokes premature cell senescence associated with accumulation of p53 and p16INK4a. *Cell.* 88:593–602. https://doi.org/10.1016/S0092-8674(00)81902-9

Sirbu, B.M., F.B. Couch, J.T. Feigerle, S. Bhaskara, S.W. Hiebert, and D. Cortez. 2011. Analysis of protein dynamics at active, stalled, and collapsed replication forks. *Genes Dev.* 25:1320–1327. https://doi.org/10.1101/gad.2053211

Vassilev, L.T., B.T. Vu, B. Graves, D. Carvajal, F. Podlaski, Z. Filipovic, N. Kong, U. Kammlott, C. Lukacs, C. Klein, et al. 2004. In vivo activation of the p53 pathway by small-molecule antagonists of MDM2. *Science.* 303:844–848. https://doi.org/10.1126/science.1092472

Vernier, M., V. Bourdeau, M.F. Gaumont-Leclerc, O. Moiseeva, V. Bégin, F. Saad, A.M. Mes-Masson, and G. Ferbeyre. 2011. Regulation of E2Fs and senescence by PML nuclear bodies. *Genes Dev.* 25:41–50. https://doi.org/10.1101/gad.1975111

Ward, I.M., and J. Chen. 2001. Histone H2AX is phosphorylated in an ATR-dependent manner in response to replicational stress. *J. Biol. Chem.* 276:47759–47762. https://doi.org/10.1074/jbc.C100569200

Wei, S., X. Chen, K. McGraw, L. Zhang, R. Komrokji, J. Clark, G. Caceres, D. Billingsley, L. Sokol, J. Lancet, et al. 2013. Lenalidomide promotes p53 degradation by inhibiting MDM2 auto-ubiquitination in myelodysplastic syndrome with chromosome 5q deletion. *Oncogene.* 32:1110–1120. https://doi.org/10.1038/onc.2012.139

Wu, X., J. Wu, J. Huang, W.C. Powell, J. Zhang, R.J. Matusik, F.O. Sangiorgi, R.E. Maxson, H.M. Sucov, and P. Roy-Burman. 2001. Generation of a prostate epithelial cell-specific Cre transgenic mouse model for tissue-specific gene ablation. *Mech. Dev.* 101:61–69. https://doi.org/10.1016/S0925-4773(00)00551-7

Yaswen, P., and J. Campisi. 2007. Oncogene-induced senescence pathways weave an intricate tapestry. *Cell.* 128:233–234. https://doi.org/10.1016/j.cell.2007.01.005

Zhou, B.B., and S.J. Elledge. 2000. The DNA damage response: putting checkpoints in perspective. *Nature.* 408:433–439. https://doi.org/10.1038/35044005

Zhou, B.P., Y. Liao, W. Xia, Y. Zou, B. Spohn, and M.C. Hung. 2001. HER-2/neu induces p53 ubiquitination via Akt-mediated MDM2 phosphorylation. *Nat. Cell Biol.* 3:973–982. https://doi.org/10.1038/ncb1101-973

Supplemental material

Parisotto et al., https://doi.org/10.1084/jem.20171207

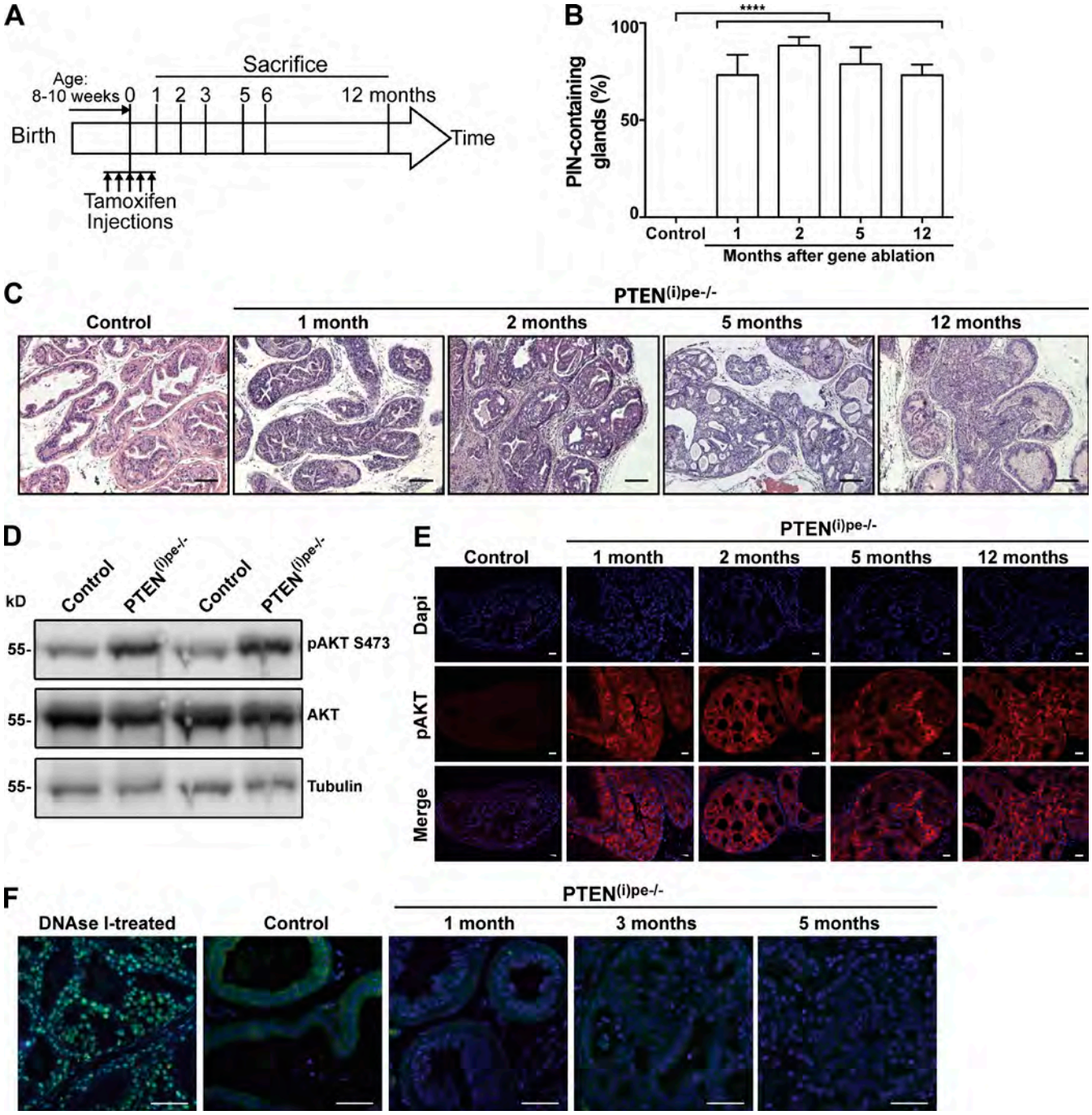

Figure S1. **Generation and characterization of PTEN$^{(i)pe-/-}$ mice. (A)** Schematic description of the timeline of gene ablation (Tam administration) and time points of sacrifice of PTEN$^{(i)pe-/-}$ and control mice. **(B)** Proportion of DLP glands affected by PIN lesions in PTEN$^{(i)pe-/-}$ and control mice over 12 mo after gene ablation. Values are mean of four to six mice ± SEM; ****, P value < 0.0001. **(C)** Representative views of H&E-stained DLP sections from PTEN$^{(i)pe-/-}$ and control mice sacrificed at indicated time points after gene ablation. Four to eight PTEN$^{(i)pe-/-}$ mice per time point and eight control mice were analyzed. **(D)** Western blot analysis of pAKT S473 and of total AKT in prostate extracts of PTEN$^{(i)pe-/-}$ and control mice sacrificed 1 mo after gene ablation. Tubulin was used as internal loading control. Data are representative of three experiments. **(E)** Representative AKT pS473 immunofluorescence staining (red) of prostate sections of PTEN$^{(i)pe-/-}$ and control mice sacrificed at indicated time points after gene ablation. Four to eight PTEN$^{(i)pe-/-}$ mice per time point and eight control mice were analyzed. **(F)** Representative TUNEL staining (green) of DLP sections of PTEN$^{(i)pe-/-}$ and control mice sacrificed at indicated time points after gene ablation. Positive control: DNase I–treated DLP section of a PTEN$^{(i)pe-/-}$ mouse sacrificed 3 mo after gene ablation. Blue, Dapi. Bars: 100 µm (C); 25 µm (E); 250 µm (F). Three PTEN$^{(i)pe-/-}$ mice per time point and three control mice were analyzed.

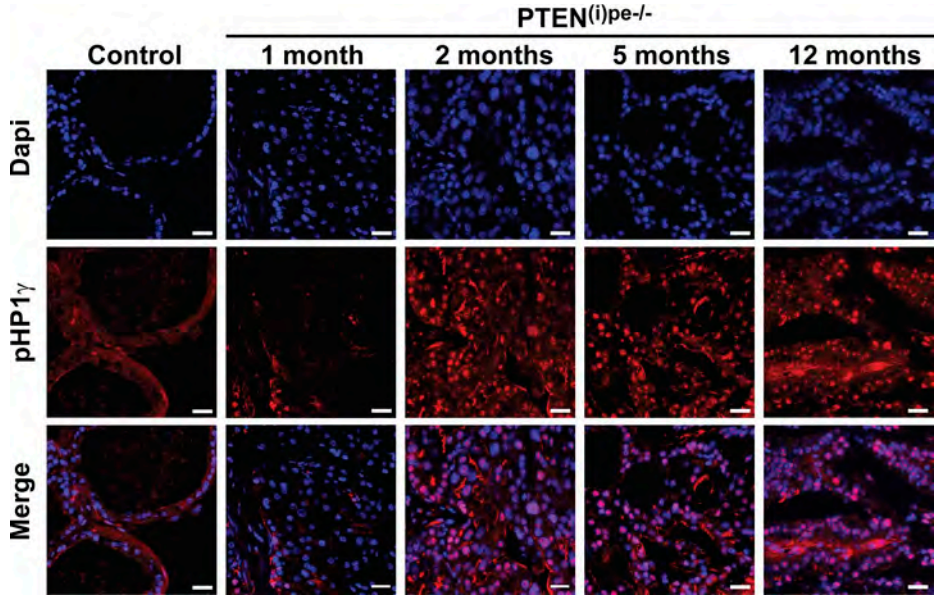

Figure S2. **Immunodetection of pHP1γ in PEC of PTEN$^{(i)pe-/-}$ mice.** Representative pHP1γ immunofluorescence staining (red) of DLP sections of PTEN$^{(i)pe-/-}$ and control mice sacrificed at indicated time points after gene ablation. Blue, Dapi. Bars, 20 µm. Data are representative of three experiments with n = 3–4 mice per time point

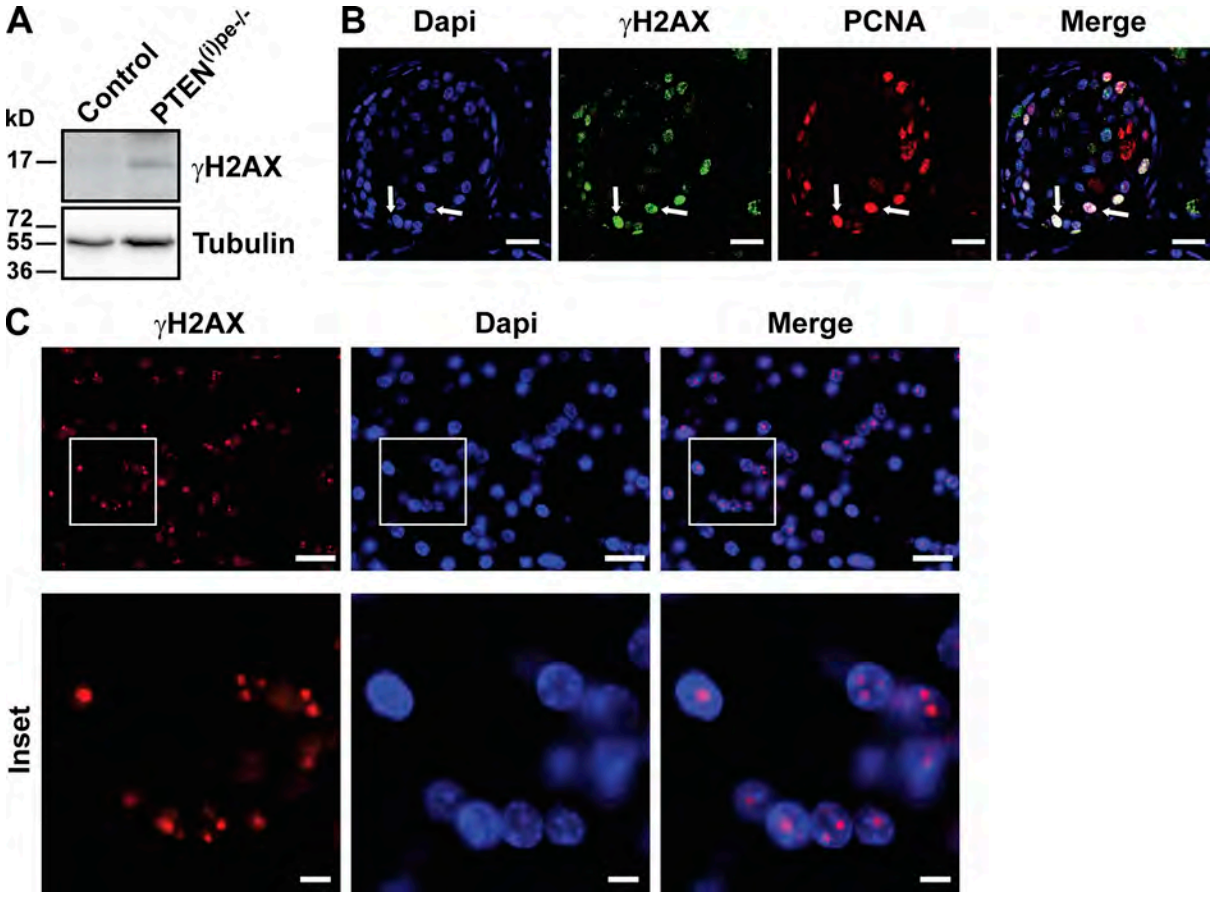

Figure S3. **Immunodetection of DDR markers in PEC of PTEN$^{(i)pe-/-}$ mice. (A)** Representative Western blot analysis of prostatic extracts from PTEN$^{(i)pe-/-}$ and control mice sacrificed 1 mo after *PTEN* ablation with antibodies directed against γH2AX. Tubulin was used as internal loading control. Three PTEN$^{(i)pe-/-}$ mice and three control mice were analyzed. **(B)** Representative immunofluorescence staining of γH2AX (green) and PCNA (red) of DLP sections of PTEN$^{(i)pe-/-}$ and control mice sacrificed 1 mo after gene ablation. White arrows, examples of double-stained nuclei. Three mice were analyzed. **(C)** Representative γH2AX immunofluorescence staining (red) of DLP sections of a PTEN$^{(i)pe-/-}$ sacrificed 5 mo after gene ablation. Blue, Dapi. Bars: 25 µm (B and C, main images); 5 µm (C, insets). Three mice were analyzed.

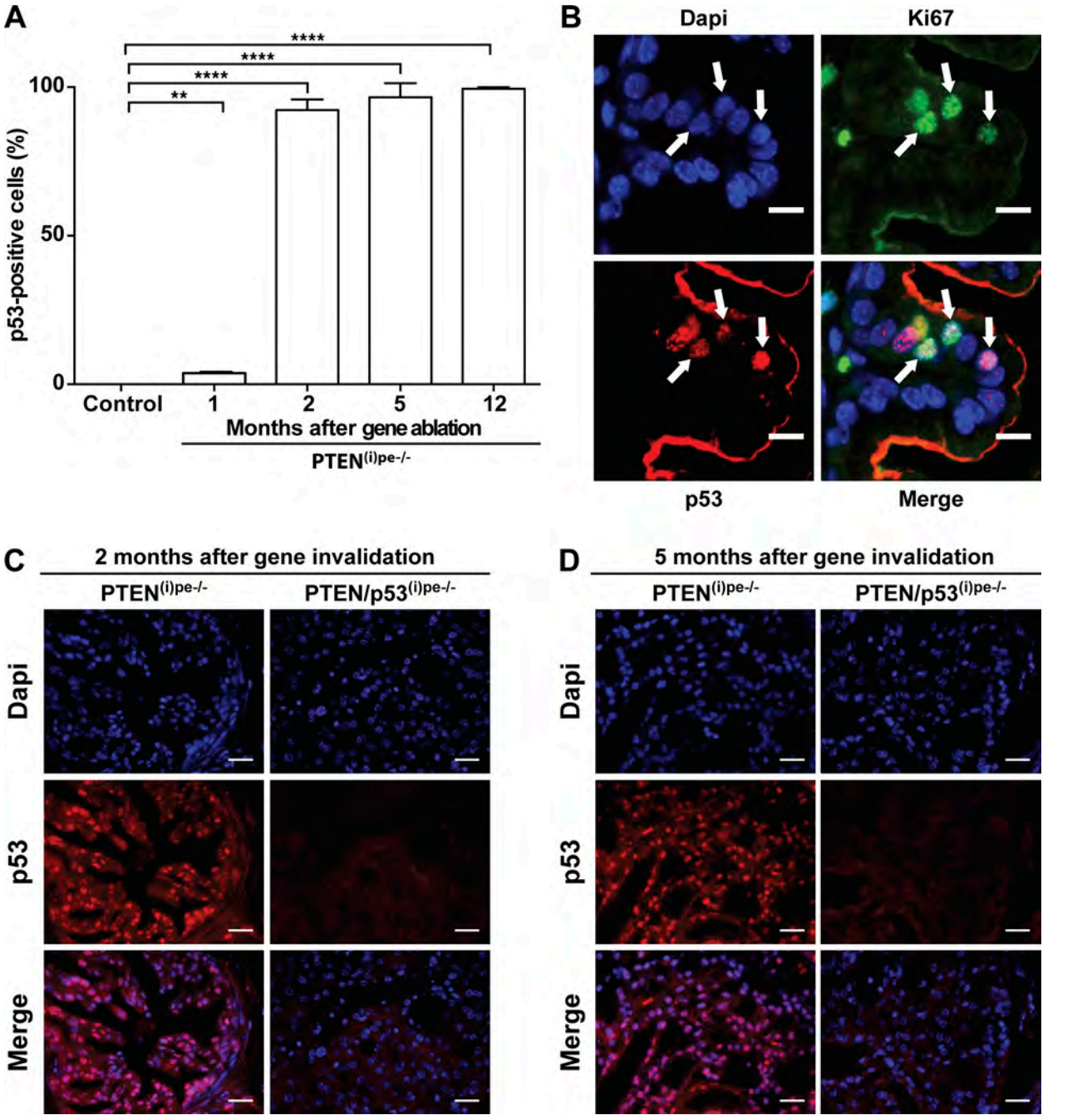

Figure S4. **Characterization of p53 expression in PEC of PTEN$^{(i)pe-/-}$ and PTEN/p53$^{(i)pe-/-}$ mice. (A)** Quantification of p53-positive PECs in the DLP epithelium of PTEN$^{(i)pe-/-}$ and control mice over 12 mo after gene ablation. Values are mean of four to six mice ± SEM. **, P value < 0.01; ****, P value < 0.0001. Data are representative of two experiments with n = 3–4 mice per time point. **(B)** Representative p53 (red) and Ki67 (green) immunofluorescence staining of DLP sections of PTEN$^{(i)pe-/-}$ and control mice sacrificed 1 mo after gene ablation. White arrow, example of double stained nuclei. Three mice were analyzed. **(C and D)** Representative p53 immunofluorescence staining (red) of DLP sections of PTEN$^{(i)pe-/-}$ and PTEN/p53$^{(i)pe-/-}$ mice sacrificed 2 (C) and 5 (D) months after gene ablation. Blue, Dapi. Bars: 10 µm (B); 25 µm (C and D). Data are representative of two experiments with n = 3–4 mice per time point.

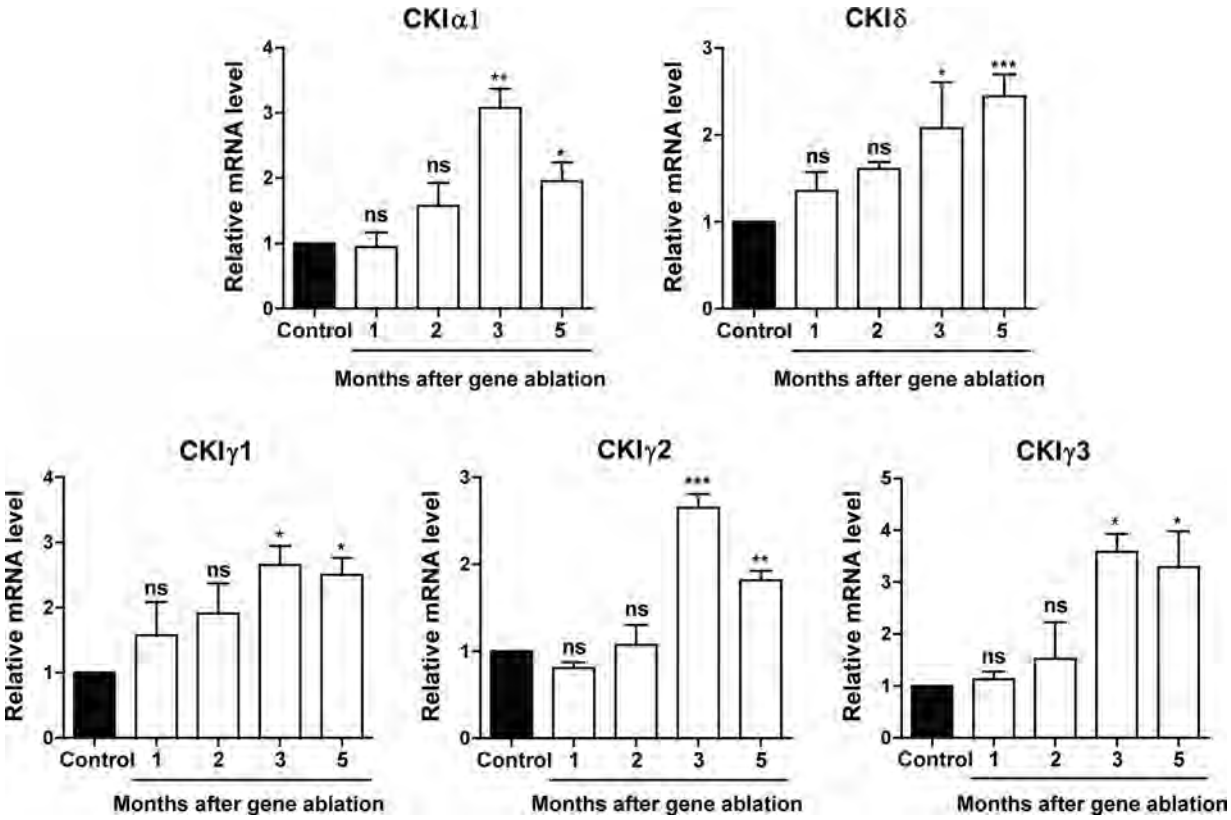

Figure S5. **Relative transcript levels of CKIα1, CKIδ, CKIγ1,-2, and -3 isoforms in the prostate of PTEN$^{(i)pe-/-}$ and control mice at 1–5 mo after gene invalidation.** *n* = 3 for control mice at 5 mo and *n* = 4, *n* = 4, *n* = 4, *n* = 3, and *n* = 10 for PTEN$^{pe-/-}$ mice at 1, 2, 3, and 5 mo after gene ablation, respectively. Bars represent the mean ± SEM. One way ANOVA. ns; not significant; *, P < 0.05; **, P < 0.01; ***, P < 0.001.

PART II

Manuscript II

Summary Part II: Role of Trp53 in Pten-null prostatic epithelial cells *in vivo*

The tumor suppressor genes PTEN and p53 are among the most frequently mutated genes in prostate cancer. Genetic ablation of Pten in prostatic epithelial cells (PECs) was reported to induce cell senescence in a p53-dependent manner, which can be antagonized by combined inactivation of Trp53 *in vivo*. However, unlike previous mouse models that lack the ability to strictly control the time of Pten and Trp53 ablation, we took advantage from our Pten/Trp53$^{(i)pe-/-}$ mice in which Pten and Trp53 are selectively ablated in mature prostatic luminal cells, via the Tamoxifen (Tam)-dependent Cre-ER^{T2} system.

Although Pten/Trp53-null PECs proliferation is stimulated at 2 months, PECs of 76 % of Pten/Trp53$^{(i)pe-/-}$ mice develop prostatic intraepithelial neoplasia (PINs) that enter senescence. However, only PECs of 24% of Pten/Trp53$^{(i)pe-/-}$ mice develop either adenocarcinoma or sarcomatoid tumors and more than one-third of the latter develop metastases. Thus, although Trp53 attenuates Pten-null PECs proliferation, it is not mandatory for cell senescence induction.

Importantly, along with the senescence phenotype in prostatic lesions, loss of Trp53 in Pten-deficient PECs enhances stemness, promotes the formation of cell entity exhibiting both luminal and basal characteristics, and induces focal neuroendocrine differentiation of luminal PECs.

Thus, Trp53 is not necessary for senescence induction, but is definitely required for sustaining cell identity of Pten-deficient PECs in prostatic lesions. Therefore, identification of luminal/basal stem cell characteristics is needed for the development of new targeted therapies.

Keywords: prostate cancer, prostatic epithelial cells, prostatic intraepithelial neoplasia, cell senescence, stemness and neuroendocrine differentiation.

Graphical abstract II:

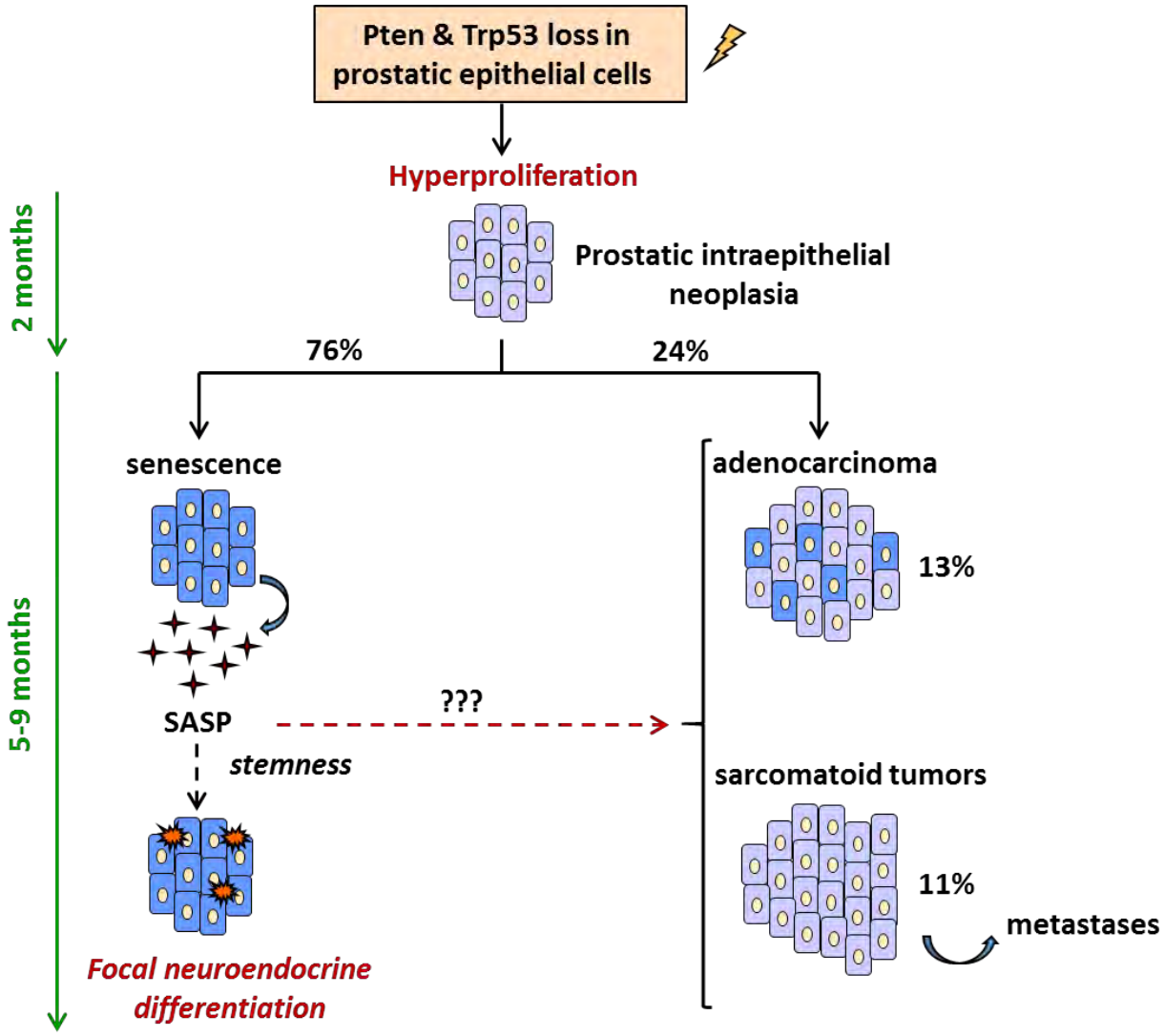

Figure 28: Schematic representation describing the key events of prostate cancer progression upon the loss of Pten and Trp53 in prostatic luminal epithelial cells.

Manuscript II

Trp53 deficiency promotes stemness and neuroendocrine differentiation, but is not mandatory to induce senescence in Pten-null prostatic epithelial cells

Rana El Bizri et al., in preparation

Introduction

Prostate cancer (PCa) is the third leading cause of cancer-related deaths in males of industrialized countries, and its associated mortality remains a major health problem (Siegel et al., 2017). Human PCa progression takes decades and proceeds through multistage process including prostatic intraepithelial neoplasia (PIN), locally/and invasive adenocarcinoma and metastasis (Abate-Shen and Shen, 2000). Less than 2% of human PCa develops neuroendocrine prostate cancer (NEPC) (Grignon, 2004), and the latter is often associated with the resistance of PCa to therapeutic castration (Yu Ku et al., 2017; Zou et al., 2017). NEPC is associated with altered histology, reduced androgen receptor (AR) levels, and expression of neuroendocrine markers such as Synaptophysin, Chromogranin A and Neuron Specific Enolase (NSE) (Beltran et al., 2011; Yu Ku et al., 2017; Zou et al., 2017). Notably, human and mouse neuroendocrine prostate cancer (NEPC) exhibit deregulation of stem cell reprogramming factors (Yu Ku et al., 2017).

PCa includes alterations of several tumor suppressor genes such as PTEN and p53 (Di Cristofano and Pandolfi, 2000; Vogelstein et al., 2000). Loss of tumor suppressor genes (e.g. Pten) opposes neoplastic transformation by triggering an irreversible cell growth arrest *in vivo*, which is termed cellular senescence (Chen et al., 2005). Moreover, it was shown that complete loss of Pten can restrict prostate tumorigenesis through a Trp53-dependent cellular senescence response both *in vitro* and *in vivo*, which can be antagonized by combined loss of Trp53 (Chen et al., 2005). Combined inactivation of Pten and Trp53 was reported to trigger invasive and lethal PCa (Chen et al., 2005).

Senescent cells are metabolically active and secrete a number of cytokines and chemokines, which are components of the senscence-associated secretory phenotype (SASP) (Coppé et al., 2010). Chemokines and their receptors contribute to the recruitment of immunosuppressive cells such as myeloid-derived suppressor cells (MDSCs) that can oppose senescence and promote tumorigenesis (Katoh et al., 2013). Moreover, it was reported that the SASP promotes the stem cell reprogramming factors of neighboring cells, in a paracrine fashion, and in turn reprogrammed cells induce damage and senescence to other cells *in vivo* (Mosterio et al., 2016; Ritschka et al., 2017).

To investigate the relevance of these observations in a strictly controlled mouse model for prostate tumor progression, we generated mice in which Pten and Trp53 genes are selectively ablated in prostatic luminal epithelial cells after puberty (Pten/Trp53$^{(i)pe-/-}$ mice). Our results show that although loss of Trp53 accelerates Pten-null PECs proliferation 2 months after gene ablation, 76 % of Pten/Trp53$^{(i)pe-/-}$ mice develop PINs that enter senescence and express higher levels of senescence markers, and only 24 % of them develop either adenocarcinoma or sarcomatoid tumors within 9 months after gene ablation, and more than one-third of the latter develop metastases. Thus, even though Trp53 attenuates the proliferation peak of Pten-null PECs, it is not mandatory for senescence induction. Importantly, loss of Trp53 in Pten-null PECs of prostatic lesions enhances stemness, promotes the formation of cell population expressing both luminal and basal markers, and induces focal neuroendocrine differentiation of luminal PECs. Taken together, our results indicate that Trp53 is not absolutely required for senescence induction, but is necessary for maintaining cell identity of Pten-null PECs.

Results

Pten/Trp53-deficient prostatic epithelial cells generate PINs, adenocarcinoma and sarcomatoid tumors

To determine the role of Trp53 in Pten-deficient prostatic epithelial cells (PECs) of adult mice, we analyzed Pten/Trp53$^{(i)pe-/-}$ mice, in which both Pten and Trp53 are selectively ablated in prostatic luminal epithelial cells after puberty (Parisotto et al., 2018) **(Figures S1A and S1B)**. The prostate weight increased in both Pten/Trp53$^{(i)pe-/-}$ and Pten$^{(i)pe-/-}$ mice from 50 mg to ~ 150 mg between 1 and 4.5 months after gene ablation **(Figure S1C)**. Between 5 and 9 months, it slightly increased up to 250 mg (small size prostate; SSP) in 76 % of Pten/Trp53$^{(i)pe-/-}$ mice, whereas it increased to 250-500 mg (intermediate size prostate; ISP) in 13 % of them, and to more than 500 mg (large size prostate; LSP) in 11 % of them **(Figures 1A and 1B)**. Histological analyses revealed that the DLP and AP of SSP of Pten/Trp53$^{(i)pe-/-}$ mice contained low and high grade PINs, as seen in Pten$^{(i)pe-/-}$ mice at 5 months **(Figures 1C, S1D and data not shown)** (Parisotto et al., 2018). ISP contained mainly high grade PINs in DLP and adenocarcinoma (ADK) in AP **(Figures 1C and S1D)**. In contrast, the prostate weight of Pten$^{(i)pe-/-}$ mice remained below 250 mg at 9 months after gene ablation, and the DLP and AP contained low and high grade PINs but no adenocarcinoma **(Figures 1C, S1D and data not shown)** (Ratnacaram et al., 2008). LSP of Pten/Trp53$^{(i)pe-/-}$ mice contained mainly sarcomatoid tumors (SARC) and more than 40 % of them developed metastases. In contrast, no metastases were observed in mice with only SSP and ISP **(Figures 1C, S1E and data not shown)**. PECs of PINs, adenocarcinoma and sarcomatoid tumors of Pten/Trp53$^{(i)pe-/-}$ mice expressed pAKT S473, an indicator for PTEN loss **(Figures 1C and S1D)**. In agreement with previous results (Parisotto et al., 2018), whereas PECs in PINs of Pten$^{(i)pe-/-}$ mice displayed nuclear Trp53 staining 5-6 months after gene ablation **(Figure 1C)**, PECs of PINs, adenocarcinoma and sarcomatoid tumors were Trp53 negative in Pten/Trp53$^{(i)pe-/-}$ mice **(Figures 1C, S1D and S1F)**. Thus, even though both Pten and Trp53 are efficiently ablated in PEC, most PINs do not progress, and only some generate adenocarcinoma or sarcomatoid tumors.

To determine the proliferation rate of PECs at various time after gene ablation, we performed Ki67 immunofluorescence staining. At 1 month, the percentage of Ki67 positive PECs in DLP was ~ 5-6 fold higher in Pten/Trp53$^{(i)pe-/-}$ mice than in control mice, and similar to that of Pten$^{(i)pe-/-}$ mice **(Figure S1G)**. At 2 months, it further increased in Pten/Trp53$^{(i)pe-/-}$ mice and was ~ 3 fold higher than in Pten$^{(i)pe-/-}$ mice **(Figure S1G)**. Importantly, at 5-6 months, percentage of Ki67-positive PECs of PIN-containing prostates in Pten/Trp53$^{(i)pe-/-}$ mice was ~ 2-3 fold lower than at 2 months and similar to that of age-matched Pten$^{(i)pe-/-}$ mice, but was still ~ 2-3 fold higher than in control mice **(Figures 1C, 1D and S1G)**, in agreement with previous results (Parisotto et al., 2018). Interestingly, the proliferation of PECs of

adenocarcinoma in AP and of sarcomatoid tumors in Pten/Trp53$^{(i)pe-/-}$ mice was ~ 2-4 fold higher than that of PINs in AP and DLP **(Figures 1C, 1D, S1D and S1H)**. Thus, even though loss of Trp53 enhances Pten-null PECs proliferation 2 months after gene ablation, the proliferation rate of PECs in PIN-containing prostates is low ~ 5-6 months after gene ablation in both Pten$^{(i)pe-/-}$ and Pten/Trp53$^{(i)pe-/-}$ mice. In contrast, PECs of 24% of Pten/Trp53$^{(i)pe-/-}$ mice actively proliferate in adenocarcinoma and sarcomatoid tumors, and ~ 40 % of Pten/Trp53$^{(i)pe-/-}$ mice with sarcomatoid tumors develop peritoneal metastases within 9 months after gene ablation.

Pten/Trp53-deficient PECs of PINs are senescent

To further characterize PECs in Pten/Trp53$^{(i)pe-/-}$ mice, we analyzed the expression of cell cycle regulators between 1 and 6 months after Pten and Trp53 ablation. RT-qPCR showed that transcript levels of negative cell cycle regulators (e.g. p16, p19^{ARF}, p27 and Rb1) were low at 1 month in the DLP and AP of control, Pten$^{(i)pe-/-}$ and Pten/Trp53$^{(i)pe-/-}$ mice, whereas those of p21 were ~ 5-6 fold higher in Pten$^{(i)pe-/-}$ and Pten/Trp53$^{(i)pe-/-}$ mice than in control mice **(Figure S2A)**. At 2 months, transcript levels of p16, p19^{ARF}, p21, p27 and Rb1 were similarly increased in Pten$^{(i)pe-/-}$ and Pten/Trp53$^{(i)pe-/-}$ mice **(Figure S2B)**. Five to six months after gene ablation, the transcript levels of p16, p19^{ARF} and p21 were further increased in PIN-containing prostates of Pten/Trp53$^{(i)pe-/-}$ mice, but not of Pten$^{(i)pe-/-}$ mice **(Figure 2A)**, whereas p27 and Rb1 levels were similar. Interestingly, at this time point, most PINs in Pten$^{(i)pe-/-}$ and Pten/Trp53$^{(i)pe-/-}$ mice exhibited staining for senescence-associated β-galactosidase (SA-βGal), a faithful marker of cell senescence (Collado and Serrano, 2006) **(Figure 2B)**. Moreover, transcript levels of lysosomal-β-galactosidase (Glb1), encoding SA-βGal, were similarly increased in PIN-containing prostates of Pten/Trp53$^{(i)pe-/-}$ and Pten$^{(i)pe-/-}$ mice 5-6 months after gene ablation **(Figure 2C)**. To further characterize PINs of Pten/Trp53$^{(i)pe-/-}$ mice, phosphorylated S83 heterochromatin protein 1 γ (pHP1γ), indicative of senescence associated heterochromatin foci (SAHF) (Adams, 2007), was immunodetected. At 1 month, few PECs of Pten/Trp53$^{(i)pe-/-}$ mice displayed nuclear pHP1γ staining, and as expected no pHP1γ staining was observed in control mice **(Figures S3A and S3B)**. In contrast, PECs of PINs were pHP1γ-positive in Pten/Trp53$^{(i)pe-/-}$ mice at 2 and 5 months after gene ablation **(Figures S3C and S3D)**, as previously seen in Pten$^{(i)pe-/-}$ mice (Parisotto et al., 2018). Thus, Trp53 attenuates the proliferation peak of Pten-null PECs, but is not mandatory for senescence induction.

To further characterize senescent PINs, we analyzed the transcript levels of genes involved in SASP in the DLP and AP of Pten$^{(i)pe-/-}$ and of Pten/Trp53$^{(i)pe-/-}$ mice at various time after gene ablation. At 1 month, the transcript levels of Il1β, Cxcl1, Cxcl2 and Cxcl5 were expressed at low levels in the prostate of control, Pten$^{(i)pe-/-}$ and Pten/Trp53$^{(i)pe-/-}$ mice, while those of Tnfα and Csf1 were higher in

Pten/Trp53$^{(i)pe-/-}$ mice than in control and Pten$^{(i)pe-/-}$ mice **(Figure S2C)**. Moreover, at 2 months, the transcript levels of Csf1, Cxcl1 and Cxcl5 were ~ 20 fold higher in Pten/Trp53$^{(i)pe-/-}$ mice than in control mice, and ~ 4-5 fold higher than in Pten$^{(i)pe-/-}$ mice **(Figure S2D)**. Five to six months after gene ablation, the transcript levels of Il1β, Tnfα, Csf1, Cxcl1, Cxcl2, Cxcl5 and Ccl2 were ~ 10-15 fold higher in PIN-containing prostates of Pten/Trp53$^{(i)pe-/-}$ mice than in control mice, whereas those of Csf1, Cxcl1, Cxcl2 and Cxcl5 were ~ 3-4 fold higher in PIN-containing prostates of Pten/Trp53$^{(i)pe-/-}$ mice than in Pten$^{(i)pe-/-}$ mice **(Figure 2D)**. In addition, as infiltrating MDSCs has been shown to oppose senescence and drive tumorigenesis (Katoh et al., 2013), we examined the transcript levels of markers of the myeloid lineage. Those of Cd11b, and of the two GR-1 variants, Ly6c and Ly6g, were higher in the prostates of Pten$^{(i)pe-/-}$ mice than of control mice at 2 and 5 months, but not at 1 month **(Figures 3A-C)**. The transcript levels of those markers were further increased in PIN-containing prostates of Pten/Trp53$^{(i)pe-/-}$ mice at 2 and 5 months **(Figures 3A-C)**. Therefore, lack of Trp53 in Pten-deficient PECs enhances the levels of factors of SASP and MDSCs recruitment, and thus might contribute to tumor progression via enhancing the reprogramming stem cell markers.

Pten/Trp53-deficient PECs in PINs express stemness and neuroendocrine markers

To further characterize PINs of Pten/Trp53$^{(i)pe-/-}$ mice, we performed transcriptomic analyses of DLP and AP at 5-6 months after gene ablation. RNA sequencing revealed that 861 genes were upregulated and 614 were downregulated in SSP from Pten/Trp53$^{(i)pe-/-}$ compared to aged-matched control mice **(Figure 2E)**. Pathway analyses using Wikipathways showed that inflammation, immune cell regulation and senescence were mainly affected (e.g. Toll-like receptor signaling, Chemokine signaling, B and T cell receptor signalling, TNFα-NFκB signalling and senescence pathways) **(Figure 2F)**. As expected, among the most upregulated genes are regulators of cell cycle arrest (e.g. Cdkn2a and p16) and genes involved in SASP (e.g. Cxcl1, Cxcl2, Cxcl5, Tnf, Il1β and Csf1). Strikingly, stem cell reprogramming factors (e.g. Cd44, Sox2, Ezh2, Nanog) and neuroendocrine markers (e.g. Syp, Eno2, Chga, Ascl1) were also affected **(Figure 2G and data not shown)**.

RT-qPCR analyes showed that the transcript levels of reprogramming factors (e.g. Sox2, Ezh2 and Nanog) involved in generating induced pluripotent stem cells (iPSCs) (Bracken et al., 2003) were higher in the prostates of Pten$^{(i)pe-/-}$ mice than of control mice **(Figure 4A)**, and those of Sox2 (sex determining region Y-box 2) and Nanog (Nanog homeobox) were significantly higher in PIN-containing prostates of Pten/Trp53$^{(i)pe-/-}$ mice than of Pten$^{(i)pe-/-}$ mice 5-6 months after gene ablation **(Figure 4A)**. In agreement with these results, immunohistochemical analyses showed that most of the PECs of PINs in Pten$^{(i)pe-/-}$ and Pten/Trp53$^{(i)pe-/-}$ mice express Ezh2 (enhancer of zeste 2 polycomb repressive complex 2 subunit),

whereas few Ezh2-positive nuclei were detected in PECs of control mice **(Figure 4B)**. Moreover, more PECs in PINs of Pten/Trp53$^{(i)pe-/-}$ mice displayed nuclear Sox2 and Nanog staining than of Pten$^{(i)pe-/-}$ mice, whereas no Sox2- and Nanog-positive nuclei were detected in PEC of control mice **(Figure 4B)**. Thus, loss of Trp53 and/or Pten in deficient PECs induces the expression of reprogramming factors that might create a stem-cell-like environment lineage plasticity. In addition, 5-6 months after gene ablation, transcript levels of the neuroendocrine markers Chga and Ascl1 were 4-8 fold higher in PIN-containing prostates of Pten$^{(i)pe-/-}$ and Pten/Trp53$^{(i)pe-/-}$ mice than in control mice **(Figure 4C)**, whereas Syp and Eno2 transcript levels were strongly induced in PIN-containing prostates of Pten/Trp53$^{(i)pe-/-}$ mice, but not of those of Pten$^{(i)pe-/-}$ mice **(Figure 4C)**. Immunohistochemical analyses of Syp showed few Syp-positive cells in PINs of Pten$^{(i)pe-/-}$ mice and clusters of Syp-positive cells in PINs of Pten/Trp53$^{(i)pe-/-}$ mice. In contrast, as expected, only neuroendocrine cells but not luminal PECs displayed Syp staining in control mice **(Figure 4D)**. Together, loss of Trp53 in Pten-deficient PECs enhances the expression of reprogramming factors and neuroendocrine markers.

The transcript levels of luminal markers Krt8 and AR were similar in prostates of Pten$^{(i)pe-/-}$, Pten/Trp53$^{(i)pe-/-}$ and aged-matched control mice 5-6 months after gene ablation **(Figure 5A)**, and immunohistochemical analyses revealed that all epithelial cells in PINs of Pten$^{(i)pe-/-}$ and of Pten/Trp53$^{(i)pe-/-}$ mice expressed Krt8 in the cytoplasm and AR in the nucleus **(Figure 5B)**. Moreover, whereas the transcript levels of the basal markers Krt5, Krt14 and Trp63 were similar in the prostate of Pten$^{(i)pe-/-}$ and control mice, those of Krt14 were selectively increased in the prostate of Pten/Trp53$^{(i)pe-/-}$ mice **(Figure 5A)**. In agreement with these results, about 30 % of PECs in PINs of Pten/Trp53$^{(i)pe-/-}$ contained high Krt14 levels, whereas only basal prostatic cells were Krt14-positive in Pten$^{(i)pe-/-}$ and control mice **(Figure 5B)**. Importantly, all Krt14-positive Pten/Trp53-deficient PECs expressed Krt8, and some of Krt8-positive Pten/Trp53-deficient PECs expressed Krt14 **(Figures 5C and 5D)**, providing the evidence of the presence of mixed population of Pten-null PECs after the loss of Trp53. Strikingly, Syp was always co-expressed with Krt8, but not with Krt14 in Pten/Trp53-deficient PECs **(Figures 5C and 5D)**. Taken together, loss of Trp53 in Pten-deficient PECs leads to the formation of mixed population of PECs exhibiting both luminal and basal characteristics in prostatic lesions, and only luminal PECs express focal neuroendocrine markers.

Characterization of sarcomatoid tumors in Pten/Trp53$^{(i)pe-/-}$ mice

Transcriptomic analyses revealed that 944 genes were upregulated in sarcomatoid tumors compared to PIN-containing prostates of Pten/Trp53$^{(i)pe-/-}$ mice, and that 400 were downregulated **(Figure S4A)**. The most upregulated genes are involved in cell adhesion and migration (e.g. Postn, Pcdh10, Itgα11

and Pcdh15) and in biomineralization process of osteoblasts (e.g. Omd) **(Figure S4B)**. Pathway analyses further support the latter in which focal adhesion and intergrin-mediated cell adhesion were enriched in sarcomatoid tumors of Pten/Trp53$^{(i)pe-/-}$ mice **(Figure S4C)**. Whereas PIN-containing DLP and AP of Pten/Trp53$^{(i)pe-/-}$ mice expressed high levels of transcripts of epithelial markers (e.g. E-cad and β-cat) and low levels of mesenchymal markers (e.g. Vim, N-cad, Slug, Snai1 and Zeb1), sarcomatoid tumors (SARC) expressed high transcript levels of the latter, and low levels of the former (e.g. E-cad and β-cat) **(Figure S4D)**. Taken together, this further indicates that sarcomatoid tumors of Pten/Trp53$^{(i)pe-/-}$ mice can develop metastases.

Importantly, transcript levels of genes involved in SASP (e.g. IL-1β, TNFα, Cxcl2 and Cxcl5) as well as of myeloid lineage markers (e.g. Ly6c and Ly6g) were lower in sarcomatoid tumors than in PIN-containing prostates of Pten/Trp53$^{(i)pe-/-}$ mice **(Figures S4E and S4F)**, indicating that MDSCs recruitment occured only in the presence of senescent cells.

Supplemental Results

Pten/Trp53 deficiency in PECs of PINs induces replication stress

As cellular senescence is induced by stress such as DNA damage response (DDR) (Coppe et al., 2008), we examined whether observed senescence in PINs of Pten/Trp53$^{(i)pe-/-}$ mice is induced by replication stress-mediated DDR signaling. Replication protein A (RPA) phosphorylation at distinct sites occurs at stalled replication forks, and DNA double-strand breaks (DSBs) produced from stalled DNA replication induce S4 and S8 phosphorylation of RPA32 (Liaw et al., 2011; Sirbu et al., 2011). Herein, we revealed that at 1 month PEC nuclei of Pten/Trp53$^{(i)pe-/-}$ mice were RPA32-pS4/S8 negative, as well as in PECs of control mice **(Figures S5A and S5B)**. Interestingly, at 2 and 5 months, many PEC nuclei in PINs of Pten/Trp53$^{(i)pe-/-}$ mice contained high levels of S4/S8 phosphorylated RPA32, indicating that DNA DSBs follow replication fork stalling **(Figures S5C and S5D)**. Numerous nuclear staining of p53-binding protein 1 (53BP1) were also observed in PECs of PINs in Pten/Trp53$^{(i)pe-/-}$ mice 1, 2, and 5 months after gene ablation, showing the activation of DDR (Lukas et al., 2011). In contrast, no 53BP1 was observed in the nuclei of PECs of control mice **(Figure S5A)**. Taken together, Pten/Trp53-deficient PECs undergo replication stress and mount a DDR at 2 months leading to PECs senescence 5 months after gene ablation, similarly as those of Pten$^{(i)pe-/-}$ mice (Parisotto et al., 2018).

Discussion

Previously, we demonstrated that Pten loss-induced cell senescence in mature PECs occurs after a phase of enhanced proliferation, and is initiated via replication stress mediated DDR activation *in vivo*. We also showed that Trp53 stabilization by replication stress-mediated DDR activation contributes to trigger senescence, as in OIS (Parisotto et al., 2018). Supporting these results, we aimed to determine the role of Trp53 in the control of senescence induced by Pten loss in PECs, and therefore we analyzed Pten/Trp53$^{(i)pe-/-}$ mice in which Pten and Trp53 genes are selectively ablated in luminal prostatic cells at adulthood. Importantly, we gain from our mouse model the potential to strictly control the time of both Pten and Trp53 ablation by the activation of CreER^{T2} recombinase in adult mice. In other models, Pten and Trp53 ablation occurs in the undifferentiated prostate of young mice in which Probasin-4 promotor is early activated (in the prostate of newborn mice) and drives the constitutively active Cre recombinase (Chen et al., 2005).

Strikingly, although Pten-null PECs proliferation is enhanced in the absence of Trp53 at 2 months after gene ablation, only PECs of 24 % of Pten/Trp53$^{(i)pe-/-}$ mice develop either adenocarcinoma or sarcomatoid tumors, and the latter develop metastases. However, PECs of 76 % of Pten/Trp53$^{(i)pe-/-}$ mice develop PINs that enter senescence and express higher levels of some senescence markers than those of Pten-null PECs. Thus, Pten-deficient PECs senescence is not fully dependent on Trp53 *in vivo*, in contrast to previous reports demonstrating the essential role of Trp53-dependent cellular senescence in restricting Pten-deficient tumorigenesis (Alimonti et al., 2010; Chen et al., 2005). Thus, therapeutic approaches for restraining Pten-deficient tumorigenesis via p53 activation in favour of cellular senescence is not a promising strategy.

As we show that Pten/Trp53-deficient PECs undergo replication stress and mount a DDR at the phase of enhanced proliferation, 2 months after gene ablation, it is likely that replication stress-mediated DDR activation contributes to trigger senescence in Pten-null PECs in the absence of Trp53. In addition, replication stress might also result in an accumulation of mutations, and thereby might contribute to the early development of adenocarcinoma in Pten/Trp53$^{(i)pe-/-}$ mice compared to Pten$^{(i)pe-/-}$ mice. However, it remains unclear whether the intensity of replication stress is higher in Pten/Trp53-null PECs than in those of Pten-null at 2 months.

It is widely accepted that MDSCs participate to cancer immune evasion by suppressing functions of T and natural killer (NK) cells (Gabrilovich and Nagaraj, 2009). However, the mechanism/s of how MDSCs contribute in cancer progression remains unclear. Di Mitri et al. reported that GR1-positive myeloid cells infiltrate the prostate of PTEN$^{pe-/-}$ mice and oppose Pten loss-induced senescence (PICs) in a paracrine fashion via interfering with SASP through the secretion of the cytokine IL-1RA, an antagonist

of IL-1R (Di Mitri et al., 2014). In addition, SASP has been shown to promote the stem cell reprogramming factors of neighboring cells in a paracrine manner *in vivo* (Mosterio et al., 2016; Ritschka et al., 2017). Herein, along with the senescent phenotype observed in the absensce of Trp53 in Pten-deficient PECs, we noticed elevated SASP and MDSCs levels, as well as increased stemness, suggesting that Trp53 restrain Pten-deficient tumorigenesis via attenuating SASP and MDSCs levels. Strikingly, SASPs and MDSCs levels in PECs of sarcomatoid tumors were markedly reduced compared to PIN-containing prostates of Pten/Trp53$^{(i)pe-/-}$ mice; however, whether SASP and MDSCs-mediated stemness is the mechanism underlying the formation of adenocarcinoma and/or sarcomatoid tumors in Pten/Trp53$^{(i)pe-/-}$ mice remains unclear.

We also show that Trp53 loss induces focal neuroendocrine differentiation of luminal Pten-null PECs in prostatic lesions. Neuroendocrine differentiation is often associated with the resistance to anti-androgen therapies in human and mouse prostate cancer (Ku et al., 2017; Zou et al., 2017). Strikingly, we also reveal that Trp53 loss in Pten-null PECs induces the formation of prostatic cell entity sharing luminal and basal markers and not differentiating into neuroendocrine cells. Therefore, lack of Trp53 promotes lineage plasticity and induces the formation of mixed stem/progenitor cell population of Pten-null PECs in prostatic lesions, which might contribute to castration-resistance and thus predict poor therapeutic outcome.

Taken together, Trp53 is not absolutely required for senescence induction, but is necessary for maintaining cell identity of Pten-null PECs. Although there is an increasing proof that epithelial cells displaying both luminal and stem/progenitor characteristics play a crucial role in prostate cancer progression (Wang et al., 2009; Yoo et al., 2016; Toivanen et al., 2013; Liu et al., 2016), the study of these cells has been hampered by the lack of specific phenotypic markers. Therefore, identification of the phenotypic characteristics of luminal/basal Pten/Trp53-null PECs is needed for the development of new efficient targeted therapies.

Material and Methods

Mouse Care

Mice were maintained in a temperature and humidity controlled animal facility, with a 12h light/dark cycle. Mice breeding and maintenance were performed in the accredited IGBMC/ICS animal house (C67-2018-37), in compliance with French and EU regulations on the use of laboratory animal's research, under the supervision of D.M. who holds animal experimentation authorization from the French Ministry of agriculture and Fisheries (N°67-209 and A 67-227). All animal experiments were approved by the Ethical committee Com'Eth (Comité d'Ethique pour l'Expérimentation Animale, Strasbourg, France). Mice were euthanized by cervical dislocation, and tissues were directly collected, weighed and frozen in liquid nitrogen, or processed for biochemical and histological analysis.

Generation of mouse models

PSA-Cre-ER^{T2} (Feil et al., 1997), Pten$^{L2/L2}$ (Suzuki et al., 2001) and Trp53$^{L2/L2}$ (Jonkers et al., 2001) mice were backcrossed on C57BL/6 mice for more than 8 generations before intercrossing. Genotyping by PCR were performed on genomic DNA isolated from ear biopsies of the mice, using the DirectPCR extraction kit (Viagen, cat # 102-T), and primers as described (Jonkers et al., 2001; Ratnacaram et al., 2008). Mice carrying one copy of the PSA-Cre-ER^{T2} transgene, expressing the tamoxifen-inducible Cre-ER^{T2} recombinase selectively in prostatic epithelium under the control of the human PSA promoter, were crossed with mice carrying loxP-flanked (floxed) alleles of Pten (L2 alleles), to generate PSA-Cre-ER$^{T2(tg/0)}$/Pten$^{L2/L2}$ (tg: transgenic) and PSA-Cre-ER$^{T2(0/0)}$/Pten$^{L2/L2}$ mice. In addition, PSA-Cre-ER$^{T2(tg/0)}$/Pten$^{L2/L2}$ mice were inter-crossed with Trp53$^{L2/L2}$ mice carrying floxed alleles of Trp53 (Jonkers et al., 2001) (see also **Figure S1A**), to generate PSA-Cre-ER$^{T2(tg/0)}$/Pten$^{L2/L2}$/trp53$^{L2/L2}$ and Cre-ER$^{T2(0/0)}$/Pten$^{L2/L2}$/trp53$^{L2/L2}$ mice. Gene ablation was induced by daily intraperitoneal injections of tamoxifen (Tam) (1 mg/mouse) for 5 days to 8 week-old PSA-Cre-ER$^{T2(tg/0)}$/Pten$^{L2/L2}$ and PSA-Cre-ER$^{T2(tg/0)}$/Pten$^{L2/L2}$/trp53$^{L2/L2}$ mice, to generate mutant Pten$^{(i)pe-/-}$ and Pten/trp53$^{(i)pe-/-}$ mice, respectively. PSA-Cre-ER$^{T2(0/0)}$/Pten$^{L2/L2}$ mice (Pten$^{pe+/+}$ mice) and Cre-ER$^{T2(0/0)}$/Pten$^{L2/L2}$/trp53$^{L2/L2}$ mice (Pten/trp53$^{pe+/+}$ mice) were similarly Tam-treated and were used as controls. [pe: prostate epithelium; (i): induced].

RNA extraction and analysis

RNA was isolated from dorsolateral and anterior prostate samples using RNeasy Mini kit (Qiagen), reverse transcribed using SuperScript II Reverse Transcriptase (Invitrogen), and amplified by quantitative PCR with the SYBER Green kit (Roche) and a LightCycler 480 (Roche Diagnostics), according to the manufacturer's instructions. Primer sequences are given in **Table 1**.

Table 1: Primer sequences

Gene	Forward (5' to 3')	Reverse (5' to 3')
18S	CGCGGTTCTATTTTGTTGGT	TCGTCTTCGAAACTCCGACT
p16	GAACTCTTTCGGTCGTACCC	CAGTTCGAATCTGCACCGTA
$p19^{ARF}$	GCTCTGGCTTTCGTGAACAT	GTGAACGTTGCCCATCATC
p21	TCTTCTGCTGTGGGTCAGGAG	GAGGGCTAAGGCCGAAGATG
p27	TTTCATGTATATCTTCCTTGCTTCA	ACGCCAGACGTAAACAGCTC
Rb1	TGCATGGCTTTCAGATTCACC	GCTGAGAGGACAAGCAGGTT
Glb1	GGATGGACAGCCATTCCGAT	CAGGGCACGTACATCTGGATA
Il1β	ACGACAAAATACCTGTGGCC	TGGGTATTGCTTGGGATCCA
Tnfα	CCCCAAAGGGATGAGAAGT	CACTTGGTGGTTTGCTACGA
Csf1	TGCTAGGGGTGGCTTTAGG	CAACAGCTTTGCTAAGTGCTCTA
Cxcl1	CTGGGATTCACCTCAAGAACATC	CAGGGTCAAGGCAAGCCTC
Cxcl2	CCAACCACCAGGCTACAGG	GCGTCACACTCAAGCTCTG
Cxcl5	TGCCCTACGGTGGAAGTCAT	AGCTTTCTTTTTGTCACTGCCC
Ccl2	CACTCACCTGCTGCTACTCA	GCTTGGTGACAAAAACTACAGC
Cd11b	CAAAGAACAACACACGCAGG	GGCTCCCCAACCAGTGTATA
Ly6c	ATAGCACTCGTAGCACTGCA	ACCTTGTCTGAGAGGAACCC
Ly6g	TGTGCTCATCCTTCTTGTGG	AGGGGCAGGTAGTTGTGTTG
Sox2	CAAAAACCGTGATGCCGACT	CGCCCTCAGGTTTTCTCTGT
Ezh2	ACTGCTTCCTACATCCCTTCC	AGAGCAGCAGCAAACTCCTT
Nanog	TTCCTGGTCCCCACAGTTTG	GGCGAGGAGAGGCAGC
Syp	CCATTCAGGCTGCACCAAGT	TTCAGCCGAGGAGGAGTAGT
Eno2	CTGTGCCGGCCTTTAATGTG	GAAAGCTCTCAGCACCCACT
Chga	AGGGGACACCAAGGTGATGA	AGCAGATTCTGGTGTCGCAG
Ascl1	AATGGACTTTGGAAGCAGGATG	CCATTTGACGTCGTTGGCG
krt8	CGGCTACTCAGGAGGACTGA	TGAAAGTGTTGGATCCCCCG
AR	CTGCCTCCGAAGTGTGGTAT	GCCAGAAGCTTCATCTCCAC
Krt5	TGGCGATGACCTTCGAAACA	GGTTGGCACACTGCTTCTTG
Krt14	CTACCTGGACAAGGTGCGTG	CCAGGATCTTGCTCTTCAGGT
Trp63	AACACAGACCACGCACAGAA	TTCGGTGGAATACGTCCAGG
E-cad	AACCCAAGCACGTATCAGGG	GAGTGTTGGGGGCATCATCA
β-cat	GTCAGTGCAGGAGGCCG	CAGGTCAGCTTGAGTAGCCA
Vim	AGGCCGAGGAATGGTACAA	TCTTCCATCTCACGCATCTG
N-cad	TTGCTTCAGGCGTCTGTGGAG	TTCGTGCACATCCTTCGGTAA
Slug	ACATTCGAACCCACACATTGC	AAGAGAAAGGCTTTTCCCCAGT
Snai1	TGTGTGGAGTTCACCTTCCAG	AGAGAGTCCCAGATGAGGGT
Zeb1	CCGCCAACAAGCAGACTAT	GGCGTGGAGTCAGAGTCAT
Zeb2	AAGTACCGCCACGAGAAGA	GAACTTGCGGTTACCTGCTC

RNA-seq data analysis

RNA-sequencing was performed by the GenomEast platform, a member of the "France Génomique" consortium (ANR-10-INBS-0009). Reads were mapped onto the mm10 assembly of mouse genome using Tophat v2.0.10 (Kim et al., 2013) and the Bowtie2 v2.1.0 aligner (Langmead and Salzberg, 2012). Only uniquely aligned reads have been retained for further analyses. Quantification of gene expression was performed using HTSeq-0.6.1. Read counts were normalized across libraries with the method proposed by Anders and Huber (Anders and Huber, 2010). Comparisons of interest were performed using the method proposed by Love et al. (Love, Huber and Anders, 2014) implemented in the DESeq2 Bioconductor library (DESeq2 v1.0.19). Resulting p-values were further adjusted for multiple testing using Benjamini and Hochberg method (Benjamini, 1995). A gene is considered to be differentially expressed if the p-value is less or equal to 10^{-5}.

Histological analysis

Prostate tissues were immediately fixed in ice-cold 4% formaldehyde supplemented with 1 tablet/10 mL of PhosSTOP (04 906 837 001, Roche). Prostate tissues were embedded in paraffin and sectioned at 5 µm. For histopathological analyses, paraffin sections were stained with hematoxylin and eosin. Immunofluorescence staining (IF) was performed as described (Ratnacaram et al., 2008; Parisotto et al., 2018). Primary antibodies used for IF were directed against AKT pS473 (4060, Cell Signaling Technology; 1/200), Ki67 (SP6, Thermo-Scientific; 1/500), p53 (CM5) (Lin-P956, Linaris; 1/500), pHP1γ (2600, Cell Signaling Technology; 1/200), RPA32 pS4/S8 (Bethyl Laboratories A300-245A; 1/200) and 53BP1 (NB100-305, Novus Biologicals; 1/200). Secondary antibodies [CY3 AffiniPure goat anti-rabbit IgG (H+L)] were from Jackson Immunoresearch. For immunohistochemistry (IHC), paraffin sections were treated with 3% H_2O_2 (in PBS 1X) to block endogenous peroxidase activity before antigen retrieval with citrate buffer (pH=6) boiled in a microwave (750 W for 10 min). Slides were then blocked with 1.5% of normal rabbit serum (Vector Laboratories) and incubated with primary antibodies against Sox2 (14962, Cell Signaling Technology; 1/100), Ezh2 (5246, Cell Signaling Technology; 1/200), Nanog (8822, Cell Signaling Technology; 1/50), Syp (SP11, Invitrogen; 1/20), krt8 (GTX109489, GeneTex; 1/200), AR (N-20) (G2613, Santa Cruz biotechnology; 1/200) and krt14 (PRB-155P, Covance; 1/400) overnight at 4°C, followed by incubation with biotinylated goat anti-rabbit IgG (Vector Laboratories) for 1h at room temperature (RT) and treatment of AB complex (Vector Laboratories) for 30 min at RT. Staining was visualized by the substrate chromogen solution (DAB) (Vector Laboratories) and then counterstained with hematoxylin.

Senescence-associated β-galactosidase staining

As previously described (Parisotto et al., 2018), 10 µm frozen prostate sections were cut with a cryostat, fixed in 2% formaldehyde and 0.2% glutaraldehyde, stained in 100 mM $K_3Fe(CN)_6$, 100 mM $K_4Fe(CN)_6$, 2 mM $MgCl_2$, 150 mM NaCl, citric acid phosphate buffer (0.2 M Na_2HPO_4, 0.1 M citric acid), 1 mg/mL X-gal (Euromedex) for 6 h at 37°C and counterstained with hematoxylin.

Statistical analysis

Statistical analyses were performed with the one-way ANOVA test and Unpaired t-Test using GraphPad Prism.

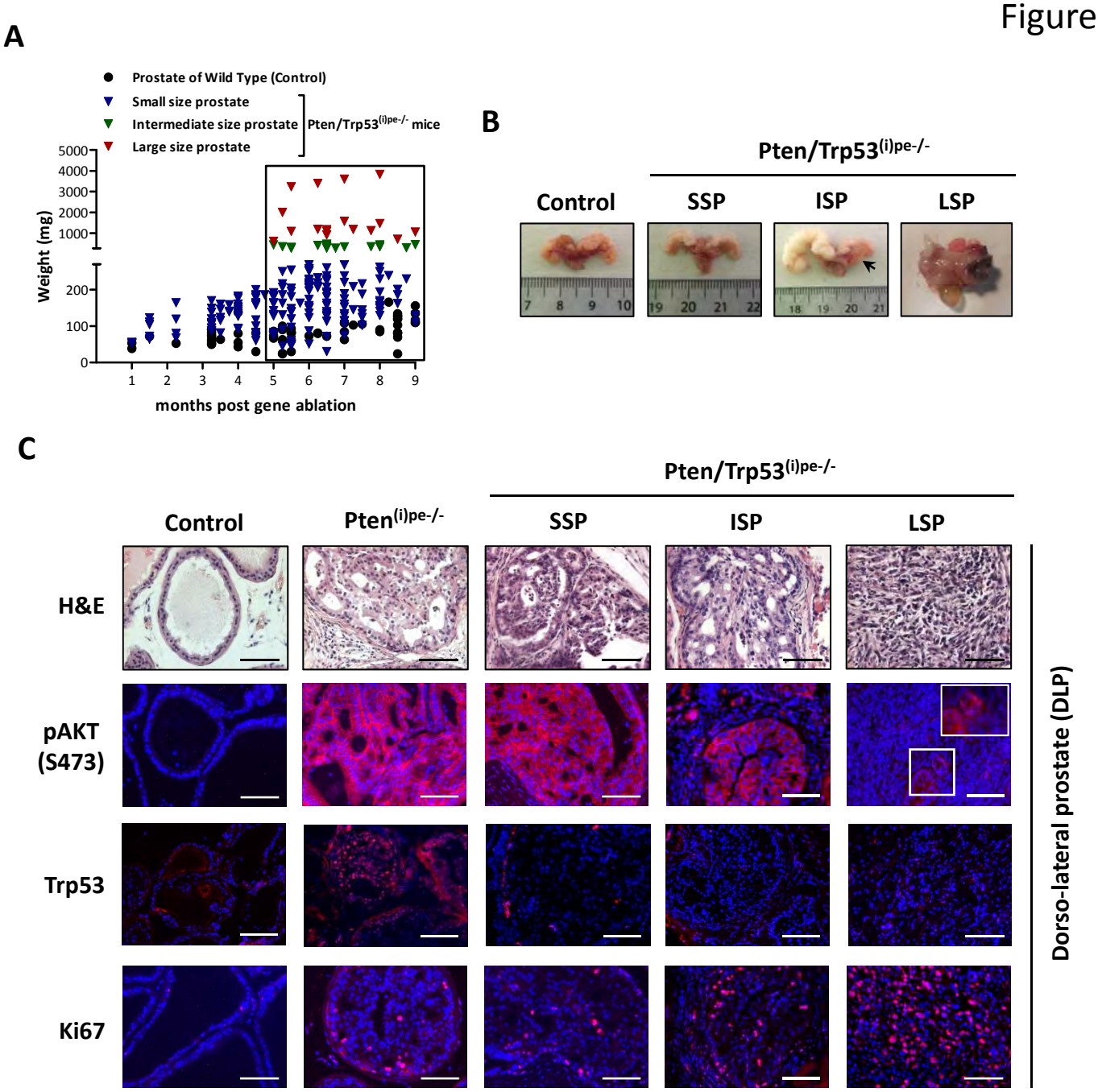

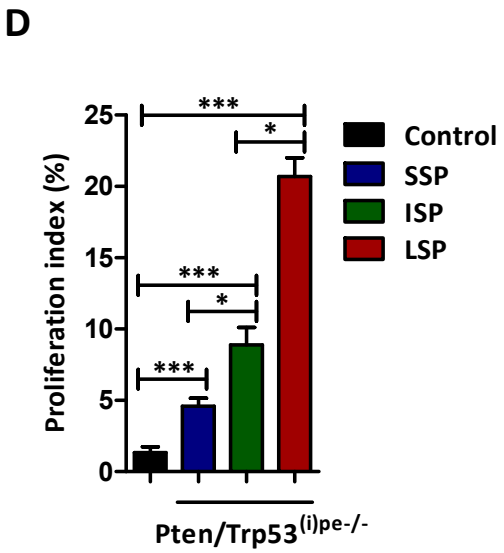

Figure 1. Characterization of prostatic lesions in Pten/Trp53$^{(i)pe-/-}$ mice.

(**A**) Prostate weight (mg) of Pten/Trp53$^{(i)pe-/-}$ and control mice over 9 months after gene ablation. (**B**) Macroscopic views of prostates of Pten/Trp53$^{(i)pe-/-}$ and control mice. Black arrow showing AP of intermediate prostate. (**C**) Representative views of DLP sections of Pten$^{(i)pe-/-}$, Pten/Trp53$^{(i)pe-/-}$ and control mice sacrificed 5-6 months after gene ablation. Sections were stained with hematoxylin-eosin (HE), or immunostained with pAKT (S473), p53 and Ki67 (red). n=4-5/group. Blue: Dapi. Scale bar: 75 µm. (**D**) Proliferation index (percentage of Ki67-positive prostatic luminal epithelial cells) in DLP of Pten/Trp53$^{(i)pe-/-}$ and control mice sacrificed 5-6 months after gene ablation. Values are mean from 4-9 mice ± SEM. One-way ANOVA. *p<0.05; ***p<0.001.

A

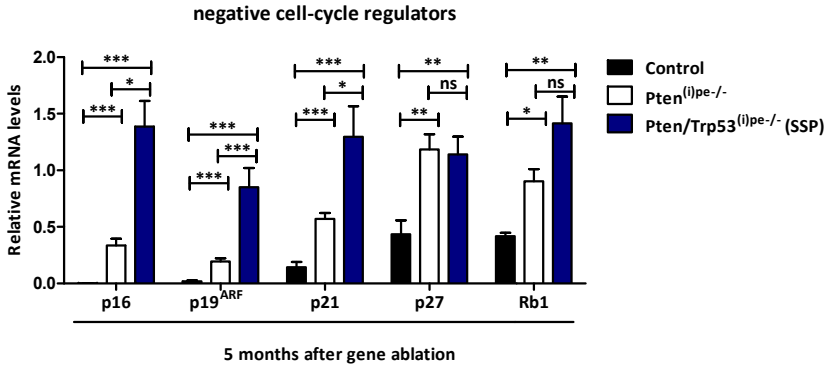

B

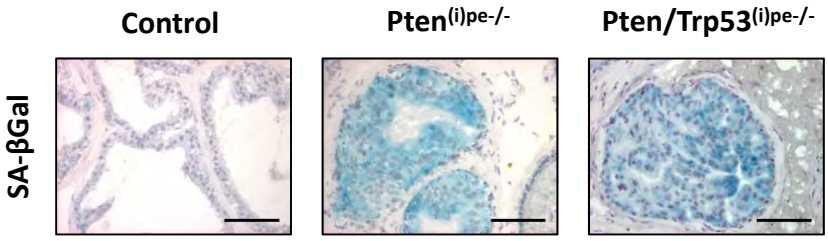

C

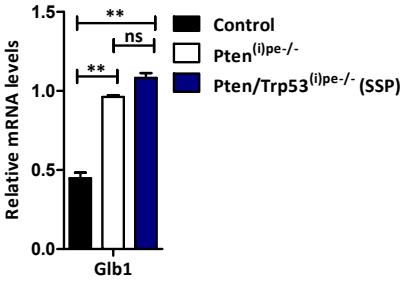

D

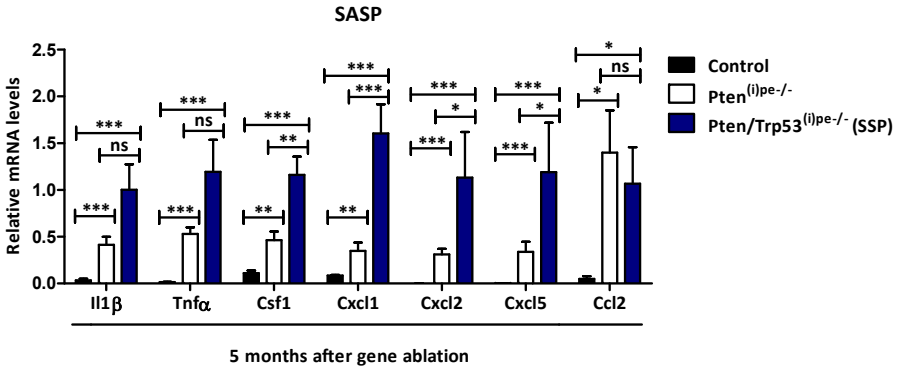

E

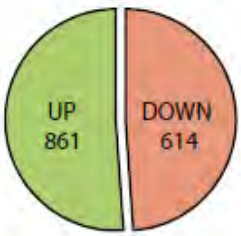

F

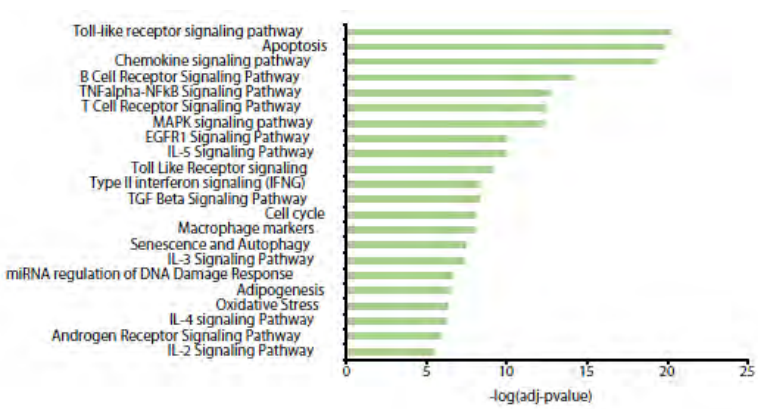

G

Upregulated gene name	LFC
Cxcl2	9.57
Cxcl5	8.92
Tnf	7.44
Il1b	7.01
Cdkn2a	6.22
Cxcl1	6.21
Cd44	4.29
Csf1	2.64

Figure 2. Characterization of senescence phenotype in PINs of Pten/Trp53$^{(i)pe-/-}$ mice.
Relative transcript levels of negative cell-cycle regulators (**A**) and genes involved in senescence-associated secretory proteins (SASP) (**D**) in the DLP and AP of Pten$^{(i)pe-/-}$, Pten/Trp53$^{(i)pe-/-}$ (SSP) and control mice sacrificed 5-6 months after gene ablation. Values are mean from 4-9 mice ± SEM. One-way ANOVA. *p<0.05; **p<0.01; ***p<0.001; ns, not significant. (**B**) Representative senescence-associated β-galactosidase (SA-βGal) staining (blue) of DLP sections of Pten$^{(i)pe-/-}$, Pten/Trp53$^{(i)pe-/-}$ (SSP) and control mice sacrificed 5-6 months after gene ablation. Pink: hematoxylin staining. Scale bar: 75 μm. (**C**) Relative transcript levels of Glb1 in the DLP and AP of Pten$^{(i)pe-/-}$, Pten/Trp53$^{(i)pe-/-}$ (SSP) and control mice sacrificed 5-6 months after gene ablation. Values are mean from 3-4 mice ± SEM. One-way ANOVA. **p<0.01; ns, not significant. Venn diagram showing upregulated and downregulated genes in PINs versus control (**E**). Pathway analyses showing significantly enriched pathways for the set of upregulated and downregulated genes in PINs versus control (**F**). Most upregulated genes in PINs versus control (**G**).

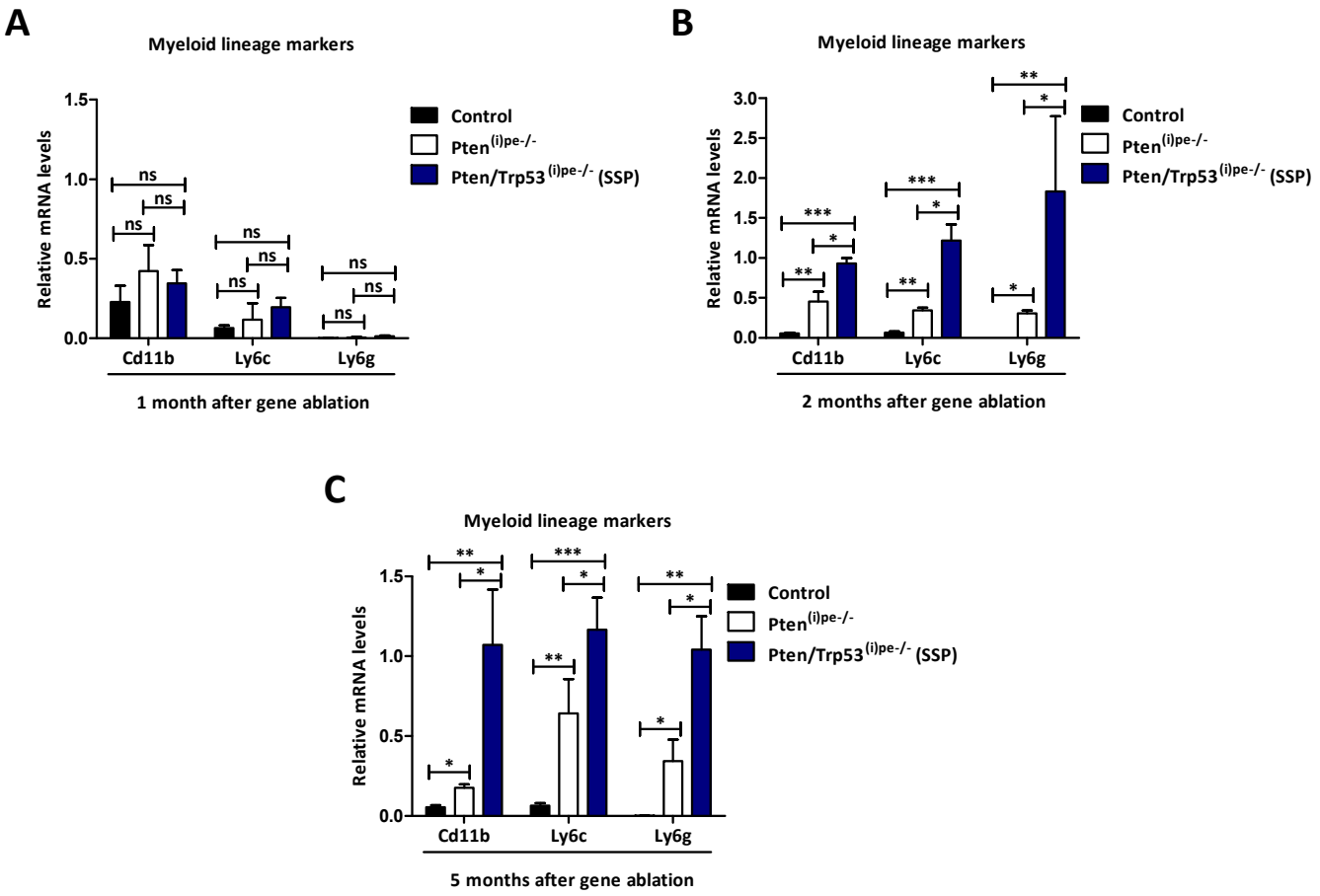

Figure 3. Analyses of myeloid lineage markers during PIN evolution in Pten$^{(i)pe-/-}$ and Pten/Trp53$^{(i)pe-/-}$ mice.

Relative transcript levels of myeloid lineage markers in the DLP and AP of Pten$^{(i)pe-/-}$, Pten/Trp53$^{(i)pe-/-}$ and control mice sacrificed 1 (**A**), 2(**B**) and 5-6 (of SSP) (**C**) months after gene ablation. Values are mean from 3-5 mice ± SEM. One-way ANOVA. *p<0.05; **p<0.01; ***p<0.001; ns, not significant.

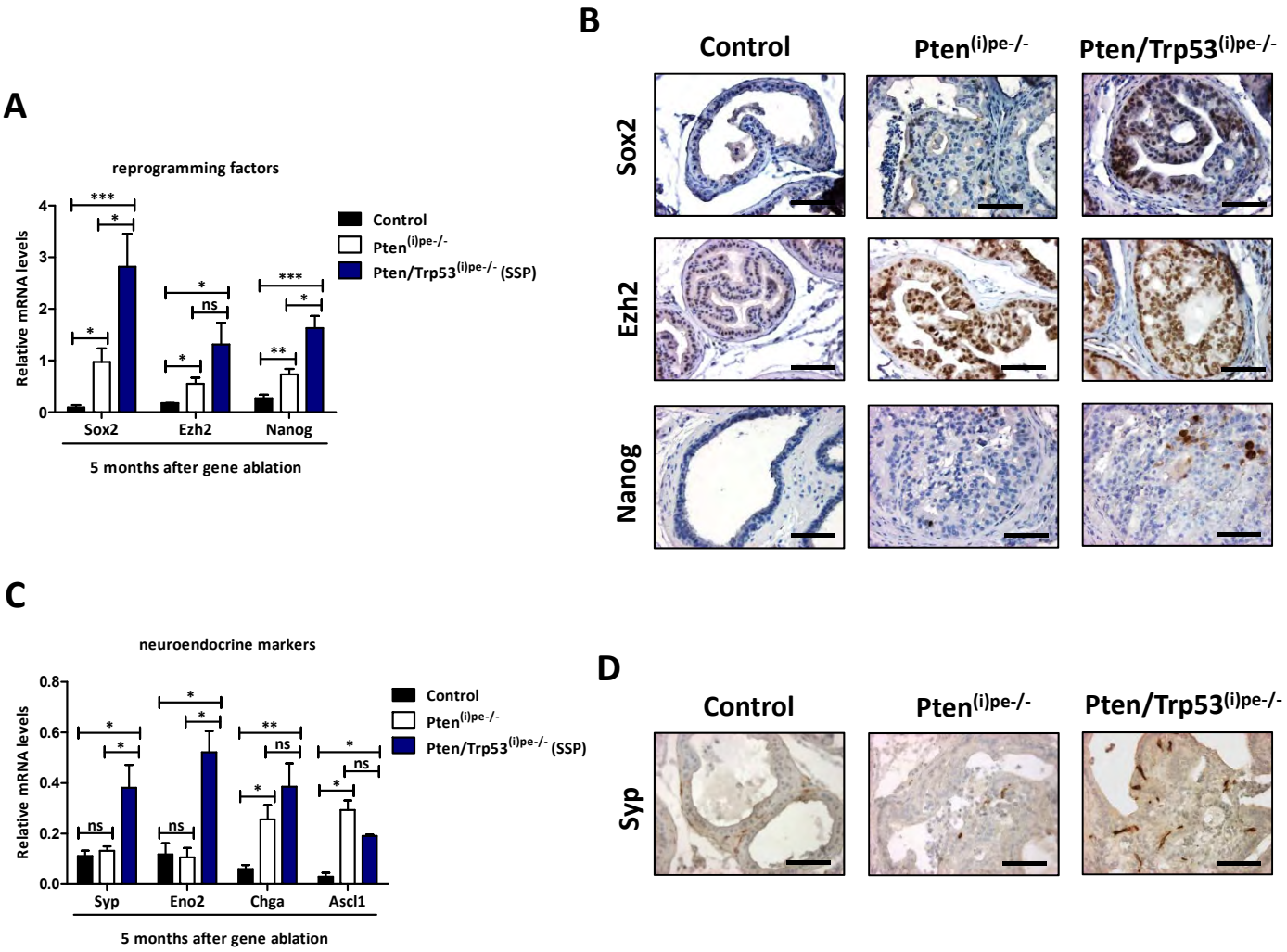

Figure 4. Characterization of cellular reprogramming and morphologic features of neuroendocrine differentiation in PINs of Pten$^{(i)pe-/-}$ and Pten/Trp53$^{(i)pe-/-}$ mice.

Transcript levels of reprogramming factors (**A**) and of neuroendocrine markers (**C**) in the DLP and AP of Pten$^{(i)pe-/-}$, Pten/Trp53$^{(i)pe-/-}$ (SSP) and control mice sacrificed 5-6 months after gene ablation. n=3-4 for each group. Values are mean from 3-4 mice ± SEM. One-way ANOVA. *p<0.05; **p<0.01; ***p<0.001; ns, not significant. Immunohistochemical analyses of reprogramming factors (Sox2, Ezh2 and Nanog) (**B**) and of neuroendocrine marker (Syp) (**D**) in the DLP of Pten$^{(i)pe-/-}$, Pten/Trp53$^{(i)pe-/-}$ (SSP) and control mice sacrificed 5-6 months after gene ablation. Blue: hematoxylin staining. Scale bar: 75 µm.

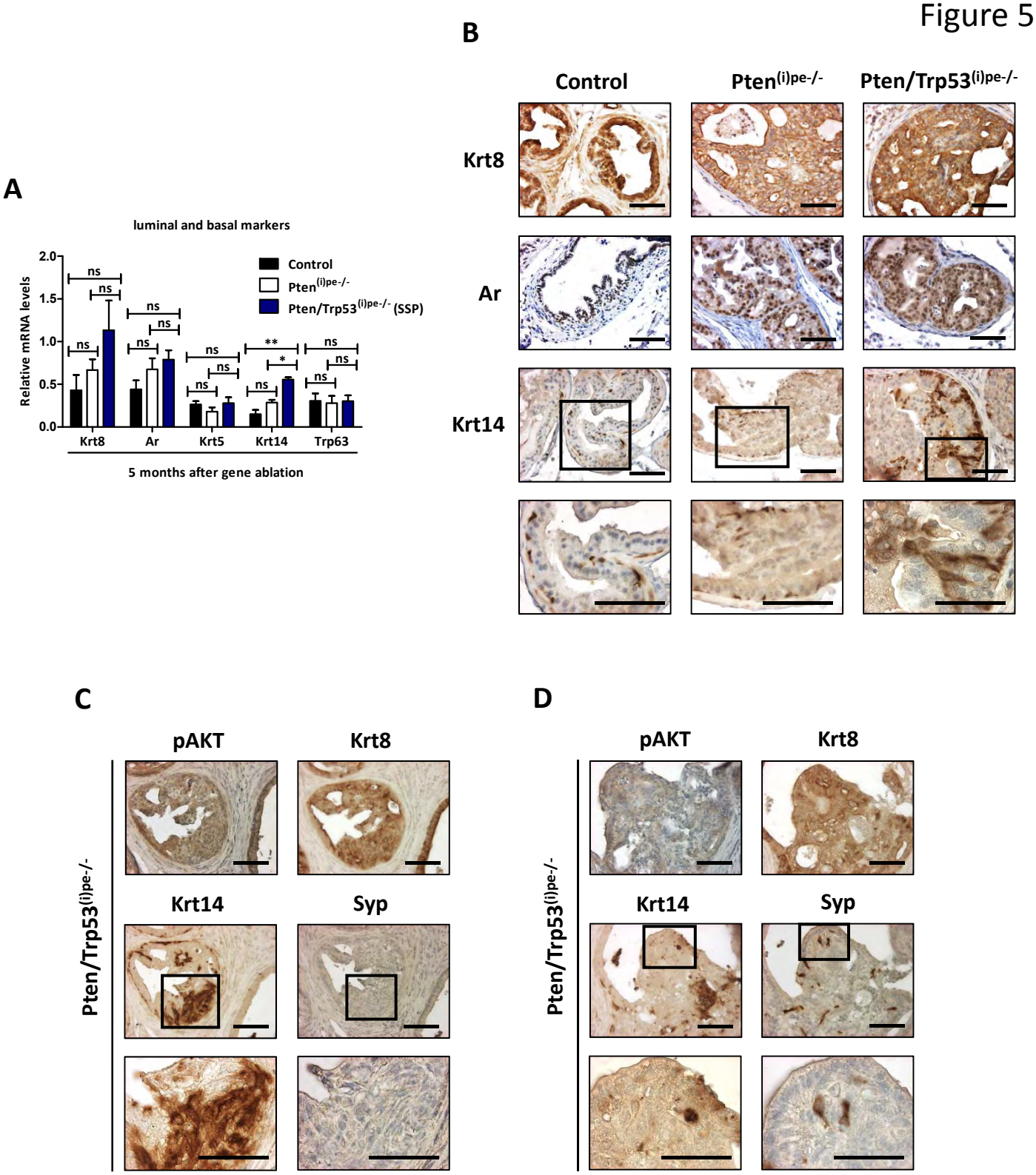

Figure 5. Characterization of luminal and basal markers in Pten$^{(i)pe-/-}$ and Pten/Trp53$^{(i)pe-/-}$ mice.
(**A**) Transcript levels of luminal and basal markers in the prostate of Pten$^{(i)pe-/-}$, Pten/Trp53$^{(i)pe-/-}$ (SSP) and control mice sacrificed 5-6 months after gene ablation. n=3-4 mice for each group. Values are mean from 3-4 mice ± SEM. One-way ANOVA. *p<0.05; **p<0.01; ns, not significant. (**B**) Immunohistochemical analyses of luminal markers (Krt8 and AR) and basal marker (Krt14) in the DLP of Pten$^{(i)pe-/-}$, Pten/Trp53$^{(i)pe-/-}$ (SSP) and control mice sacrificed 5 months after gene ablation. n=3-4 mice for each group. (**C**) and (**D**) Immunohistochemical analyses of pAKT, Krt8, Krt14 and Syp in adjacent sections of Pten/Trp53$^{(i)pe-/-}$ (SSP) mice sacrificed 5-6 months after gene ablation. n=3-4 mice. Blue: hematoxylin staining. Scale bar: 75 µm.

Supplemental figure 1

A

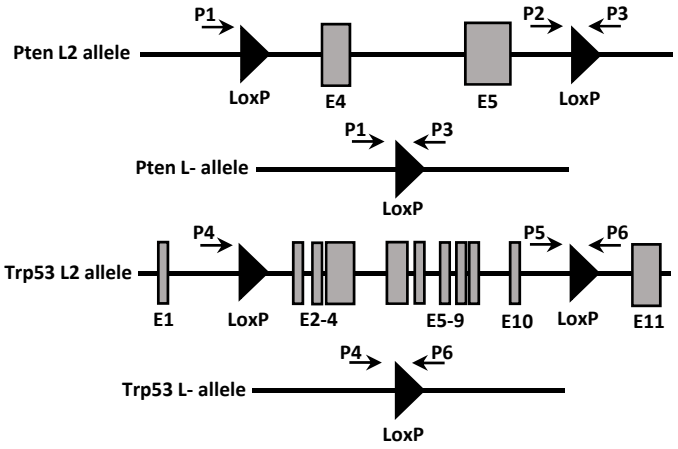

B

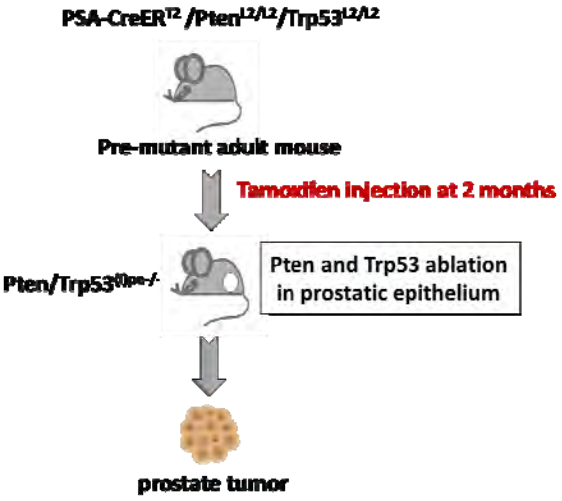

C

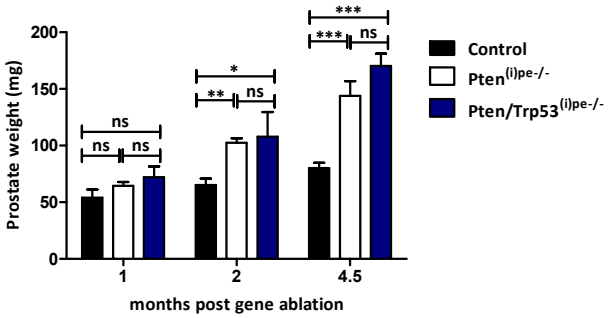

D

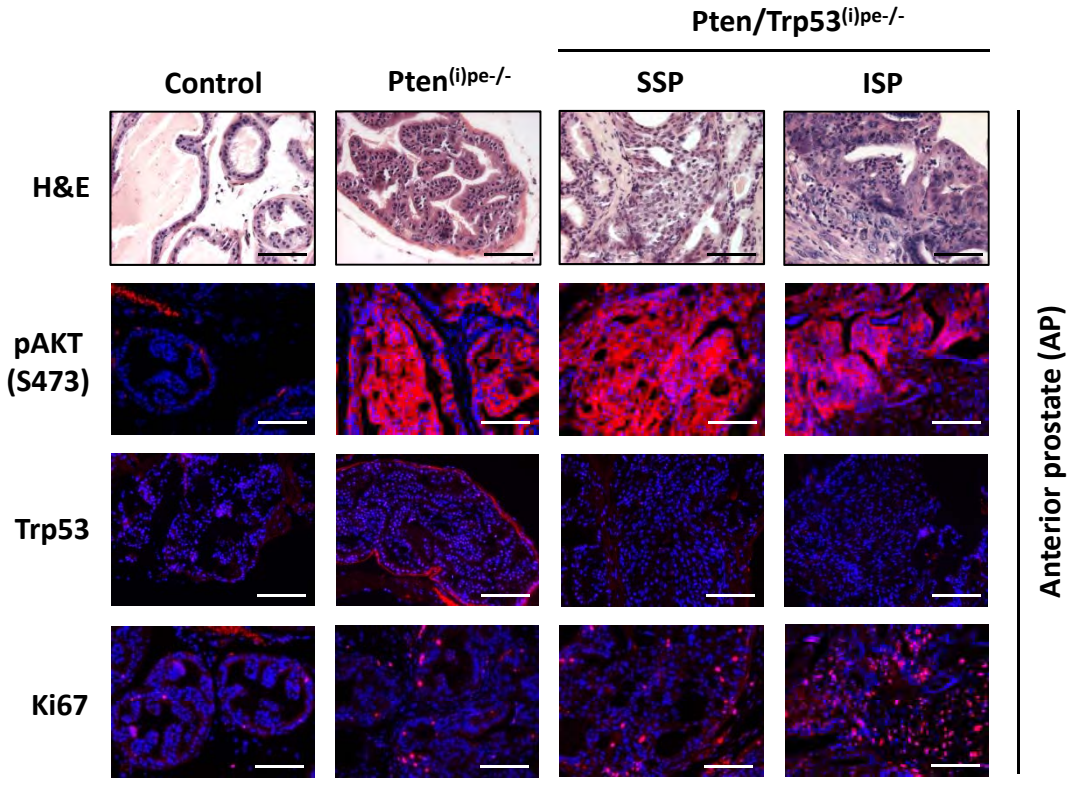

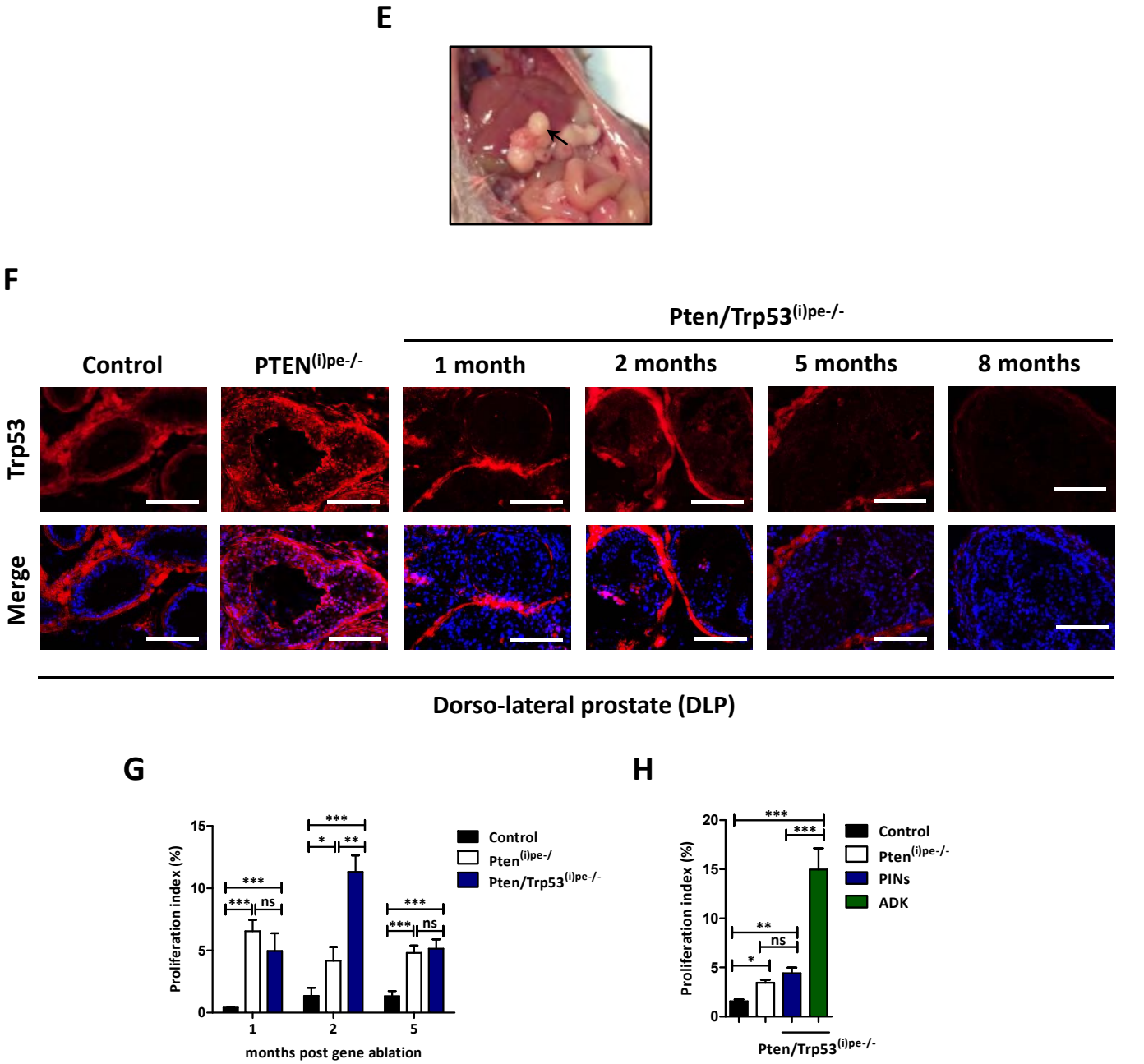

Supplemental figure 1. Generation and characterization of Pten/Trp53$^{(i)pe-/-}$ mice.
(**A**) Schematic representation of floxed (L2) and recombined (L-) Pten and Trp53 alleles. Grey boxes, arrowheads and arrows indicate exons, LoxP sites and PCR primers, respectively. (**B**) Schematic representation of Pten/Trp53$^{(i)pe-/-}$ mouse model. (**C**) Prostate weight of Pten$^{(i)pe-/-}$, Pten/Trp53$^{(i)pe-/-}$ and control mice sacrificed 1,2 and 4.5 months after gene ablation. (**D**) Representative views of AP sections of Pten$^{(i)pe-/-}$, Pten/Trp53$^{(i)pe-/-}$ and control mice sacrificed 5-6 months after gene ablation. Sections were stained with hematoxylin-eosin (HE), or immunostained with pAKT (S473), p53 and K67 (red). n=3-4/group. Blue: Dapi. Scale bar: 75 µm. (**E**) Image of representative view of metastases in the peritoneum of Pten/Trp53$^{(i)pe-/-}$ mice. (**F**) Representative p53 immunostaining (red) of DLP sections of control, Pten$^{(i)pe-/-}$ (5 months after Pten ablation) and Pten/Trp53$^{(i)pe-/-}$ mice at indicated time points after gene ablation. Blue: Dapi. Scale bar: 75 µm. (**G**) Proliferation index (percentage of Ki67-positive prostatic luminal epithelial cells) in DLP of Pten$^{(i)pe-/-}$, Pten/Trp53$^{(i)pe-/-}$ and control mice sacrificed 1, 2 and 5 months after gene ablation. (**H**) Proliferation index (percentage of Ki67-positive prostatic luminal epithelial cells) in AP of Pten/Trp53$^{(i)pe-/-}$ and control mice sacrificed 5-6 months after gene ablation. Values are mean from 4-5 mice ± SEM. One-way ANOVA. *p<0.05; **p<0.01; ***p<0.001 ; ns, not significant.

A

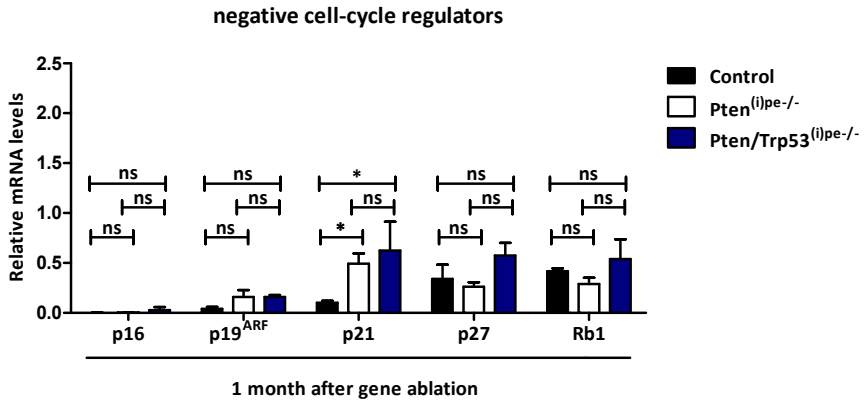
negative cell-cycle regulators
Relative mRNA levels
Control
Pten(i)pe-/-
Pten/Trp53(i)pe-/-
p16
p19ARF
p21
p27
Rb1
1 month after gene ablation

B

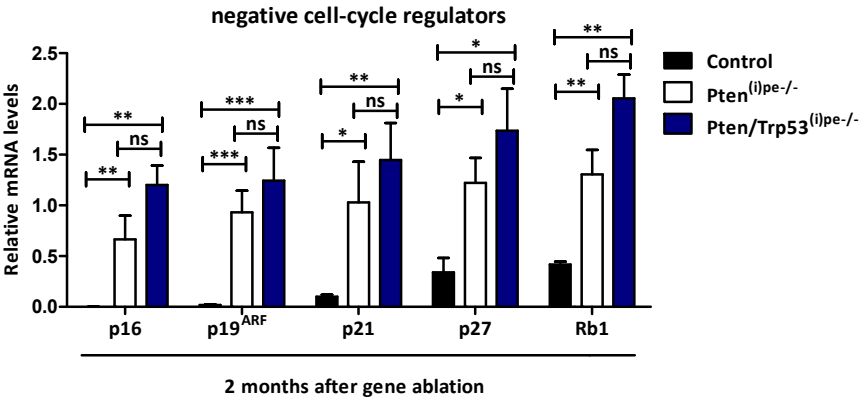
negative cell-cycle regulators
Relative mRNA levels
Control
Pten(i)pe-/-
Pten/Trp53(i)pe-/-
p16
p19ARF
p21
p27
Rb1
2 months after gene ablation

C

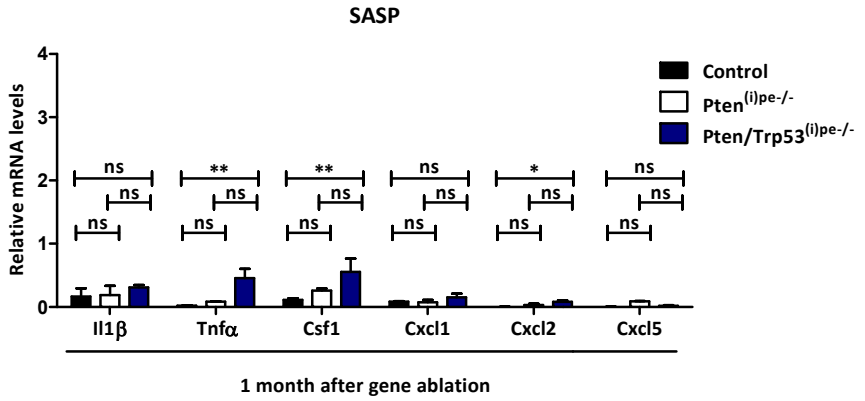
SASP
Relative mRNA levels
Control
Pten(i)pe-/-
Pten/Trp53(i)pe-/-
Il1β
Tnfα
Csf1
Cxcl1
Cxcl2
Cxcl5
1 month after gene ablation

D

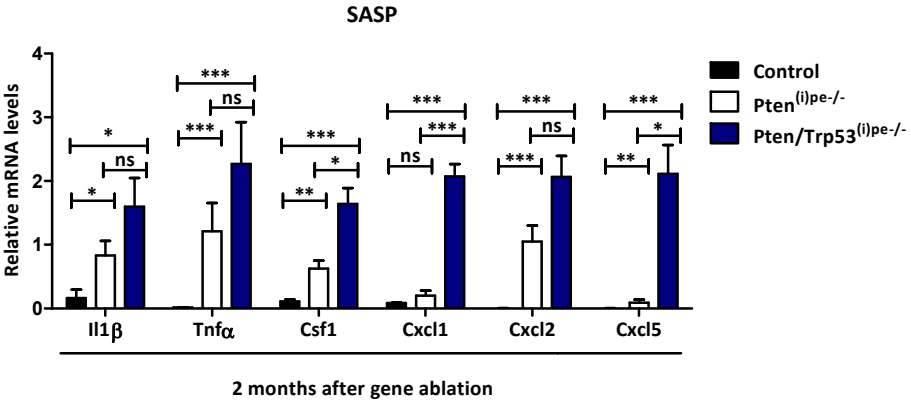
SASP
Relative mRNA levels
Control
Pten(i)pe-/-
Pten/Trp53(i)pe-/-
Il1β
Tnfα
Csf1
Cxcl1
Cxcl2
Cxcl5
2 months after gene ablation

Supplemental figure 2. Quantification of transcript levels of negative cell-cycle regulators at early stages in Pten/Trp53$^{(i)pe-/-}$ mice.

Relative transcript levels of cell-cycle negative regulators and genes involved in SASP in the DLP and AP of Pten$^{(i)pe-/-}$, Pten/Trp53$^{(i)pe-/-}$ and control mice sacrificed 1 (**A and C**) and 2 (**B and D**) months after gene ablation. Values are mean from 3-4 mice ± SEM. One-way ANOVA. *p<0.05; **p<0.01; ***p<0.001; ns, not significant.

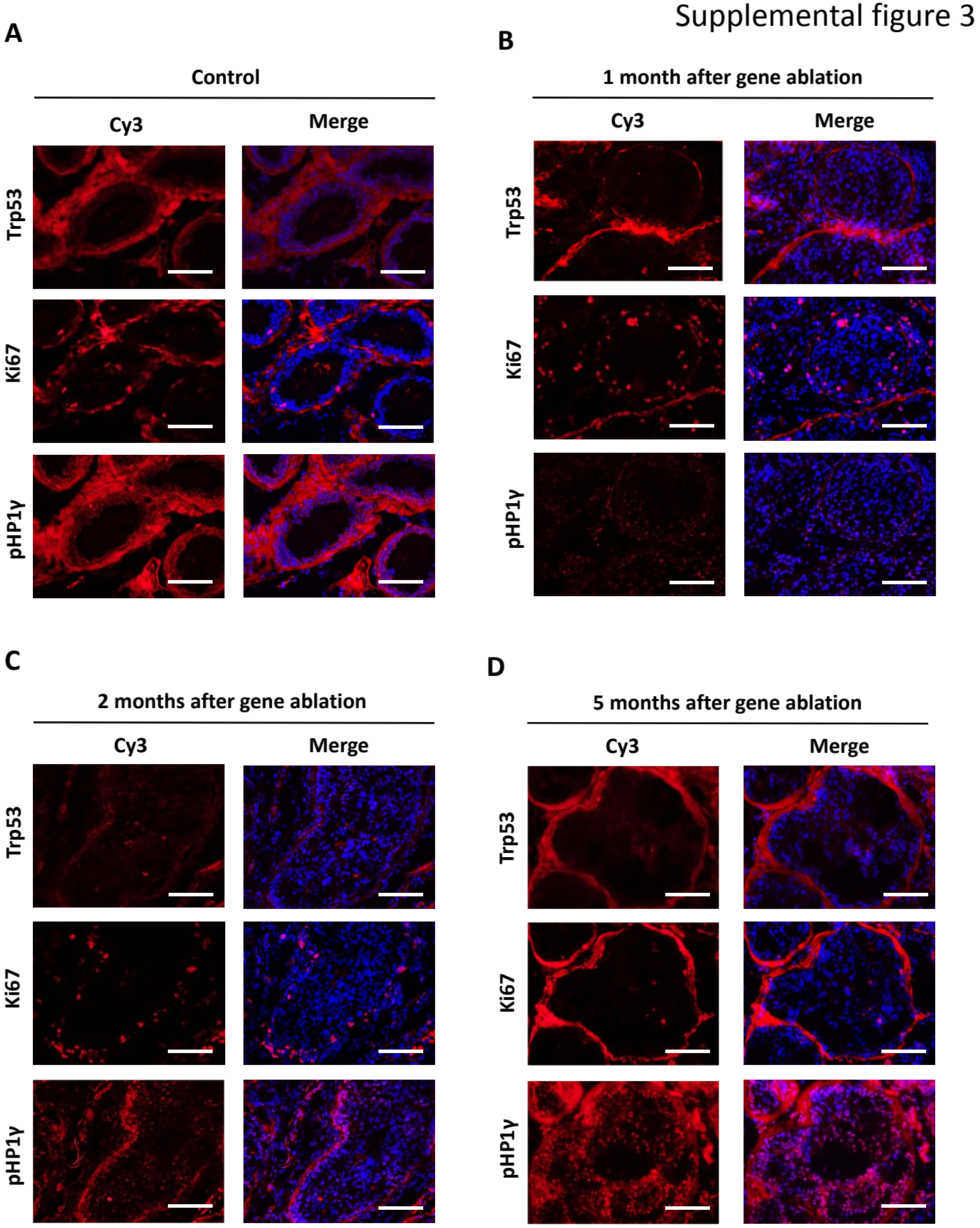

Supplemental figure 3. Immunodetection of pHP1γ in PINs of Pten/Trp53$^{(i)pe-/-}$ mice.
Representative p53, Ki67 and pHP1γ immunostaining (red) of DLP adjacent sections of control mice (**A**) and PTEN/p53$^{(i)pe-/-}$ mice sacrificed at 1 (**B**), 2 (**C**) and 5 (of SSP) (**D**) months after gene ablation. n=3/group. Blue: Dapi. Scale bar: 75 µm.

Supplemental figure 4

A

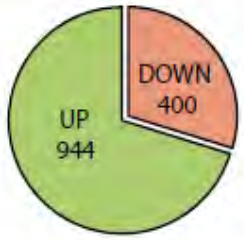

B

Upregulated gene name	LFC
Postn	6.98
Pcdh10	6.84
Itgα11	6.75
Pcdh15	6.44
Omd	6.43

C

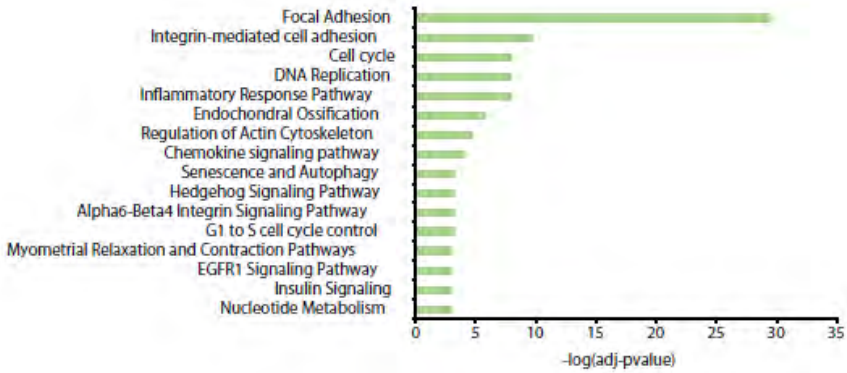

D

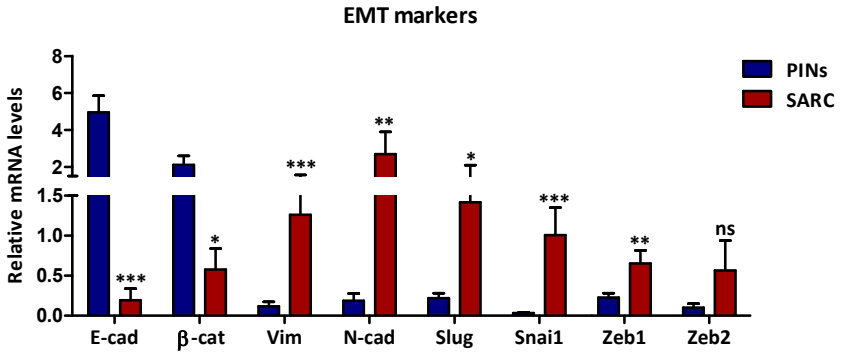

E

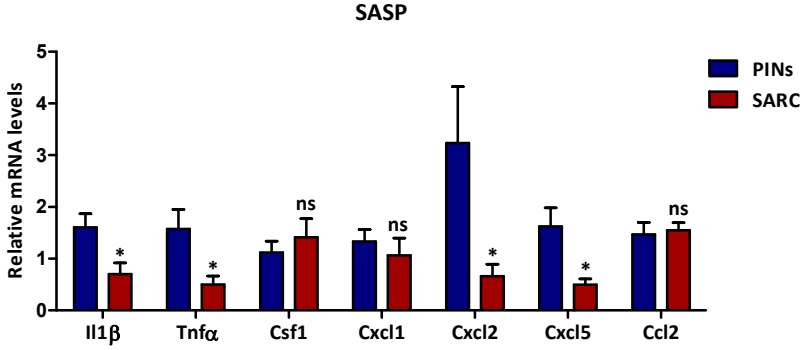

F

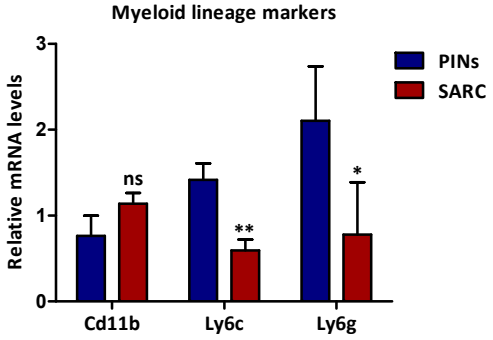

Supplemental figure 4. Characterization of sarcomatoid tumors in Pten/Trp53$^{(i)pe-/-}$ mice.
Venn diagram showing upregulated and downregulated genes in SARC versus PINs (**A**). Most upregulated genes in SARC versus PINs (**B**). Pathway analyses showing significantly enriched pathways for the set of upregulated and downregulated genes in SARC versus PINs (**C**). Relative transcript levels of genes involved in epithelial-mesenchymal transition markers (**D**), senescence-associated secretory proteins (SASP) (**E**) and myeloid lineage markers (**F**) in PIN-containing prostates and Sarc of Pten/Trp53$^{(i)pe-/-}$ mice sacrificed 5-8 months after gene ablation. n=9 for PINs and n=4-6 for Sarc. Values are mean from 4-9 mice ± SEM. Unpaired t-Test. *p<0.05; **p<0.01; ***p<0.001; ns, not significant.

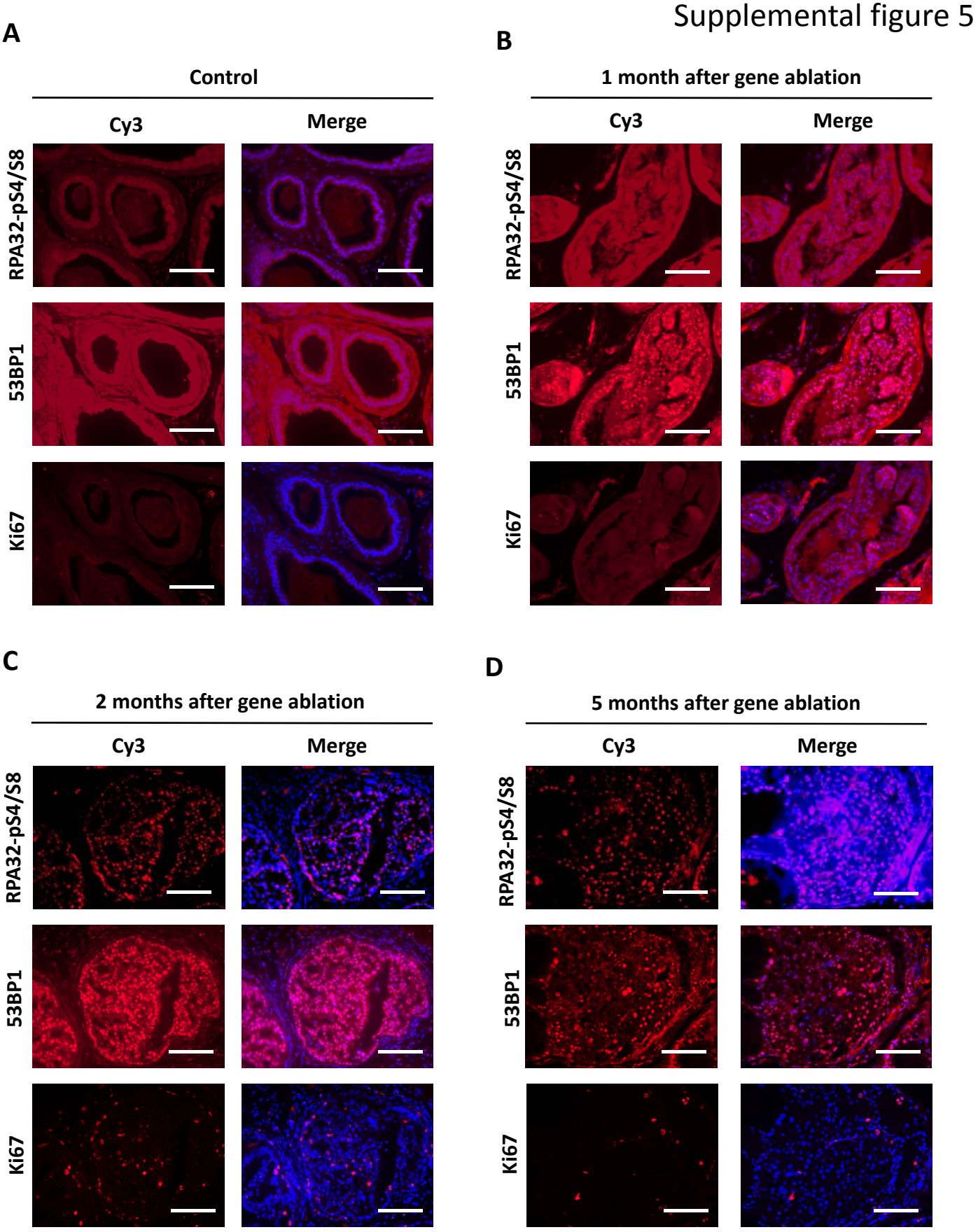

Supplemental figure 5. Immunodetection of DDR markers in PINs of Pten/Trp53$^{(i)pe-/-}$ mice.
Representative immunostaining of RPA32-pS4/S8, 53BP1 and Ki67 (red) of DLP adjacent sections of control mice (**A**) and PTEN/p53$^{(i)pe-/-}$ mice sacrificed at 1 (**B**), 2 (**C**) and 5 (of SSP) (**D**) months after gene ablation. n=3/group. Blue: Dapi. Scale bar: 75 µm.

PART III

Graphical abstract III:

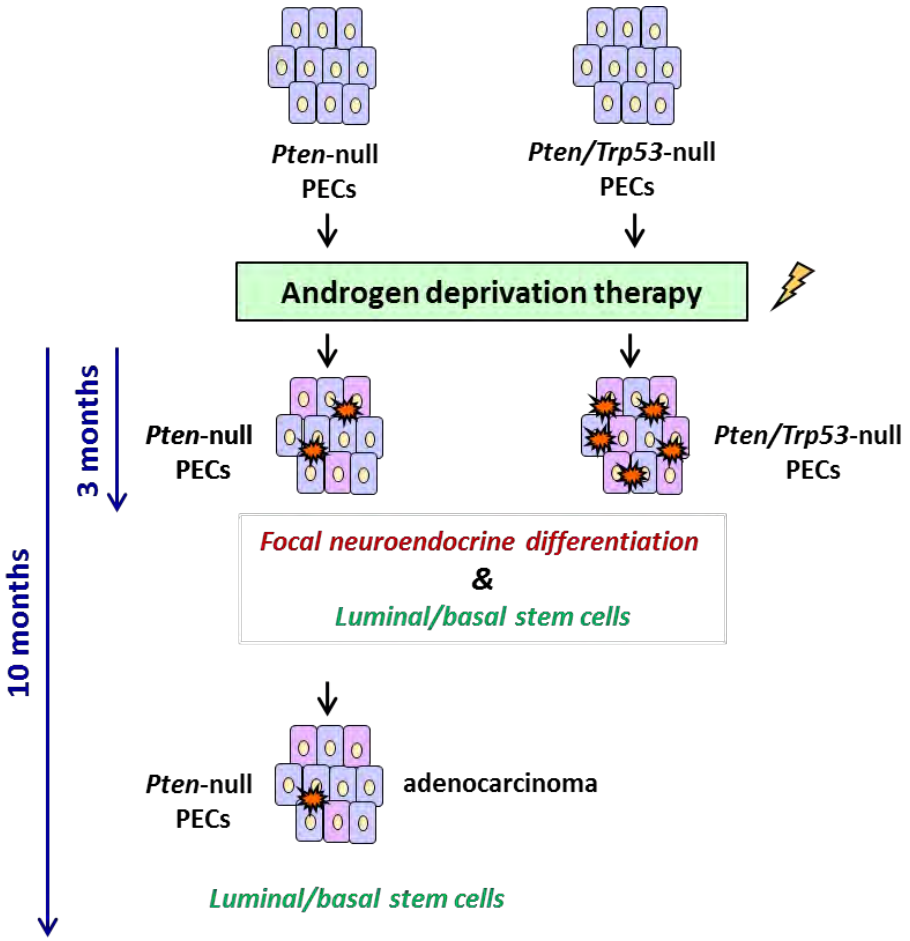

Figure 29: Schematic representation showing the key events underlying castration resistance of Pten and Pten/Trp53-null PECs.

Manuscript III

Androgen deprivation enhances stemness of Pten and Pten/Trp53-deficient prostatic epithelial cells and neuroendocrine differentiation

Rana El Bizri et al., in preparation

Introduction

Prostate cancer (PCa) remains a leading cause of cancer-related death in males of industrialized countries (Siegel et al., 2017). Co-mutations of the tumor suppressor genes PTEN and p53 are often associated with metastatic and castration-resistant prostate cancer (CRPC) (Grasso et al., 2012; Robinson et al., 2015). Hormonal therapy targeting androgen receptor (AR) is a major therapy for patients of advanced and/or metastatic PCa, since AR signaling is required for all stages of disease progression (Watson et al., 2015; Scher et al., 2005; Hussain et al., 2000). Nonetheless, due to treatment resistance, prostate tumors relapse after 1-3 years and develop aggressive forms of PCa, termed castration-resistant prostate cancer (CRPC), displaying an adenocarcinoma phenotype and is AR dependent despite androgens depletion (CRPC-Adeno) (Zou et al., 2017; Beltran et al., 2016; Watson et al., 2015; Scher et al., 2005). However, some resistant tumors show features of neuroendocrine (NE) differentiation, often mixed with adenocarcinoma, termed CRPC-NE (Zou et al., 2017; Aparicio et al., 2016; Beltran et al., 2016; Aggarwal et al., 2014; Beltran et al., 2011). NEPC emerges from pre-existing prostate adenocarcinoma (PADC) because they share clonal origin (Beltran et al., 2011; Yu Ku et al., 2017). NEPC is associated with altered histology, reduced androgen receptor (AR) levels, and expression of neuroendocrine markers such as Synaptophysin (SYP), Chromogranin A (CHGA) and Neuron Specific Enolase (NSE) (Beltran et al., 2011; Yu Ku et al., 2017; Zou et al., 2017). In addition, human and mouse neuroendocrine prostate cancer (NEPC) exhibit deregulation of stem cell reprogramming factors (Yu Ku et al., 2017).

As prostate cancer relapsing from antiandrogen therapies exhibits neuroendocrine differentiation, lineage plasticity might underlie therapeutic resistance (Yuan et al., 2007; Komiya et al., 2009; Yu Ku et al., 2017). The ability of a cancer cell to acquire a phenotypic characteristics of a cell lineage whose survival no longer depends on the drug target, is often termed lineage plasticity (Mu et al., 2017). However, the mechanisms underlying lineage plasticity hinders the identification of efficient therapies.

It was shown that castrate-tolerant luminal cells displaying stem-like properties remain quiescent after androgen deprivation and can regenerate prostatic tumors when androgen signaling is restored

(Toivanen et al., 2013). However, these cells are rarely characterized, as specific markers are yet to be identified.

To characterize the fate of Pten and Pten/Trp53-deficient prostatic epithelial cells (PECs) in response to therapeutic castration, we analyzed Pten$^{(i)pe-/-}$ and Pten/Trp53$^{(i)pe-/-}$ mice in which Pten and combined Pten and Trp53 are selectively ablated in prostatic luminal cells in adult mice, respectively, using the tamoxifen (Tam)-dependent Cre-ER^{T2} system (Ratnacaram et al., 2008; Parisotto et al., 2018). These mice were surgically castrated 2 months after gene ablation, a stage of early PINs formation, and sacrificed 3 months after (at senescence stage) (Parisotto et al., 2018). Our study reveals that Pten and Pten/Trp53-null PECs resist to castration via enhanced stemness and the presence of focal neuroendocrine differentiation. Importantly, we also show that androgen deprivation therapy promotes the expression of the basal markers without affecting those of luminal markers in Pten and Pten/Trp53-null PECs, and thus those PECs display a shared luminal and basal stem like properties. Strikingly, after long term castration, we also demonstrate that the resisting Pten-null PECs display an adenocarcinoma phenotype rather than neuroendocrine phenotype, and thus mimicking resistant human PCa to anti-androgen therapies.

Results

Pten and Pten/Trp53-deficient prostatic epithelial cells resist to androgen deprivation

To characterize the role of androgens in preneoplastic prostatic lesions, Pten$^{(i)pe-/-}$ and Pten/Trp53$^{(i)pe-/-}$ were surgically castrated 2 months after gene ablation, a stage of early PIN formation, and sacrificed 3 months later, when mature PECs are senescent (Parisotto et al., 2018; Manuscript I, in preparation) **(Figure 1A)**. As expected, castration strongly reduced the size and mass of the prostate, seminal vesicle and bulbocavernosus muscle in control, Pten$^{(i)pe-/-}$ and Pten/Trp53$^{(i)pe-/-}$ mice **(Figures 1B, S1A, S1B, S1C, S1D)**. However, the prostate mass of castrated Pten$^{(i)pe-/-}$ and Pten/Trp53$^{(i)pe-/-}$ mice was higher than that of castrated control mice **(Figure S1A)**. Prostatic glands' area in the DLP sections of Pten$^{(i)pe-/-}$ and Pten/Trp53$^{(i)pe-/-}$ mice decreased after castration, but remained higher than that of castrated control mice **(Figure 1D)**. The architecture of PINs in the DLP and AP of castrated mutant mice resembled that of sham operated mutant mice, whereas that of glands in control mice showed atrophy **(Figure 1C and data not shown)**. Importantly, PECs of castrated Pten$^{(i)pe-/-}$ and Pten/Trp53$^{(i)pe-/-}$ mice expressed pAKT S473 as those of sham operated mutant mice, and as expected, no pAKT S473 staining was detected in sham and castrated control mice **(Figure 1C)**. The proliferation rate (%Ki67) of PECs in PINs in castrated mutant mice was similar to those of respective sham operated mutant mice **(Figures 1C and 1E)**, indicating that some Pten and Pten/Trp53-deficient prostatic epithelial cells (PECs) survive and proliferate after castration.

Androgen deprivation does not influence Pten and Pten/Trp53-deficient prostatic epithelial cells from becoming senescent

As cellular senescence is induced in PINs of Pten$^{(i)pe-/-}$ and Pten/Trp53$^{(i)pe-/-}$ mice (Parisotto et al., 2018; Manuscript II, in preparation), we examined whether androgen deprivation affect PECs of PINs from becoming senescent. RT-qPCR showed that the transcript levels of negative cell cycle regulators (e.g. p16, p19^{ARF}, p21, p27 and Rb1), of genes involved in senescence-associated secretory phenotype (SASP) (e.g. Il1β and Tnfα) and lysosomal-β-galactosidase (Glb1), encoding SA-βGal, were similarly induced in DLP and AP of sham operated and castrated Pten$^{(i)pe-/-}$ and Pten/Trp53$^{(i)pe-/-}$ mice, while their levels remained basal in castrated control mice **(Figures 2A, 2B and 2C)**. To further characterize senescence in PINs of Pten$^{(i)pe-/-}$ and Pten/Trp53$^{(i)pe-/-}$ mice after castration, we immunodetected phosphorylated S83 heterochromatin protein 1 γ (pHP1γ), an indicative of senescence associated heterochromatin foci (SAHF) (Adams, 2007). In the absence of androgens, PECs of PINs in Pten $^{(i)pe-/-}$ and Pten/Trp53$^{(i)pe-/-}$ mice displayed nuclear pHP1γ staining similar to those of respective sham mutant

mice, whereas no pHP1γ staining was observed in sham and castrated control mice **(Figure 3A)**. Thus, androgen deprivation does not affect senescence in Pten and Pten/Trp53-null PECs.

Enhanced stemness and neuroendocrine differentiation in Pten$^{(i)pe-/-}$ and Pten/Trp53$^{(i)pe-/-}$ mice after castration

As it was shown that some resistant PCa to anti-androgen therapies exhibit neuroendocrine differentiation *in vivo* (Ku et al., 2017; Zou et al., 2017), we aimed to investigate whether Pten and Pten/Trp53-deficient PECs display neuroendocrine variants after androgen deprivation. Gene set enrichment analysis (GSEA) using Genomatix software and published signatures of common induced pluripotent stem cells genes (iPSCs) (Kareta et al., 2015) showed an enrichment of latter genes (e.g. mainly Sox2 and Nanog) 3 months after castration in Pten/Trp53$^{(i)pe-/-}$ mice **(Figure 4A)**. To validate this signature, we performed RT-qPCR for some iPSCs genes also referred as reprogramming factors (e.g. Sox2, Ezh2 and Nanog). Transcript levels of Sox2 and Ezh2 were higher in castrated than in sham operated Pten$^{(i)pe-/-}$ and Pten/Trp53$^{(i)pe-/-}$ mice, whereas no difference in Nanog levels was observed. In contrast, iPSCs genes were not induced in control mice after castration **(Figure 4B)**. Immunohistochemical analyses revealed higher levels of nuclear Sox2 in PINs of castrated Pten$^{(i)pe-/-}$ and Pten/Trp53$^{(i)pe-/-}$ mice than in those of respective sham operated mutant mice. In contrast, PECs of sham operated or castrated control mice were Sox2 negative **(Figure 4C)**. Thus, androgen deprivation in Pten and Pten/Trp53-deficient PECs induces reprogramming factors. Moreover, RT-qPCR showed that the transcript levels of neuroendocrine markers (e.g. Syp, Eno2, Chga, Ascl1) were markedly increased after castration in both mutant mice, whereas only Syp transcript levels increased in control mice **(Figure 4D)**. Importantly, whereas few luminal PECs in PINs of sham operated Pten$^{(i)pe-/-}$ and Pten/Trp53$^{(i)pe-/-}$ mice expressed Syp, more focal Syp expression was observed in luminal PECs of PINs in castrated respective mutant mice. In contrast, no Syp-positive staining was observed in luminal PECs of sham and castrated control mice **(Figure 4E)**. Thus, androgen deprivation stimulates stemness and induces focal neuroendocrine differentiation in PECs of PINs of Pten$^{(i)pe-/-}$ and Pten/Trp53$^{(i)pe-/-}$ mice , suggesting that lineage plasticity might underlie their therapeutic resistance.

Androgen deprivation stimulates basal expression in Pten and Pten/Trp53-deficient PECs

As castration of adult mice markedly reduced luminal cell number with few or no loss of basal cell number (English et al., 1987), we determined whether Pten and Pten/Trp53-deficient PECs express basal stem like characteristics after androgen deprivation. RT-qPCR showed similar expression of the

luminal marker (Krt8) in castrated mutant mice compared to respective sham mutant mice **(Figure 5A)**. Transcript levels of Ar were ~ 2-3 fold higher in both castrated mutant mice than in respective sham operated mutant mice, whereas their levels were similar in both sham operated and castrated control mice **(Figure 5A)**. Immunohistochemical analyses showed that Ar was expressed in all the nuclei of PECs of sham operated control, Pten$^{(i)pe-/-}$ and Pten/Trp53$^{(i)pe-/-}$ mice, whereas this expression was decreased after castration **(Figure S2A)**. Moreover, transcript levels of Ar target genes (e.g. Pbsn, Msmb and Nkx3.1) were downregulated in control, Pten$^{(i)pe-/-}$ and Pten/Trp53$^{(i)pe-/-}$ mice after castration **(Figure S2B)**. Thus, reduced nuclear AR translocation indicates the decreased Ar signaling activation in Pten and Pten/Trp53-deficient PECs after androgen deprivation.

In addition, transcript levels of basal markers (e.g. Krt5, Krt14 and Trp63) were ~ 6-7 fold higher in castrated Pten$^{(i)pe-/-}$ mice than in sham operated Pten$^{(i)pe-/-}$ mice, whereas those of krt5 and Trp63 were ~ 14-15 fold higher in castrated Pten/Trp53$^{(i)pe-/-}$ mice than in sham operated Pten/Trp53$^{(i)pe-/-}$ mice and those of Krt14 were ~ 5-6 fold higher. In contrast, their levels were similar in both sham and castrated control mice **(Figure 5A)**. Immunohistochemical analyses showed that all PECs of sham and castrated control, Pten$^{(i)pe-/-}$ and Pten/Trp53$^{(i)pe-/-}$ mice expressed Krt8. Moreover, ~ 20 % of Pten-deficient PECs and ~50 % of Pten/Trp53-deficient PECs expressed Krt14 after castration, whereas only basal prostatic cells were Krt14-positive in both sham and castrated control mice. Importantly, all Krt14-positive PECs co-expressed with Krt8 in both sham and castrated mutant mice **(Figure 5B)**. Thus, loss of Trp53 selectively enhances the expression of basal markers in Pten-null PECs without affecting the expression of their luminal marker after androgen deprivation therapy, and thus castrate-resistant Pten/Trp53-null PECs, as well as Pten-null PECs, display a shared luminal and basal stem like properties.

Characterization of Pten-deficient PECs after long term castration

To characterize prostatic tumors in Pten$^{(i)pe-/-}$ mice after long term (LT) castration, Pten$^{(i)pe-/-}$ mice were surgically castrated 2 months after gene ablation, a similar time point as previously castrated Pten$^{(i)pe-/-}$ mice, and sacrificed 10 months after, when prostatic adenocarcinoma are formed in AP (Parisotto et al., 2018) **(Figure S3A)**. Long term castration markedly reduced the mass of the prostate, seminal vesicle and bulbocavernosus muscle of Pten$^{(i)pe-/-}$ mice **(Figures S3B, S3C, S3D and S3E)**. Adenocarcinoma (ADK) were present in the AP of sham and LT castrated Pten$^{(i)pe-/-}$ mice, whereas only low and high PINs were detected in their DLP **(Figure S4A)**. PECs in ADK and in PINs in both sham and LT castrated Pten$^{(i)pe-/-}$ mice similarly expressed pAKT S473 **(Figures S4B and S4C)**. The proliferation rate (% Ki67) of PECs in PINs of both sham and LT castrated Pten$^{(i)pe-/-}$ mice was similar to that of Pten$^{(i)pe-/-}$

mice sacrificed 3 months (Short term; ST) after sham operation and castration **(Figures S4B, S4C and S4D)**, indicating that Pten-null PECs sustain their survival and proliferation after long term castration.

Decrease of Synaptophysin expression in Pten-deficient PECs after long term castration

We investigated the effect of long term castration on the expression of reprogramming factors and neuroendocrine markers. RT-qPCR showed that the transcript levels of reprogramming factors such as Sox2, Ezh2 and Nanog were similar in both sham and LT castrated $Pten^{(i)pe-/-}$ mice. Notably, their transcript levels were similarly expressed in LT and ST castrated $Pten^{(i)pe-/-}$ mice **(Figure 6A)**. Therefore, long term castration does not affect the expression of reprogramming factors in Pten-null PECs. Moreover, transcript levels of neuroendocrine markers (e.g. Eno2, Chga and Ascl1) were similarly induced in both LT and ST castrated $Pten^{(i)pe-/-}$ mice **(Figure 6B)**. However, Syp transcript levels were ~ 2 fold lower in LT castrated $Pten^{(i)pe-/-}$ mice than in those of ST castrated $Pten^{(i)pe-/-}$ mice **(Figure 6B)**. In agreement with these results, no Syp-positive PECs was detected in LT castrated $Pten^{(i)pe-/-}$ mice **(Figure 7B)**. Thus, long term after androgen deprivation, Pten-deficient PECs exhibit adenocarcinoma phenotype rather than neuroendocrine phenotype, and thus resembles resistant human PCa to anti-androgen therapies.

Mixed luminal and basal expression in Pten-deficient PECs after long term castration

The transcript levels of luminal marker Krt8 were similar in both sham and LT castrated $Pten^{(i)pe-/-}$ mice, whereas those of AR were ~ 2-3 fold higher in LT castrated $Pten^{(i)pe-/-}$ mice than in respective sham mutant mice **(Figure 7A)**. Moreover, transcript levels of basal markers such as Krt5, Krt14 and Trp63 were similarly induced in LT and ST castrated $Pten^{(i)pe-/-}$ mice **(Figure 7A)**. In agreement with these results, immunohistochemical analyses revealed that all PECs of both sham and LT castrated $Pten^{(i)pe-/-}$ mice expressed Krt8, whereas krt14 was more expressed in PECs of LT castrated $Pten^{(i)pe-/-}$ mice than in those of respective sham mutant mice **(Figure 7B)**. Notably, Krt14-positive PECs co-expressed with Krt8 in both sham and LT castrated $Pten^{(i)pe-/-}$ mice, but not with Syp, as previously seen in both sham and ST castrated $Pten^{(i)pe-/-}$ mice **(Figure 7B)**. Thus, long term of androgen deprivation, Pten-deficient PECs maintain their luminal and basal stem cell characteristics.

Discussion

While aggressive tumors initially respond to androgen deprivation therapy, they ultimately relapse to castration-resistant prostate cancer (CRPC), which is a lethal disease (Ryan and Tindall, 2011; Scher and Sawyers, 2005). Despite the global efforts to understand the mechanisms of resistance to therapeutic castration, the cell type(s) resist androgen deprivation remain poorly characterized (Sala et al., 2017).

Mutant mice were sacrificed after castration or sham operation at the time were Pten and Pten/Trp53-null PECs enter senescence. We show here that some Pten and Pten/Trp53-null PECs resist androgen deprivation, as the architecture of prostatic lesions as well as the proliferation rate of PECs in castrated mutant mice resembles that of respective sham operated mutant mice. Previously, we showed that senescent Pten and Pten/Trp53-null PECs express a large number of members of SASP (e.g. cytokines and chemokines), which in turn can accumulate other mutations and contribute to prostate tumor progression (Parisotto et al., 2018; El Bizri et al., in preparation II). Since transcript levels of genes involved in SASP are similar in both sham and castrated $Pten^{(i)pe-/-}$ and $Pten/Trp53^{(i)pe-/-}$ mice, members of SASP are unlikely to contribute in castration resistance mechanism of Pten and Pten/Trp53-null PECs.

It was reported that combined loss of Rb and Trp53 in mouse prostate leads to the upregulation of the reprogramming factors such as Sox2 and Ezh2, which promotes epithelial plasticity, and facilitates neuroendocrine differentiation (Ku et al., 2017; Mu et al., 2017). Recently, it has been shown that abiraterone-treated NPp53 prostate tumors, in which Pten and Trp53 are co-inactivated in mouse prostate based on an inducible $Nkx3.1^{CreERT2}$ driver, exhibit either focal or overt neuroendocrine differentiation. Focal neuroendocrine-like cells are non-proliferative while overt cells are highly proliferative (Zou et al., 2017). Here we show that short term castration stimulates stemness and induces focal neuroendocrine differentiation in both Pten and Pten/Trp53-null PECs. Moreover, we also show that, after long term castration, Pten-null PECs exhibit adenocarcinoma phenotype rather than focal neuroendocrine phenotype, in agreement with previous study showing the non-proliferative capacity of focal neuroendocrine cells (Zou et al., 2017). Thus, as these focal neuroendocrine cells was shown to be non-proliferative, unlikely they can contribute to the mechanism facilitating therapeutic resistance in Pten-null PECs.

Importantly, short term after castration, we demonstrate here that castrate-tolerant Pten and Pten/Trp53-null PECs share both luminal and basal stem like characteristics. In addition, as we show that these prostatic cell entity sharing luminal and basal markers survive after long term castration in $Pten^{(i)pe-/-}$ mice, they can contribute in the mechanism underlying resistance of Pten-null PECs to

androgen deprivation. Even though castrate-tolerant epithelial cells displaying both luminal and stem/progenitor cell characteristics play a crucial role in prostate tumor evolution, specific phenotypic markers are yet to be identified (Liu et al., 2016; Toivanen et al., 2013; Wang et al., 2009; Yoo et al., 2016). Supporting this idea, Sala et al. identified a rare population of castration-resistant progenitor cells in $Pten^{pe-/-}$ prostate tumors, referred as LSC^{med} ($Lin^{-}/Sca\text{-}1^{+}/CD49f^{med}$), which represents a unique cell entity that shares markers of luminal and basal/stem cells, and CK4 was validated to be a specific marker for LSC^{med} (Sala et al., 2017). Therefore, this cell entity of castrate-resistant Pten and Pten/Trp53-null PECs might resemble that of LSC^{med}, as they both share the luminal and basal stem progenitor properties.

Taken together, identification of the phenotypic characteristics of castrate-tolerant Pten and Pten/Trp53-null PECs exhibiting shared luminal and basal stem like characteristics might open new avenues to develop efficient targeted therapies for CRPC.

Material and Methods

Mouse Care

Mice were maintained in a temperature and humidity controlled animal facility, with a 12h light/dark cycle. Mice breeding and maintenance were performed in the accredited IGBMC/ICS animal house (C67-2018-37), in compliance with French and EU regulations on the use of laboratory animal's research, under the supervision of D.M. who holds animal experimentation authorization from the French Ministry of agriculture and Fisheries (N°67-209 and A 67-227). All animal experiments were approved by the Ethical committee Com'Eth (Comité d'Ethique pour l'Expérimentation Animale, Strasbourg, France). Mice were euthanized by cervical dislocation, and tissues were directly collected, weighed and frozen in liquid nitrogen, or processed for biochemical and histological analysis.

Generation of mouse models

PSA-Cre-ER^{T2} (Feil et al., 1997), Pten$^{L2/L2}$ (Suzuki et al., 2001) and Trp53$^{L2/L2}$ (Jonkers et al., 2001) mice were backcrossed on C57BL/6 mice for more than 8 generations before intercrossing. Genotyping by PCR were performed on genomic DNA isolated from ear biopsies of the mice, using the DirectPCR extraction kit (Viagen, cat # 102-T), and primers as described (Jonkers et al., 2001; Ratnacaram et al., 2008). Mice carrying one copy of the PSA-Cre-ER^{T2} transgene, expressing the tamoxifen-inducible Cre-ER^{T2} recombinase selectively in prostatic epithelium under the control of the human PSA promoter, were crossed with mice carrying loxP-flanked (floxed) alleles of Pten (L2 alleles), to generate PSA-Cre-ER$^{T2(tg/0)}$/Pten$^{L2/L2}$ (tg: transgenic) and PSA-Cre-ER$^{T2(0/0)}$/Pten$^{L2/L2}$ mice. In addition, PSA-Cre-ER$^{T2(tg/0)}$/Pten$^{L2/L2}$ mice were inter-crossed with Trp53$^{L2/L2}$ mice carrying floxed alleles of Trp53 (Jonkers et al., 2001) (see also **Figure S1A**), to generate PSA-Cre-ER$^{T2(tg/0)}$/Pten$^{L2/L2}$/trp53$^{L2/L2}$ and Cre-ER$^{T2(0/0)}$/Pten$^{L2/L2}$/trp53$^{L2/L2}$ mice. Gene ablation was induced by daily intraperitoneal injections of tamoxifen (Tam) (1 mg/mouse) for 5 days to 8 week-old PSA-Cre-ER$^{T2(tg/0)}$/Pten$^{L2/L2}$ and PSA-Cre-ER$^{T2(tg/0)}$/Pten$^{L2/L2}$/trp53$^{L2/L2}$ mice, to generate mutant Pten$^{(i)pe-/-}$ and Pten/trp53$^{(i)pe-/-}$ mice, respectively. PSA-Cre-ER$^{T2(0/0)}$/Pten$^{L2/L2}$ mice (Pten$^{pe+/+}$ mice) and Cre-ER$^{T2(0/0)}$/Pten$^{L2/L2}$/trp53$^{L2/L2}$ mice (Pten/trp53$^{pe+/+}$ mice) were similarly Tam-treated and were used as controls. [pe: prostate epithelium; (i): induced].

RNA extraction and analysis

RNA was isolated from dorsolateral and anterior prostate samples using RNeasy Mini kit (Qiagen), reverse transcribed using SuperScript II Reverse Transcriptase (Invitrogen), and amplified by quantitative PCR with the SYBER Green kit (Roche) and a LightCycler 480 (Roche Diagnostics), according to the manufacturer's instructions. Primer sequences are given in **Table 1**.

Table 1: Primer sequences

Gene	Forward (5' to 3')	Reverse (5' to 3')
18S	CGCGGTTCTATTTTGTTGGT	TCGTCTTCGAAACTCCGACT
p16	GAACTCTTTCGGTCGTACCC	CAGTTCGAATCTGCACCGTA
$p19^{ARF}$	GCTCTGGCTTTCGTGAACAT	GTGAACGTTGCCCATCATC
p21	TCTTCTGCTGTGGGTCAGGAG	GAGGGCTAAGGCCGAAGATG
p27	TTTCATGTATATCTTCCTTGCTTCA	ACGCCAGACGTAAACAGCTC
Rb1	TGCATGGCTTTCAGATTCACC	GCTGAGAGGACAAGCAGGTT
Glb1	GGATGGACAGCCATTCCGAT	CAGGGCACGTACATCTGGATA
Il1β	ACGACAAAATACCTGTGGCC	TGGGTATTGCTTGGGATCCA
Tnfα	CCCCAAAGGGATGAGAAGT	CACTTGGTGGTTTGCTACGA
Csf1	TGCTAGGGGTGGCTTTAGG	CAACAGCTTTGCTAAGTGCTCTA
Cxcl1	CTGGGATTCACCTCAAGAACATC	CAGGGTCAAGGCAAGCCTC
Cxcl2	CCAACCACCAGGCTACAGG	GCGTCACACTCAAGCTCTG
Cxcl5	TGCCCTACGGTGGAAGTCAT	AGCTTTCTTTTTGTCACTGCCC
Ccl2	CACTCACCTGCTGCTACTCA	GCTTGGTGACAAAAACTACAGC
Sox2	CAAAAACCGTGATGCCGACT	CGCCCTCAGGTTTTCTCTGT
Ezh2	ACTGCTTCCTACATCCCTTCC	AGAGCAGCAGCAAACTCCTT
Nanog	TTCCTGGTCCCCACAGTTTG	GGCGAGGAGAGGCAGC
Syp	CCATTCAGGCTGCACCAAGT	TTCAGCCGAGGAGGAGTAGT
Eno2	CTGTGCCGGCCTTTAATGTG	GAAAGCTCTCAGCACCCACT
Chga	AGGGGACACCAAGGTGATGA	AGCAGATTCTGGTGTCGCAG
Ascl1	AATGGACTTTGGAAGCAGGATG	CCATTTGACGTCGTTGGCG
krt8	CGGCTACTCAGGAGGACTGA	TGAAAGTGTTGGATCCCCCG
AR	CTGCCTCCGAAGTGTGGTAT	GCCAGAAGCTTCATCTCCAC
Krt5	TGGCGATGACCTTCGAAACA	GGTTGGCACACTGCTTCTTG
Krt14	CTACCTGGACAAGGTGCGTG	CCAGGATCTTGCTCTTCAGGT
Trp63	AACACAGACCACGCACAGAA	TTCGGTGGAATACGTCCAGG

Histological analysis

Prostate tissues were immediately fixed in ice-cold 4% formaldehyde supplemented with 1 tablet/10 mL of PhosSTOP (04 906 837 001, Roche). Prostate tissues were embedded in paraffin and sectioned at 5 µm. For histopathological analyses, paraffin sections were stained with hematoxylin and eosin. Immunofluorescence staining (IF) was performed as described (Ratnacaram et al., 2008; Parisotto et al., 2018). Primary antibodies used for IF were directed against AKT pS473 (4060, Cell Signaling Technology; 1/200), Ki67 (SP6, Thermo-Scientific; 1/500) and pHP1γ (2600, Cell Signaling Technology; 1/200). Secondary antibodies [CY3 AffiniPure goat anti-rabbit IgG (H+L)] were from Jackson Immunoresearch. For immunohistochemistry (IHC), paraffin sections were treated with 3% H_2O_2 (in PBS 1X) to block endogenous peroxidase activity before antigen retrieval with citrate buffer (pH=6) boiled in a microwave (750 W for 10 min). Slides were then blocked with 1.5% of normal rabbit serum (Vector Laboratories) and incubated with primary antibodies against Sox2 (14962, Cell Signaling Technology; 1/100), Syp (SP11, Invitrogen; 1/20), krt8 (GTX109489, GeneTex; 1/200), AR (N-20) (G2613, Santa Cruz biotechnology; 1/200) and krt14 (PRB-155P, Covance; 1/400) overnight at 4°C, followed by incubation with biotinylated goat anti-rabbit IgG (Vector Laboratories) for 1h at room temperature (RT) and treatment of AB complex (Vector Laboratories) for 30 min at RT. Staining was visualized by the substrate chromogen solution (DAB) (Vector Laboratories) and then counterstained with hematoxylin.

Statistical analysis

Statistical analyses were performed with the one-way ANOVA test and Unpaired t-Test using GraphPad Prism.

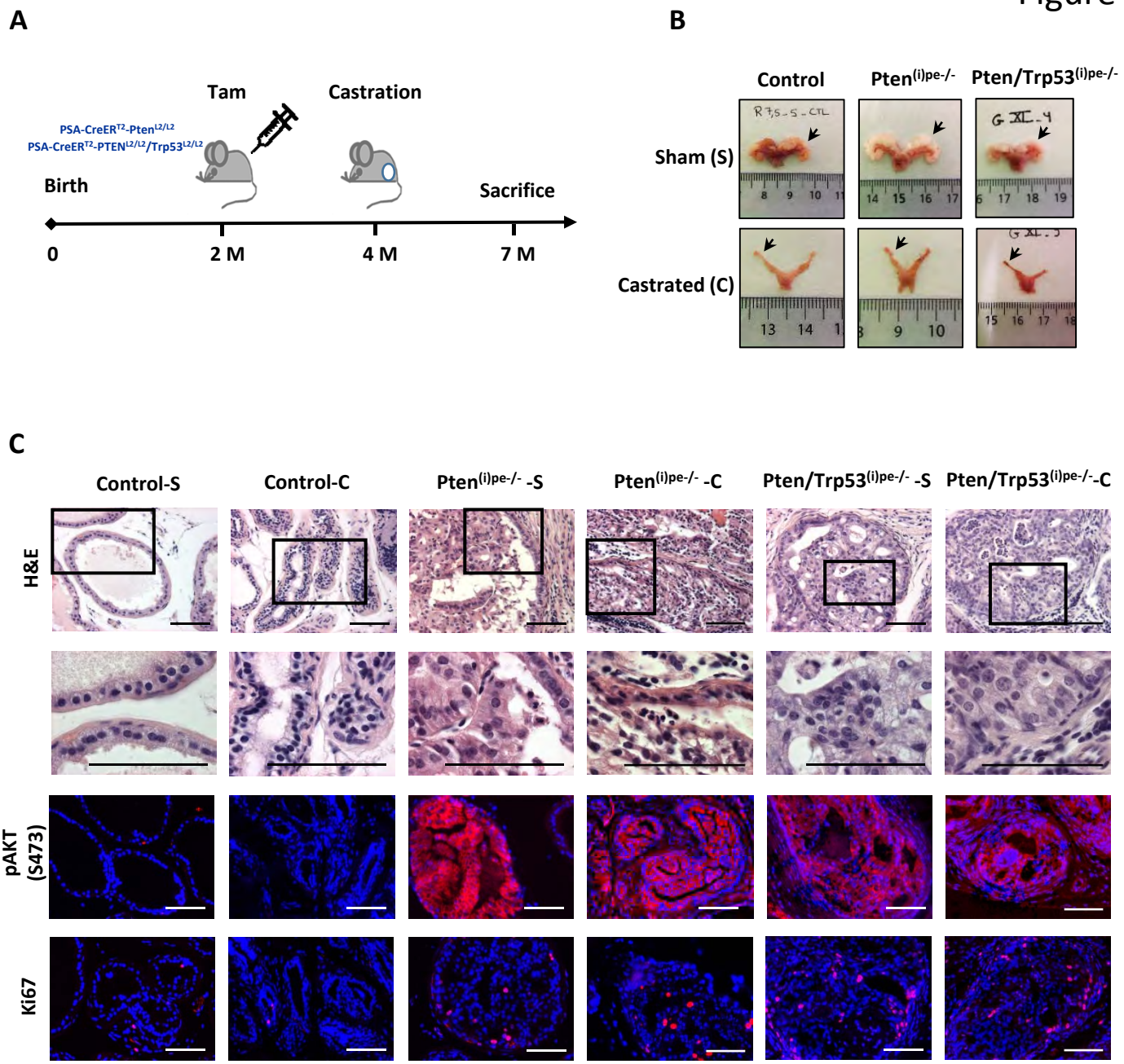
A
Tam
Castration
PSA-CreER^{T2}-Pten$^{L2/L2}$
PSA-CreER^{T2}-PTEN$^{L2/L2}$/Trp53$^{L2/L2}$
Birth
Sacrifice
0
2 M
4 M
7 M
B
Control
Pten$^{(i)pe-/-}$
Pten/Trp53$^{(i)pe-/-}$
Sham (S)
Castrated (C)
C
Control-S
Control-C
Pten$^{(i)pe-/-}$ -S
Pten$^{(i)pe-/-}$ -C
Pten/Trp53$^{(i)pe-/-}$ -S
Pten/Trp53$^{(i)pe-/-}$-C
H&E
pAKT (S473)
Ki67
D
Gland area (µm^2)
40000
30000
20000
10000
0
***
*
***
*
***
Control (S)
Control (C)
PTEN$^{(i)pe-/-}$ (S)
Pten$^{(i)pe-/-}$ (C)
Pten/Trp53$^{(i)pe-/-}$ (S)
Pten/Trp53$^{(i)pe-/-}$ (C)
E
Proliferation index (%)
15
10
5
0
*
**
ns
ns
ns
Control (S)
Control (C)
Pten$^{(i)pe-/-}$ (S)
Pten$^{(i)pe-/-}$ (C)
Pten/Trp53$^{(i)pe-/-}$ (S)
Pten/Trp53$^{(i)pe-/-}$ (C)

Figure 1. Characterization of prostatic lesions in Pten$^{(i)pe-/-}$ and Pten/Trp53$^{(i)pe-/-}$ mice after castration.
(**A**) Schematic representation of the experiment. (**B**) Images of representative prostate and seminal vesicle (black arrow) of sham (S) and castrated (C) Pten$^{(i)pe-/-}$, Pten/Trp53$^{(i)pe-/-}$ and control mice sacrificed 3 months after castration and sham operation. (**C**) Representative views of DLP sections of Pten$^{(i)pe-/-}$ and Pten/Trp53$^{(i)pe-/-}$ and control mice sacrificed 3 months after castration (C) or sham (S) operation. Sections were stained with hematoxylin-eosin (HE), or immunostained with of pAKT (S473) and Ki67 (red). Blue:Dapi. Scale bar: 75 µm. (**D**) Gland area in DLP of Pten$^{(i)pe-/-}$, Pten/Trp53$^{(i)pe-/-}$ and control mice sacrificed 3 months after castration or sham operation, respectively. (**E**) Proliferation index (percentage of Ki67-positive prostatic luminal epithelial cells) in DLP of sham (S) and castrated (C) Pten$^{(i)pe-/-}$, Pten/Trp53$^{(i)pe-/-}$ and control mice sacrificed 3 months after castration and sham operation. n=3 sham and n=5 castrated Pten$^{(i)pe-/-}$ mice, n=4 sham and n=7 castrated Pten/Trp53$^{(i)pe-/-}$ mice, n=3 sham and n=4 castrated control mice. Bars represent the mean ± SEM. One way ANOVA. *p<0.05; **p<0.01; ***p<0.001 and ns, not significant.

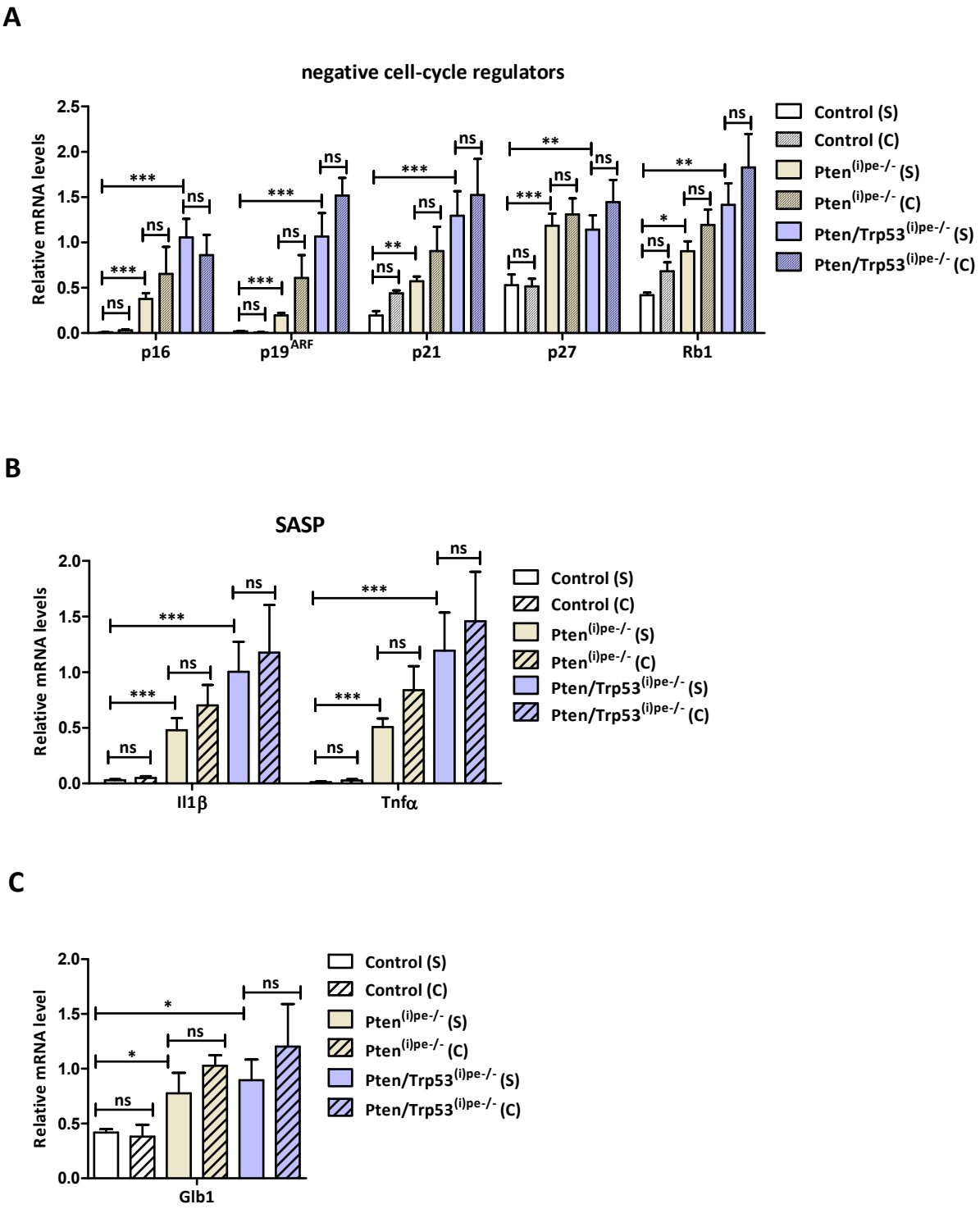

Figure 2. Characterization of senescence in Pten$^{(i)pe-/-}$ and Pten/Trp53$^{(i)pe-/-}$ mice after castration.
Relative transcript levels of negative cell-cycle regulators (**A**), genes involved in senescence-associated secretory proteins (SASP) (**B**) and Glb1 gene in the DLP and AP of Pten$^{(i)pe-/-}$, Pten/Trp53$^{(i)pe-/-}$ and control mice sacrificed 3 months after castration (C) and sham (S) operation. n=3 sham and n=5 castrated Pten$^{(i)pe-/-}$ mice, n=4 sham and n=7 castrated Pten/Trp53$^{(i)pe-/-}$ mice, n=3 sham and n=4 castrated control mice. Bars represent the mean ± SEM. One way ANOVA. *p<0.05; **p<0.01; ***p<0.001 and ns, not significant.

A

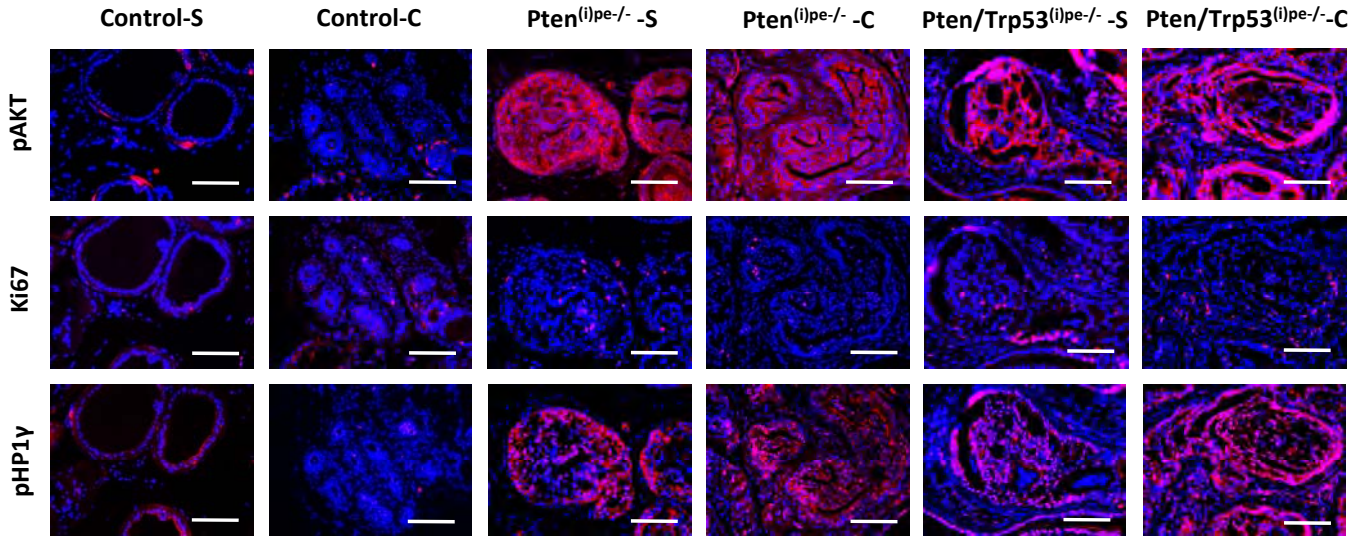

Figure 3. Immunodetection of pHP1γ in Pten$^{(i)pe-/-}$ and Pten/Trp53$^{(i)pe-/-}$ mice after castration.
(**A**) Representative pAKT (S473), Ki67 and pHP1γ immuno-fluorescence staining (red) of DLP adjacent sections of Pten$^{(i)pe-/-}$, Pten/Trp53$^{(i)pe-/-}$ and control mice sacrificed 3 months after castration (C) and sham (S) operation. n=3/group. Blue: Dapi. Scale bar: 75 µm.

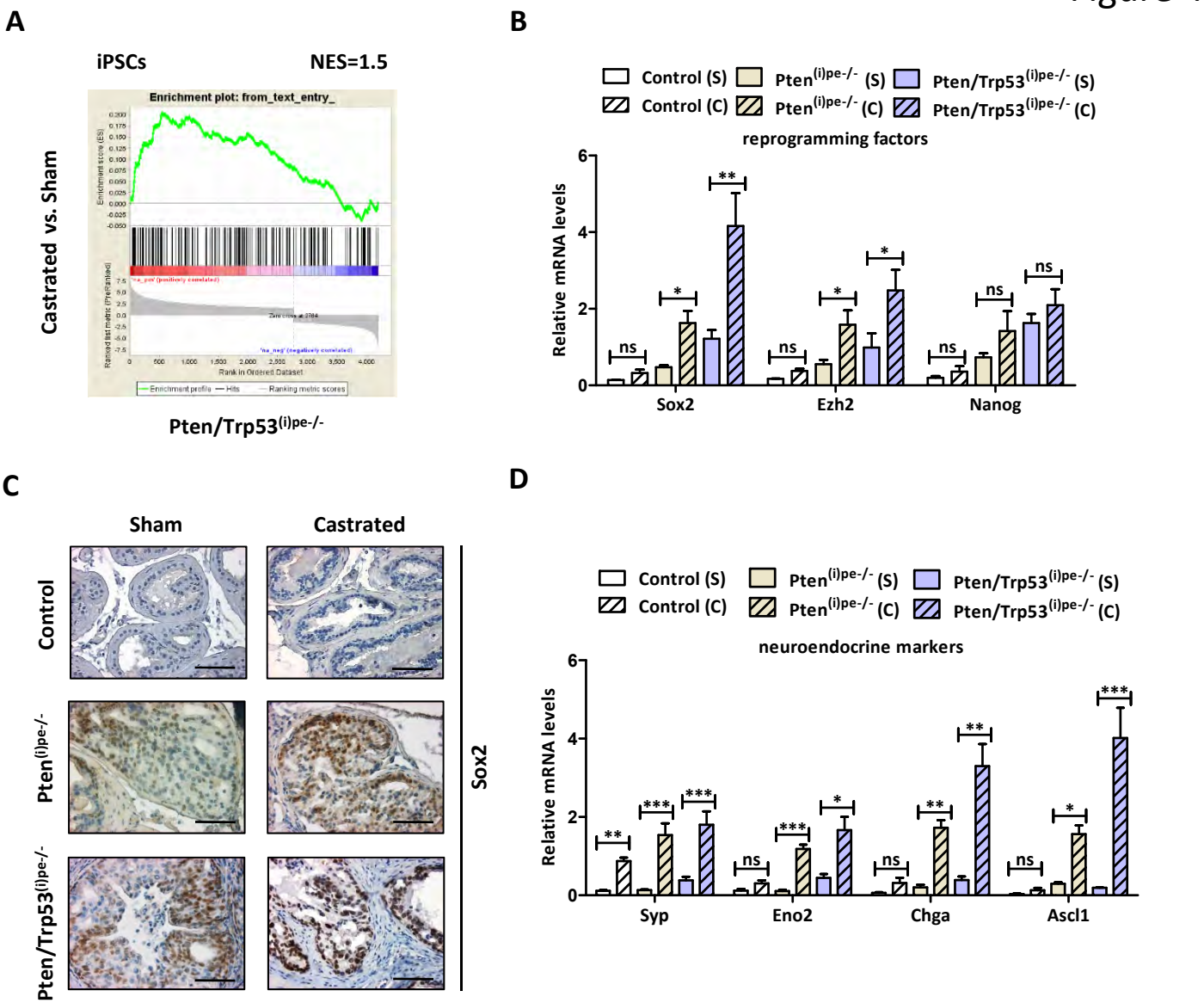

Figure 4. Characterization of cellular reprogramming and morphologic features of neuroendocrine differentiation in Pten$^{(i)pe-/-}$ and Pten/Trp53$^{(i)pe-/-}$ mice after castration.
GSEA of iPSCs genes (Kareta et al., 2015) using the gene expression profile of prostate of Pten/Trp53$^{(i)pe-/-}$ mice castrated versus sham (**A**). (NES) Normalized enrichment score for the gene sets are reported. Transcript levels of reprogramming factors (**B**) and neuroendocrine markers (**D**) in the DLP and AP of Pten$^{(i)pe-/-}$, Pten/Trp53$^{(i)pe-/-}$ and control mice sacrificed 3 months after castration (C) or sham (S) operation. n=3 sham and n=5 castrated Pten$^{(i)pe-/-}$ mice, n=4 sham and n=7 castrated Pten/Trp53$^{(i)pe-/-}$ mice, n=3 sham and n=4 castrated control mice. Bars represent the mean ± SEM. One way ANOVA. *p<0.05; **p<0.01; ***p<0.001 and ns, not significant. Immunohistochemistry of reprogramming factor (Sox2) (**C**) and neuroendocrine marker (Syp) (**E**) in the DLP of Pten$^{(i)pe-/-}$, Pten/Trp53$^{(i)pe-/-}$ and control mice sacrificed 3 months after castration (C) or sham (S) operation. Blue: hematoxylin staining. Scale bar: 75 µm.

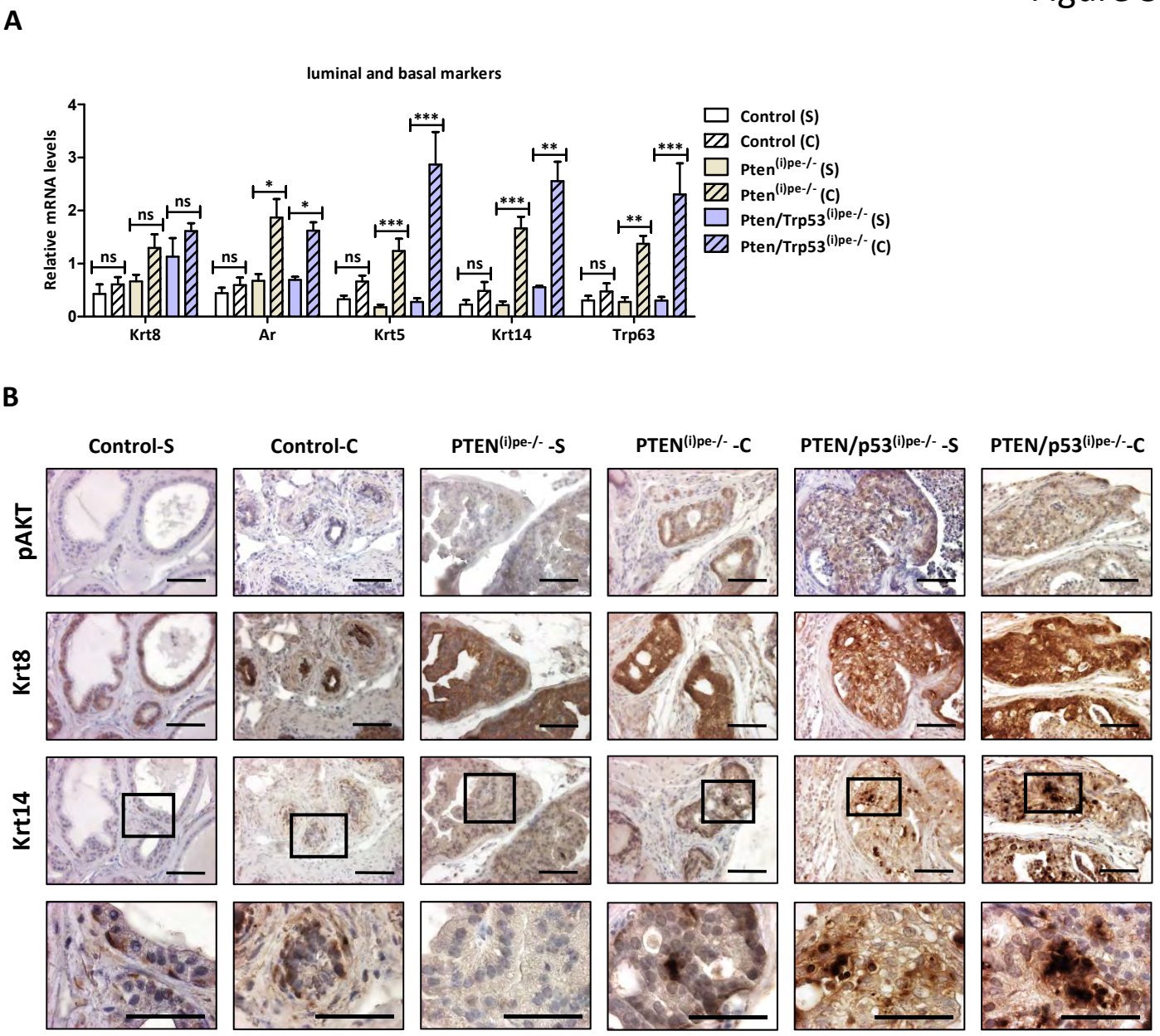

Figure 5. Expression of luminal and basal markers in Pten$^{(i)pe-/-}$ and Pten/Trp53$^{(i)pe-/-}$ mice after castration.

(**A**) Transcript levels of luminal and basal markers in the prostate of Pten$^{(i)pe-/-}$, Pten/Trp53$^{(i)pe-/-}$ and control mice sacrificed 3 months after castration (C) or sham (S) operation. n=3 sham and n=5 castrated Pten$^{(i)pe-/-}$ mice, n=4 sham and n=7 castrated Pten/Trp53$^{(i)pe-/-}$ mice, n=3 sham and n=4 castrated control mice. Values are mean from 3-4 mice ± SEM. One-way ANOVA. *p<0.05; **p<0.01; ***p<0.001; ns, not significant. (**B**) Immunohistochemistry of pAKT S473, Krt8 (luminal marker) and Krt14 (basal marker) in the DLP of adjacent sections of Pten$^{(i)pe-/-}$, Pten/Trp53$^{(i)pe-/-}$ and control mice sacrificed 3 months after castration (C) or sham (S) operation. Blue: hematoxylin staining. Scale bar: 75 µm. n=3/4 mice for each group.

A

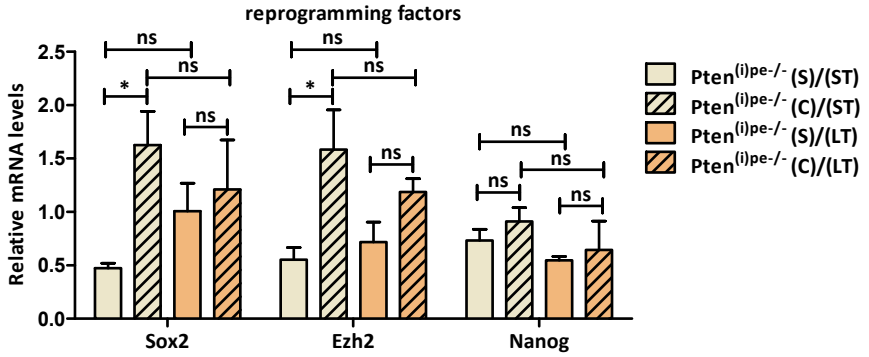

B

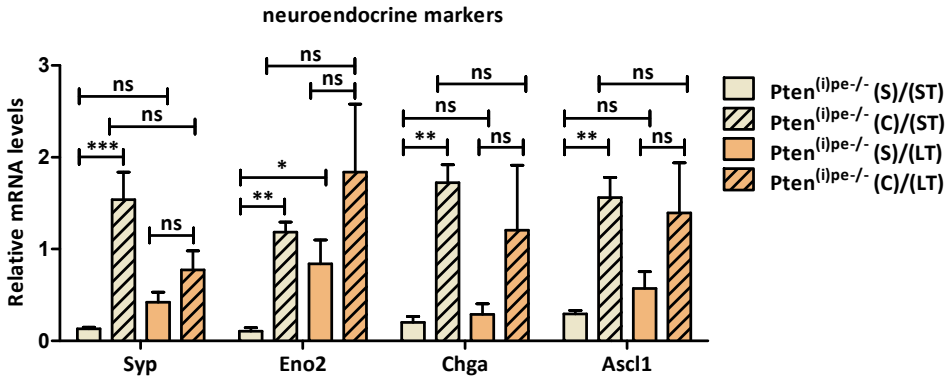

Figure 6. Expression of cellular reprogramming factors neuroendocrine markers in Pten$^{(i)pe-/-}$ mice long term after castration.

(**A**) Transcript levels of reprogramming factors (**B**) and neuroendocrine markers in the DLP and AP of Pten$^{(i)pe-/-}$ mice sacrificed 3 months (ST) and 10 months (LT) after castration (C) or sham (S) operation. n=3 sham and n=5 castrated Pten$^{(i)pe-/-}$ mice (ST), n=3 sham and n=4 castrated Pten $^{(i)pe-/-}$ mice (LT). Bars represent the mean ± SEM. One way ANOVA. *p<0.05; **p<0.01; ***p<0.001 and ns, not significant.

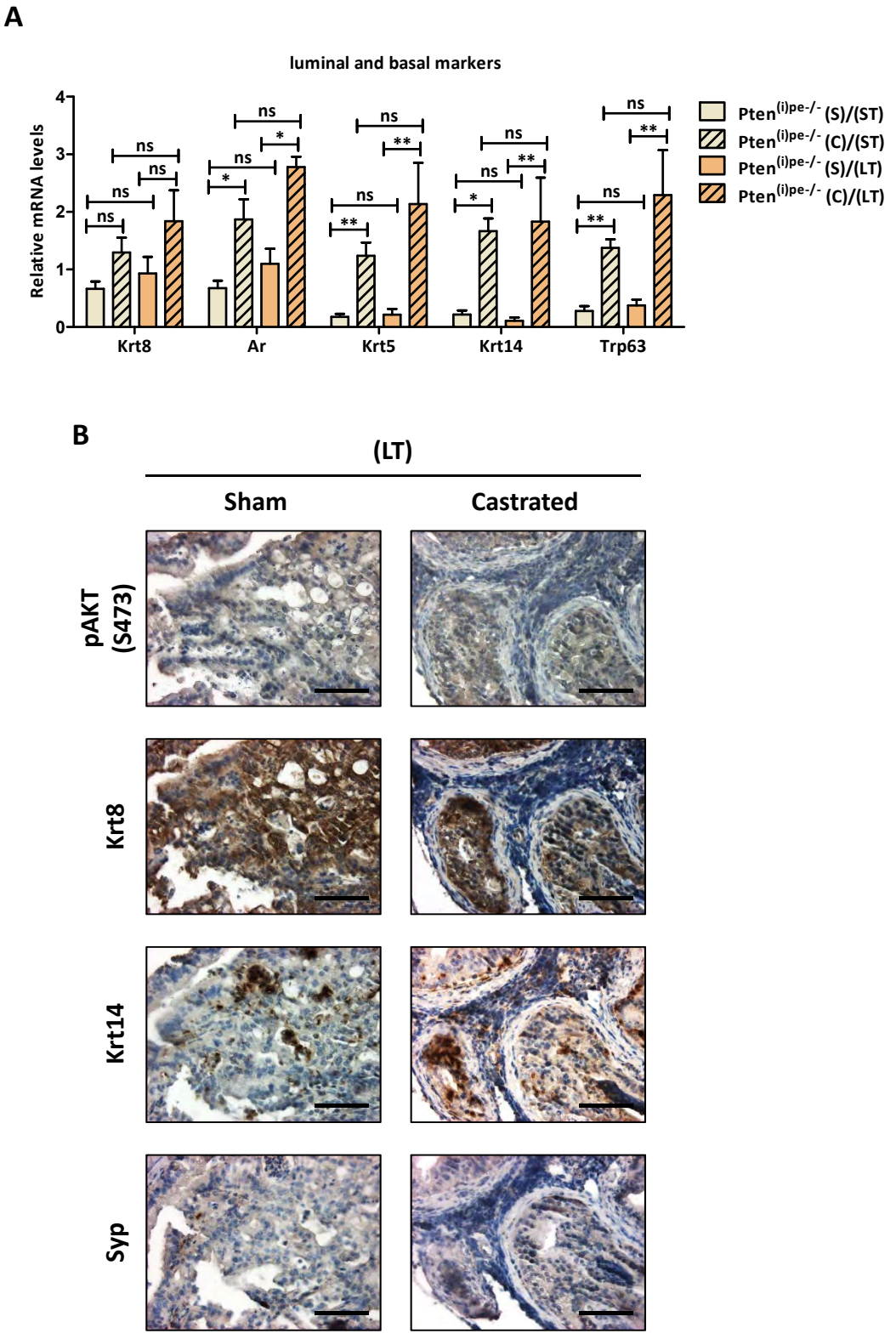

Figure 7. Expression of luminal and basal markers in Pten$^{(i)pe-/-}$ long term after castration.
(**A**) Transcript levels of luminal and basal markers in the prostate of Pten$^{(i)pe-/-}$ sacrificed 3 months (ST) and 10 months (LT) after castration (C) or sham (S) operation. n=3 sham and n=5 castrated Pten$^{(i)pe-/-}$ mice (ST), n=3 sham and n=4 castrated Pten $^{(i)pe-/-}$ mice (LT). Bars represent the mean ± SEM. One-way ANOVA. *p<0.05; **p<0.01; ns, not significant. (**B**) Immunohistochemistry of pAKT S473, Krt8 (luminal marker), Krt14 (basal marker) and Syp in the DLP of adjacent sections of Pten$^{(i)pe-/-}$ mice sacrificed 10 months (LT) after castration (C) or sham (S) operation. Blue: hematoxylin staining. Scale bar: 75 µm. n=3/4 mice for each group.

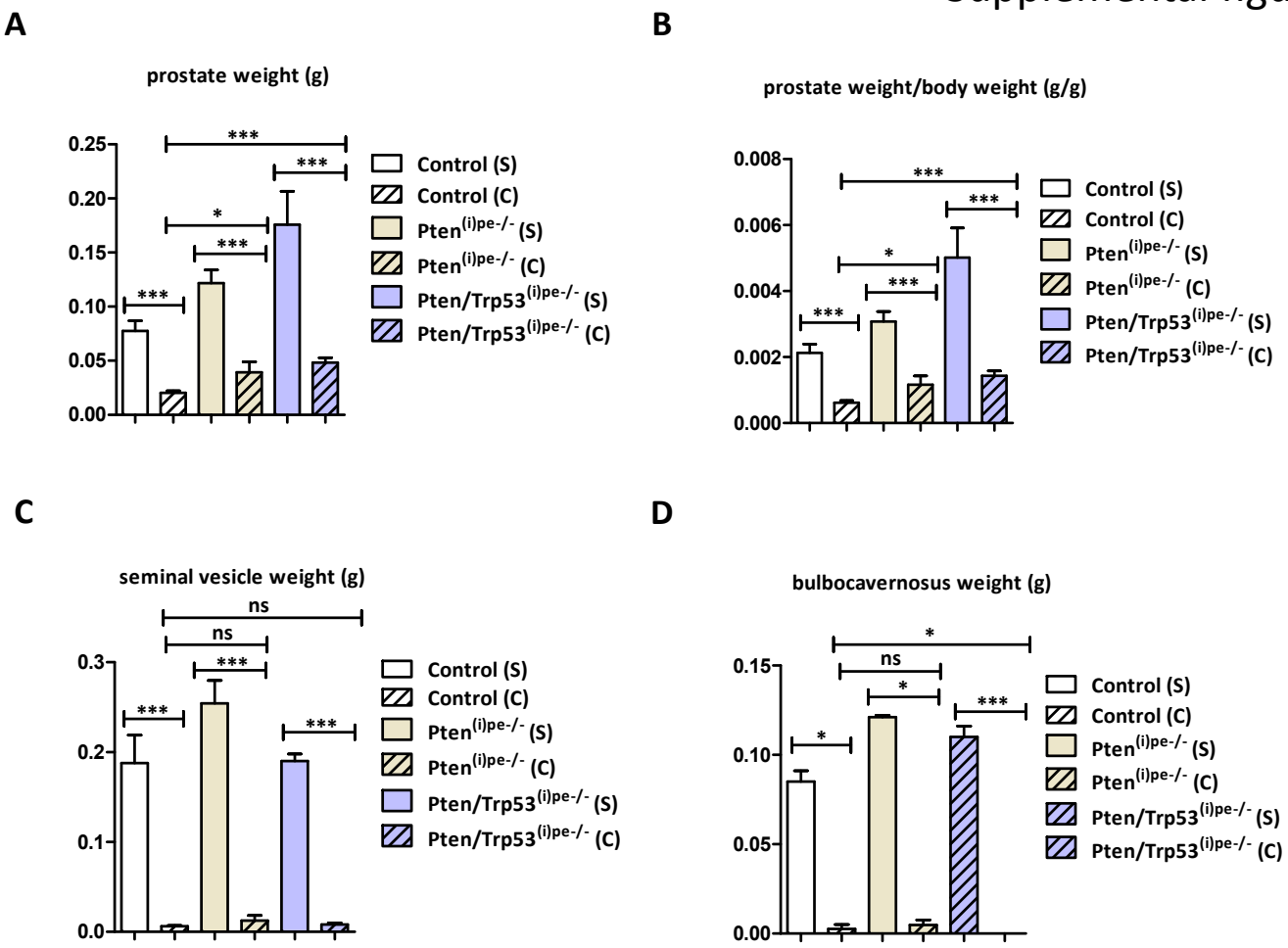

Supplemental figure 1. Effect of castration on Pten$^{(i)pe-/-}$, Pten/Trp53$^{(i)pe-/-}$ and control mice.
Prostate weight (**A**), prostate weight/body weight (**B**), seminal vesicle weight (**C**) and bulbocavernosus weight (**D**) of Pten$^{(i)pe-/-}$, Pten/Trp53$^{(i)pe-/-}$ and control mice sacrificed 3 months after castration (C) and sham (S) operation. n=3-7 sham and n=8 castrated Pten$^{(i)pe-/-}$ mice, n=6 sham and n=12 castrated Pten/Trp53$^{(i)pe-/-}$ mice, n=5 sham and n=9 castrated control mice. Bars represent the mean ± SEM. One way ANOVA. *p<0.05; ***p<0.001; ns, not significant.

A

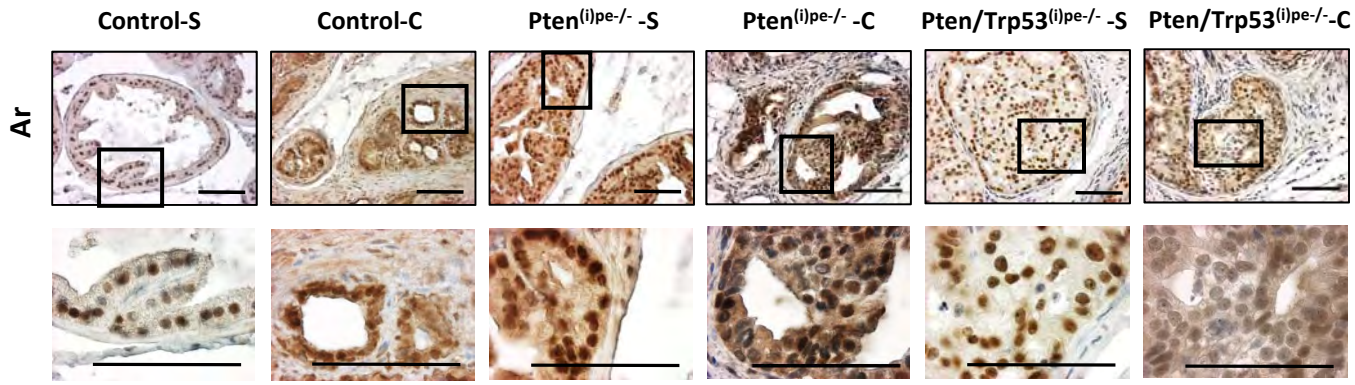

B

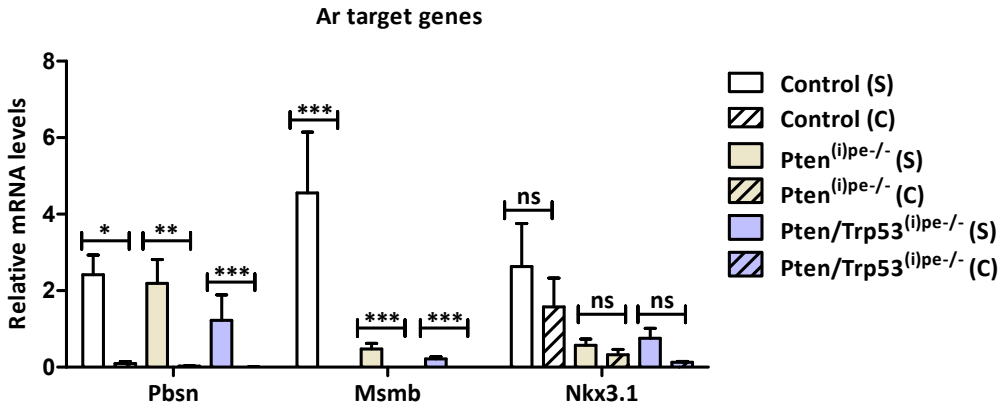

Supplemental figure 2. Characterization of Androgen receptor (AR) signaling in Pten$^{(i)pe-/-}$ and Pten/Trp53$^{(i)pe-/-}$ mice after castration.

(**A**) Immunohistochemical detection of luminal marker (AR) in the DLP of Pten$^{(i)pe-/-}$, Pten/Trp53$^{(i)pe-/-}$ and control mice sacrificed 3 months after castration (C) or sham (S) operation. Blue: hematoxylin staining. Scale bar: 75 µm. n=3/4 mice for each group. (**B**) Relative transcript levels of AR target genes in the DLP and AP of Pten$^{(i)pe-/-}$ and Pten/Trp53$^{(i)pe-/-}$ mice sacrificed 3 months after castration (C) or sham (S) operation. n=8 sham and n=5 castrated Pten$^{(i)pe-/-}$ mice, n=10 sham and n=7 castrated Pten/Trp53$^{(i)pe-/-}$ mice, n=9 sham and n=4 castrated control mice. Bars represent the mean ± SEM. One way ANOVA. *p<0.05; **p<0.01; ***p<0.001; ns, not significant.

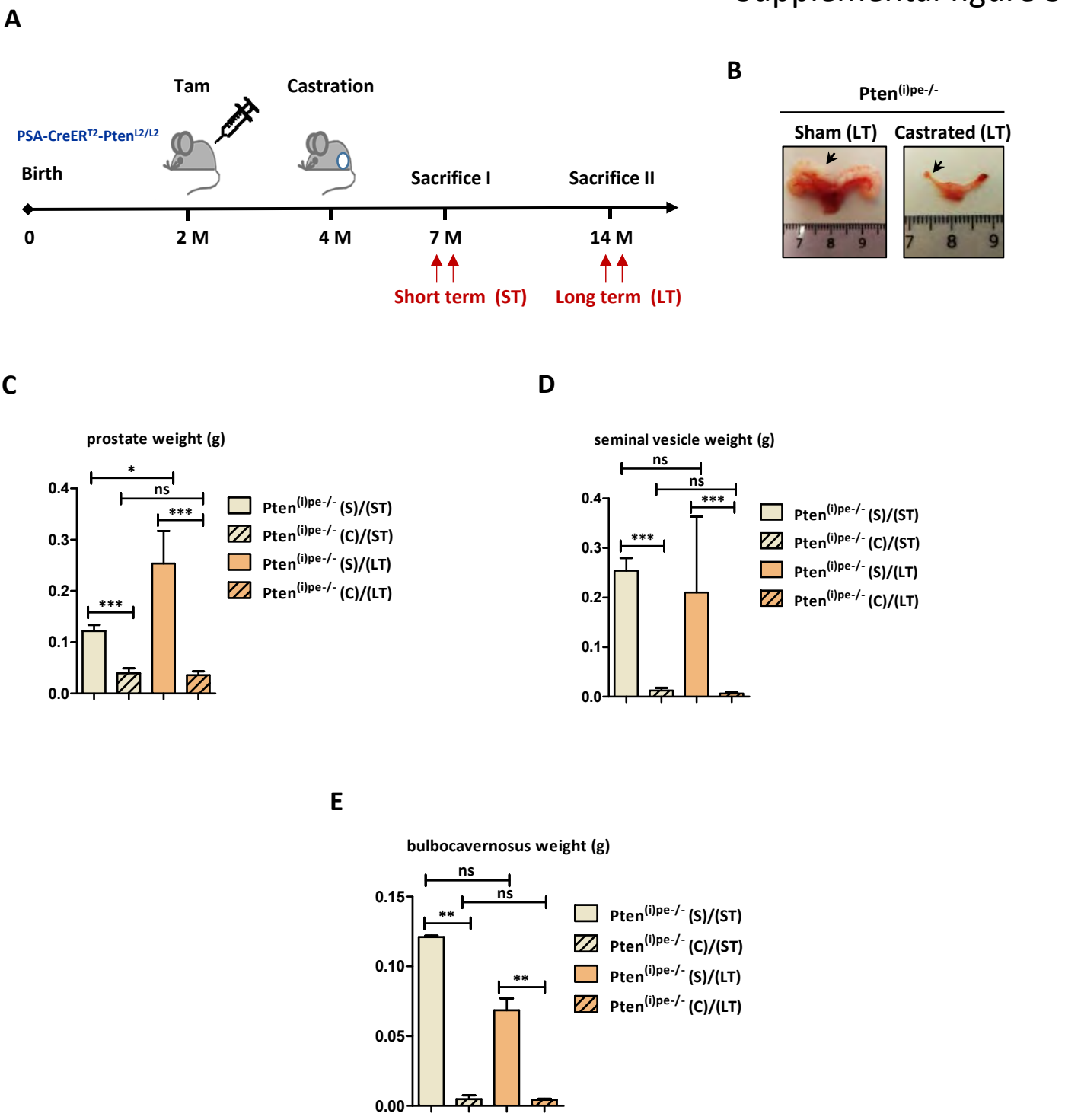

Supplemental figure 3. Effect of long term castration on Pten$^{(i)pe-/-}$ mice.
(**A**) Schematic representation of the experiment. (**B**) Images of representative prostate and seminal vesicle (black arrow) of sham (S) and castrated (C) Pten$^{(i)pe-/-}$ mice sacrificed 10 months after castration and sham operation. Prostate weight (**C**), seminal vesicle weight (**D**) and bulbocavernosus weight (**E**) of Pten$^{(i)pe-/-}$ mice sacrificed 3 months (ST) and 10 months (LT) after castration (C) or sham (S) operation. n=3 sham and n=5 castrated Pten$^{(i)pe-/-}$ mice (I), n=3 sham and n=4 castrated Pten $^{(i)pe-/-}$ mice (II). Bars represent the mean ± SEM. One way ANOVA. *p<0.05; **p<0.01; ***p<0.001 and ns, not significant.

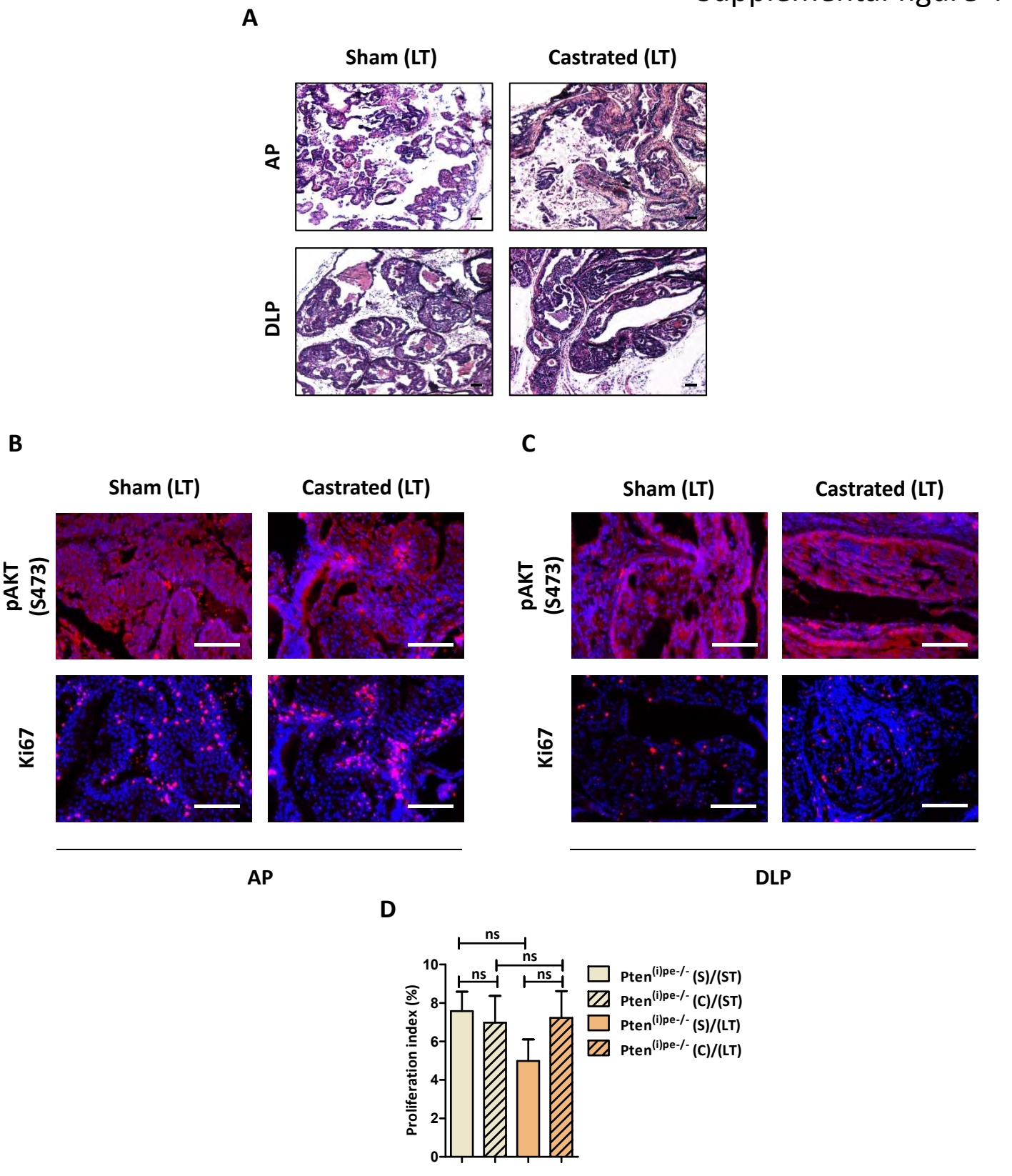

Supplemental figure 4. Characterization of prostatic lesions in Pten$^{(i)pe-/-}$ mice after long term castration. (**A**) Representative views of AP and DLP sections of Pten$^{(i)pe-/-}$ mice sacrificed 10 months after castration or sham operation. Sections were stained with hematoxylin-eosin (HE). Scale bar: 75 µm. Immunodetection of pAKT S473 and Ki67 (red) in the AP (**B**) and DLP (**C**) of Pten$^{(i)pe-/-}$ mice sacrificed 10 months after castration (C) or sham (S) operation. (**D**) Proliferation index (percentage of Ki67-positive prostatic luminal epithelial cells) in DLP of sham (S) and castrated (C) Pten$^{(i)pe-/-}$ mice sacrificed 3 months (ST) and 10 months (LT) after castration or sham operation. n=3 sham and n=5 castrated Pten$^{(i)pe-/-}$ mice (I), n=3 sham and n=4 castrated Pten $^{(i)pe-/-}$ mice (II). Bars represent the mean ± SEM. One way ANOVA. ns, not significant.

GENERAL DISCUSSION

General discussion

In agreement with previous studies *in vivo* (Chen et al., 2005; Di Mitri et al., 2014), we show here that Pten ablation in mature PECs stimulates PINs formation, the progression of which is antagonized by cellular senescence. In contrast to OIS, as no hyperproliferation phase and no signs of DDR was observed after Pten knockdown in cultured cells, PICS was reported to be a new type of cellular senescence (Alimonti et al., 2010; Astle et al., 2012). However, we demonstrate here that Pten-loss induced senescence in PECs is initiated via replication stress-mediated DDR activation after an early phase of enhanced proliferation, and thus resembles OIS (Parisotto et al., 2018). Moreover, we show that Trp53 stabilization via replication stress-mediated DDR activation in Pten-deficient PECs might contribute to trigger senescence, as in OIS (Bartkova et al., 2006; Bartek et al., 2007).

Notably, an important characteristic of our mouse model is to strictly control the time of floxed genes ablation (e.g. Pten, Trp53 and etc.) via the activation of $CreER^{T2}$ recombinase in adult mice (Parisotto et al., 2018; Ratnacaram et al., 2008). However, the use of other mouse model/s is/are hampered by the lack of the temporal control of floxed genes ablation, and gene ablation (e.g. Pten) occurs in undifferentiated prostate of young mice (Alimonti et al., 2010; Chen et al., 2005; Di Mitri et al., 2014). PIN development is accelerated (Luchman et al., 2008) and does not mimic the latency phase of human prostate cancer. In our model, the lower proliferation rate of PECs which reaches a maximum of ~ 10 %, although it reaches ~ 40 % in previously studied model (Alimonti et al., 2010; Chen et al., 2005), probably contribute to slow the establishment of senescent PECs, as the replication stress might be less intense.

It was reported that GR1-positive myeloid cells infiltrate the prostate of $PTEN^{pe-/-}$ mice and oppose PICS in a paracrine fashion by interfering with SASP through the secretion of the cytokine IL-1RA, an antagonist of IL-1R (Di Mitri et al., 2014). However, we show here that IL-1RA-producing GR-1 positive cells (MDSCs) are not present in the prostate of $Pten^{(i)pe-/-}$ mice 1 month after Pten ablation, and thus they cannot contribute to the high proliferation rate at this stage and cannot count for the delay of PECs senescence induced by Pten ablation (Parisotto et al., 2018). However, we demonstrate that AKT activation induced by Pten ablation in PECs counteract DNA-damage induced senescence via enhanced Mdm2-mediated p53 degradation. Moreover, we provide evidence that CKI contributes to Trp53 stabilization at later stages, as it has been shown that CKI family members lead to Mdm2 degradation and thus decrease p53 affinity to Mdm2 (Knippschild et al., 2014). Thus, selective inhibitors of AKT or Mdm2-p53 interaction might enforce senescence and prevent or delay prostate tumor progression.

Although Pten loss in PECs induces cellular senescence that limits tumor progression, as it involves replication stress, approaches based on PICS induction are at risk for cancer prevention and therapy.

Indeed, replication stress induced by Pten ablation might result in an accumulation of mutations such as Tp53, before Trp53 is stabilized and senescence is initiated, and/or in senescent cells, leading to senescence escape and formation of adenocarcinoma. Thus, the safest strategy might be the elimination of senescent cells (for example via inducing apoptosis in senescent cells).

To investigate the role of Trp53 in Pten-null PECs, we analyzed Pten/Trp53$^{(i)pe-/-}$ mice over a period of time. Following the loss of Trp53, Pten-null PECs proliferation is stimulated within few months, as we show that the early hyperproliferation phase is induced via Mdm2-mediated Trp53 degradation in Pten-null PECs (Parisotto et al., 2018). Unexpectedly, although Pten-null PECs proliferation is stimulated in the absence of Trp53 at 2 months, most of the PECs of Pten/Trp53$^{(i)pe-/-}$ mice develop PINs that enter senescence and even express higher levels of some senescence markers than those of Pten$^{(i)pe-/-}$ mice, demonstrating that Trp53 is not absolutely required for initiating senescence in Pten-null PECs. Thus, our results deviate from previous studies showing that Trp53 is required to generate senescent Pten-deficient PECs (Alimonti et al., 2010; Chen et al., 2005). As we show that Pten/Trp53-deficient PECs undergo replication stress and a DDR at the phase of enhanced proliferation 2 months after gene ablation, it is likely that replication stress-mediated DDR activation contributes to trigger senescence in Pten-null PECs in the absence of Trp53.

However, one-fourth of PECs of Pten/Trp53$^{(i)pe-/-}$ mice develop either adenocarcinoma or sarcomatoid, and the latter develop metastases. Importantly PECs of Pten/Trp53$^{(i)pe-/-}$ mice develop adenocarcinoma earlier than those of Pten $^{(i)pe-/-}$ mice, which is likely due to the accumulation of mutations that might result from enhanced replication stress at 2 months. However, it is currently unknown whether the replication stress is more intense in Pten/Trp53-null PECs than in those of Pten-null at 2 months. Moreover, it remains unclear whether the formation of adenocarcinoma or sarcomatoid tumors are resulted from the senescence escape of Pten/Trp53-null PECs, or they are derived from cells that do not enter senescence. Taken together, Trp53 is not mandatory to induce senescence in Pten-deficient PECs, but it can impair their subsequent growth arrest. Therefore, therapeutic strategies for suppressing Pten-deficient tumorigenesis via p53 activation in favour of cellular senescence is not a promising approach.

Forkhead Box M1 (FOXM1) and Centromere protein F (CENPF), involved in cell cycle progression and mitosis respectively, function synergistically to promote tumor growth via the activation of key signaling pathways associated with prostate cancer (e.g. PI3-kinase and MAP kinase pathways). Co-expression of FOXM1 and CENPF is a robust prognostic indicator of poor survival and metastasis. Cosilencing of FOXM1 and CENPF synergistically abrogates prostate tumor growth and induces stress pathway (Aytes et al., 2014). Thus, if these genes are downregulated in Pten/Trp53$^{(i)pe-/-}$ mice, they

might contribute to trigger senescence via inducing replication stress-mediatied DDR. In contrast, if these genes are upregulated, they might contribute to enforce the formation of adenocarcinoma or sarcomatoid tumor. Therefore, determining the status of these genes will allow us to understand prostate tumor evolution in our mouse model (Pten/Trp53$^{(i)pe-/-}$ mice).

CXCL1 is a member of SASP and one of the ligands that binds to the chemokine receptor CXCR2, which has been shown to recruit MDSCs into colonic mucosa and colitis-associated tumors, and thus promote colitis-associated carcinogenesis (Katoh et al., 2013). This study provide an evidence in the interplay between members of SASP and MDSCs in contributing to tumor progression. Moreover, SASP has been shown to promote the stem cell reprogramming factors of neighboring cells in a paracrine fashion *in vivo* (Mosterio et al., 2016; Ritschka et al., 2017). Strikingly, we show here that elevated SASP and MDSCs levels as well as increased stemness were detected along with the senescence phenotype in PIN-containing prostates of Pten/Trp53$^{(i)pe-/-}$ mice, indicating that Trp53 restrain Pten-deficient tumorigenesis via attenuating SASP and MDSCs levels. However, whether SASP and MDSCs-mediated stemness is the mechanism underlying the formation of adenocarcinoma and/or sarcomatoid tumors in Pten/Trp53$^{(i)pe-/-}$ mice remains to be established. Taken together, therapeutic approaches for suppressing MDSCs using CXCR2 antagonists in favour of restraining stemness is probably a promising strategy.

We also show that the loss of Trp53 in Pten-null PECs induces focal neuroendocrine differentiation of luminal PECs and promotes the formation of cells expressing both luminal and basal markers in prostatic lesions. Thus, loss of Trp53 in Pten-null PECs promotes lineage plasticity, which is often associated with the resistance to anti-androgen therapies in human prostate cancer (Ku et al., 2017; Zou et al., 2017). Strikingly, prostatic cell entity sharing luminal and basal characteristics does not differentiate into neuroendocrine cells. Thus, following the loss of Trp53, mixed stem/progenitor Pten-null PECs are formed, which might contribute to castration resistance and thus predict poor therapeutic outcome. Taken together, although Trp53 is not absolutely required for senescence induction, it is mandatory for maintaining cell identity of Pten-null PECs.

Following short term castration, stemness is enhanced and focal neuroendocrine differentiation is induced in castrate-tolerant Pten and Pten/Trp53-null PECs. However, as these focal neuroendocrine cells were shown to be non-proliferative (Zou et al., 2017), they might contribute in the mechanism underlying therapeutic resistance of Pten and Pten/Trp53-null PECs. In addition, several months after castration, Pten-null PECs exhibit adenocarcinoma phenotype rather than focal neuroendocrine phenotype, and thus similar to most cases of human castration-resistant prostate cancer. However, whether neuroendocrine differentiation is induced in Pten/Trp53$^{(i)pe-/-}$ mice after long term castration

remains to be investigated. Importantly, castrate-resistant Pten and Pten/Trp53-null PECs exhibiting luminal and basal markers and not differentiating into neuroendocrine cells are formed. Thus, these cells challenges the models of searching for castrate-resistant cells based on basal versus luminal markers (Lu et al., 2013) since these prostatic cell entity is sharing markers of each. Interestingly, Sala et al. identified a rare population of castration-resistant progenitor cells in $Pten^{pe-/-}$ prostate tumors, referred as LSC^{med} ($Lin^{-}/Sca\text{-}1^{+}/CD49f^{med}$), which represents a unique cell entity that shares markers of luminal and basal/stem cells, and CK4 was validated to be a specific marker for LSC^{med} (Sala et al., 2017). Therefore, castrate-resistant Pten and Pten/Trp53-null PECs might resemble that of LSC^{med}, as they both share the luminal and basal stem progenitor properties, and thus might also express CK4 as a specific marker. Moreover, we show that the activation of AR signaling is reduced after short term castration in both $Pten^{(i)pe-/-}$ and $Pten/Trp53^{(i)pe-/-}$ mice. As Sala et al. showed that LSC^{med} was enriched in low AR signaling context after castration (Sala et al., 2017), castrate-resistant Pten and Pten/Trp53-null PECs resembling LSC^{med} might also enriched due to reduced activation of AR signaling. However, the molecular mediators that contribute to LSC^{med}/and or castrate-resistant Pten and Pten/Trp53-null PECs enrichment in low AR signaling contexts remain to be determined.

Taken together, as current treatments lead to side effects and resistance, the development of therapeutic strategies to eliminate senescent cells/and or PECs expressing luminal and basal markers in pre-cancerous lesions represents promising option for prostate cancer treatment.

REFERENCES

References

Abate-Shen, C., and Shen, M. M. (2000). Molecular genetics of prostate cancer. Genes Dev *14*, 2410-2434.

Acloque, H., Adams, M. S., Fishwick, K., Bronner-Fraser, M., and Nieto, M. A. (2009). Epithelial-mesenchymal transitions: the importance of changing cell state in development and disease. J Clin Invest *119*, 1438-1449.

Adams, J. M., and Cory, S. (2007). The Bcl-2 apoptotic switch in cancer development and therapy. Oncogene *26*, 1324-1337.

Adams, P. D. (2007). Remodeling of chromatin structure in senescent cells and its potential impact on tumor suppression and aging. Gene *397*, 84-93.

Agoulnik, I. U., and Weigel, N. L. (2008). Androgen receptor coactivators and prostate cancer. Adv Exp Med Biol *617*, 245-255.

Alimonti, A., Nardella, C., Chen, Z., Clohessy, J. G., Carracedo, A., Trotman, L. C., Cheng, K., Varmeh, S., Kozma, S. C., Thomas, G.*, et al.* (2010). A novel type of cellular senescence that can be enhanced in mouse models and human tumor xenografts to suppress prostate tumorigenesis. J Clin Invest *120*, 681-693.

Andersen, R. J., Mawji, N. R., Wang, J., Wang, G., Haile, S., Myung, J. K., Watt, K., Tam, T., Yang, Y. C., Banuelos, C. A.*, et al.* (2010). Regression of castrate-recurrent prostate cancer by a small-molecule inhibitor of the amino-terminus domain of the androgen receptor. Cancer Cell *17*, 535-546.

Aparicio, A., Logothetis, C. J., and Maity, S. N. (2011). Understanding the lethal variant of prostate cancer: power of examining extremes. Cancer Discov *1*, 466-468.

Arora, V. K., Schenkein, E., Murali, R., Subudhi, S. K., Wongvipat, J., Balbas, M. D., Shah, N., Cai, L., Efstathiou, E., Logothetis, C.*, et al.* (2013). Glucocorticoid receptor confers resistance to antiandrogens by bypassing androgen receptor blockade. Cell *155*, 1309-1322.

Askew, E. B., Gampe, R. T., Jr., Stanley, T. B., Faggart, J. L., and Wilson, E. M. (2007). Modulation of androgen receptor activation function 2 by testosterone and dihydrotestosterone. J Biol Chem *282*, 25801-25816.

Astle, M. V., Hannan, K. M., Ng, P. Y., Lee, R. S., George, A. J., Hsu, A. K., Haupt, Y., Hannan, R. D., and Pearson, R. B. (2012). AKT induces senescence in human cells via mTORC1 and p53 in the absence of DNA damage: implications for targeting mTOR during malignancy. Oncogene *31*, 1949-1962.

Aytes, A., Mitrofanova, A., Lefebvre, C., Alvarez, M. J., Castillo-Martin, M., Zheng, T., Eastham, J. A., Gopalan, A., Pienta, K. J., Shen, M. M.*, et al.* (2014). Cross-species regulatory network analysis identifies a synergistic interaction between FOXM1 and CENPF that drives prostate cancer malignancy. Cancer Cell *25*, 638-651.

Bae, K. M., Su, Z., Frye, C., McClellan, S., Allan, R. W., Andrejewski, J. T., Kelley, V., Jorgensen, M., Steindler, D. A., Vieweg, J., and Siemann, D. W. (2010). Expression of pluripotent stem cell reprogramming factors by prostate tumor initiating cells. J Urol *183*, 2045-2053.

Baeriswyl, V., and Christofori, G. (2009). The angiogenic switch in carcinogenesis. Semin Cancer Biol *19*, 329-337.

Bakkenist, C. J., and Kastan, M. B. (2003). DNA damage activates ATM through intermolecular autophosphorylation and dimer dissociation. Nature *421*, 499-506.

Beltran, H., Prandi, D., Mosquera, J. M., Benelli, M., Puca, L., Cyrta, J., Marotz, C., Giannopoulou, E., Chakravarthi, B. V., Varambally, S.*, et al.* (2016). Divergent clonal evolution of castration-resistant neuroendocrine prostate cancer. Nat Med *22*, 298-305.

Beltran, H., Rickman, D. S., Park, K., Chae, S. S., Sboner, A., MacDonald, T. Y., Wang, Y., Sheikh, K. L., Terry, S., Tagawa, S. T.*, et al.* (2011). Molecular characterization of neuroendocrine prostate cancer and identification of new drug targets. Cancer Discov *1*, 487-495.

Beltran, H., Tagawa, S. T., Park, K., MacDonald, T., Milowsky, M. I., Mosquera, J. M., Rubin, M. A., and Nanus, D. M. (2012). Challenges in recognizing treatment-related neuroendocrine prostate cancer. J Clin Oncol *30*, e386-389.

Bergerat, J. P., and Ceraline, J. (2009). Pleiotropic functional properties of androgen receptor mutants in prostate cancer. Hum Mutat *30*, 145-157.

Bergers, G., and Benjamin, L. E. (2003). Tumorigenesis and the angiogenic switch. Nat Rev Cancer *3*, 401-410.

Berthold, D. R., Pond, G. R., Soban, F., de Wit, R., Eisenberger, M., and Tannock, I. F. (2008). Docetaxel plus prednisone or mitoxantrone plus prednisone for advanced prostate cancer: updated survival in the TAX 327 study. J Clin Oncol *26*, 242-245.

Berx, G., and van Roy, F. (2009). Involvement of members of the cadherin superfamily in cancer. Cold Spring Harb Perspect Biol *1*, a003129.

Bhowmick, N. A., Neilson, E. G., and Moses, H. L. (2004). Stromal fibroblasts in cancer initiation and progression. Nature *432*, 332-337.

Black, B. E., Vitto, M. J., Gioeli, D., Spencer, A., Afshar, N., Conaway, M. R., Weber, M. J., and Paschal, B. M. (2004). Transient, ligand-dependent arrest of the androgen receptor in subnuclear foci alters phosphorylation and coactivator interactions. Mol Endocrinol *18*, 834-850.

Bostwick, D. G. (1989). Prostatic intraepithelial neoplasia (PIN). Urology *34*, 16-22.

Bostwick, D. G., and Qian, J. (2004). High-grade prostatic intraepithelial neoplasia. Mod Pathol *17*, 360-379.

Branzei, D., and Foiani, M. (2005). The DNA damage response during DNA replication. Curr Opin Cell Biol *17*, 568-575.

Brooke, G. N., and Bevan, C. L. (2009). The role of androgen receptor mutations in prostate cancer progression. Curr Genomics *10*, 18-25.

Bubendorf, L., Kononen, J., Koivisto, P., Schraml, P., Moch, H., Gasser, T. C., Willi, N., Mihatsch, M. J., Sauter, G., and Kallioniemi, O. P. (1999). Survey of gene amplifications during prostate cancer

progression by high-throughout fluorescence in situ hybridization on tissue microarrays. Cancer Res *59*, 803-806.

Byun, T. S., Pacek, M., Yee, M. C., Walter, J. C., and Cimprich, K. A. (2005). Functional uncoupling of MCM helicase and DNA polymerase activities activates the ATR-dependent checkpoint. Genes Dev *19*, 1040-1052.

Cavallaro, U., and Christofori, G. (2004). Cell adhesion and signalling by cadherins and Ig-CAMs in cancer. Nat Rev Cancer *4*, 118-132.

Centenera, M. M., Harris, J. M., Tilley, W. D., and Butler, L. M. (2008). The contribution of different androgen receptor domains to receptor dimerization and signaling. Mol Endocrinol *22*, 2373-2382.

Ceraline, J., Cruchant, M. D., Erdmann, E., Erbs, P., Kurtz, J. E., Duclos, B., Jacqmin, D., Chopin, D., and Bergerat, J. P. (2004). Constitutive activation of the androgen receptor by a point mutation in the hinge region: a new mechanism for androgen-independent growth in prostate cancer. Int J Cancer *108*, 152-157.

Chan, S. C., Li, Y., and Dehm, S. M. (2012). Androgen receptor splice variants activate androgen receptor target genes and support aberrant prostate cancer cell growth independent of canonical androgen receptor nuclear localization signal. J Biol Chem *287*, 19736-19749.

Chen, Z., Trotman, L. C., Shaffer, D., Lin, H. K., Dotan, Z. A., Niki, M., Koutcher, J. A., Scher, H. I., Ludwig, T., Gerald, W.*, et al.* (2005). Crucial role of p53-dependent cellular senescence in suppression of Pten-deficient tumorigenesis. Nature *436*, 725-730.

Cheng, N., Chytil, A., Shyr, Y., Joly, A., and Moses, H. L. (2008). Transforming growth factor-beta signaling-deficient fibroblasts enhance hepatocyte growth factor signaling in mammary carcinoma cells to promote scattering and invasion. Mol Cancer Res *6*, 1521-1533.

Chmelar, R., Buchanan, G., Need, E. F., Tilley, W., and Greenberg, N. M. (2007). Androgen receptor coregulators and their involvement in the development and progression of prostate cancer. Int J Cancer *120*, 719-733.

Chrisofos, M., Papatsoris, A. G., Lazaris, A., and Deliveliotis, C. (2007). Precursor lesions of prostate cancer. Crit Rev Clin Lab Sci *44*, 243-270.

Claessens, F., Denayer, S., Van Tilborgh, N., Kerkhofs, S., Helsen, C., and Haelens, A. (2008). Diverse roles of androgen receptor (AR) domains in AR-mediated signaling. Nucl Recept Signal *6*, e008.

Cleutjens, K. B., van Eekelen, C. C., van der Korput, H. A., Brinkmann, A. O., and Trapman, J. (1996). Two androgen response regions cooperate in steroid hormone regulated activity of the prostate-specific antigen promoter. J Biol Chem *271*, 6379-6388.

Collado, M., and Serrano, M. (2006). The power and the promise of oncogene-induced senescence markers. Nat Rev Cancer *6*, 472-476.

Collado, M., and Serrano, M. (2010). Senescence in tumours: evidence from mice and humans. Nat Rev Cancer *10*, 51-57.

Coppe, J. P., Desprez, P. Y., Krtolica, A., and Campisi, J. (2010). The senescence-associated secretory phenotype: the dark side of tumor suppression. Annu Rev Pathol *5*, 99-118.

Cottard, F., Asmane, I., Erdmann, E., Bergerat, J. P., Kurtz, J. E., and Ceraline, J. (2013). Constitutively active androgen receptor variants upregulate expression of mesenchymal markers in prostate cancer cells. PLoS One *8*, e63466.

Courtois-Cox, S., Jones, S. L., and Cichowski, K. (2008). Many roads lead to oncogene-induced senescence. Oncogene *27*, 2801-2809.

Culig, Z., and Bartsch, G. (2006). Androgen axis in prostate cancer. J Cell Biochem *99*, 373-381.

Culig, Z., Hobisch, A., Cronauer, M. V., Radmayr, C., Trapman, J., Hittmair, A., Bartsch, G., and Klocker, H. (1994). Androgen receptor activation in prostatic tumor cell lines by insulin-like growth factor-I, keratinocyte growth factor, and epidermal growth factor. Cancer Res *54*, 5474-5478.

Culig, Z., Klocker, H., Bartsch, G., and Hobisch, A. (2001). Androgen receptor mutations in carcinoma of the prostate: significance for endocrine therapy. Am J Pharmacogenomics *1*, 241-249.

Culig, Z., and Santer, F. R. (2014). Androgen receptor signaling in prostate cancer. Cancer Metastasis Rev *33*, 413-427.

Cunha, G. R., Alarid, E. T., Turner, T., Donjacour, A. A., Boutin, E. L., and Foster, B. A. (1992). Normal and abnormal development of the male urogenital tract. Role of androgens, mesenchymal-epithelial interactions, and growth factors. J Androl *13*, 465-475.

Dardenne, E., Beltran, H., Benelli, M., Gayvert, K., Berger, A., Puca, L., Cyrta, J., Sboner, A., Noorzad, Z., MacDonald, T.*, et al.* (2016). N-Myc Induces an EZH2-Mediated Transcriptional Program Driving Neuroendocrine Prostate Cancer. Cancer Cell *30*, 563-577.

Davies, A. H., Beltran, H., and Zoubeidi, A. (2018). Cellular plasticity and the neuroendocrine phenotype in prostate cancer. Nat Rev Urol *15*, 271-286.

de Bono, J. S., Oudard, S., Ozguroglu, M., Hansen, S., Machiels, J. P., Kocak, I., Gravis, G., Bodrogi, I., Mackenzie, M. J., Shen, L.*, et al.* (2010). Prednisone plus cabazitaxel or mitoxantrone for metastatic castration-resistant prostate cancer progressing after docetaxel treatment: a randomised open-label trial. Lancet *376*, 1147-1154.

Dehm, S. M., and Tindall, D. J. (2005). Regulation of androgen receptor signaling in prostate cancer. Expert Rev Anticancer Ther *5*, 63-74.

Dehm, S. M., and Tindall, D. J. (2007). Androgen receptor structural and functional elements: role and regulation in prostate cancer. Mol Endocrinol *21*, 2855-2863.

Di Cristofano, A., and Pandolfi, P. P. (2000). The multiple roles of PTEN in tumor suppression. Cell *100*, 387-390.

Di Mitri, D., Toso, A., and Alimonti, A. (2015a). Molecular Pathways: Targeting Tumor-Infiltrating Myeloid-Derived Suppressor Cells for Cancer Therapy. Clin Cancer Res *21*, 3108-3112.

Di Mitri, D., Toso, A., and Alimonti, A. (2015b). Tumor-infiltrating myeloid cells drive senescence evasion and chemoresistance in tumors. Oncoimmunology *4*, e988473.

Di Mitri, D., Toso, A., Chen, J. J., Sarti, M., Pinton, S., Jost, T. R., D'Antuono, R., Montani, E., Garcia-Escudero, R., Guccini, I.*, et al.* (2014). Tumour-infiltrating Gr-1+ myeloid cells antagonize senescence in cancer. Nature *515*, 134-137.

Dirac, A. M., and Bernards, R. (2010). The deubiquitinating enzyme USP26 is a regulator of androgen receptor signaling. Mol Cancer Res *8*, 844-854.

Edwards, J., Krishna, N. S., Witton, C. J., and Bartlett, J. M. (2003). Gene amplifications associated with the development of hormone-resistant prostate cancer. Clin Cancer Res *9*, 5271-5281.

Evan, G., and Littlewood, T. (1998). A matter of life and cell death. Science *281*, 1317-1322.

Evan, G. I., and d'Adda di Fagagna, F. (2009). Cellular senescence: hot or what? Curr Opin Genet Dev *19*, 25-31.

Feldman, B. J., and Feldman, D. (2001). The development of androgen-independent prostate cancer. Nat Rev Cancer *1*, 34-45.

Ford, O. H., 3rd, Gregory, C. W., Kim, D., Smitherman, A. B., and Mohler, J. L. (2003). Androgen receptor gene amplification and protein expression in recurrent prostate cancer. J Urol *170*, 1817-1821.

Fouad, Y. A., and Aanei, C. (2017). Revisiting the hallmarks of cancer. Am J Cancer Res *7*, 1016-1036.

Freeman, D. J., Li, A. G., Wei, G., Li, H. H., Kertesz, N., Lesche, R., Whale, A. D., Martinez-Diaz, H., Rozengurt, N., Cardiff, R. D.*, et al.* (2003). PTEN tumor suppressor regulates p53 protein levels and activity through phosphatase-dependent and -independent mechanisms. Cancer Cell *3*, 117-130.
Gabrilovich, D. I., Ostrand-Rosenberg, S., and Bronte, V. (2012). Coordinated regulation of myeloid cells by tumours. Nat Rev Immunol *12*, 253-268.

Galsky, M. D., Small, A. C., Tsao, C. K., and Oh, W. K. (2012). Clinical development of novel therapeutics for castration-resistant prostate cancer: historic challenges and recent successes. CA Cancer J Clin *62*, 299-308.

Germann, M., Wetterwald, A., Guzman-Ramirez, N., van der Pluijm, G., Culig, Z., Cecchini, M. G., Williams, E. D., and Thalmann, G. N. (2012). Stem-like cells with luminal progenitor phenotype survive castration in human prostate cancer. Stem Cells *30*, 1076-1086.

Greenberg, N. M., DeMayo, F., Finegold, M. J., Medina, D., Tilley, W. D., Aspinall, J. O., Cunha, G. R., Donjacour, A. A., Matusik, R. J., and Rosen, J. M. (1995). Prostate cancer in a transgenic mouse. Proc Natl Acad Sci U S A *92*, 3439-3443.

Greene, K. L., Albertsen, P. C., Babaian, R. J., Carter, H. B., Gann, P. H., Han, M., Kuban, D. A., Sartor, A. O., Stanford, J. L., Zietman, A., and Carroll, P. (2009). Prostate specific antigen best practice statement: 2009 update. J Urol *182*, 2232-2241.

Gregory, C. W., He, B., Johnson, R. T., Ford, O. H., Mohler, J. L., French, F. S., and Wilson, E. M. (2001). A mechanism for androgen receptor-mediated prostate cancer recurrence after androgen deprivation therapy. Cancer Res *61*, 4315-4319.

Grignon, D. J. (2004). Unusual subtypes of prostate cancer. Mod Pathol *17*, 316-327.

Guo, Z., Dai, B., Jiang, T., Xu, K., Xie, Y., Kim, O., Nesheiwat, I., Kong, X., Melamed, J., Handratta, V. D., *et al.* (2006). Regulation of androgen receptor activity by tyrosine phosphorylation. Cancer Cell *10*, 309-319.

Guo, Z., Yang, X., Sun, F., Jiang, R., Linn, D. E., Chen, H., Chen, H., Kong, X., Melamed, J., Tepper, C. G., *et al.* (2009). A novel androgen receptor splice variant is up-regulated during prostate cancer progression and promotes androgen depletion-resistant growth. Cancer Res *69*, 2305-2313.

Hanahan, D., and Folkman, J. (1996). Patterns and emerging mechanisms of the angiogenic switch during tumorigenesis. Cell *86*, 353-364.

Hanahan, D., and Weinberg, R. A. (2000). The hallmarks of cancer. Cell *100*, 57-70.

Hargrave, M., Wright, E., Kun, J., Emery, J., Cooper, L., and Koopman, P. (1997). Expression of the Sox11 gene in mouse embryos suggests roles in neuronal maturation and epithelio-mesenchymal induction. Dev Dyn *210*, 79-86.

Harris, W. P., Mostaghel, E. A., Nelson, P. S., and Montgomery, B. (2009). Androgen deprivation therapy: progress in understanding mechanisms of resistance and optimizing androgen depletion. Nat Clin Pract Urol *6*, 76-85.

Hay, E. D. (2005). The mesenchymal cell, its role in the embryo, and the remarkable signaling mechanisms that create it. Dev Dyn *233*, 706-720.

Heemers, H. V., and Tindall, D. J. (2007). Androgen receptor (AR) coregulators: a diversity of functions converging on and regulating the AR transcriptional complex. Endocr Rev *28*, 778-808.

Helpap, B., Kollermann, J., and Oehler, U. (1999). Neuroendocrine differentiation in prostatic carcinomas: histogenesis, biology, clinical relevance, and future therapeutical perspectives. Urol Int *62*, 133-138.

Helt, C. E., Cliby, W. A., Keng, P. C., Bambara, R. A., and O'Reilly, M. A. (2005). Ataxia telangiectasia mutated (ATM) and ATM and Rad3-related protein exhibit selective target specificities in response to different forms of DNA damage. J Biol Chem *280*, 1186-1192.

Hemann, M. T., and Narita, M. (2007). Oncogenes and senescence: breaking down in the fast lane. Genes Dev *21*, 1-5.

Hermans, K. G., Boormans, J. L., Gasi, D., van Leenders, G. J., Jenster, G., Verhagen, P. C., and Trapman, J. (2009). Overexpression of prostate-specific TMPRSS2(exon 0)-ERG fusion transcripts corresponds with favorable prognosis of prostate cancer. Clin Cancer Res *15*, 6398-6403.

Hirano, D., Okada, Y., Minei, S., Takimoto, Y., and Nemoto, N. (2004). Neuroendocrine differentiation in hormone refractory prostate cancer following androgen deprivation therapy. Eur Urol *45*, 586-592; discussion 592.

Hollenhorst, P. C., Paul, L., Ferris, M. W., and Graves, B. J. (2011). The ETS gene ETV4 is required for anchorage-independent growth and a cell proliferation gene expression program in PC3 prostate cells. Genes Cancer *1*, 1044-1052.

Holzbeierlein, J., Lal, P., LaTulippe, E., Smith, A., Satagopan, J., Zhang, L., Ryan, C., Smith, S., Scher, H., Scardino, P*., et al.* (2004). Gene expression analysis of human prostate carcinoma during hormonal therapy identifies androgen-responsive genes and mechanisms of therapy resistance. Am J Pathol *164*, 217-227.

Hornberg, E., Ylitalo, E. B., Crnalic, S., Antti, H., Stattin, P., Widmark, A., Bergh, A., and Wikstrom, P. (2011). Expression of androgen receptor splice variants in prostate cancer bone metastases is associated with castration-resistance and short survival. PLoS One *6*, e19059.

Hu, R., Dunn, T. A., Wei, S., Isharwal, S., Veltri, R. W., Humphreys, E., Han, M., Partin, A. W., Vessella, R. L., Isaacs, W. B*., et al.* (2009). Ligand-independent androgen receptor variants derived from splicing of cryptic exons signify hormone-refractory prostate cancer. Cancer Res *69*, 16-22.

Huggins, C. (1942). Effect of Orchiectomy and Irradiation on Cancer of the Prostate. Ann Surg *115*, 1192-1200.

Huggins, C. (1944). The Treatment of Cancer of the Prostate : (The 1943 Address in Surgery before the Royal College of Physicians and Surgeons of Canada). Can Med Assoc J *50*, 301-307.

Huggins, C., and Hodges, C. V. (1972). Studies on prostatic cancer. I. The effect of castration, of estrogen and androgen injection on serum phosphatases in metastatic carcinoma of the prostate. CA Cancer J Clin *22*, 232-240.

Isikbay, M., Otto, K., Kregel, S., Kach, J., Cai, Y., Vander Griend, D. J., Conzen, S. D., and Szmulewitz, R. Z. (2014). Glucocorticoid receptor activity contributes to resistance to androgen-targeted therapy in prostate cancer. Horm Cancer *5*, 72-89.

Junttila, M. R., and Evan, G. I. (2009). p53--a Jack of all trades but master of none. Nat Rev Cancer *9*, 821-829.

Kaikkonen, S., Jaaskelainen, T., Karvonen, U., Rytinki, M. M., Makkonen, H., Gioeli, D., Paschal, B. M., and Palvimo, J. J. (2009). SUMO-specific protease 1 (SENP1) reverses the hormone-augmented SUMOylation of androgen receptor and modulates gene responses in prostate cancer cells. Mol Endocrinol *23*, 292-307.

Kastan, M. B., and Lim, D. S. (2000). The many substrates and functions of ATM. Nat Rev Mol Cell Biol *1*, 179-186.

Katoh, H., Wang, D., Daikoku, T., Sun, H., Dey, S. K., and Dubois, R. N. (2013). CXCR2-expressing myeloid-derived suppressor cells are essential to promote colitis-associated tumorigenesis. Cancer Cell *24*, 631-644.

Katsogiannou, M., Ziouziou, H., Karaki, S., Andrieu, C., Henry de Villeneuve, M., and Rocchi, P. (2015). The hallmarks of castration-resistant prostate cancers. Cancer Treat Rev *41*, 588-597.

Kawamura, T., Suzuki, J., Wang, Y. V., Menendez, S., Morera, L. B., Raya, A., Wahl, G. M., and Izpisua Belmonte, J. C. (2009). Linking the p53 tumour suppressor pathway to somatic cell reprogramming. Nature *460*, 1140-1144.

Kellokumpu-Lehtinen, P., Santti, R., and Pelliniemi, L. J. (1980). Correlation of early cytodifferentiation of the human fetal prostate and Leydig cells. Anat Rec *196*, 263-273.

Klotz, L. (2008). Maximal androgen blockade for advanced prostate cancer. Best Pract Res Clin Endocrinol Metab *22*, 331-340.

Knippschild, U., Kruger, M., Richter, J., Xu, P., Garcia-Reyes, B., Peifer, C., Halekotte, J., Bakulev, V., and Bischof, J. (2014). The CK1 Family: Contribution to Cellular Stress Response and Its Role in Carcinogenesis. Front Oncol *4*, 96.

Knudsen, K. E., and Kelly, W. K. (2011). Outsmarting androgen receptor: creative approaches for targeting aberrant androgen signaling in advanced prostate cancer. Expert Rev Endocrinol Metab *6*, 483-493.

Knudsen, K. E., and Scher, H. I. (2009). Starving the addiction: new opportunities for durable suppression of AR signaling in prostate cancer. Clin Cancer Res *15*, 4792-4798.

Kong, D., Sethi, S., Li, Y., Chen, W., Sakr, W. A., Heath, E., and Sarkar, F. H. (2015). Androgen receptor splice variants contribute to prostate cancer aggressiveness through induction of EMT and expression of stem cell marker genes. Prostate *75*, 161-174.

Ku, S. Y., Rosario, S., Wang, Y., Mu, P., Seshadri, M., Goodrich, Z. W., Goodrich, M. M., Labbe, D. P., Gomez, E. C., Wang, J.*, et al.* (2017). Rb1 and Trp53 cooperate to suppress prostate cancer lineage plasticity, metastasis, and antiandrogen resistance. Science *355*, 78-83.

Kumar-Sinha, C., Tomlins, S. A., and Chinnaiyan, A. M. (2008). Recurrent gene fusions in prostate cancer. Nat Rev Cancer *8*, 497-511.

Lee, S. O., Lou, W., Hou, M., de Miguel, F., Gerber, L., and Gao, A. C. (2003a). Interleukin-6 promotes androgen-independent growth in LNCaP human prostate cancer cells. Clin Cancer Res *9*, 370-376.

Lee, S. O., Lou, W., Hou, M., Onate, S. A., and Gao, A. C. (2003b). Interleukin-4 enhances prostate-specific antigen expression by activation of the androgen receptor and Akt pathway. Oncogene *22*, 7981-7988.

Lee, S. O., Ma, Z., Yeh, C. R., Luo, J., Lin, T. H., Lai, K. P., Yamashita, S., Liang, L., Tian, J., Li, L.*, et al.* (2013). New therapy targeting differential androgen receptor signaling in prostate cancer stem/progenitor vs. non-stem/progenitor cells. J Mol Cell Biol *5*, 14-26.

Lemmon, M. A., and Schlessinger, J. (2010). Cell signaling by receptor tyrosine kinases. Cell *141*, 1117-1134.

Levine, A. J. (1997). p53, the cellular gatekeeper for growth and division. Cell *88*, 323-331.

Liaw, H., Lee, D., and Myung, K. (2011). DNA-PK-dependent RPA2 hyperphosphorylation facilitates DNA repair and suppresses sister chromatid exchange. PLoS One *6*, e21424.

Lilja, H., Ulmert, D., and Vickers, A. J. (2008). Prostate-specific antigen and prostate cancer: prediction, detection and monitoring. Nat Rev Cancer *8*, 268-278.

Linja, M. J., and Visakorpi, T. (2004). Alterations of androgen receptor in prostate cancer. J Steroid Biochem Mol Biol *92*, 255-264.

Lipianskaya, J., Cohen, A., Chen, C. J., Hsia, E., Squires, J., Li, Z., Zhang, Y., Li, W., Chen, X., Xu, H., and Huang, J. (2014). Androgen-deprivation therapy-induced aggressive prostate cancer with neuroendocrine differentiation. Asian J Androl *16*, 541-544.

Locke, J. A., Guns, E. S., Lubik, A. A., Adomat, H. H., Hendy, S. C., Wood, C. A., Ettinger, S. L., Gleave, M. E., and Nelson, C. C. (2008). Androgen levels increase by intratumoral de novo steroidogenesis during progression of castration-resistant prostate cancer. Cancer Res *68*, 6407-6415.

Loeb, S., Bjurlin, M. A., Nicholson, J., Tammela, T. L., Penson, D. F., Carter, H. B., Carroll, P., and Etzioni, R. (2014). Overdiagnosis and overtreatment of prostate cancer. Eur Urol *65*, 1046-1055.

Lonergan, P. E., and Tindall, D. J. (2011). Androgen receptor signaling in prostate cancer development and progression. J Carcinog *10*, 20.

Lowe, S. W., Cepero, E., and Evan, G. (2004). Intrinsic tumour suppression. Nature *432*, 307-315.

Lu, T. L., Huang, Y. F., You, L. R., Chao, N. C., Su, F. Y., Chang, J. L., and Chen, C. M. (2013). Conditionally ablated Pten in prostate basal cells promotes basal-to-luminal differentiation and causes invasive prostate cancer in mice. Am J Pathol *182*, 975-991.

Macleod, K. F. (2010). The RB tumor suppressor: a gatekeeper to hormone independence in prostate cancer? J Clin Invest *120*, 4179-4182.

Manin, M., Baron, S., Goossens, K., Beaudoin, C., Jean, C., Veyssiere, G., Verhoeven, G., and Morel, L. (2002). Androgen receptor expression is regulated by the phosphoinositide 3-kinase/Akt pathway in normal and tumoral epithelial cells. Biochem J *366*, 729-736.

Manin, M., Martinez, A., Van Der Schueren, B., Reynaert, I., and Jean, C. (2000). Acquisition of androgen-mediated expression of mouse vas deferens protein (MVDP) gene in cultured epithelial cells and in vas deferens during postnatal development. J Androl *21*, 641-650.

Marcelli, M., Ittmann, M., Mariani, S., Sutherland, R., Nigam, R., Murthy, L., Zhao, Y., DiConcini, D., Puxeddu, E., Esen, A*., et al.* (2000). Androgen receptor mutations in prostate cancer. Cancer Res *60*, 944-949.

Maroulakou, I. G., Anver, M., Garrett, L., and Green, J. E. (1994). Prostate and mammary adenocarcinoma in transgenic mice carrying a rat C3(1) simian virus 40 large tumor antigen fusion gene. Proc Natl Acad Sci U S A *91*, 11236-11240.

McNeal, J. E., and Bostwick, D. G. (1986). Intraductal dysplasia: a premalignant lesion of the prostate. Hum Pathol *17*, 64-71.

McNeal, J. E., Bostwick, D. G., Kindrachuk, R. A., Redwine, E. A., Freiha, F. S., and Stamey, T. A. (1986). Patterns of progression in prostate cancer. Lancet *1*, 60-63.

Meeks, J. J., and Schaeffer, E. M. (2011). Genetic regulation of prostate development. J Androl *32*, 210-217.

Mestayer, C., Blanchere, M., Jaubert, F., Dufour, B., and Mowszowicz, I. (2003). Expression of androgen receptor coactivators in normal and cancer prostate tissues and cultured cell lines. Prostate *56*, 192-200.

Metzger, D., and Chambon, P. (2001). Site- and time-specific gene targeting in the mouse. Methods *24*, 71-80.

Micalizzi, D. S., Farabaugh, S. M., and Ford, H. L. (2010). Epithelial-mesenchymal transition in cancer: parallels between normal development and tumor progression. J Mammary Gland Biol Neoplasia *15*, 117-134.

Mohler, J. L. (2008a). Castration-recurrent prostate cancer is not androgen-independent. Adv Exp Med Biol *617*, 223-234.

Mohler, J. L. (2008b). A role for the androgen-receptor in clinically localized and advanced prostate cancer. Best Pract Res Clin Endocrinol Metab *22*, 357-372.

Montgomery, R. B., Mostaghel, E. A., Vessella, R., Hess, D. L., Kalhorn, T. F., Higano, C. S., True, L. D., and Nelson, P. S. (2008). Maintenance of intratumoral androgens in metastatic prostate cancer: a mechanism for castration-resistant tumor growth. Cancer Res *68*, 4447-4454.

Montironi, R., Mazzucchelli, R., Lopez-Beltran, A., Scarpelli, M., and Cheng, L. (2011). Prostatic intraepithelial neoplasia: its morphological and molecular diagnosis and clinical significance. BJU Int *108*, 1394-1401.

Mu, P., Zhang, Z., Benelli, M., Karthaus, W. R., Hoover, E., Chen, C. C., Wongvipat, J., Ku, S. Y., Gao, D., Cao, Z.*, et al.* (2017). SOX2 promotes lineage plasticity and antiandrogen resistance in TP53- and RB1-deficient prostate cancer. Science *355*, 84-88.

Mukherjee, B., Kessinger, C., Kobayashi, J., Chen, B. P., Chen, D. J., Chatterjee, A., and Burma, S. (2006). DNA-PK phosphorylates histone H2AX during apoptotic DNA fragmentation in mammalian cells. DNA Repair (Amst) *5*, 575-590.

Mulholland, D. J., Kobayashi, N., Ruscetti, M., Zhi, A., Tran, L. M., Huang, J., Gleave, M., and Wu, H. (2012). Pten loss and RAS/MAPK activation cooperate to promote EMT and metastasis initiated from prostate cancer stem/progenitor cells. Cancer Res *72*, 1878-1889.

Nadal, R., Schweizer, M., Kryvenko, O. N., Epstein, J. I., and Eisenberger, M. A. (2014). Small cell carcinoma of the prostate. Nat Rev Urol *11*, 213-219.

Namiki, Y., and Zou, L. (2006). ATRIP associates with replication protein A-coated ssDNA through multiple interactions. Proc Natl Acad Sci U S A *103*, 580-585.

Narita, M., Nunez, S., Heard, E., Narita, M., Lin, A. W., Hearn, S. A., Spector, D. L., Hannon, G. J., and Lowe, S. W. (2003). Rb-mediated heterochromatin formation and silencing of E2F target genes during cellular senescence. Cell *113*, 703-716.

Nieto, M. A. (2011). The ins and outs of the epithelial to mesenchymal transition in health and disease. Annu Rev Cell Dev Biol *27*, 347-376.

Nieto, M. A. (2013). Epithelial plasticity: a common theme in embryonic and cancer cells. Science *342*, 1234850.

Noel, E. E., Ragavan, N., Walsh, M. J., James, S. Y., Matanhelia, S. S., Nicholson, C. M., Lu, Y. J., and Martin, F. L. (2008). Differential gene expression in the peripheral zone compared to the transition zone of the human prostate gland. Prostate Cancer Prostatic Dis *11*, 173-180.

Ostrand-Rosenberg, S., and Sinha, P. (2009). Myeloid-derived suppressor cells: linking inflammation and cancer. J Immunol *182*, 4499-4506.

Palapattu, G. S., Wu, C., Silvers, C. R., Martin, H. B., Williams, K., Salamone, L., Bushnell, T., Huang, L. S., Yang, Q., and Huang, J. (2009). Selective expression of CD44, a putative prostate cancer stem cell marker, in neuroendocrine tumor cells of human prostate cancer. Prostate *69*, 787-798.

Parisotto, M., Grelet, E., El Bizri, R., Dai, Y., Terzic, J., Eckert, D., Gargowitsch, L., Bornert, J. M., and Metzger, D. (2018). PTEN deletion in luminal cells of mature prostate induces replication stress and senescence in vivo. J Exp Med.

Parisotto, M., and Metzger, D. (2013). Genetically engineered mouse models of prostate cancer. Mol Oncol *7*, 190-205.

Perner, S., Demichelis, F., Beroukhim, R., Schmidt, F. H., Mosquera, J. M., Setlur, S., Tchinda, J., Tomlins, S. A., Hofer, M. D., Pienta, K. G.*, et al.* (2006). TMPRSS2:ERG fusion-associated deletions provide insight into the heterogeneity of prostate cancer. Cancer Res *66*, 8337-8341.

Popov, V. M., Wang, C., Shirley, L. A., Rosenberg, A., Li, S., Nevalainen, M., Fu, M., and Pestell, R. G. (2007). The functional significance of nuclear receptor acetylation. Steroids *72*, 221-230.

Qin, J., Liu, X., Laffin, B., Chen, X., Choy, G., Jeter, C. R., Calhoun-Davis, T., Li, H., Palapattu, G. S., Pang, S.*, et al.* (2012). The PSA(-/lo) prostate cancer cell population harbors self-renewing long-term tumor-propagating cells that resist castration. Cell Stem Cell *10*, 556-569.

Ratnacaram, C. K., Teletin, M., Jiang, M., Meng, X., Chambon, P., and Metzger, D. (2008). Temporally controlled ablation of PTEN in adult mouse prostate epithelium generates a model of invasive prostatic adenocarcinoma. Proc Natl Acad Sci U S A *105*, 2521-2526.

Reitsema, T., Klokov, D., Banath, J. P., and Olive, P. L. (2005). DNA-PK is responsible for enhanced phosphorylation of histone H2AX under hypertonic conditions. DNA Repair (Amst) *4*, 1172-1181.

Resnick, M. J., Koyama, T., Fan, K. H., Albertsen, P. C., Goodman, M., Hamilton, A. S., Hoffman, R. M., Potosky, A. L., Stanford, J. L., Stroup, A. M.*, et al.* (2013). Long-term functional outcomes after treatment for localized prostate cancer. N Engl J Med *368*, 436-445.

Rogakou, E. P., Pilch, D. R., Orr, A. H., Ivanova, V. S., and Bonner, W. M. (1998). DNA double-stranded breaks induce histone H2AX phosphorylation on serine 139. J Biol Chem *273*, 5858-5868.

Salvatori, L., Caporuscio, F., Verdina, A., Starace, G., Crispi, S., Nicotra, M. R., Russo, A., Calogero, R. A., Morgante, E., Natali, P. G.*, et al.* (2012). Cell-to-cell signaling influences the fate of prostate cancer stem cells and their potential to generate more aggressive tumors. PLoS One *7*, e31467.

Sarkar, A., and Hochedlinger, K. (2013). The sox family of transcription factors: versatile regulators of stem and progenitor cell fate. Cell Stem Cell *12*, 15-30.

Schalken, J., and Fitzpatrick, J. M. (2016). Enzalutamide: targeting the androgen signalling pathway in metastatic castration-resistant prostate cancer. BJU Int *117*, 215-225.

Scher, H. I., Beer, T. M., Higano, C. S., Anand, A., Taplin, M. E., Efstathiou, E., Rathkopf, D., Shelkey, J., Yu, E. Y., Alumkal, J.*, et al.* (2010). Antitumour activity of MDV3100 in castration-resistant prostate cancer: a phase 1-2 study. Lancet *375*, 1437-1446.

Schmalhofer, O., Brabletz, S., and Brabletz, T. (2009). E-cadherin, beta-catenin, and ZEB1 in malignant progression of cancer. Cancer Metastasis Rev *28*, 151-166.

Schroder, F. H., Hugosson, J., Roobol, M. J., Tammela, T. L., Ciatto, S., Nelen, V., Kwiatkowski, M., Lujan, M., Lilja, H., Zappa, M.*, et al.* (2012). Prostate-cancer mortality at 11 years of follow-up. N Engl J Med *366*, 981-990.

Seiler, D., Zheng, J., Liu, G., Wang, S., Yamashiro, J., Reiter, R. E., Huang, J., and Zeng, G. (2013). Enrichment of putative prostate cancer stem cells after androgen deprivation: upregulation of pluripotency transactivators concurs with resistance to androgen deprivation in LNCaP cell lines. Prostate *73*, 1378-1390.

Shang, Y., Myers, M., and Brown, M. (2002). Formation of the androgen receptor transcription complex. Mol Cell *9*, 601-610.

Shang, Z., Cai, Q., Zhang, M., Zhu, S., Ma, Y., Sun, L., Jiang, N., Tian, J., Niu, X., Chen, J.*, et al.* (2015). A switch from CD44(+) cell to EMT cell drives the metastasis of prostate cancer. Oncotarget *6*, 1202-1216.

Sharma, A., Yeow, W. S., Ertel, A., Coleman, I., Clegg, N., Thangavel, C., Morrissey, C., Zhang, X., Comstock, C. E., Witkiewicz, A. K.*, et al.* (2010). The retinoblastoma tumor suppressor controls androgen signaling and human prostate cancer progression. J Clin Invest *120*, 4478-4492.

Shay, J. W., and Wright, W. E. (2000). Hayflick, his limit, and cellular ageing. Nat Rev Mol Cell Biol *1*, 72-76.

Shook, D., and Keller, R. (2003). Mechanisms, mechanics and function of epithelial-mesenchymal transitions in early development. Mech Dev *120*, 1351-1383.

Siegel, R. L., Miller, K. D., and Jemal, A. (2017). Cancer Statistics, 2017. CA Cancer J Clin *67*, 7-30.
Sirbu, B. M., Couch, F. B., Feigerle, J. T., Bhaskara, S., Hiebert, S. W., and Cortez, D. (2011). Analysis of protein dynamics at active, stalled, and collapsed replication forks. Genes Dev *25*, 1320-1327.

Smit, F. P., Salagierski, M., Jannink, S., and Schalken, J. A. (2013). High-resolution ERG-expression profiling on GeneChip exon 1.0 ST arrays in primary and castration-resistant prostate cancer. BJU Int *111*, 836-842.

Stambolic, V., MacPherson, D., Sas, D., Lin, Y., Snow, B., Jang, Y., Benchimol, S., and Mak, T. W. (2001). Regulation of PTEN transcription by p53. Mol Cell *8*, 317-325.

Steinkamp, M. P., O'Mahony, O. A., Brogley, M., Rehman, H., Lapensee, E. W., Dhanasekaran, S., Hofer, M. D., Kuefer, R., Chinnaiyan, A., Rubin, M. A.*, et al.* (2009). Treatment-dependent androgen receptor mutations in prostate cancer exploit multiple mechanisms to evade therapy. Cancer Res *69*, 4434-4442.

Sun, F., Chen, H. G., Li, W., Yang, X., Wang, X., Jiang, R., Guo, Z., Chen, H., Huang, J., Borowsky, A. D., and Qiu, Y. (2014). Androgen receptor splice variant AR3 promotes prostate cancer via modulating expression of autocrine/paracrine factors. J Biol Chem *289*, 1529-1539.

Sun, S., Sprenger, C. C., Vessella, R. L., Haugk, K., Soriano, K., Mostaghel, E. A., Page, S. T., Coleman, I. M., Nguyen, H. M., Sun, H.*, et al.* (2010). Castration resistance in human prostate cancer is conferred by a frequently occurring androgen receptor splice variant. J Clin Invest *120*, 2715-2730.

Sun, Y., Wang, B. E., Leong, K. G., Yue, P., Li, L., Jhunjhunwala, S., Chen, D., Seo, K., Modrusan, Z., Gao, W. Q.*, et al.* (2012). Androgen deprivation causes epithelial-mesenchymal transition in the prostate: implications for androgen-deprivation therapy. Cancer Res *72*, 527-536.

Suzman, D. L., and Antonarakis, E. S. (2014). Castration-resistant prostate cancer: latest evidence and therapeutic implications. Ther Adv Med Oncol *6*, 167-179.

Suzuki, H., Sato, N., Watabe, Y., Masai, M., Seino, S., and Shimazaki, J. (1993). Androgen receptor gene mutations in human prostate cancer. J Steroid Biochem Mol Biol *46*, 759-765.

Takahashi, K., and Yamanaka, S. (2006). Induction of pluripotent stem cells from mouse embryonic and adult fibroblast cultures by defined factors. Cell *126*, 663-676.

Talmadge, J. E., and Gabrilovich, D. I. (2013). History of myeloid-derived suppressor cells. Nat Rev Cancer *13*, 739-752.

Tannock, I. F., de Wit, R., Berry, W. R., Horti, J., Pluzanska, A., Chi, K. N., Oudard, S., Theodore, C., James, N. D., Turesson, I.*, et al.* (2004). Docetaxel plus prednisone or mitoxantrone plus prednisone for advanced prostate cancer. N Engl J Med *351*, 1502-1512.

Taplin, M. E. (2007). Drug insight: role of the androgen receptor in the development and progression of prostate cancer. Nat Clin Pract Oncol *4*, 236-244.

Taplin, M. E., Bubley, G. J., Ko, Y. J., Small, E. J., Upton, M., Rajeshkumar, B., and Balk, S. P. (1999). Selection for androgen receptor mutations in prostate cancers treated with androgen antagonist. Cancer Res *59*, 2511-2515.

Taplin, M. E., Bubley, G. J., Shuster, T. D., Frantz, M. E., Spooner, A. E., Ogata, G. K., Keer, H. N., and Balk, S. P. (1995). Mutation of the androgen-receptor gene in metastatic androgen-independent prostate cancer. N Engl J Med *332*, 1393-1398.

Taube, J. H., Herschkowitz, J. I., Komurov, K., Zhou, A. Y., Gupta, S., Yang, J., Hartwell, K., Onder, T. T., Gupta, P. B., Evans, K. W.*, et al.* (2010). Core epithelial-to-mesenchymal transition interactome gene-expression signature is associated with claudin-low and metaplastic breast cancer subtypes. Proc Natl Acad Sci U S A *107*, 15449-15454.

Thiery, J. P. (2002). Epithelial-mesenchymal transitions in tumour progression. Nat Rev Cancer *2*, 442-454.

Thiery, J. P., Acloque, H., Huang, R. Y., and Nieto, M. A. (2009). Epithelial-mesenchymal transitions in development and disease. Cell *139*, 871-890.

Tilley, W. D., Buchanan, G., Hickey, T. E., and Bentel, J. M. (1996). Mutations in the androgen receptor gene are associated with progression of human prostate cancer to androgen independence. Clin Cancer Res *2*, 277-285.

Timms, B. G. (2008). Prostate development: a historical perspective. Differentiation *76*, 565-577.
Tomlins, S. A., Rhodes, D. R., Perner, S., Dhanasekaran, S. M., Mehra, R., Sun, X. W., Varambally, S., Cao, X., Tchinda, J., Kuefer, R.*, et al.* (2005). Recurrent fusion of TMPRSS2 and ETS transcription factor genes in prostate cancer. Science *310*, 644-648.

Ueda, T., Bruchovsky, N., and Sadar, M. D. (2002). Activation of the androgen receptor N-terminal domain by interleukin-6 via MAPK and STAT3 signal transduction pathways. J Biol Chem *277*, 7076-7085.

Vassilev, L. T., Vu, B. T., Graves, B., Carvajal, D., Podlaski, F., Filipovic, Z., Kong, N., Kammlott, U., Lukacs, C., Klein, C.*, et al.* (2004). In vivo activation of the p53 pathway by small-molecule antagonists of MDM2. Science *303*, 844-848.

Veldscholte, J., Berrevoets, C. A., Brinkmann, A. O., Grootegoed, J. A., and Mulder, E. (1992). Anti-androgens and the mutated androgen receptor of LNCaP cells: differential effects on binding affinity, heat-shock protein interaction, and transcription activation. Biochemistry *31*, 2393-2399.

Vogelstein, B., Lane, D., and Levine, A. J. (2000). Surfing the p53 network. Nature *408*, 307-310.

Wang, H., Wang, M., Wang, H., Bocker, W., and Iliakis, G. (2005a). Complex H2AX phosphorylation patterns by multiple kinases including ATM and DNA-PK in human cells exposed to ionizing radiation and treated with kinase inhibitors. J Cell Physiol *202*, 492-502.

Wang, W., and Epstein, J. I. (2008). Small cell carcinoma of the prostate. A morphologic and immunohistochemical study of 95 cases. Am J Surg Pathol *32*, 65-71.

Wang, Y., Xue, H., Cutz, J. C., Bayani, J., Mawji, N. R., Chen, W. G., Goetz, L. J., Hayward, S. W., Sadar, M. D., Gilks, C. B.*, et al.* (2005b). An orthotopic metastatic prostate cancer model in SCID mice via grafting of a transplantable human prostate tumor line. Lab Invest *85*, 1392-1404.

Ward, I. M., and Chen, J. (2001). Histone H2AX is phosphorylated in an ATR-dependent manner in response to replicational stress. J Biol Chem *276*, 47759-47762.

Ward, I. M., Minn, K., and Chen, J. (2004). UV-induced ataxia-telangiectasia-mutated and Rad3-related (ATR) activation requires replication stress. J Biol Chem *279*, 9677-9680.

Ward, R. D., and Weigel, N. L. (2009). Steroid receptor phosphorylation: Assigning function to site-specific phosphorylation. Biofactors *35*, 528-536.

Wen, Y., Hu, M. C., Makino, K., Spohn, B., Bartholomeusz, G., Yan, D. H., and Hung, M. C. (2000). HER-2/neu promotes androgen-independent survival and growth of prostate cancer cells through the Akt pathway. Cancer Res *60*, 6841-6845.

Wesolowski, R., Markowitz, J., and Carson, W. E., 3rd (2013). Myeloid derived suppressor cells - a new therapeutic target in the treatment of cancer. J Immunother Cancer *1*, 10.

Whitson, J. M., and Carroll, P. R. (2010). Active surveillance for early-stage prostate cancer: defining the triggers for intervention. J Clin Oncol *28*, 2807-2809.

Wu, J. D., Haugk, K., Woodke, L., Nelson, P., Coleman, I., and Plymate, S. R. (2006). Interaction of IGF signaling and the androgen receptor in prostate cancer progression. J Cell Biochem *99*, 392-401.

Wu, J. N., Fish, K. M., Evans, C. P., Devere White, R. W., and Dall'Era, M. A. (2014). No improvement noted in overall or cause-specific survival for men presenting with metastatic prostate cancer over a 20-year period. Cancer *120*, 818-823.

Xu, K., Shimelis, H., Linn, D. E., Jiang, R., Yang, X., Sun, F., Guo, Z., Chen, H., Li, W., Chen, H.*, et al.* (2009). Regulation of androgen receptor transcriptional activity and specificity by RNF6-induced ubiquitination. Cancer Cell *15*, 270-282.

Yang, J., and Weinberg, R. A. (2008). Epithelial-mesenchymal transition: at the crossroads of development and tumor metastasis. Dev Cell *14*, 818-829.

Yeh, S., Lin, H. K., Kang, H. Y., Thin, T. H., Lin, M. F., and Chang, C. (1999). From HER2/Neu signal cascade to androgen receptor and its coactivators: a novel pathway by induction of androgen target genes through MAP kinase in prostate cancer cells. Proc Natl Acad Sci U S A *96*, 5458-5463.

Yu, J., Vodyanik, M. A., Smuga-Otto, K., Antosiewicz-Bourget, J., Frane, J. L., Tian, S., Nie, J., Jonsdottir, G. A., Ruotti, V., Stewart, R.*, et al.* (2007). Induced pluripotent stem cell lines derived from human somatic cells. Science *318*, 1917-1920.

Yuan, T. C., Veeramani, S., Lin, F. F., Kondrikou, D., Zelivianski, S., Igawa, T., Karan, D., Batra, S. K., and Lin, M. F. (2006). Androgen deprivation induces human prostate epithelial neuroendocrine differentiation of androgen-sensitive LNCaP cells. Endocr Relat Cancer *13*, 151-167.

Yuan, X., and Balk, S. P. (2009). Mechanisms mediating androgen receptor reactivation after castration. Urol Oncol *27*, 36-41.

Zhang, R., Poustovoitov, M. V., Ye, X., Santos, H. A., Chen, W., Daganzo, S. M., Erzberger, J. P., Serebriiskii, I. G., Canutescu, A. A., Dunbrack, R. L.*, et al.* (2005). Formation of MacroH2A-containing senescence-associated heterochromatin foci and senescence driven by ASF1a and HIRA. Dev Cell *8*, 19-30.

Zhao, X. Y., Malloy, P. J., Krishnan, A. V., Swami, S., Navone, N. M., Peehl, D. M., and Feldman, D. (2000). Glucocorticoids can promote androgen-independent growth of prostate cancer cells through a mutated androgen receptor. Nat Med *6*, 703-706.

Zhou, Z., Flesken-Nikitin, A., Corney, D. C., Wang, W., Goodrich, D. W., Roy-Burman, P., and Nikitin, A. Y. (2006). Synergy of p53 and Rb deficiency in a conditional mouse model for metastatic prostate cancer. Cancer Res *66*, 7889-7898.

Zou, L., and Elledge, S. J. (2003). Sensing DNA damage through ATRIP recognition of RPA-ssDNA complexes. Science *300*, 1542-1548.

Zou, M., Toivanen, R., Mitrofanova, A., Floch, N., Hayati, S., Sun, Y., Le Magnen, C., Chester, D., Mostaghel, E. A., Califano, A.*, et al.* (2017). Transdifferentiation as a Mechanism of Treatment Resistance in a Mouse Model of Castration-Resistant Prostate Cancer. Cancer Discov *7*, 736-749.

Rana EL BIZRI

Characterization of Pten and Trp53-deficient prostatic tumors in mice

Résumé

Le cancer de la prostate est la forme de cancer la plus fréquente et la troisième cause de décès par cancer chez l'homme dans les sociétés occidentales. Alors que la plupart des cancers de la prostate localisés sont éradiqués chirurgicalement, la plupart des tumeurs métastatiques répondant initialement aux thérapies par privation d'androgènes deviennent résistantes au traitement, causant généralement le décès du patient. Les gènes suppresseurs de tumeur PTEN et p53 étant fréquemment mutés dans les cancers de la prostate métastatiques et résistants à la castration, le laboratoire d'accueil a généré des modèles murins dans lesquels Pten et/ou Trp53 sont sélectivement invalidés à l'âge adulte dans les cellules épithéliales prostatiques dans le but de déterminer les évènements clés conduisant à la progression du cancer de la prostate. Notre étude révèle que l'invalidation de PTEN stimule la prolifération des cellules épithéliales prostatiques et conduit à des néoplasmes prostatiques intraépithéliaux en quelques mois. Cette hyper-prolifération induit un stress réplicatif et une réponse aux dommages de l'ADN qui va conduire à un arrêt progressif de la croissance cellulaire et une entrée en sénescence. Les cellules sénescentes sécrètent de nombreuses cytokines et de chimiokines, et peuvent accumuler des mutations contribuant ainsi à la progression de la tumeur. Il est notable qu'en l'absence de Trp53, les épithéliums prostatiques dépourvus de Pten développent des néoplasmes prostatiques intraépithéliaux entrant en sénescence. Cependant, la formation d'adénocarcinomes est accélérée et des tumeurs sarcomatoïdes pouvant générer à long terme des métastases apparaissent. En l'absence de Pten, certaines cellules épithéliales prostatiques perdent leur identité moléculaire en exprimant des marqueurs caractéristiques de cellules souches et différenciation neuroendocrinienne. Nous avons également mis en évidence des cellules épithéliales prostatiques déficientes en PTEN et p53 résistantes à la castration exprimant à la fois des marqueurs de cellules basales et luminales. En conclusion, nos travaux ont permis une avancée dans la compréhension des mécanismes conduisant à des formes incurables de cancer de la prostate. Les traitements actuels ayant des effets secondaires importants et pouvant générer des résistances, le développement de nouvelles stratégies thérapeutiques permettant l'élimination des cellules sénescentes mais aussi des cellules épithéliales prostatiques exprimant des marqueurs de cellules basales et luminales dans les lésions précancéreuses représente des perspectives intéressantes pour traiter le cancer de la prostate.

Keywords: cancer de la prostate, cellules épithéliales prostatiques, néoplasmes prostatiques intraépithéliaux, sénescence cellulaire, stress réplicatif, une réponse aux dommages de l'ADN, cancers de la prostate résistants à la castration.

Abstract

Prostate cancer (PCa) is a leading cause of male cancer death worldwide. While most locally PCa are curable, metastatic tumors initially respond to androgen deprivation therapy but ultimately relapse to castration-resistant prostate cancer (CRPC), which is a lethal disease. Since the tumor suppressor genes PTEN and p53 are frequently mutated in metastatic and CRPC, the host laboratory generated mouse models in which Pten and/or Trp53 are selectively ablated in adult prostatic epithelial cells (PECs) in order to unravel the key events leading to prostate cancer progression. Our study reveals that Pten ablation stimulates PECs proliferation forming prostatic intraepithelial neoplasia (PIN) within a few months. This hyper-proliferation induces replicative stress and a DNA damage response (DDR), which in turn leads to a progressive growth arrest with characteristics of cell senescence. As senescent cells secrete a large number of cytokines and chemokines, and can accumulate other mutations, they might contribute to tumor progression. Importantly, in the absence of Trp53, most Pten-null PECs develop PINs that enter senescence. However partial loss of PECs identity is detected as we show enhanced stemness and focal neuroendocrine differentiation of luminal Pten-null PECs. In some cases, adenocarcinoma and sarcomatoid tumors are formed, and more than one-third of the latter develop metastases. Strikingly, we also show formation of castration-resistant Pten and Pten/Trp53-null PECs expressing both luminal and basal markers. Taken together, as current treaments lead to side effects and resistance, the development of therapeutic strategies to eliminate senescent cells/and or PECs expressing luminal and basal/stem progenitor in pre-cancerous lesions represents promising option for prostate cancer treatment.

Keywords: prostate cancer, prostatic epithelial cells, prostatic intraepithelial neoplasia, cell senescence, replication stress, DNA damage response, castration-resistant prostate cancer.